e-ISSN 2586-9396

Current Applied Science and Technology

Vol. 21 No. 2
April - June 2021

KING MONGKUT'S INSTITUTE OF TECHNOLOGY LADKRABANG

Advisory Board

Current Applied Science and Technology or CAST, formerly KMITL Science and Technology Journal published by King Mongkut's Institute of Technology Ladkrabang (KMITL), has been established since its inception as KMITL Science Journal in 2001. The journal has been dedicated to publishing advanced and applied knowledge in the form of high-quality research and review articles covering the main areas of Biotechnology, Environmental Science, Agricultural Technology, Food Science and other fields related to Applied Science and Technology. Special issues devoted to important topics in advanced science and technology will occasionally be published.

The journal is an open access peer-reviewed and double blinded journal using Online Journal System (OJS) publishing online academic research and review articles. Previously, articles were published in print on a regular basis (two issues per year) since 2001 and since 2010 onward the articles have been published both in print and electronic forms starting from volume 10. In 2017, the journal title has been changed from *KMITL Science and Technology Journal* to *Current Applied Science and Technology* (CAST) (e-ISSN 2586-9396) to be more identifiable to the international scientific community according to the suggestion of Thai-Journal Citation Index Centre. The journal has been published online only since volume 17(2) (July-December, 2017). In addition, the journal has attracted researchers from other countries more than 22% according to the data. Because of more demands on publication in CAST, the editorial board has decided to publish online original academic research and review articles four issues per year (January-March, April-June, July-September and October-December) from 2021 onward.

Furthermore, the advisory board and editorial board comprises honorable and well-known members from around the world in which 50% of editorial board members are from various countries like U.K., Norway, Japan, India, China, Canada, Estonia and Egypt. Only 25% of Thai editorial board members are from the publisher organization and 25% from other publisher organizations. Most of advisory and editorial board members have high H-index according to SCOPUS.

The journal is also committed to maintaining the high level of integrity in the content published and has a Conflict of Interest policy in place. The journal uses plagiarism detection software to screen the submissions. The journal has been working closely with Thai-Journal Citation Index Centre to ensure that the journal complies with international standard of SCOPUS.

Current Applied Science and Technology (CAST)

(formerly KMITL Science and Technology Journal)

Editor

Dusanee Thanaboripat
King Mongkut's Institute of Technology Ladkrabang, Thailand

Editorial Board

CONTENTS

Efficiency of Ultrasonic Treatment on Postharvest Quality and Bioactive Compounds of 'Kim Ju' Guava Fruit During Short-Term Storage at Room Temperature

Suriyan Supapvanich* and Chollawit Kijka

Department of Agricultural Education, Faculty of Industrial Education and Technology, King Mongkut's Institute of Technology Ladkrabang, Bangkok, Thailand

Received: 9 May 2020, Revised: 13 August 2020, Accepted: 31 August 2020

Abstract

The purpose of this recent work was to investigate the efficiency of ultrasonic (US) treatment on the postharvest quality and bioactive compounds of 'Kim Ju' guava fruits during storage at room temperature (RT) (28±1°C) for 6 d. The fruit samples were sonicated at 40 kHz and 150 w for 10 min. Visual appearance, colour attributes, weight loss, total soluble solids (TSS), titratable acidity (TA), texture, pectin substances, antioxidant activity, total phenols and flavonoids contents of the fruits were monitored during storage. The fruits treated with US had better visual appearance than that of untreated fruits. US treatment could delay weight loss but it had no effect on all colour attributes, TSS and TA of fruits. Fruit softening was inhibited by US treatment due to delay in the formation of increased soluble pectin and decreased insoluble pectin contents. Moreover, US treatment could enhance antioxidant activity and the total phenols and flavonoids contents. Nevertheless, there was no change of ascorbic acid content in fruits during storage. These results suggest that US treatment is an effective postharvest approach, which could preserve postharvest quality and level of bioactive compounds of 'Kim Ju' guavas during short-term storage at RT.

Keywords: guava; ultrasound; bioactive compound; firmness; fruit
DOI 10.14456/cast.2021.19

1. Introduction

Guava (*Psidium guajava* L.) fruit is a commercial fruit in Southeast Asian countries including Thailand. Thailand has been widely known as a potential country producing tropical fruits such as durian, rambutan, papaya, pineapple, and guava [1]. Guava has been produced for domestic and international markets. Three commercial cultivars such as 'Klomsali', 'Salithong', and 'Kim Ju' have been commonly grown in Thailand [2]. They are white guavas and they are best consumed at full mature green stage when the flesh is still crisp. Besides their crispy texture and bright-green skin, white flesh and sweet-and-sour taste are other attractive characteristics of Thai guava. Among the commercial cultivars of guava, 'Kim Ju' is one of the most popular cultivars in the domestic and export market. In the domestic market, guava fruits are mostly kept at room temperature (RT) rather than storage in a cold room, a condition which limits its shelf-life and marketing period. Skin browning, rotting, softening, and weight loss are the main

*Corresponding author: Tel.: (+66) 900124901
E-mail: suriyan.su@kmitl.ac.th

factors affecting quality and marketability of guava fruits [3, 4]. Guava is classified as a climacteric fruit that exhibits peaks of respiratory rate and ethylene production during the ripening process [5, 6]. At the average atmospheric temperature in Thailand (28-32°C), guavas typically undergo rapid deterioration within 3-4 days [7]. Recently, many postharvest treatments such as heat treatment [8], calcium treatment [9], exogenous plant-growth regulators treatment [4, 7] have been applied to maintain postharvest quality and reduce the deterioration of guavas during storage.

The potential of ultrasonic (US) treatment has been recognized in food industry since the 1970s. It has been used in food processing and extraction due to its cavitation effect [10]. Recently, US application has been accepted as an effective physical treatment for controlling postharvest quality and inducing pathogenic resistance in fruits and vegetables such as tomatoes [11, 12], table grapes [13] and loquats [14]. Many previous works suggested that US could enhance defence mechanisms, antioxidant activities, secondary metabolites biosynthesis [12, 15, 16] as well as strengthen cell walls and membrane structures in plants [17, 18]. It has also been claimed that US treatment for an appropriate time could enhance product quality, reduce chemical hazards, lower energy consumption and be an environmentally friendly technique [10]. However, the investigation of US effects on the postharvest quality of Thai guava fruits has not been reported yet. Thus, the purpose of this study was to investigate the efficiency of US treatment on physiochemical quality and bioactive compounds of 'Kim Ju' guava during short-term storage at RT.

2. Materials and Methods

2.1 Plant materials preparation

Guava (*Psidium guajava* L.) cv. 'Kim Ju' fruits at commercial maturity (100 days after anthesis) were harvested from an orchard in Rachaburi province, Thailand. Then, the fruits were delivered to Laboratory at Department of Agricultural Education, King Mongkut's Institute of Technology Ladkrabang within 3 h. The fruit samples were then screened on the basis of uniform size (180-200 g per fruit) and quality (being without damages and diseases). Afterwards, the selected guava fruits were cleaned by rinsing with chlorinated water and dried at RT for 10 min.

2.2 Treatments

In our preliminary experiment, the effect of ultrasonic (US) treatment at 40 kHz and 150 w, for 5, 10, 15 or 20 min compared with the control treatment (without US) on visual appearance of the fruit during storage at RT (28 ± 2 °C) for 5 d was investigated. The result indicated that the visual appearance of fruit treated with US for 5 min was not different from untreated fruit. Moreover, browning skin was obviously found in the fruit samples treated with US for 20 min. US treatment for 10 or 15 min maintained the visual appearance of the fruit being storage in a superior way than other treatments (data not shown). Therefore, US treatment for 10 min was selected to study its effect on physicochemical quality of 'guavas during short-term storage at RT. In this study, the US treatment was operated using an ultrasonicator at 40 kHz and 150 w (GT-1860QTS, China). The guava fruits were treated for 10 min and the fruit samples dipped in water for 10 min were used as negative control samples. After treatment, each individual guava fruit was wrapped in a LLDPE film (commercial plastic film for guava) and then stored at RT for 6 d. The physicochemical quality parameters such as visual appearance, superficial colour attributes, total soluble solids (TSS), total acidity (TA), texture, pectin substances, antioxidant activity, phenolic compounds, flavonoids and ascorbic acid contents of both US treated and untreated guava fruits were monitored during storage.

2.3 Visual appearance and superficial colour measurement

The visual appearance of guavas during storage was evaluated by taking photographs. Photographs of the fruit samples were at day 0, 2, 4 and 6. Colour attributes such as *L**, *a**, *b**, hue and chroma values were determined using a Minolta colorimeter CR-300 (Minolta Camera Co., Japan).

2.4 Total soluble solids (TSS) and titratable acidity (TA) measurement

TSS content of guava fruit was determined using a refractometer (ATAGO, Japan). The data were expressed as percentage of TSS (%). TA content was assayed using the titration method of Association of Official Analytical Chemists [19]. The guava juice was titrated with 0.1 N NaOH using phenolphthalein as an indicator. The volume of titrated NaOH was used for calculation. The data were shown as the percentage of citric acid (% citric acid).

2.5 Texture measurement

The texture of guava fruits was measured using a TA Plus Texture Analyzer (Lloyds, England). A cylindrical probe (3 mm diameter) was used to measure the hardness of fruits at the operation rate of 1 mm sec^{-1}. The maximum force (Newton, N) was recorded as hardness.

2.6 Soluble- and insoluble-pectin substances determinations

Acetone insoluble solid (AIS) of guava was prepared according to the method of Supapvanich *et al*. [4]. All gained AIS was then used to extract pectin substances. The soluble pectin in AIS was extracted with 50 mM ethylenediaminetetraacetic acid (EDTA) consisting of 50 mM sodium acetate (pH 7) for 6 h at RT. The filtrate was collected and soluble pectin was precipitated using absolute ethanol. The cake was again extracted with 50 mM sodium carbonate (Na_2CO_3) consisting of 20 mM sodium borohydride ($NaBH_4$) for 24 h at 4±1°C followed by at ambient temperature for 2 h. The insoluble pectin was precipitated using absolute ethanol. Both the soluble and insoluble pectins were assayed using the method described by Ahmed and Labavitch [20]. The data were expressed as gram of galacturonic acid per kilogram fresh weight of sample (g kg^{-1}).

2.7 Antioxidant activity determination

Guava pulp (5g) was extracted with 60 % (v/v) ethanol. The extract was used to determine ferric reducing antioxidant potential (FRAP), and the concentrations of total phenolic compounds and flavonoids. FRAP was assayed using the method of Benzie and Strain [21]. The sample was mixed with FRAP reagent, consisting of acetate buffer (pH 3), 10 mM 2,4,6-tripyridyl-1,3,5-triazine (TPTZ) and 20 mM ferric chloride hexahydrate in the ratio of 10:1:1. The mixture was incubated at RT for 30 min and the absorbance at 630 nm wavelength was then recorded. FRAP was computed and expressed as mmole Trolox equivalents per kg fresh weight of sample (mmol kg^{-1}).

2.8 Total phenols and flavonoids contents determinations

The concentrations of total phenols and flavonoids were assayed using the methods described by Slinkard and Singleton [22] and Jia *et al*. [23], respectively. Total phenol determination was begun when 1 ml of the extract was reacted with 1 ml of 50 % (v/v) Folin-Ciocalteu reagent and 2 ml of saturated Na_2CO_3 solution. The absorbance at 750 nm wavelength was measured. The data was calculated and expressed as g gallic acid per kg fresh weight (g kg^{-1}). Flavonoids determination was initiated when 0.25 ml of the extract was mixed with 1.25 ml of distilled

water and 0.075 ml of 0.5 % $NaNO_2$, and the mixture was then incubated for 6 min. After incubation, 0.15 ml of 10 % $AlCl_3$-$6H_2O$ was added into the mixture and left for 5 min before 0.5 ml of 1.0 M NaOH was added. Absorbance at 510 nm wavelength was measured and the data were computed and shown as mg catechin equivalents per kilogram fresh weight of sample (mg kg^{-1}).

2.9 Ascorbic acid determination

A 5 g sample of guava was extracted with cold 5% metaphosphoric acid. Ascorbic acid concentration was determined using the method described by Hashimoto and Yamafuji [24]. The 0.8 ml of extract was well-mixed with 0.4 ml of 2 % 2,6-dichlorophenolindophenol and then 0.4 ml of 2 % thiourea and 0.4 ml of 1 % dinitrophenol hydrazine were added. The reaction was incubated at 37 °C for 3 h and 2 ml of 85 % H_2SO_4 was then added. Absorbance at 540 nm wavelength was measured and the data were expressed as g ascorbic acid per kilogram fresh weight of sample (g kg^{-1}).

2.10 Statistical analysis

The presented data were the mean of 4 fruit samples (n = 4) with standard deviation (SD). T-test was used for statistical analysis. Differences at $P < 0.05$ were considered as significant.

3. Results and Discussions

3.1 Visual appearance and superficial colour attributes

Figure 1 shows the visual appearance of 'Kim Ju' guava fruits treated without and with US during storage at RT for 6 d. The US treatment inhibited fruits rotten and retained desirable visual appearance during storage. The rotten fruits were detected in the control at day 4 of storage, whilst no rot was found on the US treated fruits over the storage. Brown flecks occurred evidently on the control fruits' skin after storage for 4 days but were not found on the skin of US treated fruits over the storage period. The overall colour appearance of both control and US treated fruits did not change markedly during the storage. Table 1 shows that no significant differences in colour attributes between control and US treated fruits were found throughout the storage. L^* value tended to decrease, while a^* and hue values remained constant; b^* and chroma values increased slightly in the both treatments during storage. The negative values of a^* and hue exhibited the green colour of guava fruit which were concomitant with the visual colour appearance shown in Figure 1. We also found that no significant differences in colour attributes existed between control and US treated fruits over the storage ($P > 0.05$). This s suggested that US treatment did not affect colour of the fruit skin; however, it reduced fruit decay and brown flecks on fruit skin during storage at RT for 6 day. Cao *et al*. [25] suggested that US destroys or removes contaminated microorganisms by cavitation effects. The cavitation provides free radicals in aqueous medium which attack the cell wall structures of microorganisms leading the weakening of cell wall and cell injury. Previous works reported that US treatment markedly reduced the numbers of bacteria, yeasts and mould in postharvest commodities and in turn alleviated deterioration incidence and prolonged commercial shelf-life [10, 26]. Moreover, da Silva and Dobránszki [27] suggested that US also induces antioxidative defence systems in plants. It is commonly recognised that skin browning of fruits and vegetables is caused by the oxidative reaction of polyphenol oxidase (PPO) and phenolic compounds. Lo'ay and Taher [28] suggested that the reaction of PPO and phenolic compounds caused the skin browning of guava fruit. The antioxidants induced by US prevented the oxidative reaction between PPO and phenolic compounds resulting in the inhibition of browning incidence [10]. Furthermore, Nadar

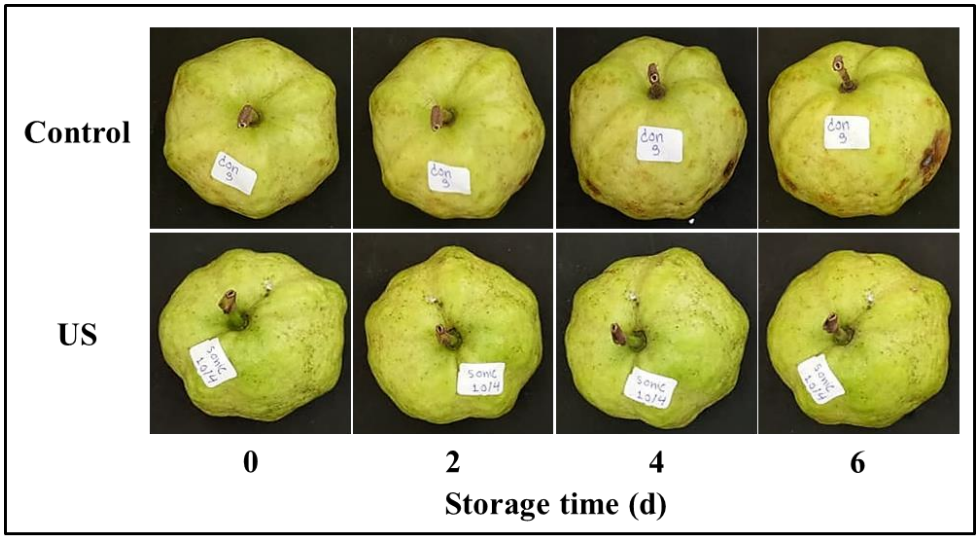

Figure 1. Visual appearance of 'Kim Ju' guava fruits treated with and without US during storage at RT (28±1ºC) for 6 days

Table 1. *L**, *a**, *b**, hue and chroma values of guava fruits treated with and without US during storage at RT (28±1ºC) for 6 days

Storage time (day)	Treatments	Colour attributes				
		L*	***a****	***b****	**hue**	**chroma**
0	Control	63.90±1.30	-7.31±1.44	37.32±0.94	101.28±1.87	37.51±0.84
	US	63.75±1.65	-7.68±0.86	37.25±1.25	101.65±1.25	38.05±1.26
2	Control	63.87±0.33	-7.90±1.24	37.94±1.92	101.21±1.66	39.41±1.37
	US	63.23±1.91	-7.65±0.56	37.53±0.95	101.53±0.98	38.31±0.89
4	Control	62.06±1.48	-7.35±1.76	38.11±1.32	100.94±2.31	38.22±1.33
	US	61.29±0.91	-7.56±0.70	37.80±0.85	101.31±1.04	38.59±0.84
6	Control	61.74±2.00	-7.02±1.96	38.36±1.52	100.41±2.45	39.04±1.75
	US	61.18±1.71	-7.71±0.85	38.26±1.12	101.42±1.42	39.13±1.00

Data are shown as mean ± SD (n = 4).

and Rathod [29] concluded that hydrodynamic cavitation from US treatment causes the damage of enzyme structure. Therefore, the skin browning of 'Kim Ju' guava fruit was inhibited by US treatment due to increased antioxidant system against oxidative browning reaction and hydrodynamic cavitation effect on enzyme structure.

3.2 Weight loss, TSS and TA

The fresh weight loss and taste-related parameters such as TSS and TA of guava fruit are shown in Figure 2. The loss of fresh weight was delayed by US which was significantly lower than that of control fruits over storage time ($P < 0.05$). The loss of fresh weight of control fruits reached

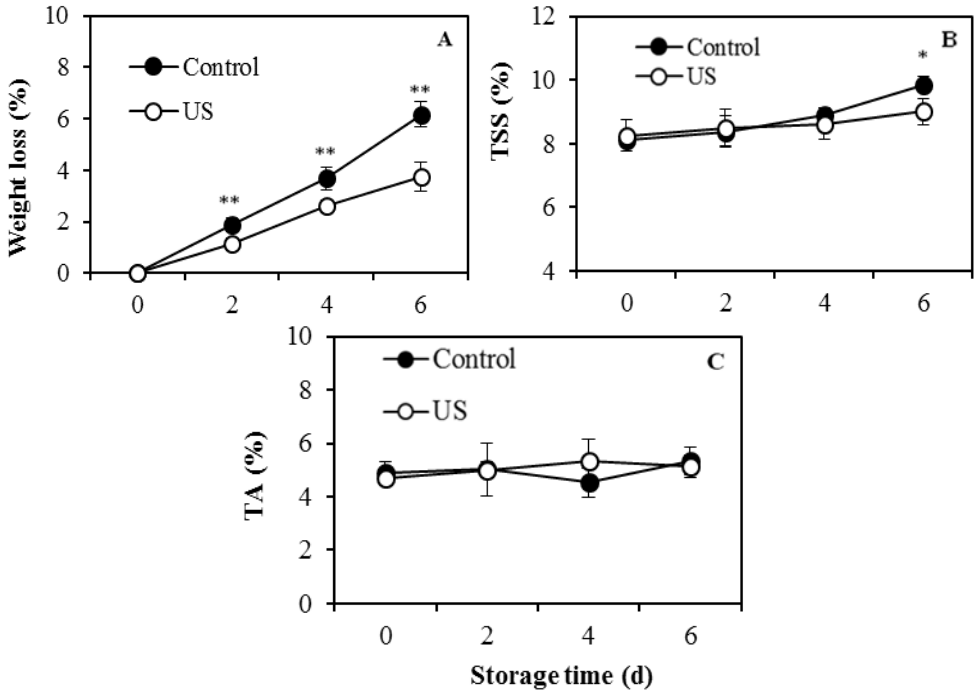

Figure 2. Weight loss (A), TSS (B), and TA (C) of guava fruits treated without and with US during storage at RT (28±1ºC) for 6 days. Vertical bars represent SD of means. Asterisks indicate the differences between treatments [** ($P < 0.01$), * ($P < 0.05$)].

6.16% whereas that of US treated fruits reached 3.74% at the end of storage. The TSS of both control and US treated fruits was not significantly different although a slight increase in TSS was found in control fruits during storage for 4 days. On day 6 of storage, an increase in TSS of both treatments was found and TSS of control fruits was significantly higher than that of US treated fruits ($P < 0.05$). However, US treatment did not significantly affect TA of the guava fruit over the storage. The increased weight loss of guavas was positively concomitant with skin browning during storage, as described by Supapvanich *et al.* [4]. The recent study showed that the lower weight loss of guava fruits was related to the lower level of skin browning. The reduction of weight loss by US might be related to the strengthening of cell walls and cell membranes. Chen *et al*. [16] reported that US reduced lipid peroxidation and dysfunction of plant membrane occurred due to the inducements of antioxidant enzymes and bioactive compounds. Zhi *et al*. [18] reported that US treatment strengthened cell wall structure and reduced membrane peroxidation of jujube fruit during storage period. Lagnika *et al.* [30] also reported that US treatment could delay the increased weight loss of white mushroom during postharvest storage. The increase in TSS of control fruits might be related to the ripening process. It is commonly recognised that guavas are a climacteric fruit for which an increase in TSS has been used as an indicator of the ripening process [1]. Xu *et al.* [10] suggested that hydrodynamic cavitation from US treatment could delay the ripening process by altering ethylene biosynthesis and ethylene signalling pathways.

3.3 Hardness and pectin substances

Fruit softening is an important factor limiting the success of Thai guava fruit industry because the fruit is typically consumed when its texture is still firm and crisp [7]. Figure 3 shows the effect of US treatment on texture (hardness) and pectin substances of 'Kim Ju' guava fruit during storage at RT. The hardness of guava fruits treated with US slightly decreased during

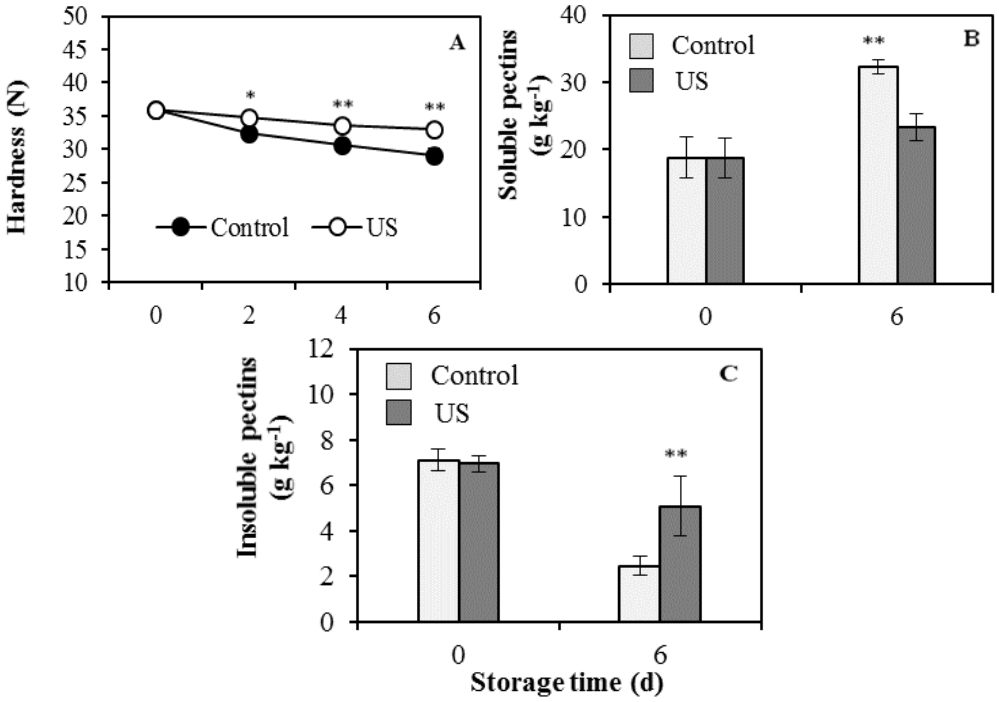

Figure 3. Hardness (A) and the concentrations of soluble pectin (B), and insoluble pectin (C) of guava fruits treated without and with US during storage at RT (28±1 ºC) for 6 days. Vertical bars represent SD of means. Asterisks indicate the differences between treatments [** ($P < 0.01$), * ($P < 0.05$)].

storage, whereas that of control was markedly decreased ($P < 0.01$). The change of texture was related to the changes of soluble and insoluble pectin substances during storage. It is commonly acknowledged that the modification of pectin substances, especially the depolymerisation of pectin polymers, causes fruit softening [7, 9]. Our previous studies found that the softening of 'Kim Ju' guava fruit was accompanied by increased soluble pectin and decreased insoluble pectin during storage [4, 7]. The recent result showed that US treatment obviously delayed the increase of soluble pectin and the reduction of insoluble pectin during storage. The soluble pectin and insoluble pectin of US treated guava fruit were significantly lower and higher, respectively, than those of control fruits ($P < 0.05$). Zhi *et al*. [18] suggested that US induced cellular calcium distribution, resulted in the creation of calcium pectate and inhibition of the generation of water- and CDTA-soluble pectin fractions in jujube fruit. Moreover, the increase of intercellular Ca^{2+} by US treatment was reported by Wang *et al*. [17].

3.4 Antioxidant activity and bioactive compounds

Figure 4 showed the effect of US on antioxidant activity (FRAP) and bioactive compound contents of 'Kim Ju' guavas during storage. It was found that US enhanced FRAP and the total contents of phenols and flavonoids of guavas compared to control fruits. However, there was no effect on ascorbic acid content of fruits during storage. This was in the agreement with the findings of Ding *et al*. [11], who observed that the combined US and slightly acidified electrolytic water treatment had no effect on ascorbic acid content of cherry tomatoes. Both FRAP and total phenols content of US treated guavas were significantly higher than those of control fruit throughout storage time ($P < 0.05$). The flavonoids content of US treated fruits was

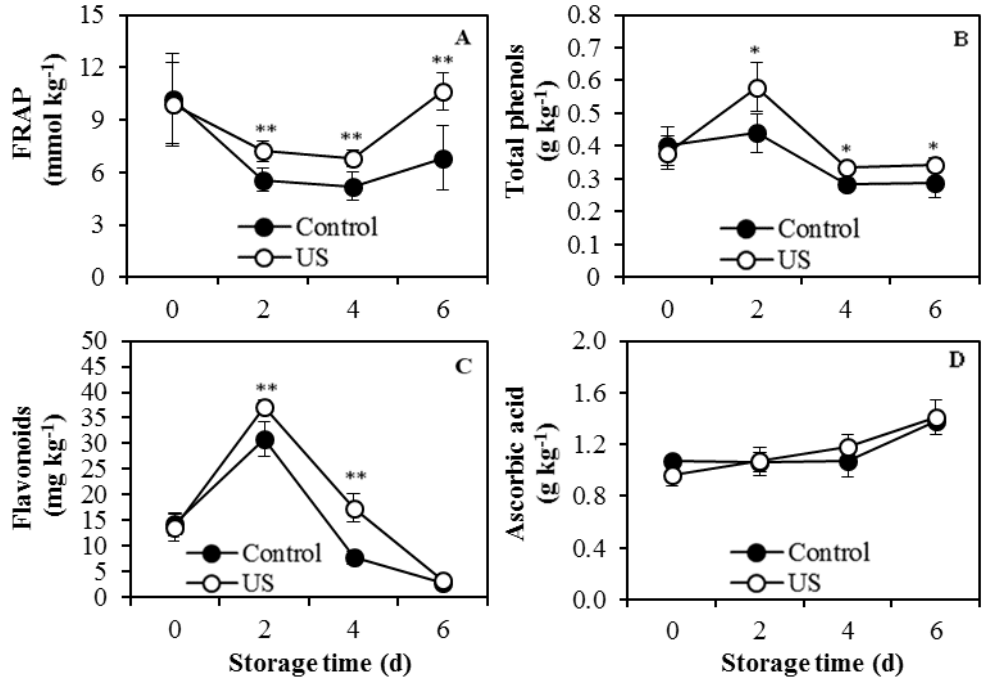

Figure 4. Antioxidant activity (FRAP) (A) and the contents of total phenols (B), flavonoids (C) and ascorbic acid (D) of guava fruit treated without and with US during storage at RT (28±1ºC) for 6 days. Vertical bars represent SD of means. Asterisks indicate the differences between treatments [** ($P < 0.01$), * ($P < 0.05$)].

significantly higher than that of control fruits during storage for the first 4 days of storage ($P < 0.01$) and it then declined and reached to the same level as the control fruits on day 6 of storage. The results indicated that US treatment enhanced antioxidant system and biosynthesis of secondary metabolites such as phenolic compounds and flavonoids contents of guava fruit during storage. It has been recognised that US is claimed as a physical elicitor of plant defence mechanisms [10]. The hydrodynamic cavitation from US creates abiotic stress in plant tissues which stimulates defence-related genes expression and the biosynthesis of secondary metabolites in order to protect against stressors [16]. Wu and Lin [15] and Chen *et al*. [16] proved that US treatment induces defence mechanism by stimulating phenylpropanoid pathway. It is widely recognised that phenylalanine ammonia lyase (PAL) is the key enzyme inducing the pathway. The effect of US treatment at hermetic dosage increases PAL activity and bioactive compounds including phenolic compounds and flavonoids, and this has been reported for tomatoes [11], fresh-cut pineapples [31], table grapes [13], and sweet potato slices [32].

4. Conclusions

The US treatment at the frequency of 40 kHz and the power of 150 w for 10 min could maintain desirable visual appearance, inhibit decay incidence and reduce increased weight loss of 'Kim Ju' guava fruits during storage at RT (28 ± 1 ºC). The US treatment could retard the increment of soluble pectin and the reduction insoluble pectin leading to the retention of fruit texture. Moreover, FRAP and the contents of total phenolic compounds and flavonoids were enhanced by US treatment. However, US treatment had no effect on colour attributes, TSS, TA and ascorbic acid content of the guava fruits. Thus, the US treatment is a potential postharvest

approach maintaining quality and enhancing nutritional values of 'Kim Ju' guava fruits during short term storage at RT.

5. Acknowledgements

We would like to thank Department of Agricultural Education for partial funding support and Asst. Prof. Dr. Chanporn Jaosap for supporting ultrasonicator.

References

[1] Food and Agricultural Organization, 2011. *Food and Agricultural Commodities Production: Guava, Mango, and Mangosteen.* [online] Available at: http://www.faostat.fao.org/site/339/default.aspx.

[2] National Bureau of Agricultural Commodity and Food Standards, 2010. *Guava, the Royal Gazette, 127 Section 147D Special dated 21 December 2010*. [online] Available at: web.acfs.go.th.

[3] Ruzaina, I., Norizzah, A.R., Zahrah, M.S.H., Cheow, C.S., Adi, M.S., Noorakmar, A.W. and Zahid, A.M., 2013. Utilization of palmbased and beeswax coating on the postharvest-life of guava (*Psidium guajava* L.) during ambient and chilled storage. *International Food Research Journal*, 20(1), 265-274.

[4] Supapvanich, S., Mahasap, B., Boonyaritthongchai, P., Techavuthiporn, C., Tepsorn, R. and Youryon, P., 2017. Salicylic acid immersion maintains physiochemical quality and enhances bioactive compounds in 'Kim Ju' guava fruit during cold storage. *Emirates Journal Food and Agriculture*, 29(8), 620-628.

[5] Eliane, B., Angelo, P.J., Ana, L.P., and Ricardo, A.K., 2005. Delay of ripening of 'Pedro Sato' guava with 1-methylcyclopropene. *Postharvest Biology and Technology*, 35, 303-308.

[6] Silip, J.J., 2013. *Quality Characteristics of Guava (Psidium guajava l. cv. kampuchea) in Response to Hydrocooling, Time, Storage, Temperature, and Storage Duration.* MS. University Putra Malaysia, Malaysia.

[7] Supapvanich, S., Kernprie, Y., Boonyaritthongchai, P., Techavuthiporn, C., Tepsorn, R. and Youryon, P., 2019. Physicochemical quality maintenance and bioactive compounds enhancement of Thai guava fruit cv. 'Kim Ju' by using combinative hot water and methyl jasmonate immersion. *Emirates Journal Food and Agriculture*, 31(5), 395-404.

[8] McGuire, R., 1997. Market quality of guavas after hot-water quarantine treatment and application of carnuba wax coating. *HortScience*, 32(2), 271-274.

[9] Goutam, M., Dhaliwal, H. S. and Mahajan, B.V.C., 2010. Effect of pre-harvest calcium sprays on post- harvest life of winter guava (*Psidium guajava* L.). *Journal of Food Science and Technology*, 47(5), 501-506.

[10] Xu, Y., Zhang, L., Zhong, J., Shu, J., Ye, X. and Liu, D., 2013. Power ultrasound for the preservation of postharvest fruits and vegetables. *International Journal of Agricultural and Biological Engineering*, 6(2), 116-125.

[11] Ding, T., Ge, Z., Shi, J., Xu, Y.T. Jones, C.L. and Liu, D.H., 2015. Impact of slightly acid electrolyzed water (SAEW) and ultrasound on microbial loads and quality of fresh fruits. *LWT-Food Science and Technology*, 60, 1195-1199.

[12] Esua, O.J., Chin, N.L., Yusof , Y.A., and Sukon, R., 2019. Effects of simultaneous UV-C radiation and ultrasonic energy postharvest treatment on bioactive compounds and antioxidant activity of tomatoes during storage. *Food Chemistry*, 270, 113-122.

[13] Bal, E., Kok, D. and Torcuk, A.I., 2017. Postharvest putrescine and ultrasound treatments to improve quality and postharvest life of table grapes (*Vitis vinifera* L.) cv. Michele Palieri. *Journal of Central European Agriculture,* 18(3), 598-615.

[14] Ling, C., Xu, J., Shao, S., Wang, L., Jin, P. and Zheng, Y., 2018. Effect of ultrasonic treatment combined with peracetic acid treatment reduces decay and maintains quality in loquat fruit. *Journal of Food Quality*, 2018, https://doi.org/10.1155/2018/7564056

[15] Wu, J. and Lin, L., 2002. Elicitor-like effects of low-energy ultrasound on plant (*Panax ginseng*) cells: induction of plant defense responses and secondary metabolite production. *Applied Microbiology and Biotechnology*, 59, 51-57.

[16] Chen, B., Huang, J., Wang, J. and Huang, L., 2008. Ultrasound effects on the antioxidative defense systems of *Porphyridium cruentum. Colloids and Surfaces B: Biointerfaces*, 61, 88-92.

[17] Wang, B., Zhao, H., Wang, X., Duan, Z., Wang, D. and Akio, S., 2002. Influence of sound stimulation on plasma membrane H^+-ATPase activity. *Colloids and Surfaces B: Biointerfaces*, 25(3), 183-188.

[18] Zhi, H., Liu, Q., Xu, J., Dong, Y., Liu, M. and Zong, W., 2017. Ultrasound enhances calcium absorption of jujube fruit by regulating the cellular calcium distribution and metabolism of cell wall polysaccharides. *Journal of the Science of Food and Agriculture*, 97(15), 5202-5210.

[19] A.O.A.C., 1990. *Official Methods of Analysis of AOAC International.* 16th ed. Washington, DC: Association of Official Analytical Chemists International.

[20] Ahmed, A.R. and Labavitch, J.M., 1978. A simplified method for accurate determination of cell wall uronide content. *Journal of Food Biochemistry*, 1(4), 361-365.

[21] Benzie, I.F.F. and Strain, J.J., 1996. The ferric reducing ability of plasma (FRAP) as a measure of "antioxidant power": The FRAP assay. *Analytical Biochemistry*, 239, 70-76.

[22] Slinkard, K. and Singleton, V.L., 1997. Total phenol analysis: Automation and comparison with manual methods. *American Journal of Enology and Viticulture*, 28, 49-55.

[23] Jia, Z., Tang, M. and Wu, J., 1999. The determination of flavonoid contents in mulberry and their scavenging effects on superoxide radical. *Food Chemistry*, 64, 555-559.

[24] Hashimoto, S. and Yamafuji, K., 2001. The determination of diketo-L-gulonic acid, dehydro-L-ascorbic acid, and L-ascorbic acid in the same tissue extract by 2, 4-dinitrophenol hydrazine method. *The Journal of Biological Chemistry*, 147, 201-208.

[25] Cao, S., Hu, Z. and Pang, B., 2010. Optimization of postharvest ultrasonic treatment of strawberry fruit. *Postharvest Biology and Technology*, 55(3), 150-153.

[26] Joyce, E., Phull, S.S., Lorimer, J.P. and Mason, T.J., 2003. The development and evaluation of ultrasound for the treatment of bacterial suspensions: A study of frequency, power, and sonication time on cultured Bacillus species. *Ultrasonics Sonochemistry*, 10(6), 315-318.

[27] da Silva, J.A.T, and Dobránszki, J., 2014. Sonication and ultrasound: impact on plant growth and development. *Plant Cell, Tissue and Organ Culture*, 117, 131-143.

[28] Lo'ay, A.A. and Taher, M.A., 2018. Influence of edible coatings chitosan/PVP blending with salicylic acid on biochemical fruit skin browning incidence and shelf life of guava fruits cv. 'Banati'. *Scientia Horticulturae*, 235, 424-436.

[29] Nadar, S.S. and Rathod, V.K., 2017. Ultrasound assisted intensification of enzyme activity and its properties: a mini-review. *World Journal of Microbiology and Biotechnology*, 33, 170, https//doi.org/10.1007/s11274-017-2322-6

[30] Lagnika, C., Zhang, M. and Mothibe, K.J., 2013. Effects of ultrasound and high pressure argon on physico-chemical properties of white mushrooms (*Agaricus bisporus*) during postharvest storage. *Postharvest Biology and Technology*, 82, 87-94.

[31] Yeoh, W.K. and Ali, A., 2017. Ultrasound treatment on phenolic metabolism and antioxidant capacity of fresh-cut pineapple during cold storage. *Food Chemistry*, 216 (1), 247-253.

[32] Pan, Y., Chen, L., Pang, L., Chen, X., Jia, X. and Li, X., 2020. Ultrasound treatment inhibits browning and improves antioxidant capacity of fresh-cut sweet potato during cold storage. *RSC Advances*, 10(16), 9193-9202.

Evaluation of Atmospheric PM10 in the Southwest Region of Nigeria

Mohammed Mohammed Ndamitso[1], Yahaya Ahmed Iyaka[1], Aishat Abdulkadir[2] and Francis Olawale Abulude[1,3]*

[1]Department of Chemistry, Federal University of Technology, Minna, Niger State, Nigeria
[2]Department of Geography, Federal University of Technology, Minna, Niger State, Nigeria
[3]Science and Education Development Institute, Akure, Ondo State, Nigeria

Received: 22 March 2020, Revised: 10 August 2020, Accepted: 8 September 2020

Abstract

Particulate matter (PM), according to World Health Organization (WHO), has caused several millions of deaths, and both the young and old have been affected. To mitigate this problem, the compositions of the elements that make up the PM and their sources must be determined. These can provide the necessary information needed by stakeholders to work on. To this end, the study determined the mass concentrations of the PM10 obtained from the Federal University of Technology, Akure (FUTA), National Museum and Monuments and Oba-Ile; for a period of ten months (January-October, 2018). A total of thirty samples was collected. The PM concentration was calculated gravimetrically and the data were subjected to statistical analyses. The results for PM in $\mu g/m^3$ were: FUTA (39.10±0.31-133.22±0.21), Museum (49.71±0.11-196.70±0.01), and Oba-Ile (34.50±0.31-161.30±0.42). The results were well above the WHO standard limits. Air Quality Index (AQI) was calculated for each location, and the results for the air quality in Akure showed that the locations were unhealthy for sensitive groups.

Keywords: particulate matter; AQI; anthropogenic activities; WHO; Akure; Nigeria
DOI 10.14456/cast.2021.20

1. Introduction

Air pollution is a major global issue due to its impact on human health and property [1-4]. Due to urbanization and industrial development, environmental quality has declined throughout the globe in recent times [5, 6]. It is thought that more than 2.4 million individuals die each year globally due to PM pollution issues [4, 7, 8]. According to Ilyas *et al*. [9] and Ndamitso *et al*. [4], PM moves into the lungs when inhaled, and thus has adverse effects that ultimately cause health-related problems such as cancer, asthma, and cardiovascular and respiratory diseases.

It has been confirmed that PM in Europe is a pollutant and has surpassed the recommended normal limits [10, 11]. Schweizer *et al*. [12] mention that PM is a complex mixture of chemical

*Corresponding author: Tel: +2348034458674
Email: walefut@gmail.com

species from anthropogenic and natural emission sources and from secondary pollutants which form in the atmosphere. In particular, in developing nations, rapid urbanization and population growth are part of the causes of the world-wide PM issue. This statement was verified by Arnfield [13], who indicated that by 2025, more than 45% of the population will live in metropolitan towns around the globe. Balogun *et al*. [14] and Owoeye and Ibitoye [15] revealed that city migration could have risen to over 30 billion over the next 30 years. A town established in 1976, Akure is no exception. Its population has been estimated at 476,159 by the National Population Commission [16] since its founding, the population, business, industrial, farming and petroleum products (bitumen) have increased which may have an impact on particulate matter and other anthropogenic pollutants.

In Akure, Nigeria, several road constructions, farming, industrial activities, and heavy traffic have been on the increase during the past years. In these areas, no doubt, metals, gas particles, and dust are transported by wind or runoff waters. Often these particles can cause negative effects on man and buildings. To this effect, it is essential to characterize the distributions and concentrations of these metals and atmospheric deposits in the environment especially air and aquatic. This research evaluates the concentration of particulate matter (PM10) obtained in Akure, Ondo State, Nigeria.

2. Materials and Methods

Three different locations [National Museum and Monuments (005 11 40.2 E, 07 15 11.6 N), Oba-Ile (005 14 29.1 E, 07 16 04.4 N), and Federal University of Technology-FUTA (005 08 06.5 E, 07 18 07.6 N)] were selected for the sampling within the town (Figure 1). These locations represent commercial, residential, and educational settings respectively. Samplings took place once every month from 8 am to 4 pm (8 h) for 10 months (January to October 2018) using a "Gent" stacked filter unit. The PM10 were filtered through quartz filters (47mm) and kept in a desiccator at room temperature. By the end of the sampling period, thirty samples (ten per sampling area) were collected monthly. The filters were put in a chamber kept at 20^{o}C, and 35% relative humidity (RH) for 48 h to stabilize the weight. The particulate mass was determined gravimetrically (the difference of filter's weight before and after sampling) using an analytical balance (0.001mg) (Model Sartorius Microbalance ME 5 Balance).

The PM mass concentration was calculated based on these parameters:

The average flow rate = averaging flow rate at the beginning and end of 8 h sampling (1)

Average PM mass concentration ($\mu g/m^3$) = Mass/total volume (2)

The data obtained from the study data were extrapolated and scaled up to 24 h mean before computing the air quality index. The AQI (Air quality index) for the particulate matter was calculated by using the equation given by Osimobi *et al*. [17].

$$AQI = \left[\frac{AQI_{max}-AQI_{min}}{PM_{max}-PM_{min}}\ x\ (PM_{meas}-PM_{min})\right] + AQI_{min} \quad (3)$$

Where:

PM_{meas} is the 24 h measured average concentration of particulate matter ($\mu g/m^3$),
PM_{max} is the maximum concentration AQI color category containing PM_{meas}
PM_{min} is the minimum concentration of AQI color category containing PM_{meas}
AQI_{max} is the maximum AQI value for color category corresponding to PM_{meas}
AQI_{min} is the minimum AQI value for color category corresponding to PM_{meas}

The results were statistically analyzed using Minitab 16 Statistical Software.

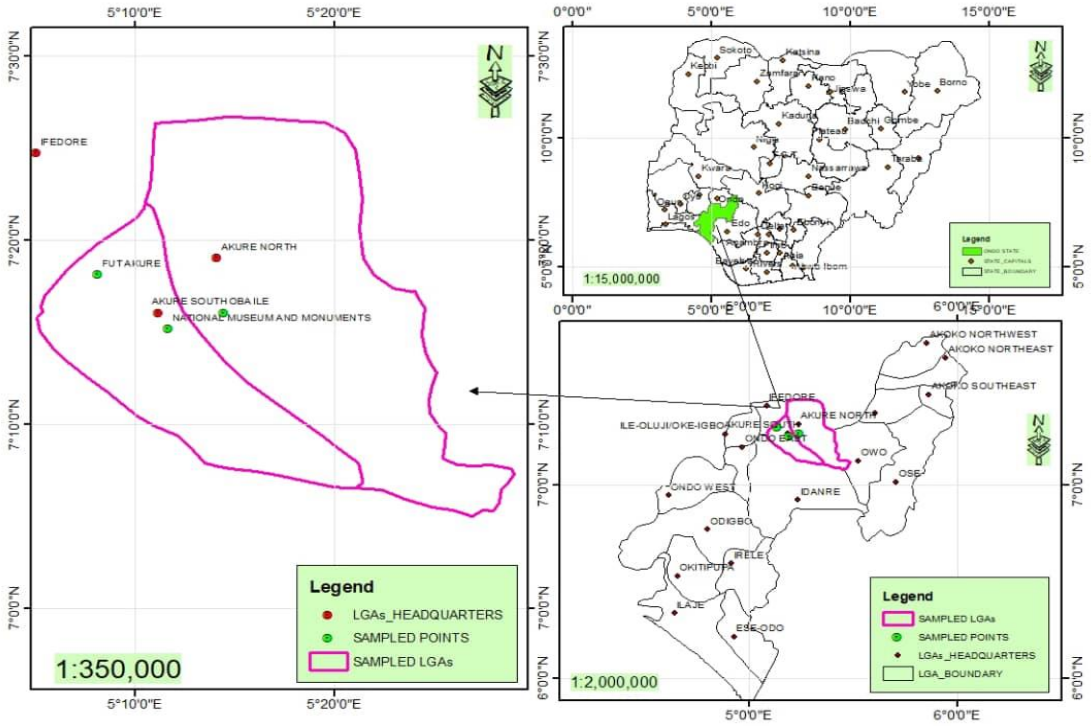

Figure 1. Map of the sampling points

3. Results and Discussion

Table 1 depicts a summary of the statistical results of the PM collected and analyzed in this study. The PM ranged between 39.10 and 133.20 (FUTA), 49.70 and 196.70 (Museum), and 34.50 and 161.30 (Oba-Ile) with mean values of 100.50, 125.20, and 112.80 µg/m^3 respectively. The Standard Error (SE) and Standard Deviation (SD) range were 10.9, 13.1 and 10.4 and 34.3, 41.3 and 33.0, while the Coefficient of Variation in percent (CV%) range was 34.17, 33.02, and 29.25, for FUTA, Museum, and Oba-Ile, respectively. The Skewness and Kurtosis gave -0.98, -0.01, -1.29 and -0.65, 0.68, and 3.80 for FUTA, Museum, and Oba-Ile, respectively. From Table 1, it could be deduced that the low standard error showed that the variability in the PM values was low during the sampling periods, while the CV (%) showed moderate variability. The variations could be due to the variations from the different months of sampling. The coefficients of variation of the PMs show that there was not much variation with locations, but the variance depicts high values due to the differences (variations) in the values obtained in each location as shown in the minimum and maximum values from each location.

The highest PM concentration occurred during the summer months when there was high temperature, solar radiation, low humidity and low wind speed. The most polluted months were April and October, which could have been due to the harsh weather conditions and high secondary transformations, as noted by Wang *et al*. [18]. The former could have been due to emissions from traffic and also agricultural burning during the April land as part of the preparation towards planting season, while the latter could have been due to the October harvest season [1]. The high PM values

Table 1. Summary of the statistical results of PM (particulate matter) (μg/m^3) measured during January to October 2018

	FUTA	**Museum**	**Oba Ile**
January	68.39	174.69	144.11
February	39.06	85.42	108.80
March	119.47	49.69	34.48
April	52.08	196.67	161.30
May	115.94	114.22	108.49
June	106.88	124.27	115.73
July	131.35	133.86	127.55
August	112.40	118.07	112.69
September	133.23	115.73	104.43
October	126.20	139.48	110.83
Mean	100.50	125.20	112.80
SE	10.90	13.10	10.40
SD	34.30	41.30	33.00
CV (%)	34.17	33.02	29.25
Min	39.10	49.70	34.50
Max.	133.20	196.70	161.30
Q1	64.30	107.00	107.50
Q3	127.50	148.30	131.70
Skewness	-0.98	-0.01	-1.29
Kurtosis	-0.65	0.68	3.80

obtained in the Museum area could have been a result of the accumulation of re-entrained and re-suspended dust resulting from vehicular emissions (low, medium and high) and unpaved terrain activities. The variations in the emissions, meteorological conditions, type of long-distance transport and secondary production are associated with the pollution levels in different seasons [19-21].

According to US. EPA [22], the air quality index of PM is categorized into good, moderate, unhealthy for sensitive groups, unhealthy, very healthy, and hazardous categories. The results were compared with this index and the results whose values were above 50 AQI range were grouped under the 'Moderate' and 'Unhealthy' groups while those with values less than this were classified as "Good" (Table 2). The average AQI in January through October of the three locations in Akure were 126.17, 131.34, and 138.96 (museum, Oba-Ile, and FUTA, respectively). All the locations were categorized as 'unhealthy for sensitive groups'. The health-related problem of PM is linked to particle sizes and particularly PM_{10} [21]. The PM deposits considered in this study were PM10, which was found in reasonable quantities in the sampling locations of this study and formed the basis of the classifications given in this study.

The values recorded in all the locations were more than 100 μg/m^3 recommended by India's Central Pollution Control Board [23], and more than three times greater than the European limit [24]. Our results (minimum-maximum values) were compared with other authors - Greilinger *et al*. [25] reported between10 and 45 μg/m^3 for Masemberg and from 20 to above 60 μg/m^3 for Bockberg, Austria; Mehta [26] gave 3.19 and 152.88 μg/m^3, for Ahmedabad, India; Abe and Miraglia [27] put that of São Paulo, Brazil to be 8 - 131 μg/m^3, and the Eastern part of Nigeria (14-504 μg/m^3) by Osimobi *et al*. [17]; Contini *et al*. [28] reported of South-Eastern Italy as 5.6 - 127.8 μg/m^3. It was observed that the minimum values from our study were higher than those reported by

Table 2. Air quality index of the selected sampling locations

Sampling Locations	Air Quality Index Categories					
	0-50 (Good)	**51-100 (Moderate)**	**101-150 (Unhealthy for sensitive groups)**	**151-200 (Unhealthy)**	**201-300 (Very Unhealthy)**	**>301 (Hazardous)**
FUTA	-	-	138.94	-	-	-
Museum	-	-	126.17	-	-	-
Oba-Ile	-	-	131.34	-	-	-

these authors. It is worthy of note that the maximum results obtained by Mehta [26] for Ahmedabad, India, and Osimobi *et al*. [17] were higher than ours. Also, the maximum results reported in this study, however, were lower than 109.60 ± 10.83 - 453.45 ± 62.92 µg/m^3 reported by Mandal *et al.* [29] for Delhi's industrial region and 584.8 µg/m^3 by Jain *et al*. [30] in Delhi, India. The variations between these results and those of others could be due to the climatic conditions of the areas, the methodology used and the natural and anthropogenic activities of the different locations. Also, the differences could be due to the differences in the weather conditions (temperature, humidity, and air exchange rates) [31].

The locational contributions of the PM to the total amount obtained in the study are shown in Figure 2. It could be noted that Oba-Ile, a residential area contributed 47% to the PM as against 36% (Museum) and 17% (FUTA) in February. The reason for the high contribution by Oba-Ile could have been the result of traffic diversion to this sampling location as a result of an accident that occurred on the Akure-Owo expressway during the sampling period. This increase in anthropogenic activities might have contributed immensely to the increase observed in the PM10 deposit of the said area during the said period (February). Likewise, the elevations in FUTA PM10 results could have been due to the waste dumps around the vicinity and also the on-going renovation activities of a lecture theater besides the sampling area [31].

4. Conclusions

To conclude, the evaluation of PM in this study shows that the concentrations were high. The results were well above the WHO standard limits. The highest value was obtained within the Museum vicinity, which could have been due to anthropogenic (dust, soil, traffic, and commercial) activities. The results, when compared with International Air Quality Index, indicate that the PM quality in Akure is unhealthy for sensitive groups. Constant monitoring of the vicinities is recommended.

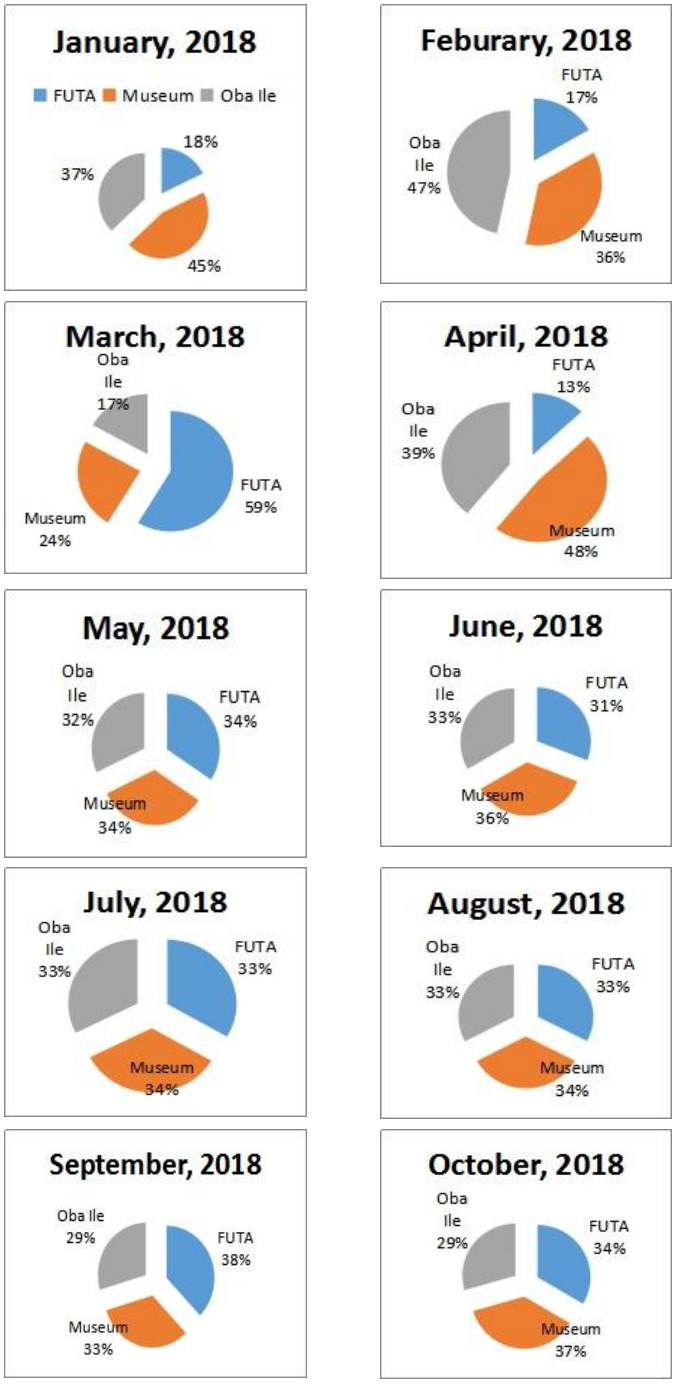

Figure 2. Distribution of PM_{10} in the locations (January-October, 2018)

5. Acknowledgements

The authors are grateful to the curator of the National Museum Commission, Akure, the Dean of Faculty of Science, Federal University of Technology, Akure (FUTA) for the permission granted to use their premises for sample collections and Mr. Edah Sunday, Department of Geography, Federal University of Technology, Minna, Niger State, Nigeria for drawing the maps.

References

[1] Zhang, J., Cheng, M., Ji, D., Liu, Z., Hu, B., Sun, Y. and Wang, Y.S., 2016. Characterization of submicron particles during biomass burning and coal combustion periods in Beijing, China. *Science and Total Environment*, 562, 812-821.

[2] Tuankrua, V., Tongdeenog, P., Tangtham, N., Aungsuratana, P. and Witthawatchuetikul, P., 2014. Assessment of aerosol-cloud-rainfall interactions in Northern Thailand. *Proceedings of the International Academy of Ecology and Environmental Sciences*, 4(4), 134-147.

[3] Zhao, L., Hu, G., Yan, Y., Yu, J., Wang, X. and Yan, Y., 2019. Source apportionment of heavy metals in urban road dust in a continental city of eastern China: Using Pb and Sr isotopes combined with multivariate statistical analysis. *Atmospheric Environment*, 201, 201-211.

[4] Ndamitso, M.M., Abdulkadir, A. and Abulude, F.O. 2016. Source apportionment: Case studies of selected African countries. *International Journal of Advancements in Research and Technology*, 5(3), 1-25.

[5] Wang, Q., Kwan, M., Zhou, K., Fan, J., Wang, Y. and Zhang, D., 2019. The impacts of urbanization on fine particulate matter ($PM_{2.5}$) concentrations: Empirical evidence from 135 countries worldwide. *Environmental Pollution*, 247, 989-998.

[6] Latif, M.T., Azmi, S.Z., Noor, A.D.M., Ismail, A.S., Johny, Z., Idris, S., Mohamed, A.F. and Mokhtar, M., 2011. The impact of urban growth on regional air quality surrounding the Langat river basin, Malaysia. *Environmentalist*, 31, 315-324.

[7] WHO, 2012. *World Health Report-Reducing Risk, Promoting a Healthy Life*. Geneva: World Health Organization.

[8] Yun, G., He, Y., Jiang, Y., Dou, P. and Dai, S., 2019. $PM_{2.5}$ Spatiotemporal Evolution and Drivers in the Yangtze River Delta between 2005 and 2015. *Atmosphere*, 10, 55, https://doi.org/10.3390/atmos10020055.

[9] Ilyas, S.Z., Khattak, A.I., Nasir S.M., Qurashi T. and Durrani R., 2009. Air pollution assessment in urban areas and its impact on human health in the city of Quetta, Pakistan. *Clean Technologies and Environmental Policy*,12(3), 291-299.

[10] Harrison, R.M. and Yin, J., 2008. Sources and processes affecting carbonaceous aerosol in central England. *Atmospheric Environment*, 42, 1413-1423.

[11] Farao, C., Caneparis, S., Perrino, C. and Harrison, R.M., 2014. Sources of PM in an industrial area: Comparison between receptor model results and semi empirical calculations of source contributions. *Aerosol and Air Quality Research*, 14, 1558-1572.

[12] Schweizer, D., Cisneros, R. and Buhler, M., 2019. Coarse and fine particulate matter components of wildland fire smoke at Devils Postpile National Monument, California, USA. *Aerosol and Air Quality Research*, 19, 1463-1470.

[13] Arnfield, A.J., 2003. Two decades of urban climate research: a review of turbulence, exchanges of energy and water, and the urban heat island. *International Journal of Climatology*, 23(1), 1-26.

[14] Balogun, I.A., Adeyewa, D.Z., Balogun, A.A. and Morakinyo, T.E., 2011. Analysis of urban expansion and land use changes in Akure, Nigeria using RS and GIS techniques. *Journal of Geography and Regional Planning*, 4(9), 533-541.

[15] Owoeye, J.O. and Ibitoye, O.A., 2016. Analysis of Akure Urban land use change detection from remote imagery perspective. *Urban Studies Research*, 2016, http://dx.doi.org/10.1155/2016/4673019

[16] National Population Commission (NPC). 2006. *The 1963, 1991 and 2006 Population Census Reports*. Abuja: National Population Commission.

[17] Osimobi, O.J., Yorkor, B. and Nwankwo, C.A., 2019. Evaluation of daily pollutant standard index and air quality index in a university campus in Nigeria using PM10 and PM2.5 particulate matter. *Journal of Science, Technology and Environment Informatics*, 7(2), 517-532.

[18] Wang, L., Li, W., Sun, Y., Tao, M., Xin, J., Song, T., Li, X., Zhang, N., Ying, K. and Wang, Y., 2018. $PM_{2.5}$ characteristics and regional transport contribution in five cities in Southern North China Plain, during 2013-2015. *Atmosphere*, 9(157), https://doi.org/10.3390/atmos 9040157

[19] Jia, M., Zhao, T., Cheng, X., Gong, S., Zhang, X., Tang, L., Liu, D., Wu, X., Wang, L. and Chen, Y., 2017. Inverse relations of $PM_{2.5}$ and O_3 in air compound pollution between cold and hot seasons over an urban area of east China. *Atmosphere*, 8(3) , 59, https://doi.org/10.3390/ atmos8030059

[20] Abulude, F.O., Ndamitso, M.M., Iyaka, Y.A. and Abdulkadir, A., 2018. Study of particulate matter of Akure, Nigeria using a sharp-cut inertial filter combined with an impactor-a preliminary study. *Journal of Atmospheric and Solar-Terrestrial Physics*, 179, 396-404.

[21] Liu, H., Scneider, P., Haugen, R. and Vogt, M., 2019. Performance assessment of a low-cost $PM_{2.5}$ sensor for a near four-month period in Oslo, Norway. *Atmosphere*, 10(41), https://doi.org/10.3390/atmos10020041

[22] US. EPA, 2009. *Patient Exposure and the Air Quality Index. Particle Pollution and Your Patients' Health.* [online] Available at: https://www.epa.gov/pmcourse/patient-exposure-and-air-quality-index#what

[23] CPCB, 2008. *Stationary Sources Emission Profiles. Central Pollution Control Board, New Delhi, India*. [online] Available at: http://cpcb.nic.in/Stationary_Sources_Emission_Profiles.xls.

[24] EEA (European Environment Agency), 2014. *Air Quality in Europe-2014 Report*. Copenhagen: European Environment Agency.

[25] Greilinger, M., Zbira, J. and Kasper-Giebl, A., 2019. Desert dust contribution to PM10 loads in Styria (Southern Austria) and impact on exceedance of limit values from 2013-2018. *Applied Sciences*, 9(11), 2265, https://doi.org/10.3390/app9112265

[26] Mehta, U., 2020. Statistical analysis of suspended and respirable suspended particulate matter (PM_{10} and $PM_{2.5}$) concentrations in urban region of Ahmedabad, India. *International Journal of Science and Research*, 9(2), 605-609.

[27] Abe, K.C. and Miraglia, S.G.E.K. 2016. Health impact assessment of air pollution in São Paulo, Brazil. *International Journal of Environmental Research and Public Health*, 13(7), 694, https://doi.org/10.3390/ijerph13070694

[28] Contini, D., Cesari, D., Donateo, A., Chirizzi, D. and Belosi, F., 2014. Characterization of PM10 and PM2.5 and their metals content in different typologies of sites in South-Eastern Italy. *Atmosphere*, 5(2), 435-453.

[29] Mandal, P., Saud, T., Sarkar, R., Mandal, A., Sharma, S.K., Mandal, T.K. and Bassin, J.K., 2014. High seasonal variation of atmospheric C and particle concentrations in Delhi, India. *Environmental Chemistry Letters*, 12(1), 225-230.

[30] Jain, S., Sharma, S.K., Mandal, T.K. and Saxena. M., 2018. Source apportionment of PM_{10} in Delhi, India using PCA/APCS, UNMIX, and PMF. *Particuology*, 37, 107-118.

[31] Kulashrestha, A., Massey, D.D., Masih, J. and Taneja, A., 2014. Source characterization of trace elements in an indoor environment at urban, rural and wayside sites in a semi-arid region of India. *Aerosol and Air Quality Research*, 14, 1738-1751.

Current Applied Science and Technology Vol. 21 No. 2 (April-June 2021)

Designing of Optimal Required Sample Sizes for Double Acceptance Sampling Plans under the Zero-Inflated Defective Data

Pramote Charongrattanasakul[1] and Wimonmas Bamrungsetthapong[2]*

[1]Division of Mathematics, Faculty of Science and Technology, Rajamangala University of Technology Krungthep, Bangkok, Thailand
[2]Division of Applied Statistics, Faculty of Science and Technology, Rajamangala University of Technology Thanyaburi, Pathumthani, Thailand

Received: 9 May 2020, Revsied: 3 August 2020, Accepted: 16 September 2020

Abstract

This research proposes an optimal double acceptance sampling plan (DSP) for manufacturing that is affected by zero-inflated data. Suppose that the number of defective items for sample inspection is considered to be under Zero-inflated Poisson (ZIP) distribution. A multi-objective optimization using Genetic Algorithm is applied to calculate the optimal parameters $(n_1, n_2, c_1, c_2)^*$ of the proposed DSP, which is concerned with maximizing the probability of acceptance sampling plan (P_a) and minimizing the total cost of inspection (TC) and the average number of samples(ASN)simultaneously. The optimal solution was focused on the design of the required sample sizes (n_1, n_2) based on three different scenarios. The results showed that the first sample and the second sample should be equal $(n_1 = n_2)$. Moreover, it was found that the probability of extra zeros $(\emptyset)$ under the ZIP distribution affects the required sample sizes and the performance of the proposed DSP. Illustrations for selecting the optimal parameters of the proposed DSP are also provided. Real data with excess zero is used to illustrate the application of the proposed DSP.

Keywords: double acceptance sampling plan; zero-inflated poisson distribution; probability of extra zeros; probability of acceptance sampling plan; Genetic Algorithm; multi-objective optimization
DOI 10.14456/cast.2021.21

1. Introduction

One important tool in the product control technique is an acceptance sampling plan (ASP). An ASP is applied in many areas to inspect the quality of items such as raw materials, some partial products of the production process, and finished products. This technique helps consumers decide whether to accept or reject a product that is produced by manufacturers based on sampling results selected from a lot. Users can decide to choose the minimum sample size from a sampling plan to achieve the acceptance criteria or the rejection criteria for that lot. Dodge and Romig's tables are widely used to

*Corresponding author: Tel.: (+66) 2549-4137 Fax(+66) 2549-4138
E-mail: wimonmas_b@rmutt.ac.th

decide on a sampling plan in which users know the lot size, percent nonconformance of the lot, producer's risk, and consumer's risk for the production process [1]. In practice, if some necessary values are unknown, then they cannot choose the optimal ASP. This problem can affect the total cost of the inspection. Recently, many researchers have studied the determination of optimal ASP model using optimization techniques as follows. Duarte and Saraiva [2] proposed a method to find the optimal value of the ASP model. The objective function was used to find the lowest value of error for the probability of accepting the ASP model for single and double sampling plans that corresponded to the sample size and the acceptable number. Kaya [3] applied a Genetic Algorithm (GA) to determine the sample size of the attribute control chart for a multi-state process. The objective function used to find the minimum cost and the maximum probability of accepting the model was found. Kobilinsky and Bertheau [4] presented a cost function for the inspection process that depended on the number of inspection groups and sample sizes for single and double ASPs based on the manufacturer's risk and the consumer's risk. Cheng and Chen [5] applied the GA methods to design a DSP. These models increased the efficiency of the design ASP and reduced errors that impacted on the manufacturer's risk and consumer's risk. Moreover, GA methods were applied to find the best information more efficiently and more accurately. Sampath and Deepa [6] designed a DSP by applying the GA methods to determine the optimal sample size and acceptance number under the manufacturer's risk and the consumer's risk. Braimah *et al*. [7] evaluated the optimal value of a mathematical model to determine the sample size and the random range for the ASP. It was found that the condition of these models provided an acceptance number equal to zero.

In addition, some researchers have studied the economic aspects of various ASPs. Hsu and Hsu [8] studied the cost aspects of a single ASP in order to evaluate the minimum cost that was appropriate for both manufacturers and consumers. Results showed that the proposed cost model was used to inspect a group of defective items. Fallahnezhad and Aslam [9] designed an economic model of the ASPs that involved Bayesian inference in which a decision was taken depending on the proposed model. Fallahnezhad and Qazvini [10] designed a new economic model of the ASP in a two-stage approach based on the Maxima Nomination Sampling (MNS) technique. Fallahnezhad *et al*. [11] presented an ASP based on the MNS method with current inspection errors. An economical model was proposed in terms of inspection errors and clarified the impact of errors from an economic point of view.

Currently, most production processes have excellent quality control. It was found that when the production process was well inspected, zero defects were more often discovered in sample inspections. For this reason, some researchers presented the idea that a zero-inflated Poisson (ZIP) distribution was appropriate for the probability distribution of the number of defects. A ZIP distribution was presented by Lambert [12], McLachlan and Peel [13]. It was a special type of mixed distribution that degenerated at zero and yet was a Poisson distribution. The ZIP distribution was applied in many disciplines such as manufacturing, public health, epidemiology, medicine, etc. Recently, many researchers developed ASPs with ZIP distributions. Loganathan and Shalini [14] considered a single sampling plans (SSP) in which the number of defective items was a ZIP distribution. The optimal plan parameters were calculated using unity values. Uma and Ramya [15] presented a Quick Switching System (QSS) that fell under a ZIP distribution. Rao and Aslam [16] designed resubmitted lots plan in which the number of defects was a ZIP distribution. The parameters of the proposed sampling plan were considered based on nonlinear optimization solutions. A nonlinear optimization is used to determine the optimal plan parameters of the proposed sampling plan. Wang and Hailemariam [17] proposed a repetitive group sampling (RGS) and multiple dependent state (MDS) sampling under a ZIP distribution. Moreover, they developed DSP and sequential sampling plans for the ZIP distribution. The unity value approach was applied to determine the optimal plan parameters of the proposed sampling plans.

The above-mentioned research showed that the production process was well inspected, the zero defects were more discovered in sample inspections. Three important objectives that the

manufacturer expected to achieve from an optimal ASP: the lowest cost, the smallest ASN, and the highest probability of acceptance. From this idea, a multi-objective optimization is used to find the optimal DSP under the proposed process. Furthermore, GA is one of the most popular methods used to find the optimal value that provides the best answer to the problem and is flexible enough to solve complex problems, like those which are developed for genetic processes [18]. Many researchers indicate that GA can be used to resolve the problem of optimizing in ASP [3, 5, 6].

The aim of this research is to design the sample sizes required to achieve an optimal DSP with zero-inflated defective data. The optimal parameters for DSP under the ZIP distribution (DSP_{ZIP}) are calculated to maximize the P_a and minimize the TC and ASN simultaneously (multi-objective function). The MATLAB software (R2019b) [19] is used to provide a simulation study of the GA with multi-objective optimization. Additionally, we focus on studying the relationship between the required sample sizes and the economic models of the proposed ASP because, in practice, smaller value of required sample sizes or ASN are more satisfactory for designing an optimal ASP. Therefore, an economic model of DSP_{ZIP} under multi-objective optimization is also considered based on three different scenarios that compare the size of the first sample (n_1) and the second sample (n_2). In illustrations, the ratio of sample size, the different scenarios of the required sample sizes, and the optimal OC function of the DSP_{ZIP} are presented. Real data example were applied to determine the optimal plan parameters under proposed DSP_{ZIP}.

2. Materials and Methods

Currently, the number of defective items for many samples will be zero when most production processes have excellent quality control, and the production process is well inspected. In this situation, the proper probability distribution function of the number of defective items for sample inspection is the Zero-Inflated (ZI) distribution.

The ZI distribution is a mixture of a process that generates zeros and the other processes that are a counted distribution under non-negative integers. Suppose X is a random variable under the ZI distribution, then the probability mass function (pmf) of X is given by

$$P(X = x|\emptyset, \Theta) = \emptyset f(x) + (1 - \emptyset) g(x;\ \Theta) \tag{1}$$

where
$$f(x) = \begin{cases} 1, & x = 0 \\ 0, & x = 1,2,3, \ldots \end{cases} \tag{2}$$

Let $\emptyset$ be a zero-inflation parameter, such that $0 < \emptyset < 1$, and $g(x;\ \Theta)$ is the pmf of X with a vector of the parameter, $\Theta = \{\theta_1, \theta_2, \ldots, \theta_n\}$.

Now, we consider a zero-inflated count model corresponding to the Poisson Binomial distribution, called zero-inflated Poisson (ZIP) distribution. Lambert [11], McLachlan and Peel [12] proposed the ZIP distribution, which is a special type of of mix of the Bernoulli distribution and Poisson distributions. From the pmf of Poisson distribution is given as $g(x;\ \lambda) = \frac{e^{-\lambda}\lambda^x}{x!};\ x = 0,1,2, \ldots,$ and substituting in eq.(1), then the pmf of ZIP distribution has the form

$$P(X = x|\emptyset, \lambda) = \begin{cases} \emptyset + (1 - \emptyset)e^{-\lambda}, & x = 0 \\ (1 - \emptyset)\frac{e^{-\lambda}\lambda^x}{x!}, & x = 1,2, \ldots, \end{cases} \tag{3}$$

where $\lambda = np, \lambda > 0, 0 < \emptyset < 1$. Furthermore, the mean and the variance of the ZIP distribution are given by $\mu_{ZIP} = (1 - \emptyset)\lambda$ and $\sigma^2_{ZIP} = \lambda(1 - \emptyset)(1 - \lambda\emptyset)$ respectively.

2.1 Design of the double acceptance sampling plan under ZIP distribution

The double acceptance sampling plan (DSP) requires the specification of four quantities which are known as its parameters. These parameters are n_1, c_1, n_2 and c_2. In a DSP, the decision of accepting or rejecting a lot is taken based on two samples.

1. The first sample: the lot is accepted if the number of defective units (d_1) in the first sample is less than the acceptance number c_1.

2. The second sample: the lot is accepted if the number of defective units $(d_1 + d_2)$ in both samples is greater than c_1 and less than or equal to the acceptance number c_2.

Therefore, if P_a^1 and P_a^2 denote the probabilities of accepting a lot on the first sample and the second sample, as shown in eq.(4) and eq.(5), respectively, then the probability of accepting a lot (P_a) of p is given by equation (6).

$$P_a^1(p) = P(d_1 \le c_1 : n_1) \tag{4}$$

$$P_a^2(p) = P(c_1 < d_1 \le c_2 : n_1) \times P(d_1 + d_2 \le c_2 : n_2) \tag{5}$$

$$P_a(p) = P_a^1(p) + P_a^2(p) \tag{6}$$

In this section, the optimal DSP under the ZIP distribution (DSP_{ZIP}) is described. From eq.(3) and eq.(6), the probability of accepting a lot for ZIP distribution is given in eq.(7).

$$\begin{aligned} P_a(p) = {} & \emptyset + (1-\emptyset)e^{-\lambda_1} \\ & + \sum_{d_1=1}^{c_1} (1-\emptyset)\frac{e^{-\lambda_1}{\lambda_1}^{d_1}}{d_1!} \\ & + \sum_{d_1=c_1+1}^{c_2} \left\{ \left[(1-\emptyset)\frac{e^{-\lambda_1}{\lambda_1}^{d_1}}{d_1!} \right] \times \left[\emptyset + (1-\emptyset)e^{-\lambda_2} + \sum_{d_2=1}^{c_2-d_1} (1-\emptyset)\frac{e^{-\lambda_2}{\lambda_2}^{d_2}}{d_2!} \right] \right\} \end{aligned} \tag{7}$$

Moreover, the average sample number function (ASN) of the DSP_{ZIP} is given in eq. (8).

$$\begin{aligned} ASN &= n_1 + n_2(1 - P_I) \\ &= n_1 + n_2 \textstyle\sum_{d_1=c_1+1}^{c_2} (1-\emptyset)\frac{e^{-\lambda_1}{\lambda_1}^{d_1}}{d_1!} \end{aligned} \tag{8}$$

where P_I is the probability of deciding on the acceptance or rejection of the lot on the first sample and is given by $P_I = P(d_1 \le c_1 : n_1) + P(d_1 > c_2 : n_1)$.

2.2 Total cost function of DSP

In this section, the total cost function of the product inspection of a lot for the DSP plan under ZI distribution is discussed. In this research, three different types of costs are considered: cost of inspection per lot, cost of internal failure per lot, and cost of an outgoing defective per lot, as presented in eq. (9).

$$\begin{aligned} TC = {} & C_I\left(n_1 P_a^1(p) + (n_1+n_2)P_a^2(p) + N\big(1 - P_a(p)\big)\right) \\ & + C_F\left((n_1+n_2)p + \big(1-P_a(p)\big)\big(N-(n_1+n_2)\big)p\right) \\ & + C_O\big(P_a(p)\big(N-(n_1+n_2)\big)p\big). \end{aligned} \tag{9}$$

where C_I is the cost of inspection per unit, C_F is the cost of the internal failure per unit, and C_O is the cost of an outgoing defective per unit.The component of the total cost function for the inspection of a lot for the DSP under the ZIP distribution can be expressed as follows:

First- term denotes the cost of inspection per lot, where $n_1 P_a^1(p) + (n_1 + n_2)P_a^2(p) + N\big(1 - P_a(p)\big)$ represents the expected number of units inspected per lot.
Second- term denotes the cost of the internal failure per lot, where $(n_1 + n_2)p + \big(1 - P_a(p)\big)\big(N - (n_1 + n_2)\big)p$ represents the expected number of defective items detected per lot.
Third- term denotes the cost of an outgoing defective per lot, where $P_a(p)\big(N - (n_1 + n_2)\big)p$ represents the expected number of defective items not detected per lot.

3. Results and Discussion

In this section, the optimal parameters of the DSP_{ZIP} are calculated to achieve the minimum value of TC and ASN when the maximum probability of accepting a lot is received. The MATLAB software (R2019b) is used to perform a simulation study of the GA with multi-objective optimization. In the optimal solution of DSP_{ZIP}, the minimum of the TC and ASN is calculated by considering the optimal values of n_1, n_2, c_1 and c_2. The constraints of the producer's risk (α) and the consumer's risk (β) are satisfied immediately by the provision of the acceptable quality level (AQL) and the lot tolerance percent defective $(LTPD)$. In practice, the constraints of α and β are satisfied immediately when AQL and $LTPD$ are provided. For the effectiveness of the proposed sampling plan, two points $(AQL, 1 - \alpha)$ and $(LTPD, \beta)$ are considered for changes on the OC curve. A manufacturer intends that the probability of acceptance of a lot of items should be greater than $1 - \alpha$ at the quality level of AQL. In reality, a customer requests that the probability of the lot acceptance should be less than β at $LTPD$. In the optimization technique, the optimal solution is considered on three objective functions simultaneously.

Multi-objective function

Minimize TC and ASN (10)
Maximize $P_a(p)$ (11)

Subject to: $P_a(AQL) \geq 1 - \alpha$ and $P_a(LTPD) \leq \beta$,
$n_1 + n_2 \leq \delta N, n_1 > 0, n_2 > 0$,
$c_1 \geq 0, c_2 > 0$ and $c_2 > c_1 \geq 0$.

The following input parameters are used to design the proposed illustrations. Some input parameters are assigned the same values for the proposed illustrations, that is the lot size $N = 1{,}000$, the proportion of sample size from lot size $\delta = (0.10, 0.20)$, the producer's risk $\alpha = 0.05$, and the consumer's risk $\beta = 0.01$. Furthermore, the input parameters of the cost function are given [8]: $C_I = 1, C_F = 2$, and $C_O = 10$, respectively. Some input parameters are assigned the different values for each sample illustrations as shown in Table 1, that is, the proportion of defective (p), the zero- inflation parameter $(\emptyset)$, the acceptable quality level (AQL), and the lot tolerance percent defective $(LTPD)$. Most studies presented a comparison between different values of AQL and $LTPD$ used to find the optimal ASP [4-11, 15-17].

Table 1. Input parameters used to design the proposed illustrations

Input parameter	Illustration 1	Illustration 2	Illustration 3
p	0.01	0.05	0 to 0.20
$\emptyset$	0.001,0.01,0.05,0.10	0.01,0.05,0.10,0.20,0.30, 0.40, 0.50	0.01,0.05,0.10
AQL	0.01,0.05	0.05	0.05
$LTPD$	0.05,0.075,0.10	0.10	0.10

3.1 Illustration 1: The three conditions of the ratio of sample size

From eq.(8) and eq.(9), we can see that the values of TC and ASN of the DSP_{ZIP} depend on the required sample sizes (n_1, n_2). Therefore, in this illustration, the sensitivity analysis of the required sample sizes (n_1, n_2) is considered based on two constraints of the proportion of sample size from lot size (δ) by assigned that $\delta = 0.10\ (n_1 + n_2 \leq 100)$, and $\delta = 0.20\ (n_1 + n_2 \leq 200)$, respectively.

Moreover, the ratio of sample size, $r = \frac{n_1}{n_2}$, is used to measure of discrimination of the DSP_{ZIP} that is concerned with the required sample sizes. There are three conditions of the ratio of sample size: $r = 1$ or $n_1 = n_2$, $r > 1$ or $n_1 > n_2$, and $r < 1$ or $n_1 < n_2$.

Depending on the above, the following multi-objective optimization problem is solved to determine the optimal plan parameters $(n_1, n_2, c_1, c_2)^*$ of the DSP_{ZIP} as per eq.(10) and eq.(11). Referring to the numerical of this illustration from Table 1, suppose $p = 0.01$ and $P_a(0.01) = 0.99$ under the different combinations of $\emptyset = (0.001,0.01,0.05,0.10), AQL = (0.01,0.05)$, and $LTPD = (0.05,0.075,0.10)$.

From Table 2, the sensitivity analyses of (n_1, n_2, c_1, c_2) under the DSP_{ZIP} are shown by considering two constraints of the required sample sizes (δ) and three conditions of the ratio of sample size (r). The investigating values are given as follows.

1. Based on two constraints of the required sample sizes with $\emptyset = 0.01$ and $AQL = 0.01$, the results show that when $LTPD$ increases the value of TC and ASN decrease. Furthermore, r further approaches to 1 when $LTPD$ increases.

2. When $\emptyset$ increases under the same values of AQL and $LTPD$, the results are not different, that is, the more $\emptyset$ increases r also approachs 1.

3. Two constraints of the required sample sizes for the same values of $\emptyset$, AQL and $LTPD$ are considered. The results indicate that the first constraint $(n_1 + n_2 \leq 100)$ is given a smaller value of TC and ASN than the second constraint $(n_1 + n_2 \leq 200)$ with $P_a(0.01) = 0.99$. On the other hand, the second constraint is given a smaller r than the first constraint respectively. This means that TC and ASN further decrease when the value of r approaches 1.

For both constraints of the required sample sizes, it can interpret that when $AQL = 0.05$, $LTPD = 0.10$, and $\emptyset$=0.10, the value of r approaches 1. This means that the required sample sizes should be equal $(n_1 = n_2)$ which provides the maximum value of P_a, and the minimum value of TC and ASN.

3.2 Illustration 2: The optimal solution under three different scenarios of the required sample sizes

In the general sampling system, the user expects that the smaller value of required sample sizes (n_1, n_2) or ASN would be more satisfactory for designing the optimal ASP. So, this illustration aims

Table 2. Optimal parameters of the DSP_{ZIP} for the minimum value of TC and ASN under the constraints of the required sample sizes with $p = 0.01$ and suppose that $P_a(0.01) = 0.99$

AQL	∅	$LTPD$	$n_1 + n_2 \leq 100$							$n_1 + n_2 \leq 200$						
			n_1	n_2	c_1	c_2	r	TC	ASN	n_1	n_2	c_1	c_2	r	TC	ASN
0.01	0.001	0.05	81	19	2	8	4.26	218	81.00	145	52	3	5	2.79	269	145.65
		0.075	71	22	2	3	3.23	186	71.18	90	67	3	8	1.34	198	90.01
		0.10	55	32	2	4	1.72	157	55.07	53	60	2	4	0.88	161	53.12
	0.01	0.05	82	16	2	3	5.13	220	82.20	148	52	3	9	2.85	277	148.00
		0.075	66	18	2	3	3.67	185	66.45	98	73	3	6	1.34	198	98.00
		0.10	55	44	2	4	1.25	151	55.0	55	85	2	4	0.65	161	55.18
	0.05	0.05	81	12	2	3	6.75	216	81.45	137	26	3	4	5.27	262	137.91
		0.075	65	35	2	3	1.86	182	65.80	83	87	2	4	0.95	201	83.71
		0.10	55	43	2	3	1.28	164	55.66	63	72	2	4	0.88	164	63.23
	0.10	0.05	81	19	2	3	4.26	212	80.63	143	56	3	5	2.55	263	143.61
		0.075	63	32	2	4	1.97	201	77.12	110	76	3	5	1.45	210	110.31
		0.10	52	47	3	4	1.10	179	80.14	51	85	1	3	0.60	195	52.01
0.05	0.001	0.05	90	10	2	5	9.00	230	90.02	158	42	4	8	3.76	261	158.01
		0.075	51	42	2	4	1.21	154	51.07	81	68	4	6	1.19	174	81.01
		0.10	44	54	3	5	0.81	137	44.01	41	103	2	4	0.40	139	41.08
	0.01	0.05	89	11	2	5	8.09	228	89.02	155	45	3	5	3.44	288	155.72
		0.075	55	18	2	4	3.06	162	55.04	66	68	3	7	0.97	162	66.01
		0.10	44	46	3	6	0.96	137	44.01	43	104	3	7	0.41	136	43.00
	0.05	0.05	51	49	1	3	1.04	199	51.60	116	84	2	4	1.38	265	117.89
		0.075	52	41	2	4	1.27	155	52.10	68	41	3	5	1.66	164	68.02
		0.10	36	48	2	5	0.75	133	36.01	58	92	4	6	0.63	142	58.01
	0.10	0.05	87	13	2	5	6.69	226	87.02	109	21	2	5	5.19	268	109.08
		0.075	52	41	2	4	1.27	155	52.07	66	42	3	5	1.57	161	66.02
		0.10	35	48	2	4	0.73	131	35.02	58	75	4	6	0.77	150	58.01

to minimize the required sample sizes (n_1, n_2) under the optimal parameters of the DSP_{ZIP}. Based on this reason, the conditions of the required sample sizes (n_1, n_2) are considered as the constraints to find the optimal DSP_{ZIP} to achieve the maximum value of P_a and the minimum value of TC and ASN simultaneously.

In this illustration, a comparison between the size of the first sample (n_1) and the second sample (n_2) is considered. The smaller value of sample size (n_1, n_2) or ASN is always more satisfactory for designing the optimal ASP.

There are three different scenarios of the required sample sizes (n_1, n_2) used to find the optimal multi-objective function of a DSP_{ZIP} as follows.

Scenario1 (S1): $n_1 = n_2$ and $n_1 + n_2 \leq \delta N(r = 1)$

Scenario2 (S2): $n_1 > n_2$ and $n_1 + n_2 \leq \delta N(r > 1)$

Scenario3 (S3): $n_1 < n_2$ and $n_1 + n_2 \leq \delta N(r < 1)$

The maximum value of $P_a(p)$ and the minimum value of TC and ASN can be determined by solving eq.10 and eq.11, with a given input parameter from Table 1. Suppose $AQL = 0.05$, and $LTPD = 0.10$ based on the reasons from the Illustration 1, the optimal parameters $(n_1, n_2, c_1, c_2)^*$ of the DSP_{ZIP} are determined by satisfying two inequalities, $P_a(AQL) \geq 1 - \alpha$ and $P_a(LTPD) \leq \beta$, and three scenarios of the required sample sizes as mentioned above.

From Table 3, the main goal is achieved (the maximum P_a and the minimum TC and ASN) by obtaining the optimal values of $(n_1, n_2, c_1, c_2)^*$ under the DSP_{ZIP}. The investigating values are given as follows.

1. Based on three different scenarios of (n_1, n_2) with $\delta = 0.10(n_1 + n_2 \leq 100)$, and $\delta = 0.20(n_1 + n_2 \leq 200)$, when $\emptyset$ increases, the value of P_a tends to increase while TC tends to decrease.

2. The three different scenarios of (n_1, n_2) are compared under the same value of δ and $\emptyset$. The results show that S1, $(n_1, n_2, c_1, c_2)^* = (50,50,1,2)^*$, provides the lowest TC and highest P_a, whereas S3, $(n_1, n_2, c_1, c_2)^* = (40,60,0,2)^*$ provides the lowest ASN.

3. Considering under the same scenario, when δ increases under the same value of $\emptyset$, the value of P_a is increasing while the value of TC and ASN is decreasing.

It can interpret that the optimal required sample sizes is Scenario 1 $(n_1 = n_2)$ because S1 provides the lowest TC and highest P_a and these parameters are an important factor in the construction of the optimal DSP_{ZIP}. Moreover, the smaller of required sample sizes (lower δ) provides the optimal DSP_{ZIP} .

3.3 Illustration 3: The optimal OC function of the DSP_{ZIP}

Illustration 2 indicates that the required sample sizes of the first and second sampling should be the smallest and equal values $(n_1 = n_2)$. In this illustration, the input parameters are assigned from Table 1. The performances of the DSP_{ZIP} with different values of $\emptyset$ under the optimal scenario (S1) are presented in Figures 1-3. The OC curves of DSP_{ZIP} are shown in Figure 1 when $(n_1, n_2, c_1, c_2)^* = (50,50,1,2)^*$. Other than that, the OC curves of DSP_{ZIP} are compared with DSP_P . Suppose DSP_P is the DSP under traditional Poisson distribution.

From Figure 1, for the same value of p and a different value of $\emptyset$, the results indicate that a higher value of $\emptyset$ under DSP_{ZIP} provides the larger P_a. Based on the same condition of optimal $(n_1, n_2, c_1, c_2)^*$, DSP_{ZIP} gives a larger P_a than DSP_P for each value of p. In practice, an optimal sampling plan should give a small ASN. From Figure 2, it can be seen that $p = 0.04$ gives the maximum value of ASN of all the proposed sampling plans. Moreover, a larger of $\emptyset$ under DSP_{ZIP}

Table 3. The optimal solution of DSP_{ZIP} under three different scenarios of the required sample sizes

δ	$\emptyset$	S1 $(50,50,1,2)^*$			S2 $(60,40,1,2)^*$			S3 $(40,60,0,2)^*$		
		P_a	TC	ASN	P_a	TC	ASN	P_a	TC	ASN
0.10	0.01	0.2944	924	62.70	0.2071	977	68.87	0.1836	990	56.08
	0.05	0.3229	913	62.18	0.2392	963	68.51	0.2150	976	55.43
	0.10	0.3586	887	61.54	0.2792	942	68.07	0.2545	946	54.62
	0.20	0.4298	844	60.26	0.3593	890	67.17	0.3341	901	52.99
	0.30	0.5011	808	58.98	0.4394	847	66.27	0.4145	855	51.37
	0.40	0.5724	764	57.70	0.5195	796	65.38	0.4958	801	49.74
	0.50	***0.6436***	***721***	***56.41***	0.5996	752	64.48	0.5778	754	48.12
		$(100,100,2,4)^*$			$(120,80,2,4)^*$			$(80,120,1,3)^*$		
		P_a	TC	ASN	P_a	TC	ASN	P_a	TC	ASN
0.20	0.01	0.1380	1024	117.37	0.0778	1056	130.60	0.1028	1038	102.21
	0.05	0.1727	1001	116.67	0.1148	1039	130.17	0.1309	1020	102.27
	0.10	0.2160	978	115.79	0.1611	1007	129.64	0.1842	987	101.10
	0.20	0.3027	924	114.04	0.2538	957	128.57	0.2747	935	98.76
	0.30	0.3896	878	112.28	0.3466	907	127.50	0.3652	884	96.41
	0.40	0.4765	823	110.53	0.4395	857	126.42	0.4557	825	94.07
	0.50	***0.5635***	***777***	***108.77***	0.5326	799	125.35	0.5463	773	91.72

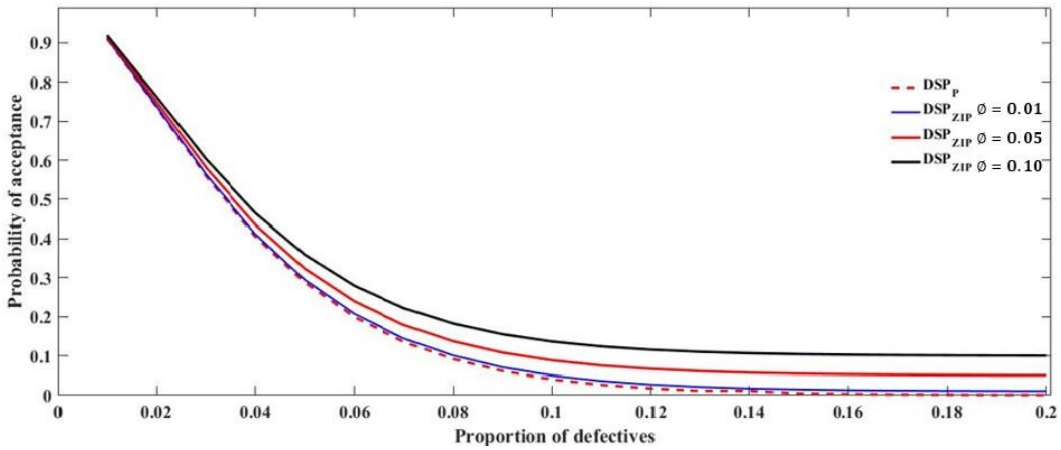

Figure 1. The optimal OC function of the DSP_{ZIP} under optimal plan $(50,50,1,2)^*$

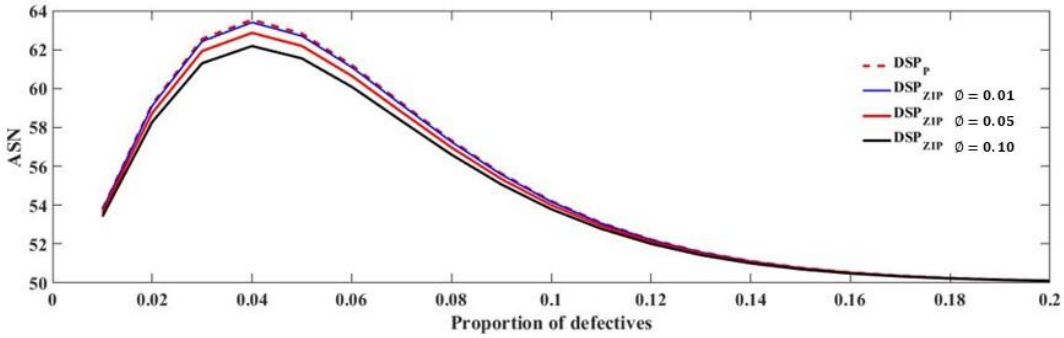

Figure 2. The optimal ASN curves of the DSP_{ZIP} under optimal plan $(50,50,1,2)^*$

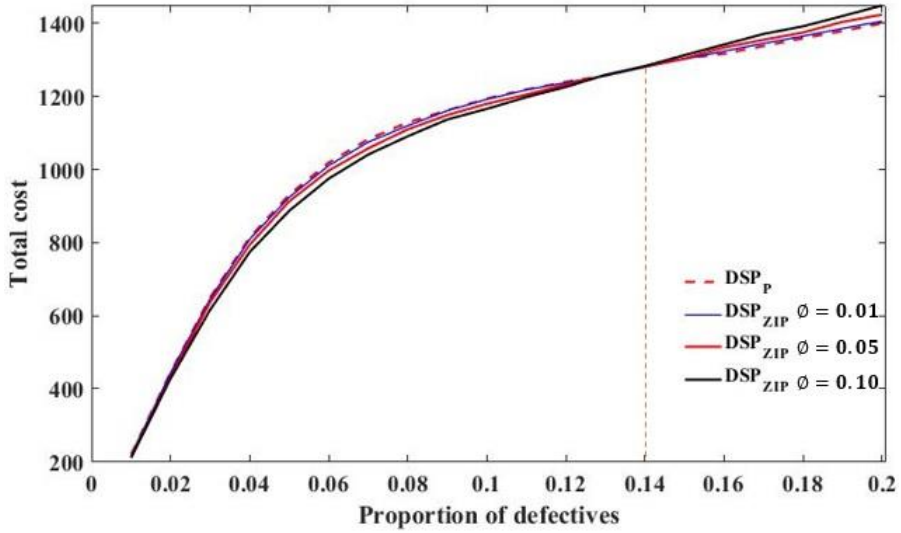

Figure 3. The optimal total cost of the DSP_{ZIP} under optimal plan $(50,50,1,2)^*$

provides smaller ASN. From Figure 3, the results show that larger values of $\emptyset$ under DSP_{ZIP} provides the lower TC for $0 < p \leq 0.13$. Furthermore, the OC function under the optimal plans $(50,50,1,2)^*$ and $(100,100,2,4)^*$ are compared in Figure 4. The result indicates that for $p = 0.01$, the optimal plan $(100,100,2,4)^*$ has a slightly larger P_a than $(50,50,1,2)^*$. On the other hand, when p increase, the optimal plans $(50,50,1,2)^*$ has a slightly larger P_a than $(100,100,2,4)^*$.

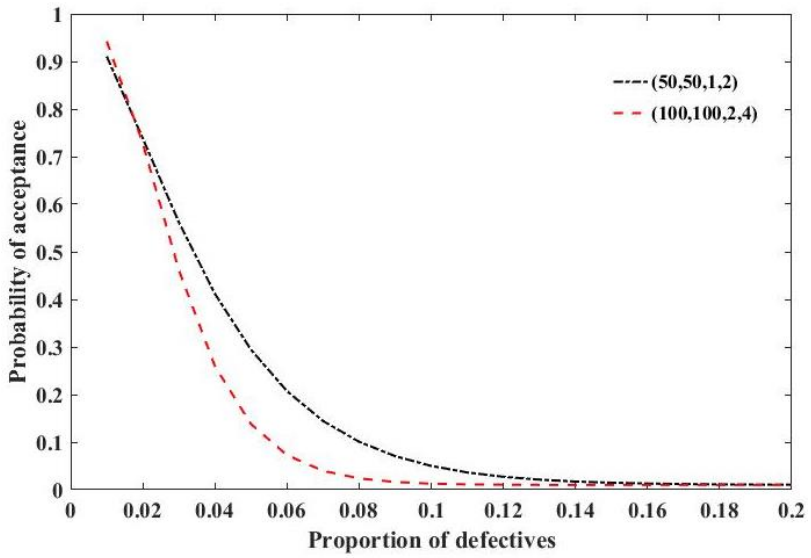

Figure 4. A comparison of the OC function under the optimal plans$(50,50,1,2)^*$and $(100,100,2,4)^*$

3.4 Real data application

In this section, a real dataset with excess zero counts is the number of read-write errors discovered in a computer hard disk in a manufacturing process (see Xie *et al*. [20]) as shown in Figure 5. This data set includes a total of 208 samples with a mean of 1.16 and a standard deviation of 1.20. From this dataset, the input parameters are calculated as follows:

$$\emptyset = \frac{Number\ of\ zero\ value\ samples}{Total\ number\ samples} = 0.87,\ p = 0.006,\ \text{and}\ \ N = 208.$$

Some of the input parameters are assigned by the user:

$$\delta = (0.10,0.20),\ \alpha = 0.05,\ \beta = 0.01, AQL = 0.05, LTPD = 0.10, C_I = 1, C_F = 2, \text{and } C_O = 10.$$

Substituting input parameters in multi-objective optimization using GA methods, we then obtained the optimal plan parameters $(n_1, n_2, c_1, c_2)^*$.The result shows that at $\delta = 0.10$ $(n_1 + n_2 \leq 20)$, the optimal plan parameters are $(10,10,0,2)$ which provide the optimal solution $P_a = 0.9917$, $TC = 37$, and $ASN = 10.27$. However, for $\delta = 0.20$ $(n_1 + n_2 \leq 40)$, the optimal plan parameters are $(20,20,0,1)$, which provide an optimal solution $P_a = 0.9911$, $TC = 47$, and $ASN = 20.95$.

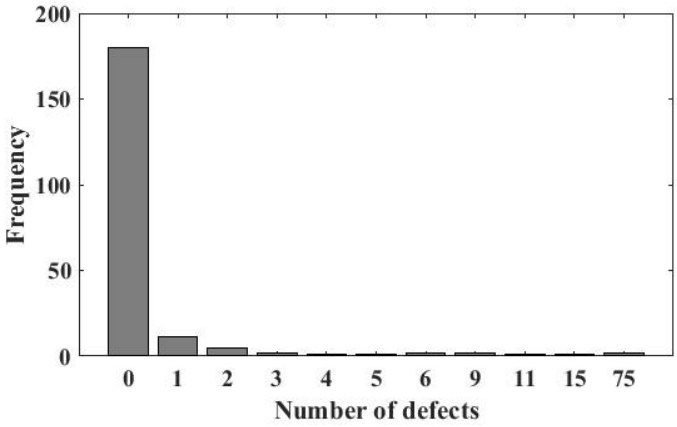

Figure 5. Number of read-write errors discovered in a computer hard disk

4. Conclusions

Nowadays, It can be observed that when the production processes are well inspected, zero defects are often found in sample inspections. There are many ways to achieve the optimal DSP that is affected by zero-inflated data. In this research, the proposed method was modified to make an optimal decision for the manufacturer. The optimal parameters were proposed to maximize the $P_a(p)$ and minimize the TC and ASN simultaneously. The proposed method was designed based on three different scenarios of the required sample sizes using multi-objective optimization with GA methods.

In conclusion, according to the proposed method, the result indicates that the values of $P_a(p)$, TC and ASN under the DSP_{ZIP} depend on the required sample sizes. Based on the same value of AQL and $LTPD$, when $\emptyset$ increases, the smaller value of required sample sizes provides the optimal DSP_{ZIP} to achieve maximum value of the $P_a(p)$ and minimum value of the TC and ASN. Furthermore, under 3 different scenarios of the required sample sizes, we found that the first sample (n_1) and the second sample (n_2) should be equal $(n_1 = n_2)$. The performance of the DSP_{ZIP} is considered by the OC function with a different value of $\emptyset$ based on $n_1 = n_2$ scenario. The results indicate that the DSP_{ZIP} provides more performance when $\emptyset$ is increased. Furthermore, under the same condition, DSP_{ZIP} provides more performance than the DSP_P in each value of p.

To apply the proposed methods, the manufacturer should know some necessary values of input parameters such as lot size, the proportion of defect per lot, cost per unit, etc. In future work, the proposed method can be applied to optimize multiple acceptance sampling plans. Moreover, the proposed method can be extended under other zero-inflated distributions such as the zero-inflated Negative binomial distribution.

5. Acknowledgements

The first author is deeply thankful to the Division of Mathematics, Faculty of Science and Technology, RMUTK. The second author thanks the Division of Applied Statistics, Faculty of Science and Technology, RMUTT for their support.

References

[1] Montgomery, D.C., 2005. *Introduction to Statistical Quality Control*. New York: John Wiley and Sons.

[2] Duarte,B.P.M. and Saraiva, P.M., 2008. An optimization- based approach for designing attribute acceptance sampling plans. *International Journal of Quality and Reliability Management*, 25, 824-841.

[3] Kaya, I., 2009. A genetic algorithm approach to determine the sample size for attribute control charts. *Information Sciences*,179, 1552-1566.

[4] Kobilinsky, A. and Bertheau, Y., 2005. Minimum cost acceptance sampling plans for grain control, with application to GMO detection. *Chemometrics and Intelligent Laboratory Systems*, 75(2), 189-200.

[5] Cheng, T.M. and Chen, Y.L., 2006. A GA mechanism for optimizing the design of attribute-double-sampling-plan. *Automation in Construction*, 16(3), 345-353.

[6] Sampath, S. and Deepa, S.P., 2012. Determination of optimal double sampling plan using Genetic Algorithm. *Pakistan Journal of Statistics and Operation Research*, 8(2), 195-203.

[7] Braimah, O.J., Saheed, Y.K., Owonipa, R.O. and Adegbite, I.O., 2015. Economic reliability acceptance sampling plan design with zero acceptance. *African Journal of Computing and ICT*, 8(3), 69-84.

[8] Hsu, L.F. and Hsu, J.T., 2012. Economic design of acceptance sampling plans in a two-stage supply chain. *Advances in Decision Sciences*, 2012, https://doi.org/10.1155/2012/359082

[9] Fallahnezhad, M.S. and Aslam, M., 2013. A new economical design of acceptance sampling models using Bayesian inference. *Accreditation and Quality Assurance*,18(3), 187-195.

[10] Fallahnezhad, M.S. and Qazvini, E., 2017. A new economical scheme of acceptance sampling plan in a two-stage approach based on the maxima nomination sampling technique. Published online in *Transactions of the Institute of Measurement and Control*, 39(7), https://doi.org/ 10.1177/0142331216629203

[11] Fallahnezhad, M.S., Qazvini, E. and Abessi, M., 2018. Designing an economical acceptance sampling plan inthe presence of inspection errors based on maxima nomination sampling method. *Scientia Iranica*, 25(3), 1701-1711.

[12] Lambert, D., 1992. Zero-inflated Poisson regression, with application to defects in manufacturing. *Technometrics*, 34, 1-14.

[13] McLachlan, G. and Peel, D., 2000. *Finite Mixture Models*. New York: John Wiley and Sons.

[14] Loganathan, A. and Shalini, K., 2014. Determination of single sampling plans by attributes under the conditions of zero-inflated Poisson distribution. *Communication in Statistics-Simulation and Computation*, 43, 538-548.

[15] Uma, G. and Ramya, K., 2016. Determination of quick switching system by attributes under the conditions of zero- inflated Poisson distribution. *International Journal of Statistics and Systems*, 11, 157-165.

[16] Rao, G.S. and Aslam, M., 2017. Resubmitted lots with single sampling plans by attributes under the conditions of zero-inflated Poisson distribution. *Communication in Statistics-Simulation and Computation*, 46, 1814-1824.

[17] Wang, F.K. and Hailemariam, S.S., 2018. Sampling plans for the zero- inflated Poisson distribution in the food industry. *Food Control*, 85, 359-368.

[18] Holland, J.H., 1975. *Adaptation in Natural and Artificial Systems*. Ann Arbor: University of Michigan Press.

[19] The Math Works™, 9.7.0 (R2019b), License Number 40791029.

[20] Xie, M., He, B. and Goh, T.N., 2001. Zero- inflated Poisson model in statistical process control. *Computational Statistics and Data Analysis*, 38(2), 191-201.

In Vitro Antilithiasis Activity and Cytoprotective Properties of *Acalypha indica* Extracts

Nandakumar Arumugam[1], Arulvel Ramaswamy[2] and Sundramurthy Venkatesa Prabhu[3]*

[1]Department of Biotechnology, KIT-Kalaignarkarunanidhi Institute of Technology, Coimbatore, Tamil Nadu, India
[2]Department of Biotechnology, Saveetha School of Engineering, Institute of Medical and Technical Sciences, Chennai, Tamil Nadu, India
[3]Department of Chemical Engineering, Addis Ababa Science and Technology University, Addis Ababa, Ethiopia

Received: 3 February 2020, Revised: 15 July 2020, Accepted: 30 September 2020

Abstract

Kidney stone is a major health problem occurring in many individuals, especially men, and it is caused by dietary intake and excess excretion of chemicals in the urine. The aim of this study was to evaluate the inhibitory potential of *Acalypha indica* Linn. against calcium oxalate stones. Various solvent extracts of *A. indica* Linn. were prepared using cold extraction method. These extracts were then used for analyzing inhibitory action against three stages of crystal formation: nucleation, growth, and aggregation. The ethanolic extracts were found to have maximum inhibitory potential of approximately 90±0.0011%, 99.4±0.002%, and 93±0.002% against the crystal nucleation, growth, and aggregation of calcium oxalate. The inhibitory potential of calcium oxalate precipitation in artificial urine by the ethanolic extract was found to be approximately 99.231±0.0001%. The ethanolic extract was fractionated by column chromatography and the bioactive compound was identified as an aliphatic group from the structural characteristics of the ethanolic extract obtained from ^{13}C nuclear magnetic resonance. Finally, the effectiveness of partially purified extract was tested on calcium oxalate stones, which were highly dissolved by the ethanolic extract (61.82±0.133%) compared to calcium phosphate stones (35.71±0.06%). It was also tested on oxalate induced Vero cell lines and the cell viability was found to be approximately 70.5±2.99%. On the basis of the present study, it was concluded that the crude extract had higher activity against calcium oxalate stones than a partially purified extract.

Keywords: aggregation; artificial urine; calcium oxalate; crystal growth; kidney stone; nucleation; Vero cell lines
DOI 10.14456/cast.2021.22

*Corresponding author: Tel.: +251 908773764, Fax: (+251) 01-189-6144
E-mail: venkatchemdata@gmail.com

1. Introduction

Renal calculi are generally called kidney stone. Being able to successively treat kidney stone these days is a milestone because it eventually leads to the death of the affected individuals. Kidney stone affects approximately 4-8% of population in the UK, 15% in the USA, and 11% in India [1]. Different forms of kidney stones that are present worldwide are calcium-containing stones of approximately 75-90%, followed by struvite crystals (10-15%), uric acid (3-10%), and cysteine (0.5-1%) [2, 3]. Lithiasis is a process in which calcium oxalate (CaC_2O_4 or CaOx) is formed in the kidney. Calcium oxalate stones are present in two forms: calcium oxalate monohydrate (COM) or whewellite, and calcium oxalate dihydrate (COD) or weddellite. COM stones are thermodynamically more stable than COD and have more affinity for the formation of renal calculi in the kidney [4-6]. It is noteworthy that the lifestyle and dietary intake of individuals also play a role in the formation of stones in the kidney. The major causes are high intake of calcium- and phosphorus-rich cereals and oxalate-rich vegetables, as well as lack of animal proteins [7]. There are several ways to treat renal stones. Some of the practices such as surgical approaches are endoscopic stone removal lithotripsy and extracorporeal shock wave lithotripsy, which cause traumatic effect and reduction in renal function with acute renal injury [8]. The alternative resource for the treatment of renal stones is the use of herbal extracts. The plants used to prepare these extracts are commonly found and the technique is also a cost-effective [9, 10]. This study deals with assessing the inhibitory effects of *Acalypha indica* Linn. leaves compared to *in vitro* analysis and on Vero cell lines.

2. Materials and Methods

2.1 Collection and authentication of plant materials

Acalypha indica Linn. plants were collected from nearby K. S. Rangasamy College of Technology, Tiruchengode, Tamil Nadu, India, from March to April 2014. The validation of plants was accomplished by Botanical Survey of India, Tamil Nadu Agricultural University, Coimbatore, Tamil Nadu, India. Renal stone formation can be identified by three stages, via calcium oxalate crystal nucleation, growth and aggregation, and these can be analyzed by the following *in vitro* techniques in the presence and absence of leaf extracts.

2.2 Preparation of plant extracts and nucleation assay

The plant leaves of *A. indica* Linn. were washed with distilled water, dried, and powdered. The powdered leaves were used for cold extraction process with different solvents such as chloroform, ethyl acetate, acetone and ethanol in the ratio of 1:10 based on their polarity. After 48 h of interval, the extracts were filtered through Whatman Grade 40 filter paper and air dried. Different concentrations of dried leaf extracts were prepared (1%, 3%, 5%, 7%, and 10%) in respective solvents for *in vitro* analysis. The nearness of nuclei prompts the emergence of kidney stones, and this was studied using the modified method [11] in which a 1.5 ml aliquot of 3.5 mmol/l calcium chloride (in TBS pH 6.5) and 150 µl of the extracts were mixed, then a 1.5 ml aliquot of 6 mmol/l sodium oxalate (in TBS pH 6.5) was included, and absorbance was estimated at 620 nm for different time intervals. Rate restraint was determined using the equation below.

$$\% \, Inhibition = \frac{C-S}{C} * 100 \quad (1)$$

where *C* is the turbidity without leaf extracts and *S* is the turbidity with leaf extracts.

2.3 Growth assay

The hindrance of the development of COM crystal was contemplated with small alterations [12] where 1.5 ml of each calcium chloride and sodium oxalate solutions of 1 mmol were prepared in the TBS buffer (pH 7.2) and mixed with 2.5 mg/ml COM crystal slurry (in acetate buffer). The absorbance was estimated at 214 nm with and without leaf extracts, and inhibition percentage was determined as follows:

$$\%\ Inhibition = \frac{C-S}{C} * 100 \quad (2)$$

where *C* is the oxalate reduction rate without leaf extracts and *S* is the oxalate reduction rate with leaf extracts.

2.4 Aggregation assay

At the point when crystals are present in the solution, they bunch together and form large particles as aggregates. The formation of aggregates can be inhibited with the help of leaf extracts with some changes in the method [13]. For this, a COM crystal can be shaped with solutions of calcium chloride and sodium oxalate at 75 mmol/l. These solutions were blended and kept in a water bath at 60°C for 1 h and then dried to collect the COM crystals. Then, 2 mg/ml COM crystals were prepared in the TBS buffer (pH 6.5). On the basis of the turbidity with and without leaf extracts, the rate of aggregation was analyzed. The rate of aggregation inhibition (Ir) was broken down by estimating the slope of turbidity with the leaf extracts and control, as follows.

$$Ir\ =\ 1\ -\frac{Turbidity\ in\ sample}{Turbidity\ in\ control} * 100 \quad (3)$$

2.5 Precipitation of calcium oxalate in artificial urine

Artificial urine (AU) was prepared with compositions containing sodium chloride (105.5 mmol/l), sodium phosphate (32.3 mmol/l), sodium citrate (3.21 mmol/l), magnesium sulfate (3.85 mmol/l), sodium sulfate (16.95 mmol/l), potassium chloride (63.7 mmol/l), calcium chloride (4.5 mmol/l), ammonium hydroxide (17.9 mmol/l), and ammonium chloride (0.0028 mmol/l) [14]. The AU was prepared freshly each day and the pH was adjusted to 6.0. The examination was directed by adding 2 ml AU, 0.5 ml extract, and 1.5 ml sodium oxalate (0.01 M), and absorbance was estimated at 620 nm. Percentage inhibition was determined using the following equation:

$$\%\ Inhibition\ =\ 1\ -\frac{Si}{Sc} * 100 \quad (4)$$

where S_i is the slope of the graph with leaf extracts and *S* is the slope of the graph without leaf extracts.

2.6 Separation of bioactive compounds by column chromatography

The potential leaf extract was identified by the above methods, and the extract was subjected to column chromatography. The column was packed with activated silica gel of 60-120 mesh and filled with respective solvent. Then, approximately 3 g extract was added and fractions were eluted out at constant time intervals and stored for further analysis.

2.7 TLC Analysis

The collected fractions were analyzed by thin-layer chromatography, and the mobile phase selected was chloroform/ethanol/methanol (8:2:1) [9, 15, 16]. This helps to identify the bioactive compound containing fractions. The plates were observed under UV light and the spots were identified.

2.8 Fourier Transform-Nuclear Magnetic Resonance (FT-NMR) analysis

The bonding regions and type of carbons present in the bioactive compound were analyzed using FT-NMR. The ^{13}C nuclear magnetic resonance (NMR) was used for the distinguishing proof of the carbon atoms in the bioactive compounds. The sample was prepared with DMSO and the spectra were read on a Bruker Advance Ultra Shield 400 spectrometer (Bruker Biospin GmbH, Rheinstetten, Germany), working at 400.13 MHz, using a broadband inverse probe head. The raw data points were obtained from the spectra.

2.9 Kidney stone analysis

Precisely expelled kidney stones were obtained from Senthil Multispeciality Hospital, Erode, Tamil Nadu, India. These stones were categorized into calcium oxalate stones and calcium phosphate stones (Figure 7 (a-b)). The initial size and weight of the stones were noted. The stones acted towards various concentrations of plant extracts and control (NaCl 10 g/l) for a period of 4 weeks with constant stirring. The stones were removed from the extracts at the end of each week and weighed after drying at 100°C. The parameters determined were decrease in weight and size of the stone, rate weight decrease, and disintegration rate [7].

$$\%\, Reduction\ in\ stone\ weight\ =\ 1\ -\frac{Final\ weight\ (\mathrm{g})}{Intial\ weight\ (\mathrm{g})} * 100 \tag{5}$$

$$Dissolution\ rate\ =\ \frac{Intial\ weight\ (\mathrm{g})\ -\ Final\ weight\ (\mathrm{g})}{Time\ (\mathrm{h})} \tag{6}$$

2.10 MTT assay

African Green Monkey Kidney cell lines (Vero cells) were acquired from the National Culture for Cell Sciences (NCCS, Pune). The cells were maintained in minimal essential medium (MEM) attuned with penicillin (100 units/ml), streptomycin (1 mg/ml), and 10% fetal bovine serum, and kept in a 25 cm^2 tissue-culture-treated flasks at 37°C and 5% CO_2 in humidified chambers. For oxalate induced cell injury, cells were refined with MEM medium alongside with 100 µg/ml sodium oxalate and various concentrations of plant extracts for 72 h [17, 18]. Cytotoxicity was measured by 3-(4,5-dimethyl-2-thiazolyl)-2,5-diphenyl-tetrazolium bromide (MTT) assay.

The viability of the cells was evaluated and estimated by the measure of decrease of MTT to purple formazan and it was evaluated by an altered method [19, 20]. The 96-well plates were used for culturing the Vero cells (1 × 105/wells). The cells were hatched at various concentrations of extracts and hatched at 37°C for 48 h. In the wake of gathering, the cells were cultured with MTT (5 mg/ml) in phosphate buffer (pH 7.4) and incubated at 37°C for 2 h. The absorbance was estimated at 540 nm by adding 0.2% DMSO to the treated cells and wells containing cells without extracts. Cell viability (%) was calculated from the following equation:

$$\%\, Cell\ viability\ =\ \frac{A540\ of\ treated\ cells}{A540\ of\ control\ cells} * 100 \tag{7}$$

2.11 Statistical analysis

All experiments were done in triplicates. These were presented as mean ± SD of three independent filters. Statistical analysis was performed by using the Analysis of Variance (ANOVA) with GraphPad Prism, V5.0, software. The distinction in the experiments was viewed significant if *P*-value was <0.05.

3. Results and Discussion

3.1 Inhibition of calcium oxalate crystal nucleation

The inhibitory potential of leaf extracts of *A. indica* Linn. was measured against crystal nucleation, which is the most critical stage in kidney stone development. Figure 1 shows the inhibitory activity in nucleation formation. It is observable that the ethanolic extracts of 1% and 5% concentration, and 1% of ethyl acetate had higher inhibition of approximately 90±0.0011% compared to all the other extracts. There is a deviation and decrease in the inhibitory activity against nucleation of the CaOx crystals, even after increasing the concentration of extracts. The results obtained by studies in *Bergenia ciliata* [5] show approximately 32%-92% inhibition in the nucleation formation.

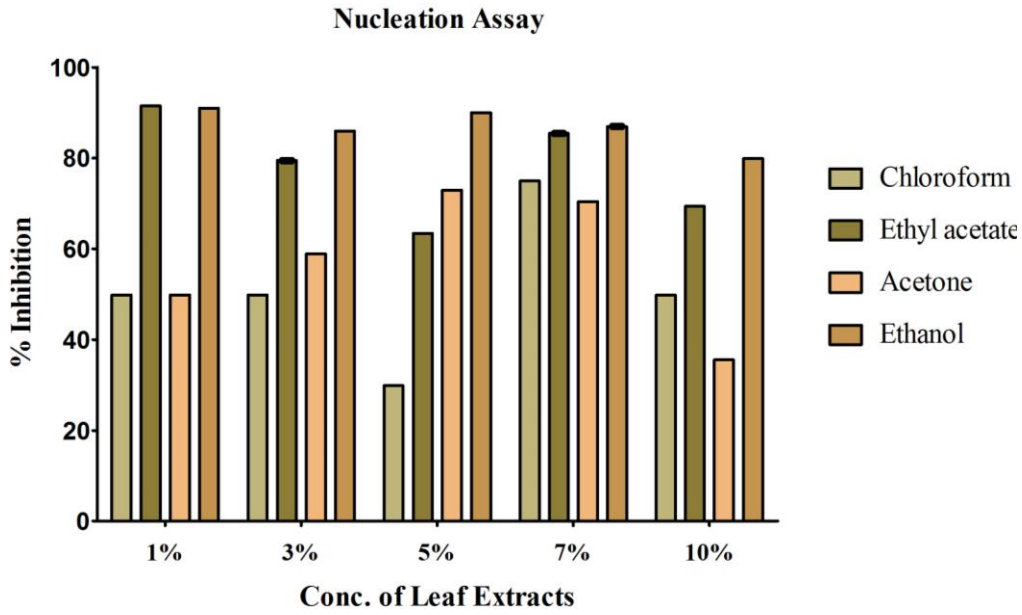

Figure 1. Effect of *Acalypha indica* Linn. leaf extracts on CaOx nucleation. Statistical analysis was depicted as p value < 0.0001.

3.2 Calcium oxalate crystal growth inhibition

Figure 2 illustrates that the concentration of ethyl acetate and ethanolic extracts has a comparable inhibition rate. The 5% concentration of both ethyl acetate and ethanolic extracts yielded 99.4±0.002% ($P < 0.0001$). The percentage inhibition of growth of CaOx crystals was comparable on increasing the concentration of leaf extracts. In banana cultivator Monthan [8] and in *Tribulus terrestris* [2], the inhibitory activity was found to increase in the inhibition of growth about 84% and 85.7% in ethanol extract respectively.

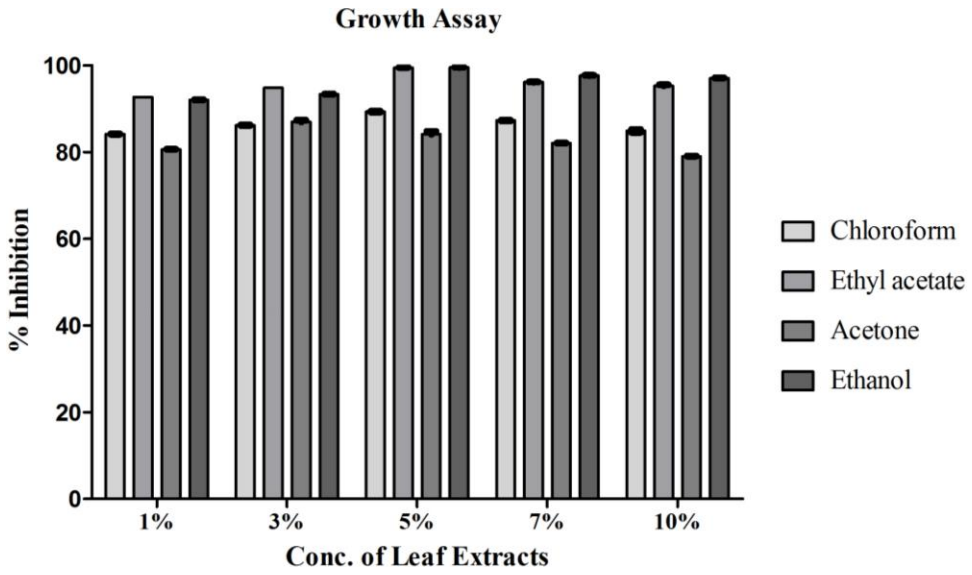

Figure 2. Effect of *Acalypha indica* Linn. leaf extracts on CaOx growth. Statistical analysis was depicted as p value < 0.0001.

3.3 Inhibition of calcium oxalate aggregation

The process of binding of kidney stone crystals to one another, called aggregation, is induced by a strong electric field. This is important in the lithiasis process. The inhibitory activity of different extracts is shown in Figure 3, which depicts that the ethanolic extracts at 3% and 5% concentrations have higher activity (93±0.002%) than other extracts. On increasing the concentration of ethanolic extract, a fall in the inhibitory activity against CaOx aggregation was observed. *Aerva lanata* [21] and *Bergenia ciliata* (Haw.) [22] showed considerable inhibition of 58%-97% against aggregation and decreased inhibition with increased concentration, and the results obtained in plants such as *Tachyspermum ammi*, [23] *Terminalia arjuna* [9], and *Tetraclinis articulate* [24] showed approximately 28%-78% inhibition.

3.4 Inhibition of calcium oxalate precipitation in artificial urine

In general, dissolved stones can be eliminated and excreted via urine. The inhibitory potential of CaOx precipitation in AU was studied with the help of leaf extracts of *A. indica* Linn. An increasing percentage of inhibition was observed for increasing concentration of ethanolic extracts and reached 99.231±0.0001% at 5% concentration (Figure 4). This is far greater compared to that of all the other

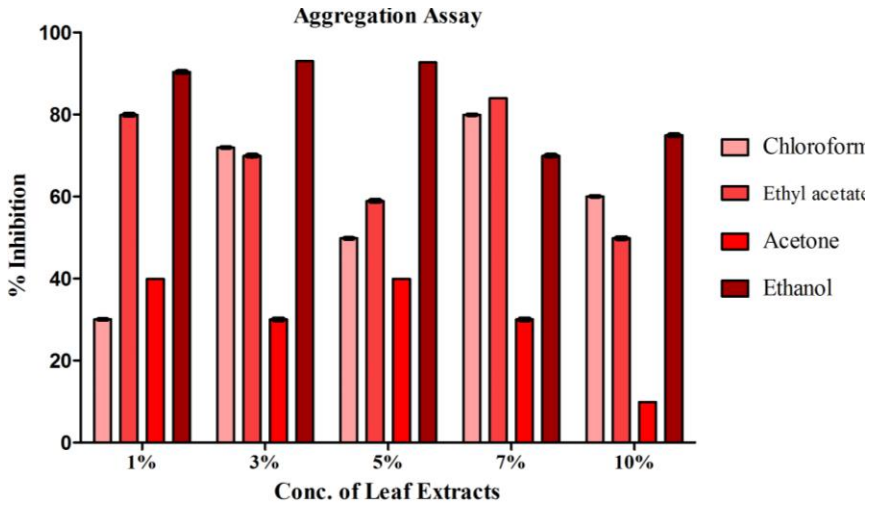

Figure 3. Effect of *Acalypha indica* Linn. leaf extracts on CaOx aggregation. Statistical analysis was depicted as p value < 0.0001.

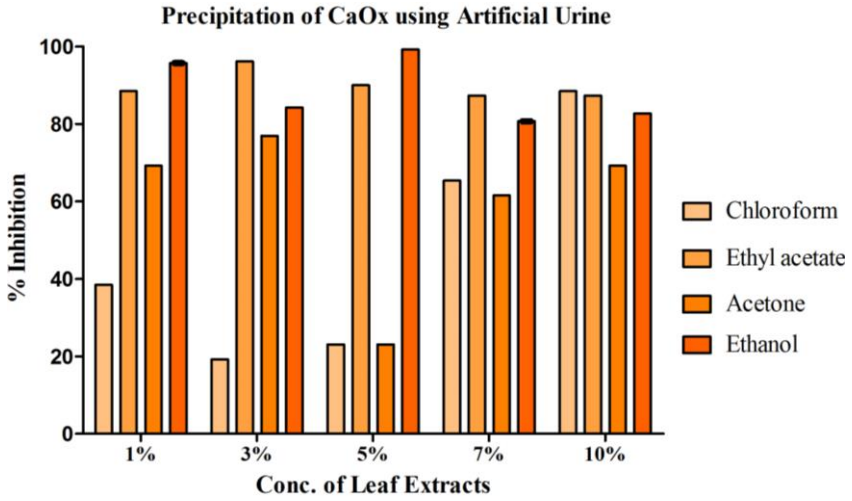

Figure 4. Effect of *Acalypha indica* Linn. leaf extracts on CaOx precipitation in artificial urine. Statistical analysis was depicted as p value < 0.0001.

extracts. A small increase in the concentration will have a negative effect on the inhibition rate. The formation of CaOx crystals in AU was considerably reduced by 99.23% with the ethanolic extract of *A. indica* Linn. The results acquired in *Achyranthes indica* Linn [10] and *Achyranthus aspera* [25] showed reductions of approximately 67%-95%.

3.5 Analysis of bioactive compounds

The ethanolic extract was found to have higher potential than other extracts based on the *in vitro* studies performed. The crude extract was subjected to column chromatography and purified fractions were obtained. The fractions were collected at definite time intervals and 53 fractions were obtained after elution. The fractions were analyzed by thin-layer chromatography for identifying the potential fractions and single band was observed in fractions 17-23 (Figure 5). The fractions 17-23 were pooled together and were analyzed using ^{13}C NMR for the carbon shift data and the results are shown in Figure 6. The peak shift data are shown in Table 1, which illustrates the compounds present in the extract. The peak 74.58 represents C=N group. Peaks 58.49-53.86 denote the presence of OCH3 group; DMSO is indicated from 38.91 to 38.33 and 17.21 shows the occurrence of the CH2 group. From these data, it can be inferred that the bioactive compound has aliphatic nature. The ethanolic extract was subjected to column chromatography and 53 fractions were obtained. Then, the single-band fractions were identified by TLC and pooled together for further process [15].

3.6 Analysis of efficacy of ethanolic extracts on kidney stone

The reduction in various properties of surgically removed stones was tested using ethanolic extracts on calcium oxalate and calcium phosphate stones. The results, tabulated as reduction in weight of the stone (g), % solubility, size reduction (cm) and mean dissolution rate (g/h), are depicted in Table 2. Figure 7(c-e) shows the kidney stones after treatment with ethanolic extract for 4 weeks. This shows the weight of the calcium oxalate and calcium phosphate stones and control stone reduced after 4 weeks (61.82±0.133%, 35.71±0.06%, and 58.75±0.03%, respectively). Similarly, the reduction in size of the kidney stones for calcium oxalate and calcium phosphate stones and control stones was 0.23±0.002, 0.30±0.017, and 0.28±0.0006, respectively. The solubility percentage and mean dissolution rate of the kidney stones after 4-week treatment with ethanolic extracts in calcium oxalate and calcium phosphate stones and control were 35.55±0.03 and 25±0.173, 15±0.115 and 0.018±0.016, and 0.04±0.06 and 0.02±0.01, respectively. From these results, it can be inferred that ethanolic extracts have less inhibitory potential against calcium phosphate stones.

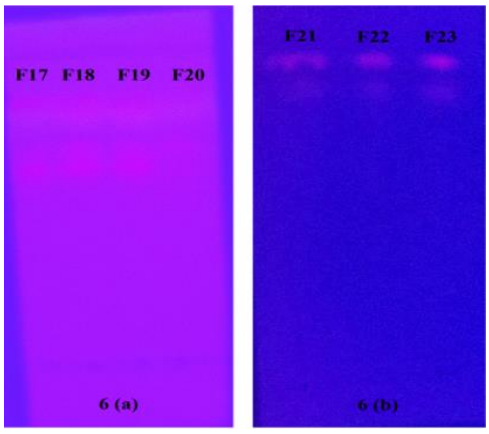

Figure 5. TLC plates showing bands of ethanolic extracts viewed under UV light
(a) Fractions 17-20, and (b) Fractions 20-23

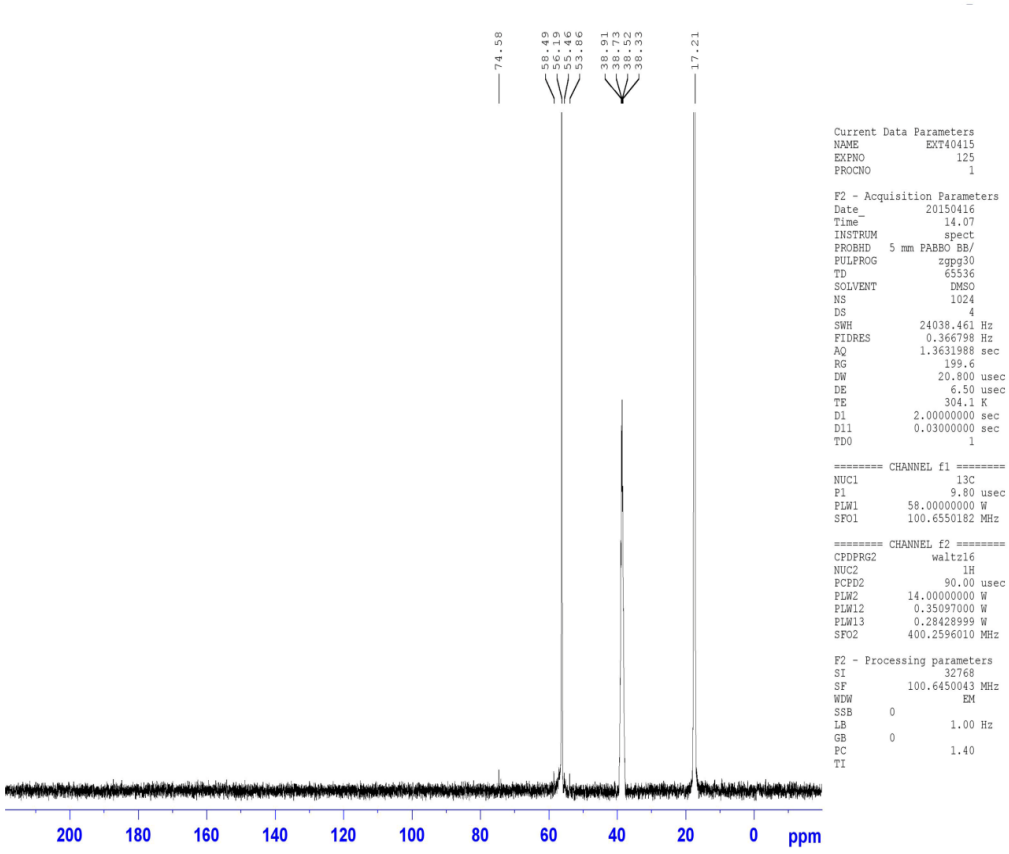

Figure 6. ^{13}C NMR spectrum of ethanolic extract of *Acalypha indica* Linn. at 400 MHz

Table 1.^{13}C NMR chemical shift data and their carbon types

S. No.	Chemical Shift (ppm)	Type of Carbon
1.	74.58	-C=N
2.	58.49	-OCH_3-
3.	56.19	-OCH_3-
4.	55.46	-OCH_3-
5.	53.86	-OCH_3-
6.	38.91	DMSO Solvent
7.	38.73	DMSO Solvent
8.	38.52	DMSO Solvent
9.	38.33	DMSO Solvent
10.	17.21	-CH_2-

Table 2. Weight reduction, % solubility, size reduction, and mean dissolution rate of calcium oxalate and calcium phosphate stones after treatment with ethanolic extracts

Particulars	Control				Calcium oxalate stone				Calcium phosphate Stone			
Initial weight of the stone (g)	0.08				0.11				0.56			
Initial Size of stone (cm)	0.6				0.6				1.1			
Week	**1**	**2**	**3**	**4**	**1**	**2**	**3**	**4**	**1**	**2**	**3**	**4**
Weight of the stone (g)	0.07	0.006	0.045	0.033	0.103	0.1	0.08	0.042	0.56	0.56	0.5	0.36
% in weight reduction after 4th week	58.75±0.03				61.82±0.133				35.71±0.06			
Solubility of stone (g)	0.01	0.01	0.015	0.012	0.007	0.003	0.02	0.038	0	0	0.06	0.14
% Solubility of stone after 4th week	15±0.115				35.55±0.03				25±0.173			
Size of stone (cm)	0.55	0.53	0.44	0.32	0.59	0.57	0.45	0.37	1.1	1.1	1	0.8
Reduction in size of stone (cm) after 4th week	0.28±0.006				0.23±0.002				0.3±0.017			
Dissolution rate (g/h)	0.006	0.012	0.021	0.028	0.0042	0.006	0.018	0.04	0	0	0.036	0.12
Mean Dissolution rate (g/h) after 4th week	0.02±0.01				0.018±0.016				0.04±0.06			

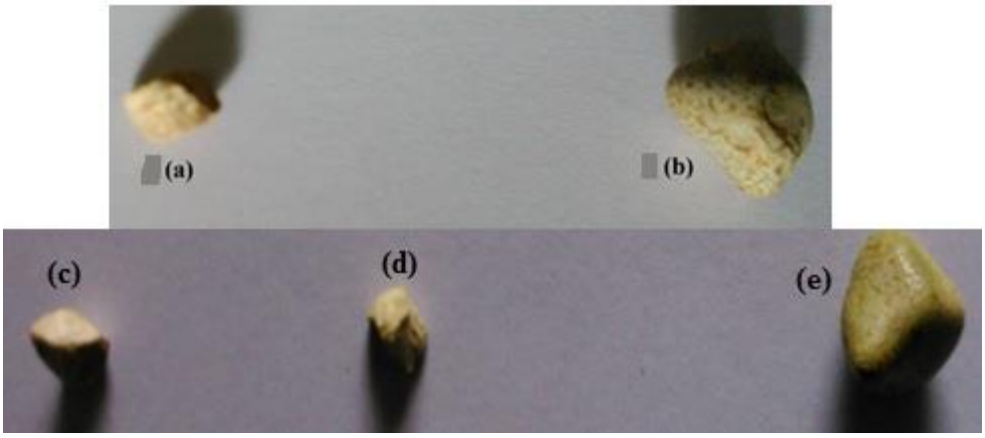

Figure 7. Stones before and after treatments with ethanolic extracts.
Before treatment with ethanolic extract; (a) calcium oxalate stone,
(b) calcium phosphate stone, and (c) control,
After Treatment with ethanolic extract; (d) calcium oxalate stone,
and (e) calcium phosphate stone

Comparable results were produced with food extracts having 9.09%-39.9% activity in dissolving the kidney stones [7] and in Phy and Art having inhibitory activity of 40.5%-52.1% [26]. *Solanum xanthocarpum*, *Rhamnus prushinae*, *S. granulate* and *Tribulus terrestris* extracts dissolved the kidney stones by approximately 15%-76.5% [27].

3.7 MTT Assay

The cytoprotective activity of ethanolic extracts of *A. indica* Linn. on oxalate-induced Vero cell lines (renal epithelial cell lines) was studied and results are shown in Figure 8. It was clearly visible that the purified extract with 1000 µg/ml concentration showed some white spots of viable cells along with untreated cells and with crude extract and all other concentration of the extracts showed little variations in the viable cells. Cell viability (%) was measured and shown in Figure 9. It was revealed that the crude extract alone can maintain the viability up to 77.4%, whereas 1000 µg/ml of purified extract can only retain the cell viability up to 70.5±2.99% compared to crude extracts and untreated cells. The viability of cells was measured and found to be high at 1000 µg/ml concentration of the ethanolic extracts. Similar results were observed in other studies [2, 28].

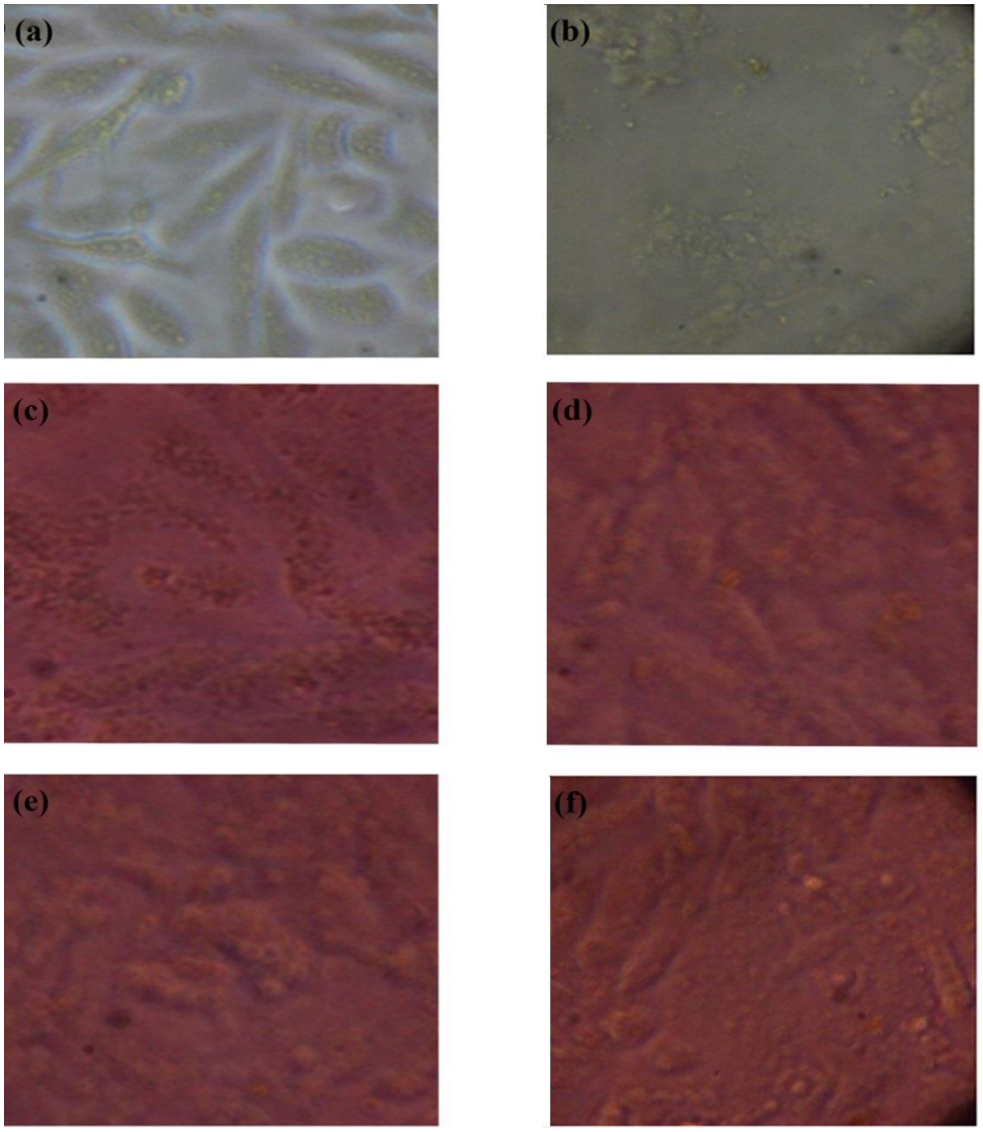

Figure 8. Viability of oxalate induced Vero cells treated with purified ethanolic extract of *Acalypha indica* Linn. (a) untreated cells, (b) extract alone, (c) 125 µg/ml extract, (d) 250 µg/ml extract, (e) 500 µg/ml extract, and (f) 1000 µg/ml extract.

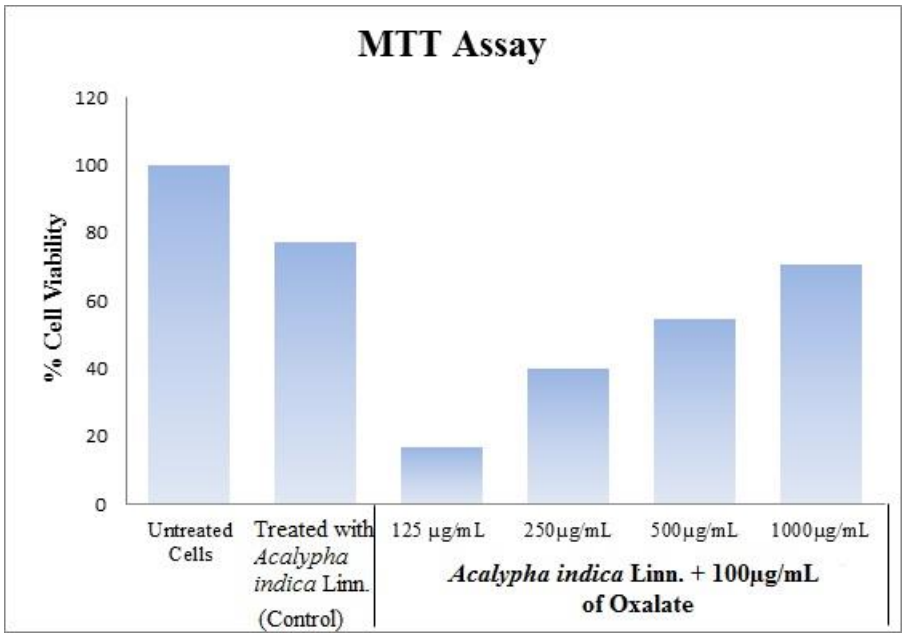

Figure 9. Effect of purified ethanolic extract of *Acalypha indica* Linn. on the viability of Vero cells

4. Conclusions

From the present study it can be concluded that *Acalypha indica* Linn. leaves show potential inhibitory activity against calcium oxalate stones. The three stages of formation and occurrence of kidney stones are nucleation, aggregation and growth of the CaOx crystal, and formation of calcium oxalate in the artificial urine was highly inhibited in the presence of the ethanolic extracts at an optimum concentration of about 5%. The efficiency of the partially purified and pooled fractions of ethanolic extracts was tested against surgically removed stones and oxalate-induced Vero cells (renal epithelial cell lines). The calcium oxalate stones were highly dissolved in the ethanolic extracts, whereas the calcium phosphate stones showed small amount of inhibition. This shows that the crude extract had higher activity compared to the partially purified extracts. Furthermore, this can be efficiently tested against animal models for the analysis of the inhibitory activity against calcium oxalate stones.

5. Acknowledgements

The authors acknowledge Senthil Multispeciality Hospital, Erode, Tamil Nadu, India for providing kidney stones, VIT University for providing NMR facilities, and to Chromopark (Namakkal) for the cell lines to be carried out in this project.

References

[1] Pareta, S.K., Patra, K.C., Mazumder, P.M. and Sasmal, D., 2011. Prophylactic role of *Boerhaavia diffusa* in ethylene glycol induced calcium oxalate urolithiasis. *African Journal of Urology,* 17(2), 28-36.

[2] Aggarwal, A., Tandon, S., Singla, S.K. and Tandon, C., 2010. Diminution of oxalate induced renal tubular epithelial cell injury and inhibition of calcium oxalate crystallization *in vitro* by aqueous extract of *Tribulus terrestris*. *International Brazilian Journal of Urology*, 36(4), 480-489.

[3] Atodariya, U., Barad, R., Upadhyay, S. and Upadhyay, U. 2013. Anti-urolithiatic activity of *Dolichos biflorus* seeds. *Journal of Pharmacognosy and Phytochemistry,* 2(2), 209-213.

[4] Srinivasa, A.K.B., Kuruba, L., Khan, S. and Saran, G.S., 2013. Antiurolithiatic activity of Gokhsuradi Churan, an ayurvedic formulation by *in vitro* method. *Advanced Pharmaceutical Bulletin,* 3(2), 477-479.

[5] Saha, S. and Verma, R.J., 2013. Inhibition of calcium oxalate crystallisation *in vitro* by an extract of *Bergenia ciliata*. *Arab Journal of Urology*, 11(2), 187-192.

[6] Saranya, R. and Geetha, N., 2014. Inhibition of calcium oxalate (CaOx) crystallization *in vitro* by the extract of beet root (*Beta vulgais* L.). *International Journal of Pharmacy and Pharmaceutical Sciences,* 6, 361-365.

[7] Rajeswari, M. and Sudha, R.K.S., 2013. *In vitro* study of the litholytic effects of selected food extracts on renal stones. *International Journal of Scientific Research,* 2(10), 1-2.

[8] Kalpana, S., Nirmaladevi, R., Rai, T.S. and Karthika, P., 2013. Inhibition of calcium oxalate crystallization *in vitro* by extract of banana cultivar Monthan. *International Journal of Pharmacy and Pharmaceutical Sciences,* 5(4), 649-653.

[9] Chaudhary, A, Singla, S.K. and Tandon, C., 2010. *In vitro* evaluation of *Terminalia arjuna* on calcium phosphate and calcium oxalate crystallization. *Indian Journal of Pharmaceutical Sciences*, 72(3), 340-345.

[10] Pareta, S.K., Patra K.C. and Harwansh, R., 2011. *In vitro* calcium oxalate crystallization inhibition by *Achyranthes indica* Linn. hydroalcoholic extract: an approach to antilithiasis. *International Journal of Pharma and Bio Sciences*, 2(1), 432-437.

[11] Hennequin, C., Lalanne, V., Daudon, M., Lacour, B. and Drueke, T., 1993. A new approach to studying inhibitors of calcium oxalate crystal growth. *Urological Research,* 21(2), 101-108.

[12] Shiekh, F.A., Khullar, M. and Singh, S.K., 2006. Lithogenesis: induction of renal calcifications by nanobacteria. *Urological Research*, 34(1), 53-57.

[13] Hess, B., Meinhardt, U., Zipperle, L., Giovanoli, R. and Jaeger, P., 1995. Simultaneous measurement of calcium oxalate crystal nucleation and aggregation: Impact of various modifiers. *Urological Research,* 23(4), 231-238.

[14] Burns, J.R. and Finlayson, B., 1980. A proposal for standard reference artificial urine in in vitro urolithiasis experiments. *Investigative Urology*, 18(2), 167-169.

[15] Sharifa, A.A., Jamaludin, J., Kiong, L.S., Chia, L.A. and Osman, K., 2012. Anti-urolithiatic terpenoid compound from *Plantago major* Linn. (Ekor Anjing). *Sains Malaysiana*, 41(1), 33-39.

[16] Atmani, F. and Khan, S.R., 2000. Effects of an extract from *Herniaria hirsuta* on calcium oxalate crystallization *in vitro. BJU International* 85(6), 621-625.

[17] Jeong, B.-C., Kwak, C., Cho, K.S., Kim, B.S., Hong, S.K. and Kim, J.-I., 2005. Apoptosis induced by oxalate in human renal tubular epithelial HK-2 cells. *Urological Research,* 33(2), 87-92.

[18] Moriyama, M.T., Miyazawa, K., Noda, K., Oka, M., Tanaka. M. and Suzuki, K., 2007. Reduction in oxalate-induced renal tubular epithelial cell injury by an extract from *Quercus salicina* Blume/*Quercus stenophylla* Makino. *Urological Research*, 35(6), 295-300.

[19] Mosmann, T., 1983. Rapid calorimetric assay for cellular growth and survival: application to proliferation and cytotoxicity assays. *Journal of Immunological Methods*, 65(1-2), 55-63.

[20] Verkoelen, C.F., Romijin, J.C., de Bruijn, W.C., Boeve, E.R., Cao, L.-C. and Schroder, F.H., 1995. Association of calcium oxalate monohydrate crystals with MDCK cells. *Kidney International*, 48, 129-138.

[21] Nirmaladevi, R., Jayaraman, U.C., Gurusamy, A., Kalpana, S. and Shirinidhi, R.T., 2013. Evaluation of *Aerva lanata* flower extract for its antilithiatic potential in vitro and in vivo. *International Journal of Pharmacy and Pharmaceutical Science Research*, 3(2), 67-71.

[22] Byahatti, V.V., Pai, K.V. and D'Souza, M.G., 2010. Effect of phenolic compounds from *Bergenia ciliata* (Haw.) Sternb. leaves on experimental kidney stones. *Ancient Science of Life*, 30(1), 14-17.

[23] Kaur, T., Bijarnia, R.K., Singla, S.K. and Tandon, C., 2009. Purification and characterization of an anticalcifying protein from the seeds of *Trachyspermum ammi* (L.). *Protein and Peptide Letter*, 16, 173-181.

[24] Beghalia, M., Ghalem, S., Allali, B., Belouatek, A. and Marouf, A., 2007. Effect of herbal extracts of *Tetraclinis articulata* and *Chamaerops humilis* on calcium oxalate crystals *in vitro. Gomal Journal of Medical Sciences*, 5(2), 55-58.

[25] Aggarwal, A., Tandon, S., Singla, S. and Tandon, C., 2010. Reduction of oxalate-induced renal tubular epithelial (NRK-52E) cell injury and inhibition of calcium oxalate crystallization *in vitro* by aqueous extract of *Achyranthes aspera. International Journal of Green Pharmacy*, 31, 159-164.

[26] Xiang-Bo, Z., Zhi-Ping, W., Jian-Min, D., Jian-Zhong, L. and Bao-liang, M., 2005. New chemolysis for urological calcium phosphate calculi-a study *in vitro. BMC Urol*ogy, 5, https://doi.org/10.1186/1471-2490-5-9

[27] Chungde, V.H., Kulkarni, C.G., Jadhav, P.H., Dhekale, P.S. and Satyajeet, S., 2012. Urinary calculi dissolving activity of Indian herbs-an *in vitro* Study: a step towards rationalization. *Research Journal of Pharmaceutical, Biological and Chemical Sciences*, 3(4), 1001-1007.

[28] Banu, N. and Pavithra, S., 2015. Anticarcinogenic effect of chlorophyllin from *Morinda citrifolia* L. on HEPG2 cells. *International Journal of Pharma and Bio Sciences*, 6, 145-159.

Current Applied Science and Technology Vol. 21 No. 2 (April-June 2021)

Evaluation of Nutrient Contents, Antioxidant and Antimicrobial Activities of Two Edible Mushrooms Fermented with *Lactobacillus fermentum*

Clement Olusola Ogidi[1]* and Racheal Bukola Agbaje[2]

[1]Biotechnology Unit, Biological Sciences, Kings University, Odeomu, Nigeria
[2]Department of Food Science and Technology, Rufus Giwa Polytechnic, Owo, Nigeria

Received: 15 May 2020, Revised: 22 September 2020, Accepted: 7 October 2020

Abstract

In this study, the edible mushrooms; *Termitomyces robustus* and *Pleurotus ostreatus* were fermented with lactic acid bacterium. The proximate composition, minerals, amino acids and fatty acids of unfermented and lacto-fermented mushrooms (mushrooms fermented with *Lactobacillus fermentum*) were revealed. The free radical scavenging and antimicrobial activities of ethanolic extracts from the mushrooms were carried out. The protein content of *P. ostreatus* and *T. robustus* fermented with *L. fermentum* increased ($p<0.05$) up to 17.7±1.9% and 10.4±0.4%, respectively. The crude fiber (7.8±0.0%) and total carbohydrates (76.6±7.9%) in lacto-fermented *T. robustus* as well as crude fiber (9.0±0.6%) and total carbohydrates (67.3±8.4%) in lacto-fermented *P. ostreatus* were reduced ($p<0.05$) when compared to unfermented mushroom samples. Lacto-fermented *P. ostreatus* had the highest valine content of 11.1±0.2 mg/100 g mushroom, while palmitic acid was found to be the most abundant saturated fatty acids (SFA) with 23.0±2.1 % in lacto-fermented *T. robustus*. The phenolic content of the studied mushrooms ranged from 5.6±0.0-7.8±0.0 mg GAE/g extract, while flavonoid was within 3.1±0.0 - 4.9±0.1 mg QE/g extract. The scavenging activity of the unfermented and lacto-fermented mushrooms against DPPH ranged from 62.8±6.8% to 91.3±10.2%. The extracts from lacto-fermented mushrooms showed better zones of inhibition ranging from 5.0±0.0 mm to 12.5±0.7 mm against tested isolates. The research suggests that the probiotic fermentation of mushrooms is a food processing method that can be adopted to enhance nutritional and functional properties of edible mushrooms.

Keywords: fermentation; preservatıon; lactic acid; fatty acid; amino acid
DOI 10.14456/cast.2021.23

*Corresponding author: Tel.: (+234)7033830019
E-mail: clementogidi@yahoo.com

1. Introduction

Edible mushrooms are often regarded as vegetables or meat substitutes due to their culinary usage [1]. Mushrooms are commonly consumed as popular dishes and are frequently used as partial substitutes for red meat due to their attractive sensory attributes like flavour, texture, aroma and taste [2]. Edible mushrooms are highly appreciated and in demand for human consumption due to the significant amounts of nutrients [3]. Nutritional excellence and biological activities of edible mushrooms contribute to their efficacious uses as fresh ingredients in soups, salads, sauces, stuffing and meat dishes, and to their inclusion as value-adding ingredients into novel products like pickles, chips, paste, soup-powder formulation, ketchup, pâté, noodles and pasta, biscuits, and nuggets [4, 5].

Mushrooms are widely consumed and can be eaten in various processed forms following different innovative and unconventional food processing methods like drying, frying, canning, salting, blanching, and freezing [5]. In recent times, some traditional methods have been adopted to preserve wild-grown and cultivated edible fungi [6, 7]. Lactic fermentation is a simple food biotechnological approach to preserve, to enhance the nutritional quality and improve functional properties of mushrooms. The studies of Jabłonska-Rys *et al*. [8] and Liu *et al*. [9] reported the effect of lactic acid bacteria (LAB) fermentation on the nutritional and functional activities of edible mushrooms. Mushrooms such as *Lenzites quercina, Lactarius deliciosus*, *Boletus edulis*, *Suillus luteus*, *Armillaria* spp., *Leccinum* spp., *Paxillus* spp., *Cantharellus cibarius, Amanita muscaria, Russula* spp., *Ganoderma* spp., *T. robustus*, *Flammulina velutipes*, *Agaricus bisporus, Pleurotus* spp. and certain members of the genus of *Tricholoma* were reportedly fermented to improve their nutritional profiles and their free radical scavenging and antimicrobial properties [10, 11]. Hence, edible macrofungi are very good sources of bioactive constituents and are increasingly used as functional foods, dietary supplements, and traditional medicines [12].

Lactic fermentation expedites food preservation and renders food products resistant to microbial spoilage due to the availability of naturally occurring secondary metabolites. Thus, it provides foods with attractive organoleptic qualities and longer shelf life [13]. The presence of viable LAB and their secreted metabolites in fermented foods enhances the health-promoting properties of the final product [14]. On this note, lactic fermentation is widely available and acceptable as a cheap technique that can be adopted for various types of food processing [15]. Hence, there is a need for more research about nutritional composition and functional potentials of certain mushrooms fermented via lactic fermentation. In this study, the nutrient contents, free radical scavenging and antimicrobial potentials of *T. robustus* or and *P. ostreatus* fermented with *L. fermentum* were investigated.

2. Materials and Methods

2.1 Chemical reagents

Folin-Ciocalteu's-reagent, 1,1-diphenyl-2-picrylhydrazyl (DPPH), butylated hydroxytoluene (BHT), gallic acid, quercetin, and dimethyl sulfoxide (DMSO) were products of Sigma-Aldrich (Steinheim, Germany); trichloro acetic acid, hydrogen peroxide (H_2O_2) were from Acros Organics (Geel, Belgium); deoxyribose, aluminium trichloride, and ethylenediaminetetraacetic acid (EDTA) were from Amresco (Ohio, USA); sodium carbonate (anhydrous), chloroform, and methanol were from Univar (Downers Grove, IL, USA), boron trifluoride, Fatty Acid Methyl Ester (FAME) Standards (C_4-C_{22}) were from Sigma-Aldrich (Saint Louis, MO, USA). All the reagents used during this study were of analytical grade.

2.2 Source of microorganisms

Termitomyces robustus and *Pleurotus ostreatus* were harvested from a farmland in Akure, Nigeria. *Lactobacillus fermentum* was isolated from a locally fermented cereal food (Ogi) using standard microbiological techniques described by Cheesbrough [16] and identified according to Cowan *et al*. [17]. The indicator microorganisms were Methicillin Resistant *Staphylococcus aureus* (MRSA), *Escherichia coli*, *Shigella dysenteriae*, *Pseudomonas aeruginosa*, *Candida troplicalis* and *Candida albicans*. The microorganisms were obtained from Nigeria Institute of Medical Research (NIMR), Lagos. The microorganisms were maintained at -4^{o}C until they were needed for the experimental study.

2.3 Fermentation of mushrooms and extract preparation

The fermentation procedure reported by Liu *et al*. [9] with a little modification was adopted. Briefly, freshly harvested mushrooms were cleaned with 75% v/v alcohol and rinsed with sterile distilled water. The mushrooms were blanched in boiling water at 96^{o}C for 4 min. The pre-treated mushrooms (500 g each) were placed in 2000 ml glass jars followed by the addition of 2% w/w NaCl and 3% sucrose at a solid-liquid ratio of 2:1 (w: v). The starter culture (*L. fermentum*) was adjusted to 10^5 cfu/ml and mixed with the prepared samples. The mixtures were incubated at 20±2^{o}C for 14 days in 3.5 l anaerobic culture jar (Sigma-255, Sigma Scientific Glass Company, India). Thereafter, the mushroom samples were freeze dried at -65±3^{o}C using a vacuum freeze dryer (FD-10-MR, Xiangtan Xiangyi Instrument Ltd, China) until constant weight was achieved. Then, the unfermented and lacto-fermented mushroom powder (100 g) samples were separately soaked in ethanol (1000 ml of 95% v/v) for 48 h. Thereafter, the samples were filtered with Whatman No. 1 filter paper. The filtrates were concentrated in a rotary evaporator (RE-52A, UNION Laboratories, England) and lyophilized. The extracts obtained were re-dissolved in 0.1 % v/v DMSO prior to further analysis.

2.4 Proximate and mineral analysis of mushrooms

The proximate composition like moisture, ash, crude fiber, protein, fat, total carbohydrates the mineral content of unfermented and lacto-fermented mushrooms were carried out according to the methods of Association of Official Analytical Chemists [18]. Minerals were analyzed by using mushroom ash obtained at 600^{o}C. The ash (1.0 g) was digested in 5 ml of HCl and 2 ml of 5 % v/v lanthanum chloride, boiled, filtered and made up to standard volume with deionized water. Atomic Absorption Spectrometer (Buck Scientific, Model 200, Inc. East Norwalk, Connecticut, U.S.A) was used at the appropriate wavelength to determine minerals; Zn, Fe, Ca, Mg, Na, and K. In order to determine Na and K contents in mushroom samples, a flame photometer (Jenway PFP 7, Staffordshire, UK) was used.

2.5 Determination of amino acids and fatty acids in mushrooms

The unfermented and lacto-fermented mushrooms (2.0 g) were defatted with chloroform: methanol (1:1v/v) in a Soxhlet apparatus equipped with a thimble. Defatted mushrooms (40 mg) were weighed into glass ampoules followed by the addition of 7.0 ml of 6 M HCl. Nitrogen gas was passed into each ampoule to expel oxygen, which can cause oxidation of amino acid during hydrolysis. After sealing the ampoules, they were put in an oven at 105±3^{o}C for 22 h and cooled to remove humins through filtration. Filtrate obtained was concentrated at 40^{o}C in a rotary evaporator, and the residue was dissolved with acetate buffer (5 ml), stored in a specimen bottle

and kept at 4ºC. The amount of hydrolysate loaded was between 5-10 μl and each aliquot was dispensed into the cartridge of the analyzer. Technicon Sequential Multisample (TSM-1 Technicon Instruments Company Ltd, Basingstoke, UK) was used to analyze free acidic, neutral and basic amino acids of the hydrolysate for 76 min. The net height of chromatogram peak representing an amino acid was measured. The approximate area of each peak was obtained by multiplying height with width at half-height [19]. The fatty acids of mushroom samples were determined by the trans-esterification method described by Stojković *et al*. [20]. Briefly, fat extracted from the mushrooms was esterified with 0.5 M KOH in methanol (3.4 ml) for 5 min at 95°C. After neutralizing the mixture with 0.7 M HCl, 3 ml of boron trifluoride (14%) in methanol was added and heated for 5 min at 90 °C. To obtained Fatty Acid Methyl Esters (FAMEs), each mixture was extracted with *n*-hexane three times and concentrated to 1 ml. From concentrated sample, 1 µl was injected into gas chromatography (GC-2010, Shimadzu, Japan) with auto injector (AOI) and capillary column (BPX-70). Quantification of FAMEs was achieved using a mix standard (C_4-C_{22}). The concentration and area of each peak of FAMEs was computed using GC post-run analysis software (Shimadzu, Japan).

2.6 Total phenolic content in mushroom extracts

Total phenolic content in extracts from the unfermented and lacto-fermented mushrooms was determined using the method of Singleton *et al*. [21]. Briefly, 2.5 ml of 10% Folin-Ciocalteu's reagent was mixed with the extract (0.5 ml). After 2 min, 2 ml of 7.5% sodium carbonate was added. The blank contained all the reaction reagents except the mushroom extract. The solution was incubated for 1 h at 25ºC. Thereafter, absorbance was measured at 765 nm and compared to a gallic acid calibration curve. Total phenols were determined as gallic acid equivalents from a standard curve, which was prepared with a calibration range of 0-100 µg/ml (coefficient of determination R^2=0.9941) and the results were expressed as mg of gallic acid equivalents (GAE)/g of extract).

2.7 Flavonoid content in mushroom extracts

The total flavonoid content of the extracts from the unfermented and lacto-fermented mushroom was determined using aluminum chloride method described by Meda *et al*. [22]. Mushroom extract (0.5 ml) and 0.5 ml of methanol were mixed with 0.1 ml of 10% w/v aluminum trichloride ($AlCl_3$), followed by 0.5 ml of potassium acetate (1.0 M) and 1.4 ml of distilled water. Each solution was incubated at 28ºC for 30 min. Absorbance was taken at 415 nm in a spectrophotometer. Quercetin was used to prepare a standard curve. The concentration of total flavonoids in mushroom samples was calculated as equivalent of quercetin (mg Quercetin (QE)/g extract).

2.8 Ferric reducing property of mushroom extracts

The reducing power of the unfermented and lacto-fermented mushroom was determined by assessing the ability of extracts to reduce $FeCl_3$ solution as described in the studies of Oyaizu [23]. Extract (2.5 ml) of each sample was mixed separately with 2.5 ml of 200 mM sodium phosphate buffer and potassium ferricyanide (2.5 ml of 1%). After incubation of the mixture at 50ºC for 20 min, 2.5 ml of 10% trichloroacetic acid was added and centrifuged. Each resulting supernatant, after centrifugation at 650 rpm for 10 min, was mixed with an equal volume of water and 1 ml of 0.1% ferric chloride. Absorbance was measured at 700 nm. Ascorbic acid at various

concentrations was used to prepare calibration curve and the reducing property of each extract was expressed in mg of Ascorbic Acid Equivalent (AAE) per g of extract.

2.9 DPPH scavenging activity of mushroom extracts

The free radical scavenging ability of the mushroom extracts against DPPH (1, 1-diphenyl-2-picryhydrazyl) was determined using the method described previously by Gyamfi *et al*. [24]. Each extract (0.1 ml) was mixed with 1.0 ml of 0.4 mM DPPH in methanol. The mixture was then incubated at 29°C for 30 min in the dark. Butylated hydroxytoluene (BHT) was used as a positive control and absorbance was measured at 517 nm using a UV-visible spectrophotometer. The capacity of free radical scavenging was calculated using the following equation:

Scavenging activity (%) = {(A control –A sample) / A control} x 100%

2.10 Scavenging ability of mushroom extracts on hydroxyl radical

The scavenging potential of the mushroom extracts against hydroxyl radical was assessed using the method of Halliwell *et al*. [25]. The reaction mixture containing an aliquot of each extracts (0.1 ml) or standard, 20 mM deoxyribose (120 µl), 0.1 M phosphate buffer (400 µl), 20mM hydrogen peroxide (40 µl), 500 µM $FeSO_4$ (40 µl), and the volume was made up to 800 µl with distilled water. The reaction mixture was incubated at 37°C for 30 min. Thereafter, 0.5 ml of trichloro acetic acid (2.8%) was added, followed by 0.4 ml thiobarbituric acid (0.6%). The mixture was heated for 20 min and cooled. The absorbance of solution was measured at 532 nm in spectrophotometer.

Scavenging activity (%) = {(Ab – As)/ Ab} × 100

Where Ab is absorbance of blank and As is absorbance of the sample at 532 nm.

2.11 Nitric oxide radical scavenging assay

The scavenging activity of the mushroom extracts against nitric oxide was performed according to the method described by Jagetia and Baliga [26]. Sodium nitroprusside (1.0 ml) in 0.5 mM phosphate buffer saline was mixed with extract (100 µl). The mixture was incubated at 25°C for 48 h. Thereafter, 1.0 ml of aliquot solution was mixed with 1.0 ml of Griess reagent containing 1% sulphanilamide, 2% o-phosphoric acid and 0.1% naphthyl ethylenediamine dihydrochloride. After incubating the solution at 34°C for 30 min, absorbance was recorded at 546 nm and scavenging activity was calculated using:

NO Scavenging activity (%) = {(A control –A sample) / A control}x 100%

2.12 Antimicrobial activity of mushroom extracts

The antimicrobial activity of the extracts was tested against microorganisms using the agar well diffusion method [16]. Briefly, the microorganisms were cultivated on nutrient broth or potatoes dextrose broth for bacterial or fungi at 37°C for 24 h and 25°C for 48 h, respectively. The inoculum size was adjusted to 0.5 McFarland turbidity standard at 600 nm using a visible spectrophotometer. A sterile swab stick was moistened with inoculum and spread on Mueller Hinton agar. Subsequently, wells of 4 mm diameter were bored into the agar medium and filled with 50 µl of 50 mg/ml of crude extract. Amoxicillin and ketoconazole were used as positive control against bacteria and fungi, respectively, while sterile distilled water served as a negative control. The plates were incubated at 37°C for 24 h and 25°C at 48-72 h for fungi and bacteria,

respectively. After incubation, zones of inhibition were measured and recorded in millimeters (mm).

2.13 Statistical analysis

Data from the experimental study were reported as mean ± standard deviation (SD) of replicates (n=3). Data were subjected to One-way Analysis of Variance (ANOVA) using SPSS version 20 software (USA). For all tests, mean values were compared by Duncan's new multiple range test and significance was determined at $p \leq 0.05$.

3. Results and Discussion

Lactic fermentation contributes to nutritional enhancement or dietary significance of various foods, and also improve the shelf life of different foods with possible production of new functional foods with nutraceutical potentials [27, 28]. In this study, the nutritional composition and functional properties of unfermented mushrooms and mushrooms fermented with *L. fermentum* was studied. Table 1 shows the proximate composition and mineral contents of unfermented and lacto-fermented mushrooms. Unfermented and fermented mushrooms have very low fat content, with values ranging from 0.5±0.0 to 1.0±0.0%. This agreed with the findings of Adebiyi *et al.* [29], who reported that fresh *T. robustus* was virtually low in fat, and had no cholesterol. The nutritional benefits of low fat content in commonly consumed mushrooms implies that *P. ostreatus***,** *T. robustus* and their fermented products can be recommended for people with cholesterol related ailments or as a suitable component of body weight management. Reduced fat content was recorded after fermentation of *P. ostreatus* or *T. robustus* with *L. fermentum* with the values of 0.5±0.0% and 0.6±0.0%, respectively. The findings of Khetarpaul and Chauhan (30) revealed that natural fermentation increased the fat content whereas pure culture fermentation involving *Lactobacillus brevis* and *L. fermentum* decreased the fat content of fermented food. Hence, the choice of starter cultures and type of substrates may affect the nutritional composition of fermented foods. In this study, the contents of fat, protein, carbohydrates, crude fiber, fatty acids and amino acids in the studied unfermented and lacto-fermented mushrooms were within the recommended Dietary reference intakes (DRI) by Food and Nutrition Board of the Institute of Medicine [31].

The protein contents of fermented *P. ostreatus* and *T. robustus* with *L. fermentum* increased to 17.7±1.9% and 10.4±0.4% and were significantly different ($p<0.05$) when compared to unfermented *P. ostreatus* and *T. robustus* which have values of 4.7±0.0 % and 6.8±1.0%. The increase in protein content of the lacto-fermented mushrooms could have occurred due to the separation of proteins bound with polysaccharides within the cell wall of mushrooms and could also have occurred in connection with the proteolytic activity of LAB metabolites. Ogidi *et al*. [10] reported that an increase in protein content of fermented *Lenzites quercina* occurred as a result of dissociation of protein bound with polysaccharides at the fungal cell wall. The increased protein content in the lacto-fermented mushrooms could also have been due to the protein-like metabolites (bacteriocins and enzymes) produced by LAB biomass during fermentation. This study found appreciable quantities of crude fiber in unfermented mushrooms, at the level of 11.5±1.6% for *T. robustus* and 13.8±0.0% for *P. ostreatus*, respectively, which were reduced to 7.8±0.0% and 9.0±0.6% in *T. robustus* and *P. ostreatus* fermented with *L. fermentum.* This is an indication that LAB is capable of utilizing mushroom crude fiber to produce other metabolites. The studies of Liang *et al*. [32] revealed that some fermenting microorganisms have the ability to degrade crude fiber of food depending on the food composition. The total carbohydrates of

unfermented and lacto-fermented mushrooms varied from 67.3±8.4 to 78.4±11.0%. The studies of Guillamón *et al.* [33] revealed that carbohydrates are the largest portion (35% to 70%) in fruiting bodies, which are the main ingredient in mushrooms and could serve as a raw material for lactic fermentation. Fungal carbohydrates like -saccharides, sugar alcohols, polysaccharides (glucans), glycogen, and chitin serve as a short-term energy source for the growth of microorganisms [34].

The mineral contents (Na, K, Mg, Ca, Zn and Fe) of unfermented and fermented mushrooms with *L. fermentum* are shown in Table 1. The reduction of Ca and Na contents in fermented mushrooms may have been due to ability of lactic acid organisms to utilize the minerals for their metabolism. Potassium was the most abundant element in *P ostreatus* fermented with *L. fermentum*, having the highest value of 1408.8±40.5 mg/100g, while the potassium concentration in *T. robustus* fermented with *L. fermentum* was 1126.0±30.7 mg/100g. The levels of Fe, Mg and Zn increased in fermented mushrooms. Fermentation has reportedly increased the bioavailability of some minerals like potassium, calcium, phosphorous, magnesium, zinc, and iron. Utilization of carbohydrates, protein and anti-nutrients by microorganisms during fermentation improves mineral contents of fermented products [35, 36]. Calcium, potassium, iron, zinc, and magnesium have been reported with high concentrations in edible mushrooms [37, 38]. These macro- and micro-elements are important in various metabolic and physiological functions in humans, which include regulation or maintaining of cellular functions, acid-base balance, osmotic fluid and oxygen transport in the body, catalysis of metabolic growth and enzyme activities, lowering of blood pressure, and the building of immune systems [39].

Table 1. Proximate (DW%) and mineral (mg/100 g) contents of unfermented and fermented mushrooms with *L. fermentum*

Proximate	***T. robustus***	***P. ostreatus***	**Lacto-fermented *T. robustus***	**Lacto-fermented *P. ostreatus***
Fat	$1.0^{ab} \pm 0.0$	$0.8^{b} \pm 0.0$	$0.6^{c} \pm 0.0$	$0.5^{c} \pm 0.0$
Protein	$6.8^{c} \pm 1.0$	$4.7^{d} \pm 0.0$	$10.4^{b} \pm 0.4$	$17.7^{a} \pm 1.9$
Crude fiber	$11.5^{a} \pm 1.6$	$13.8^{a} \pm 0.0$	$7.8^{b} \pm 0.0$	$9.0^{b} \pm 0.6$
Ash	$2.3^{c} \pm 0.0$	$3.3^{b} \pm 0.0$	$4.6^{a} \pm 0.0$	$5.5^{a} \pm 0.0$
Carbohydrates	$78.4^{a} \pm 11.0$	$77.4^{a} \pm 9.6$	$76.6^{a} \pm 7.9$	$67.3^{b} \pm 8.4$
Na	$3.0^{a} \pm 0.0$	$4.0^{a} \pm 0.0$	$0.6^{b} \pm 0.0$	$0.4^{b} \pm 0.0$
K	$681.0^{d} \pm 20.3$	$884.7^{c} \pm 27.0$	$1126.0^{b} \pm 30.7$	$1408.8^{a} \pm 40.5$
Mg	$442.0^{a} \pm 17.0$	$340.1^{b} \pm 8.1$	$223.3^{c} \pm 11.6$	$458.6^{a} \pm 20.4$
Ca	$103.1^{c} \pm 8.0$	$215.2^{a} \pm 18.2$	$84.0^{d} \pm 9.7$	$164.4^{b} \pm 10.6$
Fe	$346.7^{c} \pm 27.0$	$282.0^{d} \pm 11.5$	$710.7^{a} \pm 21.0$	$583.1^{b} \pm 9.2$
Zn	$208.4^{b} \pm 13.7$	$115.2^{c} \pm 9.3$	$261.2^{a} \pm 8.4$	$210.5^{b} \pm 3.8$

Values are mean±SD of replicates (n=3), values with different alphabets along row are significantly different from each other when $p \leq 0.05$. SD of 0.0 is <0.1.

The amino acids profile of unfermented and lacto-fermented mushrooms is shown in Table 2. Unfermented and lacto-fermented mushrooms contain valuable amino acids. Edible mushrooms contain proteins, having quality more satiating than meat [40]. Fermented mushrooms with *L. fermentum* showed increased levels of both essential and non-essential amino acids. The highest amino acid content found in lacto-fermented *P. ostreatus* was valine (11.1±0.2 mg/100 g mushroom) followed by alanine (10.2 mg/100g mushroom), while lacto-fermented *T. robustus* had the highest value of methionine (10.4 mg/100g mushroom). High concentrations of essential amino acids were found in *Agaricus bisporus*, *A. brasiliensis*, *Flammulina velutipes*, *Lentinula edodes*, *Pleurotus djamor*, *P. eryngii* and *P. ostreatus*, thus indicating that edible mushrooms are a potential and alternative source of amino acids [41]. The use of *L. fermentum* as a starter culture in mushroom fermentation increased amino acids contents. Akabanda *et al*. [42] revealed that different amino acids were secreted when milk was fermented with various single and combined starter cultures (LAB) during production of 'Nunu'. The proteolytic system of LAB with different enzymes such as cell-wall bound proteinase PrtP, aminopeptidases: PepC, PepN and PepM, and proline peptidases: PepX and PepQ, converts proteins to oligopeptides, peptides and then to amino acids [43]. With the presence of these enzymes in LAB, this study evidently showed that the lacto-fermented mushrooms are rich sources of essential and non-essential amino acids.

The fatty acids (%) of unfermented and fermented mushrooms with *L. fermentum* is shown in Table 3. Palmitic acid (C16:0) was the most abundant saturated fatty acid (SFA) in lacto-fermented *T. robustus* with value of 23.0±2.1% and 20.4±0.8% in lacto-fermented *P. ostreatus*, 10.3±1.5% in *P. ostreatus* and 6.0±0.0% in *T. robustus*. Palmitoleic acid (C16:1) is 22.2±2.8% in lacto-fermented *P. ostreatus* and 17.0±1.1% in lacto-fermented *T. robustus*, 21.0±4.2% in *P. ostreatus* and 10.0±1.1% in *T. robustus*. Oleic acid was the most abundant monounsaturated fatty acid (MUFA) with 21.8±4.8% in lacto-fermented *P. ostreatus*, 13.3±0.9% in lacto-fermented *T. robustus*, while in unfermented mushrooms, it was 9.4±0.2% in *P. ostreatus* and 10.4±0.6% in *T. robustus*. The findings of Barros *et al*. [44] and Ribeiro *et al*. [45] revealed fatty acids in some edible mushrooms ranging from 0.03 to 76.50% and 30 to 3175 mg/kg, respectively. The presence of linoleic, oleic and palmitic acids as important fatty acids in human diet is evidence for edible mushrooms being a healthy food. Several edible mushrooms that are nutritionally well-balanced with monounsaturated and polyunsaturated fatty acids are receiving increased attention due to their functionality and nutraceutical potential [46]. Polyunsaturated fatty acids (PUFAs) such as linoleic acid is an essential nutrient required by the body; plays distinctive roles in the structure and function of biological membranes in the retina, central nervous system and in the prevention of cardiovascular diseases [47].

Table 4 shows the total phenolic and flavonoid contents of unfermented and lacto-fermented edible mushrooms. The phenolic contents of 5.6±0.0, 6.4±0.0, 7.1±0.1 and 7.8±0.0 mg GAE/g extract were obtained for *T. robustus*, *P. ostreatus*, *T. robustus* fermented with *L. fermentum*, and *P. ostreatus* fermented with *L. fermentum*, respectively. Lacto-fermented *P. ostreatus* had the highest flavonoid of 4.9±0.1 mg QE/g extract, followed by lacto-fermented *T. robustus* with value of 4.4±0.0 mg QE/g. In the findings of Skąpska *et al*. [48], the total polyphenol content of 12.3 g/kg d.m. and 5.8 g/kg d.m. (expressed as gallic acid) were reported for *Agaricus bisporus* and *P. ostreatus*, respectively. Phenolic content of 67.6 mg GAE/g extract was obtained for fermented *Lenzites quercina*, a wild medicinal mushroom [49] when compared to an unfermented sample. Microbial fermentation is a method that enhances release of bound phenolic compounds through some biological processes like glycosylation, deglycosylation, ring cleavage, methylation, glucuronidation, and sulfate conjugation [50]. The ferric reducing property of the mushroom extracts ranged from 72.8±6.3 to 121.8±10.1 mg AAE/g extract. The scavenging activities of unfermented and lacto-fermented mushrooms against DPPH, HO^- and NO ranged from 62.8±6.8% to 91.3±10.2%, 50.5±5.4 to 80.5±6.1% and 40.3±2.7% to 70.3.6±7.2%,

Table 2. Amino acids (mg/100 g mushroom) of unfermented and lacto-fermented mushrooms

Amino acids	*T. robustus*	*P. ostreatus*	Lacto-fermented *T. robustus*	Lacto-fermented *P. ostreatus*
Alanine	3.0 ^{d} ±0.0	5.5 ^{c} ±0.0	8.6 ^{b} ±0.7	10.2 ^{a} ±0.0
Arginine	2.2 ^{c} ±0.2	3.2 ^{b} ±0.0	6.1 ^{a} ±0.3	6.5 ^{a} ±0.0
Aspartic	2.1 ^{d} ±0.0	5.5 ^{b} ±0.0	4.8 ^{c} ±0.0	7.2 ^{a} ±0.0
Cysteine*	3.0 ^{c} ±0.0	1.8 ^{d} ±0.1	4.9 ^{a} ±0.0	4.1 ^{b} ±0.0
Glutamine	8.1 ^{a} ±0.3	5.9 ^{c} ±0.2	6.8 ^{b} ±0.2	5.0 ^{d} ±0.0
Glycine	4.5 ^{a} ±0.0	3.5 ^{b} ±0.0	1.0 ^{d} ±0.0	2.0 ^{c} ±0.0
Histidine^	0.7 ^{a} ±0.0	0.5 ^{b} ±0.0	0.6 ^{a} ±0.0	0.4 ^{b} ±0.0
Isoleucine*	2.3 ^{b} ±0.2	2.9 ^{b} ±0.4	5.3 ^{a} ±0.2	5.1 ^{a} ±0.0
Leucine*	5.3 ^{b} ±0.0	2.7 ^{d} ±0.0	6.3 ^{a} ±0.0	4.2 ^{c} ±0.0
Lysine*	2.6 ^{c} ±0.0	2.5 ^{c} ±0.0	6.8 ^{b} ±0.2	8.3 ^{a} ±0.8
Methionine*	6.8 ^{bc} ±0.0	6.1 ^{c} ±0.0	10.4 ^{a} ±0.2	8.2 ^{ab} ±1.1
Phenylalanine*	3.6 ^{c} ±0.2	2.6±0.0	6.0 ^{a} ±0.1	6.2 ^{a} ±0.6
Proline	2.5 ^{c} ±0.0	1.2 ^{d} ±0.0	3.8 ^{b} ±0.0	4.5 ^{a} ±0.1
Serine	2.6 ^{b} ±0.0	2.0 ^{b} ±0.0	5.2 ^{a} ±0.0	4.6 ^{a} ±0.0
Threonine*	0.3 ^{d} ±0.0	4.3 ^{bc} ±0.1	5.5 ^{b} ±0.0	7.1 ^{a} ±0.0
Tyrosine*	4.0 ^{b} ±0.0	3.8 ^{b} ±0.0	4.0 ^{b} ±0.0	5.7 ^{a} ±0.0
Tryptophan*	5.1 ^{c} ±0.4	6.2 ^{b} ±0.0	6.3 ^{b} ±0.0	8.6 ^{a} ±0.0
Valine*	5.6 ^{d} ±0.0	7.0 ^{c} ±0.8	9.8 ^{b} ±0.3	11.1 ^{a} ±0.2

^ An indispensable amino acid in human adults according to FAO/WHO/UNU [39]
* Essential amino acids
Values are mean±SD of three replicates (n=3)
Values with different alphabets along row are significantly different from each other when $p \leq 0.05$.
SD of 0.0 is <0.1.

Table 3. Fatty acids (%) of unfermented and lacto-fermented mushrooms

Fatty acids	No. of carbon	*T. robustus*	*P. ostreatus*	Lacto-fermented *T. robustus*	Lacto-fermented *P. ostreatus*
Butyric acid	C4:0	5.9 ^{c} ±0.7	6.8 ^{b} ±0.2	7.0 ^{a} ±0.0	4.0 ^{d} ±0.0
Caproic acid	C6:0	11.0 ^{c} ±2.6	4.8 ^{d} ±0.0	16.0 ^{a} ±2.8	13.0 ^{b} ±1.4
Caprylic acid	C8:0	4.0 ^{d} ±0.0	4.8 ^{c} ±0.0	8.6 ^{b} ±0.9	10.7 ^{a} ±1.2
Capric acid	C10:0	13.4 ^{a} ±0.8	10.1 ^{b} ±0.0	13.0 ^{a} ±1.7	9.4 ^{b} ±0.0
Lauric acid	C12:0	3.0 ^{c} ±0.1	13.0 ^{a} ±2.1	10.7 ^{b} ±2.5	10.4 ^{b} ±0.0
Myristic acid	C14:0	8.0 ^{a} ±0.4	5.0 ^{b} ±0.0	4.5 ^{b} ±0.2	7.0 ^{a} ±0.2
Myristoleic	C14:1	17.0 ^{a} ±3.0	9.4 ^{b} ±0.6	6.0 ^{c} ±0.0	17.3 ^{a} ±1.9
Palmitic acid	C16:0	6.0 ^{d} ±0.0	10.3 ^{c} ±1.5	23.0 ^{a} ±2.1	20.4 ^{b} ±0.8
Palmitoleic acid	C16:1	10.0 ^{d} ±1.1	21.0 ^{b} ±4.2	17.0 ^{c} ±1.1	22.2 ^{a} ±2.8
Margaric acid	C17:0	12.1 ^{a} ±2.6	8.5 ^{b} ±0.1	11.0 ^{a} ±0.9	3.2 ^{c} ±0.0
Stearic acid	C18:0	7.8 ^{b} ±0.3	6.8 ^{c} ±0.0	8.0 ^{b} ±0.0	14.2 ^{a} ±1.1
Oleic acid	C18:1	10.4 ^{c} ±0.6	9.4 ^{c} ±0.2	13.3 ^{b} ±0.9	21.8 ^{a} ±4.8
Linoleic	C18:2	8.3 ^{c} ±0.0	10.6 ^{c} ±1.0	12.6 ^{b} ±0.0	14.4 ^{a} ±1.8
Linolenic	C18:3	9.0 ^{c} ±0.0	15.9 ^{a} ±3.1	9.1 ^{c} ±0.3	11.1 ^{b} ±1.5
Behenic acid	C22:0	4.0 ^{a} ±0.1	2.8 ^{c} ±0.2	4.4 ^{a} ±0.0	3.2 ^{b} ±0.0
Erucic acid	C22:1	1.8 ^{bc} ±0.0	2.1 ^{a} ±0.0	1.6 ^{c} ±0.0	1.9 ^{a} ±0.0
Arachidonic acid	C22:4	3.7 ^{b} ±0.0	1.3 ^{c} ±0.0	6.0 ^{a} ±0.0	3.5 ^{b} ±0.3

Values are mean±SD of replicates (n=3)
Values with different alphabets along row are significantly different from each other when $p \leq 0.05$.
SD of 0.0 is <0.1.

Table 4. Total phenolic, flavonoid contents and FRAP of unfermented and lacto-fermented mushrooms

Extract	Phenol mg GAE/ g of extract	Flavonoid mg QE/g extract	FRAP mg AAE /g of extract
T. robustus	5.6 ^{b}±0.0	3.8 ^{b} ±0.0	72.8 ^{d} ±6.3
P. ostreatus	6.4 ^{b} ±0.0	3.1 ^{c} ±0.0	90.0 ^{c} ±8.1
T. robustus fermented with *L. fermentum*	7.1 ^{a} ±0.1	4.4 ^{ab} ±0.0	102.6 ^{b} ±4.7
P. ostreatus fermented with *L. fermentum*	7.8 ^{a} ±0.0	4.9 ^{a} ±0.1	121.8 ^{a} ±10.1

Values are mean±SD of replicates (n=3), Values with different alphabets along column are significantly different from each other when $p \leq 0.05$. SD of 0.0 is <0.1.

respectively (Figure 1). The scavenging activity of ethanolic extract from lacto-fermented *P. ostreatus* against DPPH were not significantly different ($p<0.05$) when compared to BHT. Jabłonska-Rys *et al.* [8, 51] reported that blanching reduced the phenolic content of edible mushrooms but fermented mushrooms with probiotic strains possessed higher level of phenolic compounds and often displayed better antioxidant activities. The scavenging activity of unfermented and lacto-fermented mushrooms could be attributed to the presence of phenolic compounds in the extracts. Medicinal mushrooms contain many polyphenolic compounds that are able to transfer electrons to free radicals and thereby scavenge free radicals [6]. The synergistic action of bioactive molecules in mushrooms have led to their emerging as pleasing sources of nutraceuticals, antioxidants, anticancer, prebiotic, immune-modulating, anti-inflammatory, anti-viral, antimicrobial, and antidiabetic [52].

The zones of inhibition displayed by ethanolic extracts of unfermented and lacto-fermented mushrooms are presented in Table 5. Extracts from lacto-fermented mushrooms exhibited better inhibition of 5.0±0.0 to 12.5±0.7 mm against tested microorganisms than extracts from unfermented mushrooms, which ranged from 5.5±0.0 to 8.4±0.1 mm. The inhibitory potential of studied extracts against the growth of Gram-negative, Gram-positive and fungi was of great interest. The ability of extracts to inhibit all tested organisms suggests that unfermented and lacto-fermented mushroom contain potential antimicrobial agents. This is an indication that mushrooms contain biologically active compounds that possess antimicrobial properties [53]. In addition, the pronounced inhibition displayed by lacto-fermented mushrooms could be linked to antagonistic metabolites, which are mainly organic acids, hydrogen peroxide, bacteriocins, and reuterin produced by *L. fermentum* [54]. Bacteriocins are small peptides (bioactive proteins) that are ribosomally synthesized by Gram-positive and Gram-negative bacteria with antimicrobial activity [55], and may exert bio-preservative effects on mushrooms. This is in accordance with the findings of Bintsis [56] who reported that bacteriocins produced by LAB during fermentation prevented food spoilage by inhibiting food pathogens. The health benefits of LAB-induced fermentation are attributed to the inhibition of enteropathogenic bacteria, the promotion of safe metabolic activity, improvements in palatability and acceptability of food products as a result of change in texture, flavour, and colour [57].

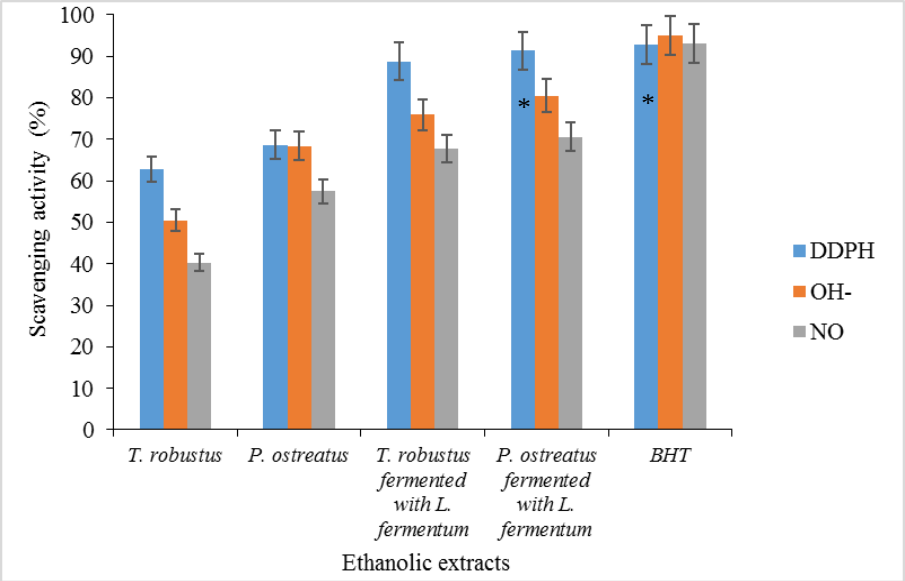

Figure 1. Scavenging activity of unfermented and lacto-fermented mushrooms at 1.0 mg/ml
* Indicates scavenging activity against DPPH were not significantly different from each other at p≤0.05. Error bar is SD.

Table 5. Zones of inhibition (mm) displayed by ethanolic extracts from unfermented and lacto-fermented mushrooms at 50 mg/ml

Extracts	**MRSA**	***E. coli***	***S. dysenteriae***	***P. aeruginosa***	***C. troplicalis***	***C. albicans***
T. robustus	7.4 [b] ±0.0	6.0 [c] ±0.0	8.0 [a] ±0.1	0.0	5.5 [c] ±0.0	0.0
P. ostreatus	8.0[a]±0.0	0.0	8.4[a]±0.1	0.0	0.0	0.0
T. robustus fermented with *L. fermentum*	12.5 [a] ±0.7	7.5 [b] ±0.1	10.0 [b] ±0.4	0.0	7.0 [b] ±0.0	6.0 [c] ±0.0
P. ostreatus fermented with *L. fermentum*	11.7 [a] ±0.9	5.0 [c] ±0.0	11.0 [a] ±1.8	0.0	9.5 [b] ±0.2	5.0 [c] ±0.0
amoxicillin / ketoconazole*	15.0 [a] ±1.2	10.6 [c] ±0.8	14.0 [a] ±2.1	8.0 [d] ±0.0	11.0 [b] ±0.0	12.2 [b] ±0.0

0.0: no zones of inhibition at 50 mg/ml, MRSA: Methicillin resistant *Staphylococcus aureus* and *tested against fungi. Values are mean±SD of replicates (n=3). Values with different alphabets along row are significantly different from each other when p≤0.05. SD of 0.0 is <0.1

4. Conclusions

Mushrooms fermented with *Lactobacillus fermentum* have the highest protein and ash contents. Presence of some essential amino acids and fatty acids as well as minerals in lacto-fermented mushrooms was higher than unfermented mushrooms. Hence, fermented mushrooms, as rich sources of proteins, amino acids, fatty acids, minerals, and antioxidants, can have positive effects on human health. *Lactobacillus fermentum* can be used as a starter culture to ferment edible mushrooms. The results in this study for free radical scavenging and antimicrobial activities indicate that lactic acid fermentation cannot reduce the bioactivity of edible mushroom.

References

[1] Chang, S.-T. and Miles, P.G., 2008. *Mushrooms: Cultivation, Nutritional Value, Medicinal Effect, and Environmental Impact.* 2nd ed. Boca Raton: CRC Press.

[2] Miller, A.M., Mills, K., Wong, T., Drescher, G., Lee, S.M., Sirimuangmoon, C., Schaefer, S., Langstaff, S., Minor, B. and Guinard, J.-X., 2014. Flavor-enhancing properties of mushrooms in meat-based dishes in which sodium has been reduced and meat has been partially substituted with mushrooms. *Journal of Food Science*, 79(9), S1795-S1804.

[3] Feeney, M.J., Miller, A.M. and Roupas, P., 2014. Mushrooms-biologically distinct and nutritionally unique. Exploring a "Third Food Kingdom". *Nutrition Today*, 49(6), 301-307.

[4] Xue, Z., Hao, J., Yu, W. and Kou, X. 2017. Effects of processing and storage preservation technologies on nutritional quality and biological activities of edible fungi: a review. *Journal of Food Process Engineering*, 40(3), https://doi.org/10.1111/jfpe.12437

[5] Diamantopoulou, P.A. and Philippoussis, A.N., 2015. Cultivated mushrooms: preservation and processing. In: Y.H. Hui and E. Özgül Evranuz, eds. *Handbook of Vegetable Preservation and Processing.* Boca Raton: CRC Press, pp. 495-526.

[6] Zhang, K., Pu, Y.-Y. and Sun, D.-W., 2018. Recent advances in quality preservation of postharvest mushrooms (*Agaricus bisporus*): A review. *Trends in Food Science and Technology*, 78, 72-82.

[7] Zheng, H.-G., Chen, J.-C. and Ahmad, I., 2018. Preservation of king oyster mushroom by the use of different fermentation processes. *Journal of Food Processing and Preservation*, 42(1), https://doi.org/10.1111/jfpp.13396

[8] Jabłonska-Rys, E., Sławnska, A. and Szwajgier, D., 2016. Effect of lactic acid fermentation on antioxidant properties and phenolic acid contents of oyster (*Pleurotus ostreatus*) and chanterelle (*Cantharellus cibarius*) mushrooms. *Food Science and Biotechnology*, 25(2), 439-444.

[9] Liu, Y., Xie, X-X., Ibrahim, S.A., Khaskheli, S.G., Yang, H., Wang, Y-F. and Huang, W., 2016. Characterization of *Lactobacillus pentosus* as a starter culture for the fermentation of edible oyster mushrooms (*Pleurotus* spp.). *LWT - Food Science and Technology*, 68, 21-26.

[10] Ogidi, C.O., Oyetayo, V.O., Akinyele, B.J., De Carvalho, C.A. and Kasuya, M.C.M., 2018. Food value and safety status of raw (unfermented) and fermented higher basidiomycetes, *Lenzites quercina* (L) P. Karsten. *Preventive Nutrition and Food Science*, 23(3), 228-234.

[11] Jabłonska-Rys, E., Skrzypczak, K., Sławnska, A., Radzki, W. and Gustaw, W., 2019. Lactic acid fermentation of edible mushrooms: tradition, technology, current state of research: a review. *Comprehensive Reviews in Food Science and Food Safety*, 18(3), 655-669.

[12] Lu, H., Lou, H., Hu, J., Liu, Z. and Chen, Q., 2020. Macrofungi: a review of cultivation strategies, bioactivity, and application of mushrooms. *Comprehensive Reviews in Food Science and Food Safety*, 19(5), 2333-2356.

[13] Singh, V.P., 2018. Recent approaches in food bio-preservation - a review. *Open Veterinary Journal*, 8(1), 104-111.
[14] Rhee, S.J., Lee, J.-E. and Lee, C.-H., 2011. Importance of lactic acid bacteria in Asian fermented foods. *Microbial Cell Factories*, 10, https://doi.org/10.1186/1475-2859-10-S1-S5
[15] Petrova, P. and Petrov, K. 2020. Lactic acid fermentation of cereals and pseudocereals: ancient nutritional biotechnologies with modern applications. *Nutrients*, 12(4), 1118, https://doi.org/10.3390/nu12041118
[16] Cheesbrough, M., 2006. *District Laboratory Practices in Tropical Countries Part 2*. 2nd ed. Cambridge: Cambridge University Press.
[17] Cowan, S.T., Feltham, R.K.A., Steel, K.J. and Barrow, G.I., 1993. *Cowan and Steel's Manual for the Identification of Medical Bacteria*. 3rd ed. Cambridge: Cambridge University Press.
[18] AOAC, 2012. *Official Methods of Analysis*, 19th ed. Washington D.C.: Association of Official Analytical Chemists.
[19] Spackman, D.H., Stein, W.H. and Moore, S., 1958. Automatic recording apparatus for use in the chromatography of amino acids. *Analytical Chemistry*, 30(7), 1190-1206.
[20] Stojković, D., Reis, F.S., Barros, L., Glamočlija, J., Ćirić, A., van Griensven, L.J.I.D., Soković, M. and Ferreira, I.C.F.R., 2013. Nutrients and non-nutrients composition and bioactivity of wild and cultivated *Coprinus comatus* (O.F. Müll.) Pers. *Food and Chemical Toxicology*, 59, 289-296.
[21] Singleton, V.L., Orthofer, R. and Lamuela-Raventos, R.M., 1999. Analysis of total phenols and other oxidation substrates and antioxidants by means of folin-cioalteau reagents. *Methods in Enzymology*, 299, 152-178.
[22] Meda, A., Lamien, C.E., Romito, M., Milligo, J. and Nacoulma, O.G., 2005. Determination of the total phenolic, flavonoid and proline contents in Burkina Fasan honey as well as their radical scavenging activity. *Food Chemistry*, 91(3), 571-577.
[23] Oyaizu, M., 1986. Studies on product of browning reaction. Antioxidative activities of products of browning reaction prepared from glucosamine. *The Japanese Journal of Nutrition and Dietetics*, 44(6), 307-315.
[24] Gyamfi, M.A., Yonamine, M. and Aaniya, Y., 1999. Free-radical scavenging action of medicinal herbs from Ghana: *Thonningia sanguine* on experimentally-induced liver injuries. *General Pharmacology*, 32(6), 661-667.
[25] Halliwell, B., Gutteridge, J.M.C. and Aruoma, O.I., 1987. The deoxyribose method: A simple 'test-tube' assay for determination of rate constants for reactions of hydroxyl radicals. *Analytical Biochemistry*, 165(1), 215-219.
[26] Jagetia, G.C. and Baliga, M.S., 2004. The evaluation of nitric oxide scavenging activity of certain Indian medicinal plants *in vitro*: a preliminary study. *Journal of Medicinal Food*, 7(3), 343-348.
[27] Achi, O.K. and Asamudo, N.U., 2019. Cereal-based fermented foods of Africa as functional foods. In: J.M. Mérillon, K. Ramawat, eds. *Bioactive Molecules in Food*. Cham: Springer, pp.1527-1558.
[28] Rollán, G.C., Gerez, C.L. and LeBlanc, J.G., 2019. Lactic fermentation as a strategy to improve the nutritional and functional values of pseudocereals. *Frontiers in Nutrition*, 6, 98, https://doi.org/10.3389/fnut.2019.00098
[29] Adebiyi, A.O., Tedela, P.O. and Atolagbe, T.T., 2016. Proximate and mineral composition of an edible mushroom, *Termitomyces robustus* (Beeli) Heim in Kwara State, Nigeria. *American Journal of Food and Nutrition*, 6(3), 65-68.
[30] Khetarpaul, N. and Chauhan, B.M., 1989. Effect of fermentation on protein, fat, minerals and thiamine content of pearl millet. *Plant Foods for Human Nutrition*, 39, 169-177.

[31] Institute of Medicine, 2005. *Dietary Reference Intakes for Energy, Carbohydrate, Fiber, Fat, Fatty Acids, Cholesterol, Protein, and Amino Acids*. Washington, DC: The National Academies Press.
[32] Liang, J., Han, B.-Z., Nout, M.J.R. and Hamer, R.J., 2008. Effects of soaking, germination and fermentation on phytic acid, total and in vitro soluble zinc in brown rice. *Food Chemistry*, 110(4), 821-828.
[33] Guillamón, E., García-Lafuente, A., Lozano, M., D´Arrigo, M., Rostagno, M.A., Villares, A. and Martinez, J.A., 2010. Edible mushrooms: role in the prevention of cardiovascular diseases. *Fitoterapia*, 81(7), 715-723.
[34] Eggleston, G., Finley, J.W., deMan, J.M., 2018. Carbohydrates. In: J.M. deMan, J.W. Finley, W.J. Hurst and C.Y. Lee, eds. *Principles of Food Chemistry*. Cham: Springer, pp. 165-229.
[35] Day, C.N. and Morawicki R.O., 2018. Effects of fermentation by yeast and amylolytic lactic acid bacteria on grain sorghum protein content and digestibility. *Journal of Food Quality*, 2018, https://doi.org/10.1155/2018/3964392
[36] Nkhata, S.G., Ayua, E., Kamau, E.H. and Shingiro, J.B., 2018. Fermentation and germination improve nutritional value of cereals and legumes through activation of endogenous enzymes. *Food Science and Nutrition*, 6(8), 2446-2458.
[37] Falandysz, J. and Borovička, J., 2013. Macro and trace mineral constituents and radionuclides in mushrooms: health benefits and risks. *Applied Microbiology and Biotechnology*, 97(2), 477-501.
[38] Siwulski, M., Mleczek, M., Rzymski, P., Budka, A., Jasińska, A., Niedzielski, P., Kalač, P., Gąsecka, M., Budzyńska, S. and Mikołajczak P., 2017. Screening the multi-element content of *Pleurotus* mushroom species using Inductively Coupled Plasma Optical Emission Spectrometer (ICP-OES). *Food Analytical and Methods*, 10, 487-496.
[39] Keen, C.L., Uriu-Adams, J.Y., Ensuma, J.L. and Gershwin, M.E., 2004. Trace elements/ minerals and immunity. In: M.E. Gershin, P. Nestel and C.L. Keen, eds. *Handbook of Nutrition and Immunity*. Totowa: Humana Press, pp. 117-140.
[40] Hess, J.M., Wang Q., Kraft, C. and Slavin, J.L., 2017. Impact of *Agaricus bisporus* mushroom consumption on satiety and food intake. *Appetite*, 117, 179-185.
[41] Bach, F., Helm, C.V., Bellettini, M.B., Maciel, G.M., Windson, C. and Haminiuk, I., 2017. Edible mushrooms: a potential source of essential amino acids, glucans and minerals *International Journal of Food Science and Technology*, 52 (11), 2382-2392.
[42] Akabanda, F., Owusu-Kwarteng, J., Tano-Debrah, K., Parkouda, C. and Jespersen, L., 2014. The use of lactic acid bacteria starter culture in the production of *Nunu*, a spontaneously fermented milk product in Ghana, *International Journal of Food Science*, 2014, https://doi.org/10.1155/2014/721067
[43] Novik, G., Meerovskaya O. and Savich, V., 2017. *Waste Degradation and Utilization by Lactic Acid Bacteria: Use of Lactic Acid Bacteria in Production of Food Additives, Bioenergy and Biogas*. [online] Available at: https://www.intechopen.com/books/food-additives/waste-degradation-and-utilization-by-lactic-acid-bacteria-use-of-lactic-acid-bacteria -in-production-
[44] Barros, L., Cruz, T., Baptista, P., Estevinho, L.M. and Ferreira, I.C.F.R., 2008. Wild and commercial mushrooms as source of nutrients and nutraceuticals. *Food and Chemical Toxicology*, 46(8), 2742-2747.
[45] Ribeiro, B., de Pinho, P.G., Andrade, P.B., Baptista, P. and Valentao, P., 2009. Fatty acid composition of wild edible mushrooms species: a comparative study, *Microchemical Journal*, 93(1), 29-35.
[46] Sande, D., de Oliveira, G.P., Moura, M.A.F.E., Martins, B.A., Lima, M.T.N.S. and Takahashi, J.A., 2019. Edible mushrooms as a ubiquitous source of essential fatty acids. *Food Research International*, 125, https://doi.org/10.1016/j.foodres.2019.108524

[47] National Research Council (US) Committee on Diet and Health, 1989. *Diet and Health: Implications for Reducing Chronic Disease Risk*. Washington (DC): National Academies Press (US).
[48] Skąpska, S., Owczarek, L., Jasińska, U., Hasińska, A., Danielczuk, J. and Sokołowska, B., 2008. Changes in the antioxidant capacity of edible mushrooms during lactic acid fermentation. *ŻYWNOŚĆ Nauka Technologia Jakość,* 4(59), 243-250.
[49] Ogidi, C.O., Oyetayo, V.O. and Akinyele B.J., 2018. Estimation of total phenolic, flavonoid content and free radical scavenging activity of a wild macrofungus, *Lenzites quercina* (L.) P. Karsten. *Current Research in Environmental and Applied Mycology*, 8(4), 425-437.
[50] Huynh, N.T., Van Camp, J., Smagghe, G. and Raes, K., 2014. Improved release and metabolism of flavonoids by steered fermentation processes: a review. *International Journal of Molecular Sciences*, 15(11), 19369-19388.
[51] Jabłonska-Rys, E., Sławinska, A., Radzki, W. and Gustaw, W., 2016. Evaluation of the potential use of probiotic strain *Lactobacillus plantarum* 299v in lactic fermentation of button mushroom fruiting bodies. *Acta Scientiarum Polonorum, Technologia Alimentaria*, 15(4), 399-407.
[52] Gupta, S., Summuna, B., Gupta, M. and Annepu, S.K., 2019. Edible mushrooms: cultivation, bioactive molecules, and health benefits. In: J.M. Mérillon and K. Ramawat, eds. *Bioactive Molecules in Food*. *Reference Series in Phytochemistry*. Cham: Springer, pp. 1815-1847.
[53] Shen, H-S., Shao, S., Chen, J-C. and Zhou T., 2017. Antimicrobials from mushrooms for assuring food safety. *Comprehensive Reviews in Food Science and Food Safety*, 16 (2), 316-329.
[54] Pancheniak, E.F., Maziero, M.T., Rodriguez-León, J.A., Parada, J.L., Spier, M.R. and Soccol C.R., 2012. Molecular characterisation and biomass and metabolite production of *Lactobacillus reuteri* LPB P01-001: a potential probiotic. *Brazilian Journal of Microbiology*, 43(1), 135-147.
[55] da Costa, R.J., Voloski, F.L.S., Mondadori, R.G., Duval, E.H. and Fiorentini, A.M., 2019. Preservation of meat products with bacteriocins produced by lactic acid bacteria isolated from meat, *Journal of Food Quality*, 2019, https://doi.org/10.1155/2019/4726510.
[56] Bintsis, T., 2018. Lactic acid bacteria: their applications in foods. *Journal of Bacteriology and Mycology*, 6(2), 89-94.
[57] Debabandya, M., Manoj, K.T., Sumedha, D. and Sadvatha, R.H., 2017. Sorghum fermentation for nutritional improvement. *Advances in Food Science and Engineering*, 1(4), 175-195.

Current Applied Science and Technology Vol. 21 No. 2 (April-June 2021)

Harmonic Reduction of a Synchronous Generator in a Wind Energy System

Ameer Aqeel Kamoona[1]*, Ahmed Najm Alfadli[2], Israa Ali Alshabeeb[1] and Ali Salah AlKhafaji[1]

[1]Computer System Department, Babylon Technical Institute, Al-Furat Al-Awsat Technical University, Iraq
[2]Ministry of Education, Al Mothana, Iraq

Received: 16 May 2020, Revised: 29 September 2020, Accepted: 23 October 2020

Abstract

Among the various sources of renewable energy, wind power is one of the fastest growing and most promising sources of electricity in the world, and it is considered as a free energy source. In spite of that, harmonics are regarded as a problem faced by wind system due to its power electronic converters. In general, it is very impotant to provide electricity with less harmonically polluted voltage, so in this paper, the design of a tuned filter that can reduce the total harmonic distortion of a synchronous generator (SG) in wind energy system is proposed. The simulation results show that the proposed design eliminates a 7^{th} harmonic effectively, and the waveform output of voltage and current are in low total harmonic distortion (THD). The proposed design improves the power quality, in addition to the improving of the other factors, resulting in reduced loss of power and enhanced performance under abnormal conditions.

Keywords: wind energy; harmonic reduction; synchronous generator; total harmonic distortion
DOI 10.14456/cast.2021.24

1. Introduction

The demand for energy in the growing society has created a concern in the last decades, especially that the conventional sources of energy are exhaustible rapidly. Therefore, the need has arisen to find alternative sources of energy which must be characterized by several features, such as sustainably and friendly to the environment. Wind energy can be considered as one of the solutions to this problem. Compared with the induction generator, SG has a clear advantage as it does not need a gearbox and a reactive magnetizing current [1]. SG is considered to be one type of variable speed wind turbine generator system. A permanent magnet synchronous generator (PMSG) can be used to create a magnetic field in the SG or used with a traditional field winding. Then, a power electronic converter AC-DC-AC connects the stator to the power grid, and a DC link is supplied energy from the generator output and then inverted to the grid as an ac energy [2].

*Corresponding author: Tel.: (+9647809690812)
E-mail: Amer@atu.edu.iq

One of the main problems with modern variable-speed wind turbines is harmonic. For this reason, harmonics measurements are required by relevant standards. A wave that has a frequency that is a whole number multiple of the fundamental frequency is called harmonic. Some harmonics are even frequencies, for example, 2f, 4f, 6f ... etc. and some are odd harmonics such as 3f, 5f, 7f ... etc. The signal is considered as a perfect sin wave if its energy is at the fundamental frequency. Today, there are many sources for harmonics, load harmonic content differs according to the load type, and each load responds according to the harmonics. Harmonics can cause voltage waveform distortion, which is a biggest problem, since it may lead to a number of defects such as overheating in the transformer, failure of power motors, fuse damage and dysfunction of control system of devices. Furthermore, harmonics may cause mal-operation of the exciting protection system, which in turn can lead to healthy system interruption and make the entire system unstable, unless an extra means for harmonic filtering or blocking is provided and especially for numerical relays [3, 4].

Different applications require high power and quality signal with low harmonics. Therefore, a lot of pervious works conducted on reducing harmonic and enhancing wind system output. Lata and Tiwari [5] used a harmonic filter for wind energy conversation system (WECS) that involved doubly fed induction generator (DFIG) and featured an efficient power electronic interface with harmonic filters to reduce the total harmonic distortion (THD) and improve power quality. Gidwani *et al*. [6] studied the use of an unconventional power electronic interface (UPEI) to reduce the total harmonic distortion (THD) and enhance power quality during disturbances, and hence the models used in the study included a pitch-angled controlled wind turbine model, a DFIG model, a power system model and an UPEI that had controlled converters and was able to increase the effectiveness of the utilization of wind energy. Schwanz *et al*. [7] studied the use of active harmonic filters placed at different locations inside a wind power plant, and the results for current and voltage harmonic distortion were compared and discussed in order to determine the most suitable location for placing active harmonic filters within a wind power plant. This study did not deal with a certain type of wind system. In addition to the above work, Wang and Lu [8] used a C-type filter for a wind or solar power plant harmonic mitigation, and the results showed that a C-type filter reduced harmonics and eliminated natural oscillation frequency, reducing THD and increasing the stability of the power system. Finally, Silva *et al*. [9] studied the use of a grid-side converter (GSC) as an active filter for harmonic filtering through the power control of a permanent magnet synchronous generator (PMSG). Referring to all above studies, passive filters and active filters can be used, and each type has advantages and disadvantages. Passive filters are considered to be cheaper and more practical to use, and smaller in size. So, in this research, we deal with the optimization of passive filters, particularly a single-tuned filter for a wind power plant of the synchronous generator type. The main objective is to analyze harmonics that are present in a wind power system, design passive filters to eliminate or control harmonic distortions, and optimize the filter for various parameters. A harmonic filter has been applied to the output of a wind farm synchronous generator (WFSG) using MATLAB/Simulink environment, and the results show the effectiveness of the experimental system in reducing the THD.

2. Materials and Methods

2.1 Harmonic filters and their effects

Voltage distortion in power systems can be decreased by using three-phase harmonic filters, which can be reflected on the power factor correction. The design of the harmonic filters are capacitive behavior at fundamental frequency, therefore, they produce reactive power. All filter types consist of RLC elements. The value of these elements are determined depending on the filter type and the parameters below:

• Nominal voltage reactive power
• Frequencies of tuning
• Quality factor

The measure of the sharpness for the tuning frequency is called quality factor and is determined by the value of resistance. Until 1980, all loads were considered to be linear except in some applications, like factories, but most items of electrical equipment these day, such as UPS, battery chargers printers, and PCs, have nonlinear loads and create harmonics. In such equipment, the fundamental waveforms and the distorted one have a relationship between them, and can be found by dividing the square root of the sum of the squares of all harmonics produced by an individual load, on the fundamental 50 or 60 Hz waveform value [10]. As explained in the Fast Fourier Transform method, this theorem calculates the (THD) included in nonlinear current or voltage waveforms. When THD is unacceptable, many troubles in sensitive equipment and loads occur. Placing a harmonic filter, which is a low impedance device, in parallel near a harmonics source will reduce the harmonic distortion as it draws harmonic current from harmonic sources in the system and consumes it as heat. Due to the fact that these filters do not have any active component such as transistors or do not need an external source of power, they are called passive filters [11].

2.2 Mathematical analysis for a single-tuned filter

The single-tuned filter is one of the simplest filter, and an optimal design means minimizing the cost of the filters and reduces the total harmonic distortion of currents and voltages. Figure 1 shows a single-tuned filter. The quality and size of the filter can be considered as a main notion in the design of the filter, and the reactive power which is supplied at fundamental frequency, determines the filter size. The filter shows a capacitive characteristics at a frequency that has a value less than tuning frequency.

Figure 1. Single-tuned filter

According to the following equations, the tuning of a single-tuned filter can be achieved to mitigate any harmonic order [12]. The order of tuning harmonic frequency (n) can be calculated from:

$$n = \frac{f_r}{f_1} \tag{1}$$

where $f1$ is a fundamental frequency and fr is the resonance or tuning frequency. The frequency, which causes the LC circuit to resonate is giving by:

$$f_r = \frac{1}{2\pi\sqrt{LC}} \tag{2}$$

where L is inductance of the filter in henry and C is the capacitance of the filter in farad. For any frequency not equal to the resonance frequency, the filter shows high impedance while it shows a low impedance for the resonance frequency. By applying the equation below, it is possible to calculate filter fundamental and harmonic reactive power:

$$Q_f = C\ \omega_f\ V_L^2\ (1-\frac{1}{n^2}) \tag{3}$$

where ω_f is the fundamental value of the angular frequency and measured in (rad/sec), and the reactive power is Qf. C is the capacitance in farad (F) and V_L represents the fundamental value of the line voltage where filter is located and n represents the harmonic order.

For given Qf and using equation (3), the value of C can be computed by:

$$C = \frac{n^2}{n^2+1}\ \frac{Q_f}{\omega_f V_L^2} \tag{4}$$

The maximum value of the frequency deviation must be taken in account in the determining of the tuning frequency in addition to the system characteristics if it is inductive or capacitive. In most cases, tuning frequency is made less than harmonic frequency due to the inductive characteristics of the power system, so the trouble of resonance does not happen. The design cannot control two operators such as system frequency deviation and impedance of the network. The two factors are considered to be in bad conditions. The maximum (ϕm) phase angle and (δm) frequency deviation are utilized in the design of the filter.

$$f_r = f_n + \Delta f = f_n + \delta_m f_n \tag{5}$$

Where, fr and fn are the tuning and harmonic frequency, respectively. δ_m is maximum frequency deviation. The optimum (L) is calculated from equation (2). For minimum value of harmonic voltage, the optimum quality factor Q_{opt} of a filter in resonant case for worst condition is given by:

$$Q_{opt} = \frac{1+\cos(\phi_m)}{2\delta_m \sin(\phi_m)} \tag{6}$$

And the optimum value of (R) can be computed by:

$$R = \frac{X_0}{Q_{opt}} = \frac{1}{Q_{opt}}\sqrt{\frac{L}{C}} \tag{7}$$

where X_o is the resonant reactance of the filter. Normally, higher Q_{opt} is considered for loss reduction. The optimal operation of the frequency band for the filter decides the filter quality (Q), which is the representation for the filter tuning sharpness. Best harmonic suppression, in addition to

harmonic voltage and power losses reduction, can be achieved by a high quality factor which may lead to an increment in the resonance problem between system and filter [13, 14]. The total harmonic distortion block is used in this simulation to measure the total harmonic distortion (THD) of a periodic distorted signal. The signal can be a measured voltage or current. The. THD is defined as the root mean square (RMS) value of the total harmonics of the signal, divided by the RMS value of its fundamental signal, and then multiplied by 100 % as shown in the following equation:

$$\text{THD} = \frac{\sqrt{I_2^2+I_3^2+\cdots I_n^2}}{I_1} \times \quad 100 \tag{8}$$

where I_n is the rms value of the harmonic current wave and I_1 is the rms value of the fundamental current, same equation can be used for voltage signal.

3. Results and Discussion

The proposed filter design has been validated and optimized via experimental tests using test system as shown in Figure 2. All the system components have been simulated in MATLAB/Simulink platform using simulink library blocks as shown in Figure 3. Hence, the system contains a wind farm of 10 MW power output, which consist of five units, each one of 2MW, 575V. The wind farm has been simulated using a MATLAB wind farm block (PMSG), and the wind block configuration parameters are listed in Table 1.

The wind farm block in the simulation as shown in Figure 2 provides measurement for its internal quantities and contains the main parts of the wind system, which are the wind turbine that is synchronous generator type in addition to the 3 stage of conversion. The first stage is through a 3ph diode rectifier which consists of power diodes connected in a bridge configuration that convert the AC generator output to DC in order to make it controllable. The next step is the DC/DC IGBT-based PWM boost converter which steps up the DC output to higher level and passes it to the DC/AC IGBT-based PWM converter, which converts it to the controllable AC output and passes it on to the grid. This design of the system with three stage of conversion is to extract maximum power for a given wind speed. Moreover, these converters are embedded in one block, i.e. “a wind farm block”, and Figure 4 shows the internal content of the block as modeled in the simulink library, which is available as a ready to use unit, so there are limited number of parameters for the user to modify, as in Table 1. The synchronous generator type of wind turbine has the advantage of increasing the output efficiency during low wind speed and reducing the turbine stresses during high wind speed, so it is the most implemented type in wind turbine. The wind farm output power is delivered to the power grid through a 30km transmission feeder of pi configuration with the aid of two step-up transformers, a 575V/ 25kV star/delta and a 25/120 kV delta/star from both sides of wind farm and grid. The earth point that forms the transmission feeder has been provided through a zigzag transformer as shown in Figure 3, and Table 2 provides all the configuration parameters for the previously mentioned equipment, since the transformer's impedances are the same for primary and secondary sides. The filter connection state can be controlled by the circuit breaker.

Two test cases were performed on the system; the first case was done without the filter to analyze the system components and to find out the harmonics content of both voltage and current waveforms which were injected into the system from the wind farm. With the aid of Powergui tool in Matlab/Simulink, as seen in Figure 5, the FFT analysis was performed on voltage and current waveforms at bus 575V to get their harmonic spectrums and THDs and the results are shown in Figures 6 and 7. The first order is the fundamental one and represents the fundamental wave itself.

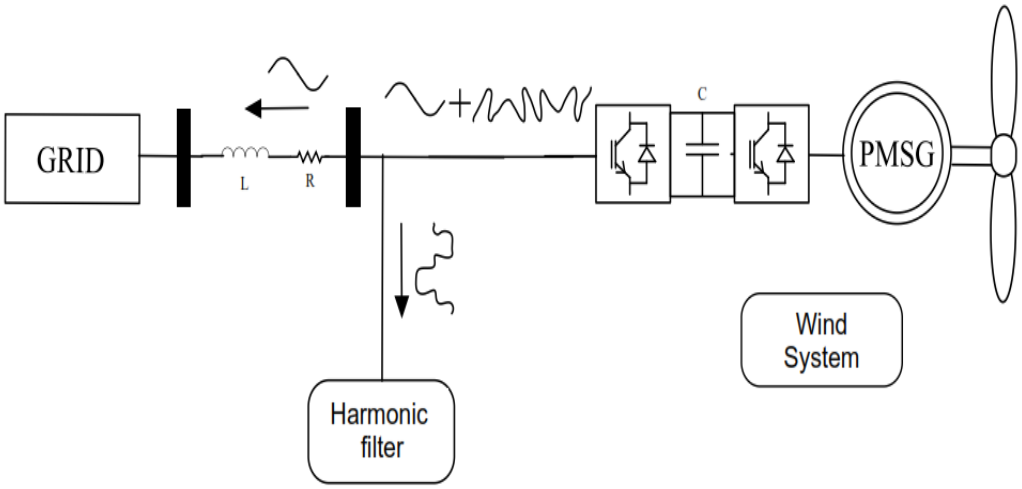

Figure 2. Test system general structure

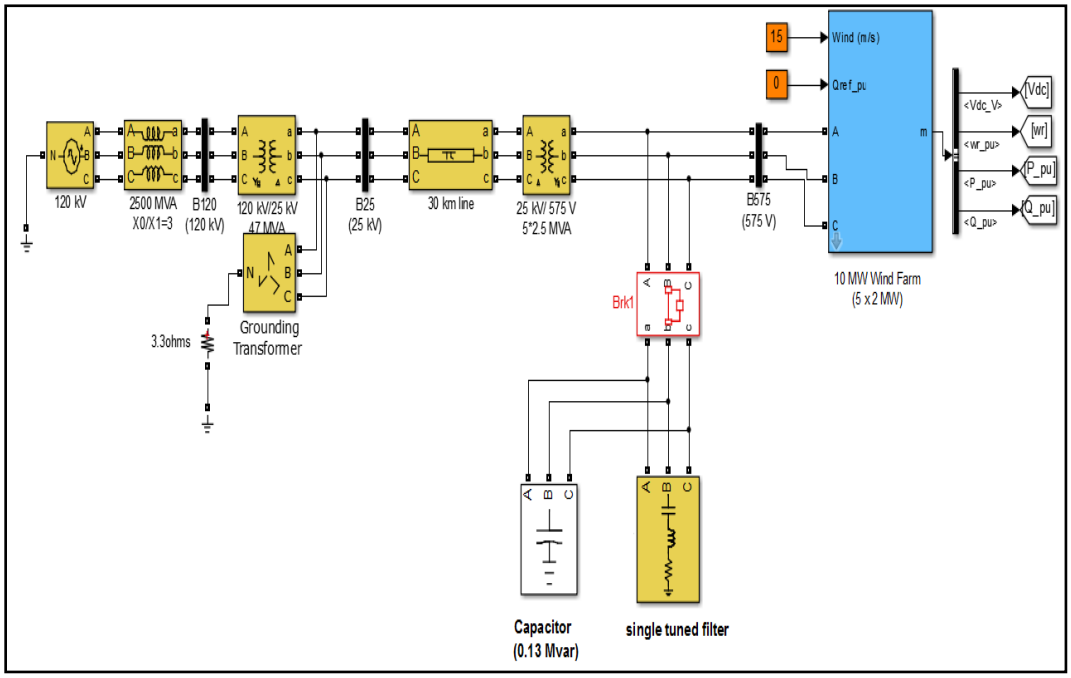

Figure 3. Matlab/Simulink model for the test system with harmonic filter representation

Table 1. Wind farm parameters

Name	Value
Nom. Power VA	10
L-L volt. V	575
Freq. Hz	60
"Controller Parameter"	
Dc bus volt. Reg. gain	1.1, 27.5
Grid-side con. var Reg. gain	0.05
Grid-side con. Volt. Reg. gain	2
Grid-side con. Ct. reg. gains	1, 50
Speed reg. gains	5, 1
Boost inductor Ct. reg. gains	0.025, 100
Pitch controller gain	15
Pitch compensation gains	1.5, 6
"Converter Parameter"	
Grid-side conv. AC Volt. V	575
Grid-side conv. AC Ct. pu	1.1
DC bus Volt. And Capc. V, F	1100, 90000e-6
Boost Conv. Induc. H, Ω	0.0012, 5e-3

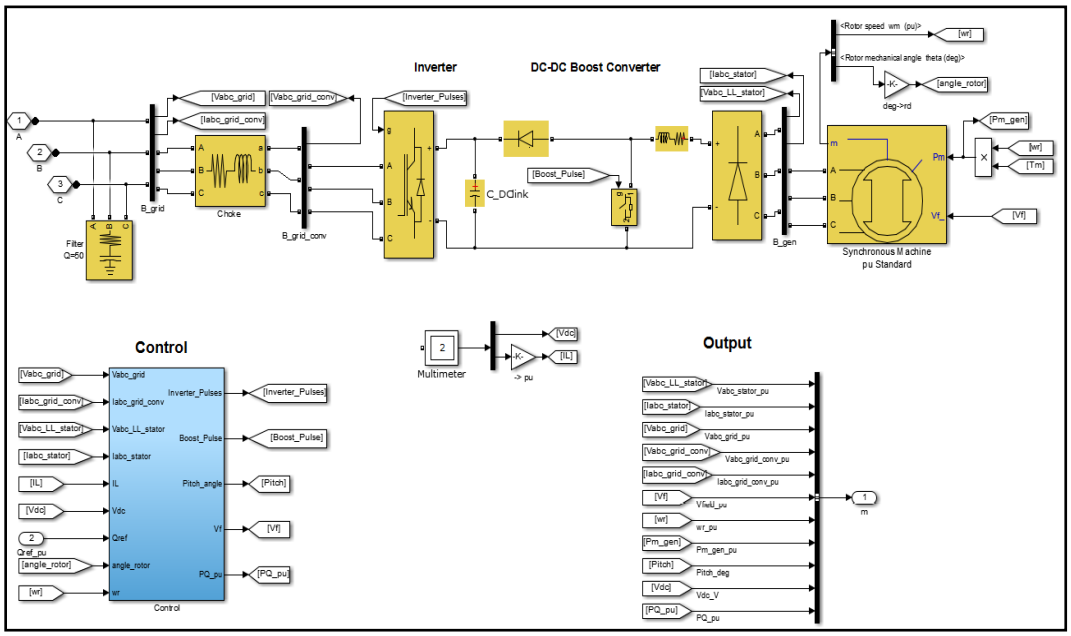

Figure 4. Under mask view for the wind farm block

Table 2. Parameters for equipment at 60 Hz

Equipment	R1	Ro	L1	Lo	C1	Co
Feeder 30 km	0.1153Ω/km	0.413Ω/km	1.05e-3H/km	3.32e-3H/km	11.33e-9F/km	5.01e-9F/km
575V/ 25kV Tr.	8.33e-4pu	----	0.025pu	----	-----	-----
25/120 kV Tr.	0.0026pu	----	0.08pu	----	----	----

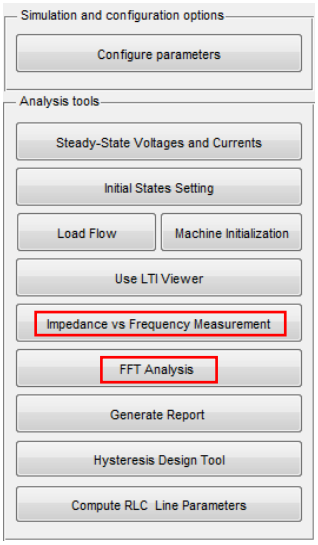

Figure 5. Powergui tools for FFT analysis

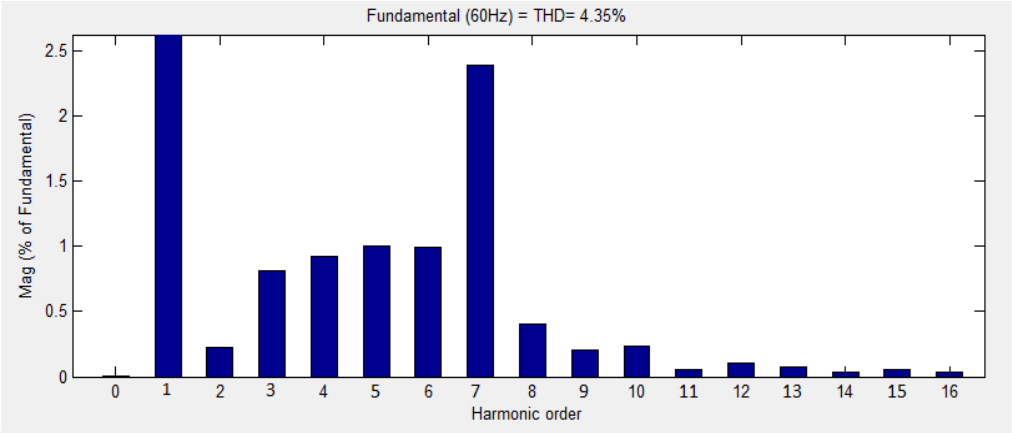

Figure 6. Spectral diagram of AC voltage without filter

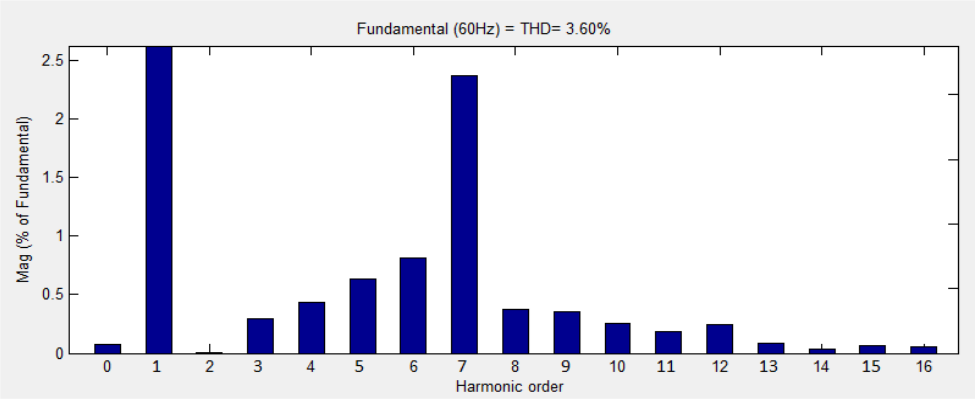

Figure 7. Spectral diagram of AC current without filter

On the other hand, a comparison of the harmonics reveals that the 7th order harmonic is dominant on the spectrum, and its value is shown as a percentage of the fundamental value.

According to the first test, the harmonic filter was designed and optimized using previously presented mathematical analysis equations in order to reduce the effect of the 7th order harmonic. Hence, Figure 8 shows the designed filter impedance vs frequency characteristic and Table 3 includes the parameters used for the filter. The second test case was performed with the filter present in the system to investigate to which extent that the 7th order harmonic could be reduced by the filter, which is assumed to supply 0.8 MVar under normal conditions.

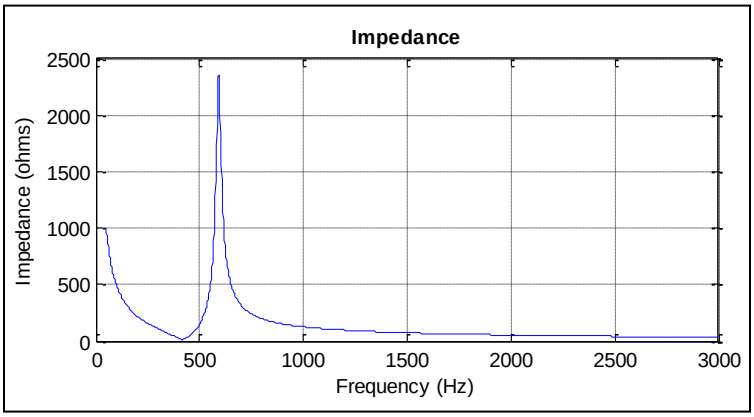

Figure 8. Filter impedance vs frequency characteristic

Table 3. Values of the designed filter

Parameter	Value
C(μf)	6289
L(mH)	0.0229
R(Ω)	0.03
Q	20

Figures 9 and 10 show the FFT analysis for voltage and current waveforms respectively with filter connected to the system. It is clear that all harmonic components fall approximately in the same negligible range. Figure 11 shows a comparison between voltages with and without filter. From the above results, the role of the filter can be noted in reducing harmonic and make voltage smoother.

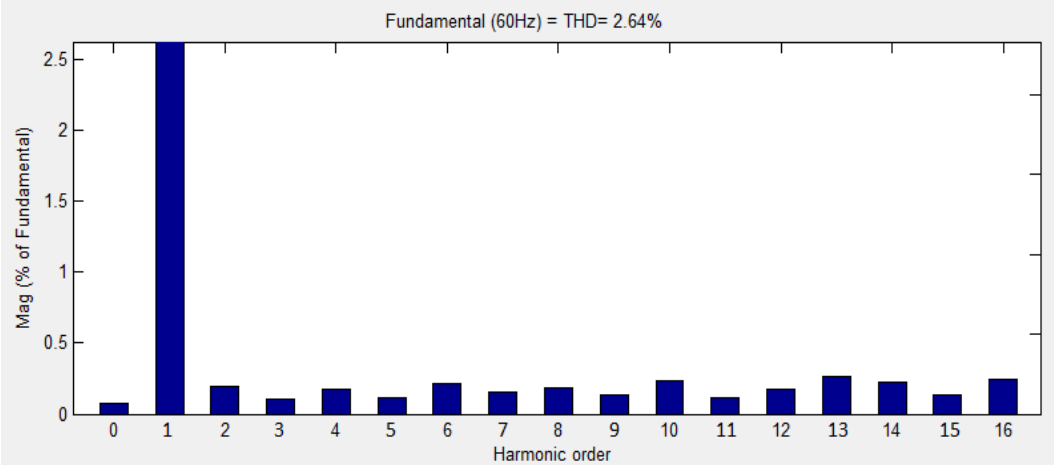

Figure 9. Spectral diagram of AC voltage with filter

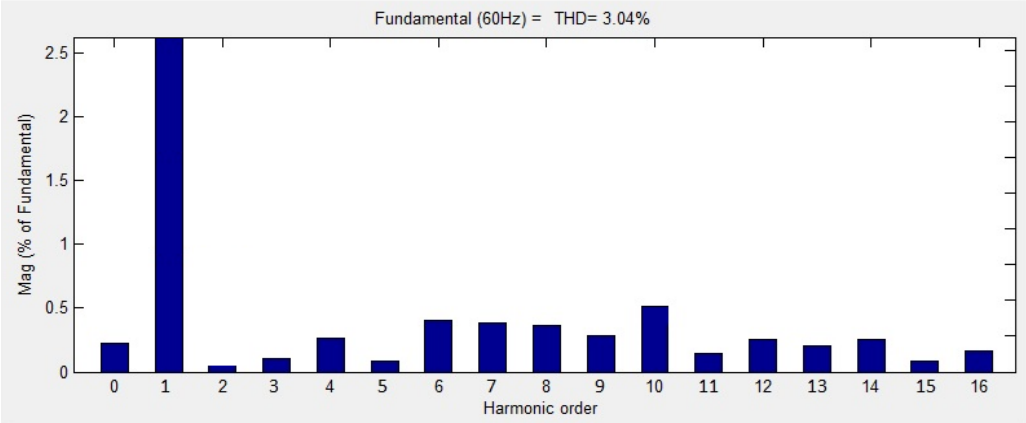

Figure 10. Spectral diagram of AC current with filter

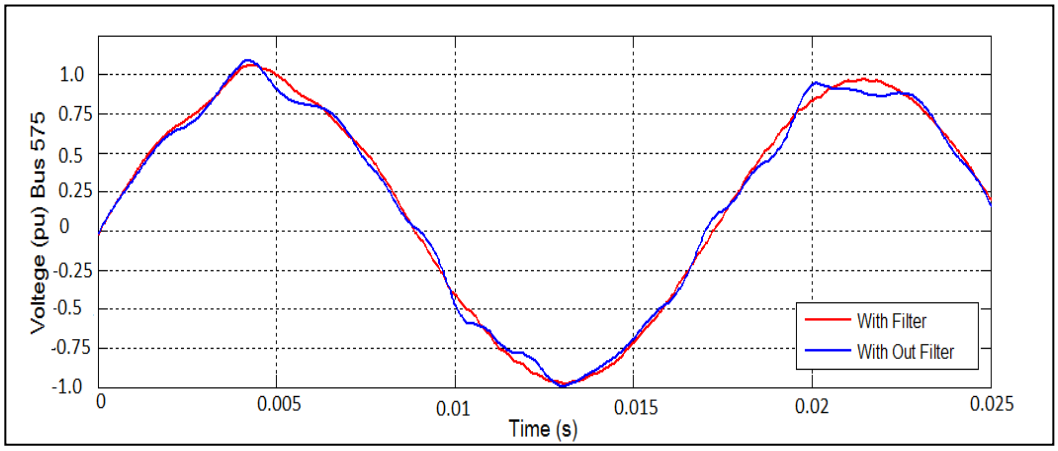

Figure 11. Enlarged scale of voltage (pu) at bus 575

In comparing the results of the two tests cases, form Figures 6 and 9, it can be noted that the 7th order harmonic of the voltage wave has been reduced from 2.16% to 0.17% when expressed as percentage of the fundamental value in the case of filter added. From Figures 7 and 10, it is clear that the 7th order harmonic has been reduced in the output current from 2.39% to 0.4%, expressed as percentage of the fundamental value. In addition, the total harmonic distortion (THD) of the output current and voltage has also been reduced due to the addition of the filter, as shown in Table 4.

Table 4. Summary of simulation results

THD	Without filter	With filter	Percentage of improvement
Voltage wave	4.35%	2.64%	39.3 %
Current wave	3.60 %	3.04%	15.5 %

4. Conclusions

This paper presents an analysis of single-tuned filter connected to a wind farm type synchronous generator (SG) to reduce total harmonic distortion using MATLAB/Simulink software. The single-tuned filter is commonly used because its advantage makes it the best choice in most cases, like simplicity installation and low cost. Single-tuned filters also have some disadvantages such as energy loss and incidence of resonance, but this can be minimized through design by choosing the appropriate value tuning frequency and Q values. The simulation results show that the 7th order harmonic and THD for the output current and voltage of the wind farm can be significantly reduced by the use of the single-tuned filter and also enhances power quality in system. Lastly, the above procedure can be used in different power system to eliminate any harmonic order.

5. Acknowledgements

The authors would like to thank the support from their home institution to finish this work.

References

[1] Ackermann, T., 2005. *Wind Power in Power Systems.* Stockholm: John Wiley & Sons.

[2] Abbas, A.J., 2010. *Optimum Power Extraction from Wind Turbine Generator to the Load*. M.Sc., University of Baghdad.

[3] McGranaghan, M.F. and Mueller, D.R., 1999. Designing harmonic filters for adjustable-speed drives to comply with IEEE-519 harmonic limits. *IEEE Transactions on Industry Applications*, 35(2), 312-318.

[4] Kamoona, A.A., Alfadli, A.N. and Alshabeeb, I.A., 2020. New method for OC relay coordination. *Journal of Electrical and Computer Engineering*, 2020, https://doi.org/10. 1155/2020/6312975

[5] Lata, G. and Tiwari, H.P., 2010. Improving power quality of wind energy conversion system with harmonic filters. *Proceeding of the International MultiConference of Engineers and Computer Scientists*, London, UK, July 4-6, 2011, 1016-1021.

[6] Gidwani, L., Tiwari, H. and Bansal, R.C., 2013. Improving power quality of wind energy conversion system with unconventional power electronic interface. *International Journal of Electrical Power and Energy Systems*, 44(1), 445-453.

[7] Schwanz, D., Bollen, M., Larsson, A. and Kocewiak, Ł.H., 2016. Harmonic mitigation in wind power plants: Active filter solutions. *17th International Conference on Harmonics and Quality of Power (ICHQP)*, Belo, Horizonte, Brazil, October 16-19, 2016, 220-225.

[8] Wang, S.-K. and Lu, C.-Y., 2020. Analysis and design of a C-type filter for a wind or solar power plant. *2020 IEEE 3rd International Conference on Electronics Technology (ICET)*, Chengdu, China, 2020, May 8-12, 2020, 404-408.

[9] Silva, L.P.S., Mota, D.D.V., Ruiz, F.P., Cavalcante, L.R., Medeiros, L.T.P., Teixeira, V.S.C., and Moreira, A.B., 2019. Power control and harmonic current mitigation from a wind power system with PMSG. *2019 IEEE 15th Brazilian Power Electronics Conference and 5th IEEE Southern Power Electronics Conference (COBEP/SPEC)*, Santos, Brazil, December 1-4, 2019, 1-6.

[10] Kaiwart, J. and Raju, U.P.B., 2016. Harmonic mitigation techniques: a review. *International Journal of Advanced Research in Electrical, Electronics and Instrumentation Engineering*, 5(11), 8346-8352.

[11] Kumar, B., 2011. *Design of Harmonic Filters for Renewable Energy Applications*. M.Sc., University of Sweden.

[12] Das, J.C., 2004. Passive filters-potentialities and limitations. *IEEE Transactions on Industry Applications*, 40(1), 232-241.

[13] Turkay, B., 2001. Harmonic filter design and power factor correction in a cement factory. *2001 IEEE Porto Power Tech Proceedings (Cat. No. 01EX502)*, Porto, Portugal, 10-13 Sept. 2001, 4.

[14] Cheng, H., Sasaki, H. and Yorino, N., 1995. A new method for both harmonic voltage and harmonic current suppression and power factor correction in industrial power systems. *Proceedings of 1995 Industrial and Commercial Power Systems Conference*, San Antonio, Texas, USA., 1995, 27.

Current Applied Science and Technology Vol. 21 No. 2 (April-June 2021)

Prediction of Tuber Peeling Rate Based on Classical Particle Removal Theories

Adeshina Fadeyibi*, Rasheed Amao Busari and Olusola Faith Ajao

Department of Food and Agricultural Engineering, Kwara State University, Malete, Nigeria

Received: 24 June 2020, Revised: 24 September 2020, Accepted: 5 November 2020

Abstract

Classical particulate modeling is a mathematical approach that is suitable for describing the behavior of a processing machine because of its ability to accommodate varying degrees of technical parameters. This research was carried out to predict the peeling rate of an existing multi-tuber peeling machine using classical particle removal theories. The machine was designed to peel fresh cassava, sweet potatoes, and cocoyam tubers at a speed range of 350-750 rpm using a selection gear system. The tuber peeling rate were determined over 1-h of machine operation at intervals of 5 min. The classical Weibull and Jennings models, formulated for removing impurities from the outer surface of solids, were used to constitute the models for predicting the peeling rate and the amount of tuber peels removed. The machine was rerun for another 30 min, and the values of the peeling rates and the amount of peels removed were computed and used for the independent validation of the resulting models. Results show a log increase in the peeling rate of the machine with an increase in the residence time and the speed of the machine operation ($p< 0.05$). Also, the Weibull model parameters were better estimator of the peeling rate with $R^2 > 95\%$ and Mean Square Error less than 10%, irrespective of the speed and the residence time of machine operation. Therefore, the models can be used for predicting the peeling rate of the machine within its operating speed limits.

Keywords: classical particle removal theory; multi-tuber peeling machine; peeling rate; Weibull model; Jennings model
DOI 10.14456/cast.2021.25

1. Introduction

Root and tuber crops are essential commodities of human diet all over the world. Almost all the food we eat daily is made of tubers, perhaps because they provide the energy needed for our work. Just like other crops grown in the tropics, the production of root and tuber crops is seasonal [1]. Therefore, the demand and supply of the crops are critical to their availability for processing. But this is usually limited due probably to the limitations in production systems. The general pattern of the supply of root crops from the surpluses of subsistence farming may eventually lead to high

*Corresponding author: Tel.: (+234) 7034867681
E-mail: adeshina.fadeyibi@kwasu.edu.ng

marketing costs for the product. Therefore, the processing of the crops is essential to meet the market availability challenges.

Processing of root and tuber crops can be done either manually or mechanically. Unlike manual processing, the latter is more important because it enhances productivity both in terms of yield and performance. Although the mechanical operations have been successfully applied to the processing of root and tuber crops [2-8], a major issue that remains is the unusually low peeling rate of the technology as depreciation sets in with age [9-11]. Most of these technologies have now become obsolete and unreliable for their intended use. The way to address this is not to design a new working machine, but in modeling the existing machine operations to predict defects and processes for routine maintenance. The mechanism of the mechanical cassava tuber peeling technology has been described by Adetan *et al.* [12], Seth [13] and Olukunle and Akinnuli [14]. The authors developed mathematical models for predicting the peeling efficiency of the cassava peeling machine; and recommended the peeling concept as a reliable tool for studying the behavior of the peeling technology. However, their research was limited in application since the model was specifically developed for the understanding of the concept of the peeling operation of the cassava tuber. Also, their tool was not general and might not be suitable for the understanding of the concept of a multi-tuber peeling machine operation. Asonye *et al.* [15] and Mohammed *et al.* [16] also explained the relationship between the peeling rate and geometry of the peeling operation by developing models. But the peeling behavior predicted was largely empirical and thus not easily scaled-up for industrial applications. There is therefore the need to develop a mathematical model for predicting the peeling rate of tubers in processing. This makes research and validation experiments more straight forward since food products are complex systems that undergo various changes and reactions when processed. The objective of this research was to develop mathematical models for predicting the peeling rate of an existing machine operating at different speeds.

2. Materials and Methods

2.1 Materials and samples preparation

A 30 kg each of the freshly harvested cassava, sweet potato and cocoyam tubers were purchased from the central market in Omuaran Market, Kwara State Nigeria. The produce samples were transported to the Landmark University, Omuaran for experimentation. Initially, the tubers were manually clean with running water to remove mud and clay, and thereafter spread under the sun to dry for 1 h. The tubers were sorted into various categories of different sizes ranging from small, medium, and large to facilitate machine processing.

2.2 Description of existing tuber peeling machine

An existing multi-tuber peeling machine was used to carry out the peeling operation, as shown in Figure 1. A detailed design of the machine has been reported by Fadeyibi and Ajao [2]. The machine consists of a rotating drum, eccentrically placed on a shaft, and powered with a 5 HP electric motor. With the help of a gear system arrangement, the machine was operated at speeds of 350, 550 and 750 rpm. Tubers are fed via the inlet, and the operation began by engaging the gear to the predetermined speed. The peeling force was applied to the tubers by the scraping and scratching action of the rotating perforated wire gauze drum. The peels were discharged through the perforations and collected underneath the machine via a chaff collector bowl. The peeled tubers were then collected via the same inlet opening used for feeding.

Figure 1. Multi-tuber peeling machine [2]

2.3 Evaluation of peeling rate

The peeling rate of the machine can be defined as the mass of the peels obtained divided by the residence time of the machine operation. By engaging the gear to 350 rpm, 20 kg of each of the tubers was fed gently through the opening for inlet made on the peeling drum. The existing peeling machine was operated for a period of 1 h, and the peeling rate was evaluated at intervals al of 5 min. The peeling rate was determined using the expression in equation (1). The procedure was repeated at 550 rpm and 750 rpm, and the peeled products are shown in Figure 2. A total of ten samples of peels each from the cassava, potato and cocoyam tubers were used to constitute the models for predicting the rate of tuber peeling.

$$\dot{m} = \frac{\Delta m}{t} \quad (1)$$

where;
$\dot{m}$ = peeling rate (kg/min)
Δm = mass change in tuber peels (kg)
t = Time taken to peel the required quantity (min)

(a) Sweet potatoes (b) cassava (c) cocoyam

Figure 2. Peeled tubers

2.4 Classical particle removal theory

2.4.1 Modeling based on Weibull model

The removal of peels from tubers is a multiplex procedure that requires adequate details for real practice. To improve the practical peeling procedure, a mathematical model would be helpful [16]. We used the Weibull probability distribution to analyze the data since the data are classified field data with significant variabilities resulting from the influence of the environment and some uncontrolled variables associated with the machine operation [17]. Based on this and according to Calabria and Pulcini [18], we viewed the machine data as a set of random variables, which are independent statistically. A univariate probability distribution function was used to model the random variables according to equation (2) [19-21].

$$F(t, \emptyset) = p(T \leq t) \qquad -\infty < t < \infty \tag{2}$$

where; $\emptyset$ = set of parameters for the distribution,
T = lifetime of the peeling machine (min),
t = time of machine operation (min)

Thus, the Weibull model was developed based on equation (2), by expressing a 2-parameter special case of the model as shown in equation (3).

$$F(t, \emptyset) = 1 - \exp\left[-\left(\frac{t}{\alpha}\right)^{\beta}\right] \qquad t \geq 0 \tag{3}$$
$$F(t, \emptyset) = 1 - \exp\left[-(\lambda t)^{\beta}\right] \qquad t \geq 0$$

where $\lambda = 1/\alpha$, α (scale parameter) > 0 and β (shape parameter) > 0

We later mimic this approach to describe the amount of peels remaining after processing of the tubers by further modifying the 2-parameter special case Weibull model as in equation (4) [16, 22].

$$r = e^{-k_R t} \tag{4}$$

where; r = remaining peels (kg)
k_R = peeling constant

However, the peeling variables in equation (4) were adjusted to reflect the peeling removal characteristics of the machine as shown in equation (5) [23].

$$r = e^{-(\frac{t}{T})R} \tag{5}$$

where; T = theoretical peeling time constant to reach 100% of the peels removal rate
t = peeling or residence time (min)
R = slope of the peeling characteristics

According to the procedure reported by Dürr and Graßhoff [24], we can express the peeling removal characteristics of the machine as a percentage of the amount of peels removed based on the scale, shape, and location constraints of a general Weibull model (Figure 3). Apparently, the amount of the tuber peels removed varies with the peeling time and the peeling resistance for each of three

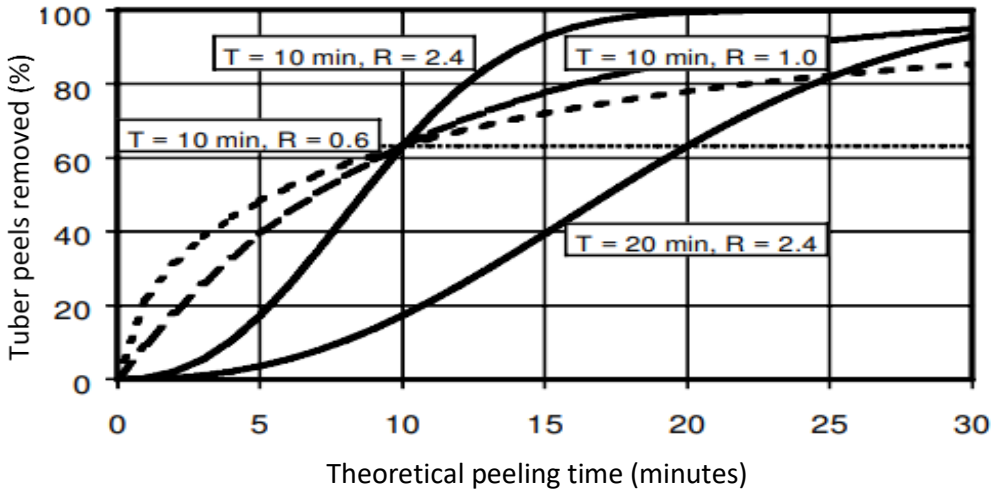

Figure 3. A typical Weibull model showing the relationships between peeling time and the amount of peels removed [24]

curves, which represent the parameters of the Weibull model. The fourth curve or broken line represents the effective peeling resistance between 10 to 20 min of the theoretical peeling time. The general formula for the time co-ordinates of the point of inflection of the curves in the model is represented in equation (6) [24].

$$t_i = T\left(\frac{R-1}{R}\right)^{1/R} \tag{6}$$

Therefore, the peeling rate is the time derivative of the mass of peels removed. Combining equations (4) and (5), a relationship for the peeling rate is apparent in equation (7).

$$\dot{m} = \frac{ds}{dt} = -\frac{dr}{dt} = \left(\frac{R}{T}\right)\left(\frac{t}{T}\right)^{R-1} e^{-(t/T)^R} \tag{7}$$

The relative peeling rate, which is defined as the ratio of the peeling rate to the amount of peels remaining, was therefore

$$\dot{m} = \frac{v}{r} = \left(\frac{R}{T}\right)\left(\frac{t}{T}\right)^{R-1}$$

$$\ln \dot{m} = \ln\left(\frac{R}{T}\right) + (R-1)\ln\left(\frac{t}{T}\right)$$

where, r_p = relative peeling rate (kg/s).

Interesting features of the peeling process becomes apparent by plotting the relative peeling rate versus the amount of peels removed. Thus, we computed the relative peeling rate as a function of the amount of peels removed.

2.4.2 Modeling based on Jennings model

A new mathematical model is presented here, initially developed by Jennings for describing the cleaning rate of soil on contact surfaces. Accordingly, Jennings model was proposed for describing the mechanism of particle removal from the tubers during the peeling operation as expressed in equation (8) [25, 26].

$$\frac{dm}{dt} = -K_R.m \tag{8}$$

$$\int_0^m \frac{dm}{m} = -K_R.\int_0^t dt$$

$$\ln\ m = -K_r.t + c$$

where, K_r and c are Jennings model parameters, m = mass of peels removed (kg), t = peeling time (min).

2.4.3 Parameter estimation

The peeling rate and the relative amount peels obtained from the performance analysis were used to constitute the models based on the Weibull and Jennings models. A linear relationship was established, and the values of the parameters were obtained experimentally. The values of the parameters, K_r and c were estimated from the Jennings models, while the values of R-1 and R/T were estimated from the Weibull models for the cassava, sweet potatoes, and cocoyam tubers.

2.4.4 Verification of the models

An independent validation was used to verify the degree fitness of the models using experimental data. In this approach, the tuber peeling machine was operated again for 30 min, and the peeling rate and the relate amount of peels were computed, as presented in Table 1. The data obtained were analyzed independently for the model verification, based on the mean square error (MSE) and the coefficients of determination (R^2), using equations (9) and (10).

$$MSE = \frac{1}{a}\sum_{i=1}^{k}(M - M_i)^2 \tag{9}$$

$$R^2 = \frac{\sum_{i=1}^{k}(\widehat{M}-M)^2}{\sum_{i=1}^{k}(M-\bar{M})^2} \tag{10}$$

where, M = tuber peeling rate and amount of peels removed, $\widehat{M}$ = model estimated response, $\bar{M}$ = mean response, k = sample size, a = number of runs for each tuber peeling (6).

3. Results and Discussion

3.1 Effect of residence time and speed on peeling rate and amount of tuber peels

The tuber peeling rate was obtained by differentiating the peeling efficiency with respect to time. The effects of the residence time of the machine operation on the relative amount of tuber peels obtained from the 750, 550 and 350 rpm speed of the rotating shaft are presented in Figures 4-6. The relative weight of the tuber peels increases with an increase in the residence time irrespective of the speed of operation of the peeling machine. There was a log increase in the peeling rate of tuber peels with an increase in the residence time and speed of the machine operation based on the

Weibull particle removal theory. Also, an increase in the relative amount of peels with an increase in the residence time and speed operation was observed based on the Jennings particle removal theory. This behavior may be due to increasing load intensity on the peeling drum at high speeds. According to the theories, multiple particles of tuber peels may inadvertently affect the flow of air effecting peeling [25, 27]. Similarly, Rothaug *et al.* [28] and Ferraz *et al.* [29] also suggested that larger amount tuber particles may decrease the performance of the peeling unit and hence the throughput capacity of the machine. The performance will be enhanced with an increase in the inertia of the speed of the machine and a decrease in the residence time. Although the peeling rate was lower at 750 rpm, the machine performance was observed to increase with decreasing speed up to 350 rpm. Thus, the peeling rate and the relative amount of peels were high at the beginning of the machine operation.

Table 1. Experimental data for independent validation

Tuber		**750 rpm**		**550 rpm**		**350 rpm**	
	t	**m**	**ṁ**	**m**	**ṁ**	**m**	**ṁ**
Cassava	5	11.63	0.074	18.87	6.130	18.98	6.020
	10	10.77	0.123	17.01	7.990	17.11	7.890
	15	10.11	0.126	16.00	9.000	16.01	8.990
	20	9.830	0.109	13.89	11.11	15.00	10.00
	25	8.820	0.127	12.57	12.43	13.98	11.02
	30	8.150	0.128	11.18	13.82	12.33	12.67
Sweet potato	5	14.23	0.770	13.78	1.220	13.16	1.840
	10	13.15	1.850	12.45	2.550	12.44	2.560
	15	12.22	2.780	11.84	3.160	11.63	3.370
	20	11.78	3.220	10.11	4.890	10.18	4.820
	25	10.13	4.870	9.670	5.330	9.460	5.540
	30	9.670	5.330	8.190	6.810	8.190	6.810
Cocoyam	5	11.63	0.370	11.06	0.940	10.44	1.560
	10	10.77	1.230	10.79	1.210	10.04	1.960
	15	10.11	1.890	10.14	1.860	9.760	2.240
	20	9.830	2.170	9.580	2.420	8.440	3.560
	25	8.820	3.180	8.880	3.120	8.160	3.840
	30	8.150	3.850	8.010	3.990	7.770	4.230

m = amount of tuber peels (kg); ṁ = tuber peeling rate (kg/min), t = residence time (min)

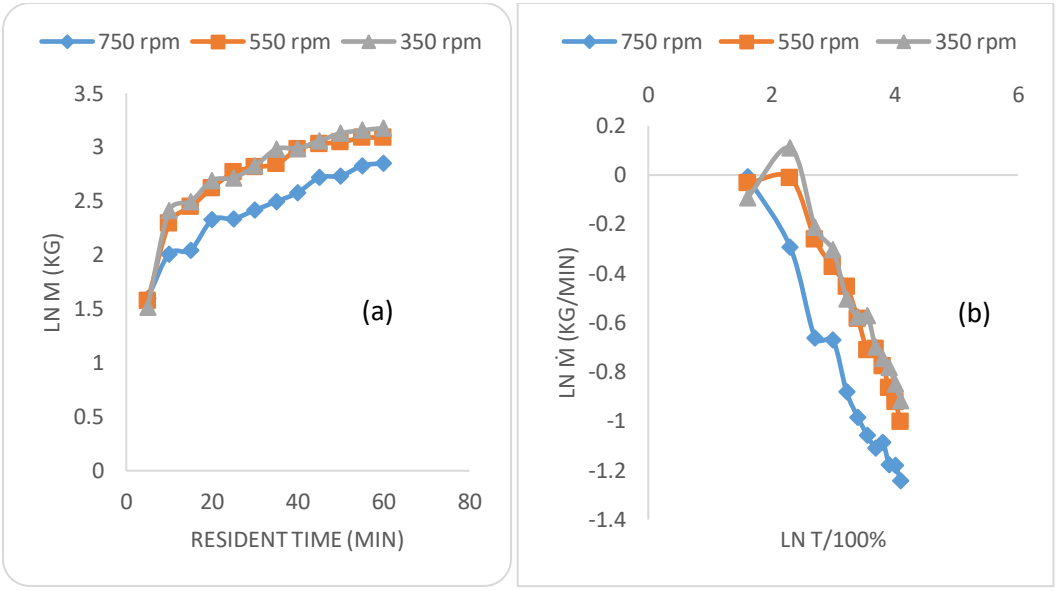

Figure 4. Jennings model prediction for cassava tuber peeling based on (a) effect of residence time on relative weight and (b) effect of theoretical peeling time constant on the peeling rate

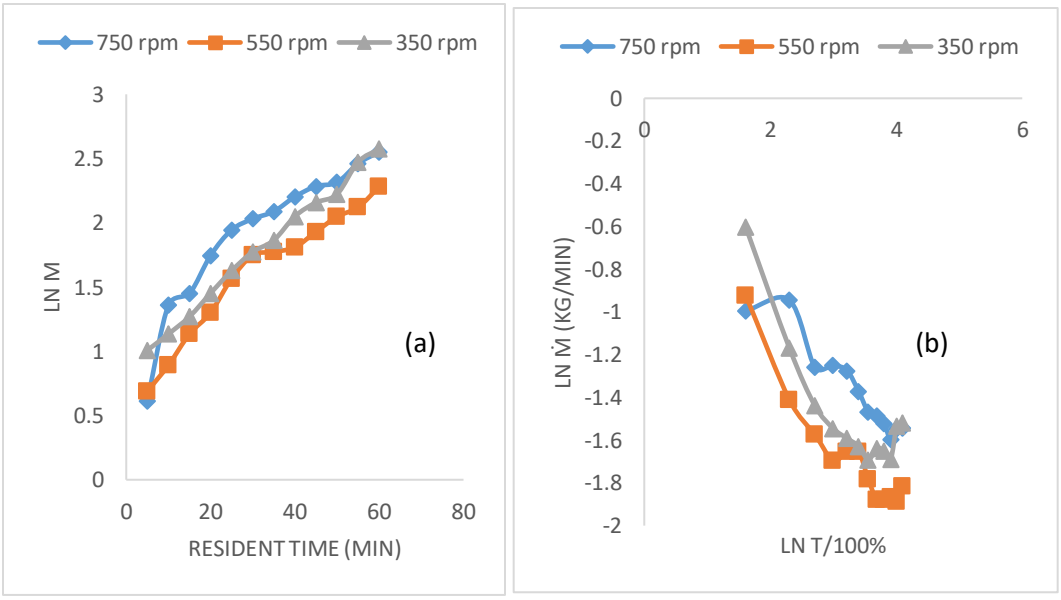

Figure 5. Jennings model prediction for sweet potato peeling based on (a) effect of residence time on relative weight and (b) effect of theoretical peeling time constant on the peeling rate

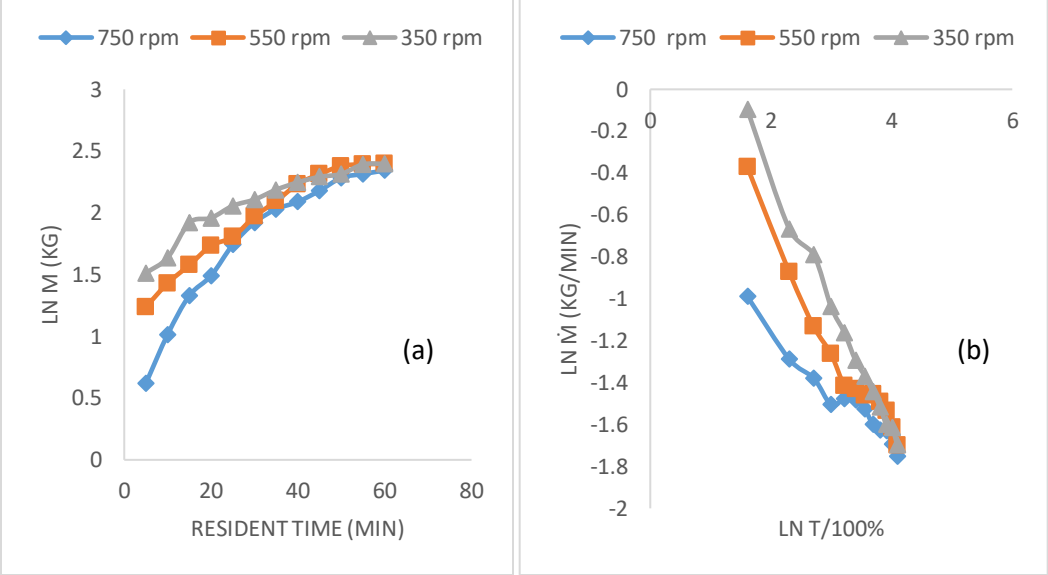

Figure 6. Jennings model prediction for cocoyam peeling based on (a) effect of residence time on relative weight and (b) effect of theoretical peeling time constant on the peeling rate

3.2 Prediction of peeling rate

The parameters for predicting the peeling rates of the cassava, sweet potatoes and cocoyam tubers are shown in Tables 2 and 3. The Weibull model parameters appears to be a better estimator of the tuber peeling rate than the Jennings model because of the higher values of the determination coefficient and lower mean square error. Simonyan and Yiljep [30] reported similar results in their study on the grain separation and cleaning efficiency of conventional sorghum thresher. Also, Peng *et al.* [31] corroborated our findings in their work on the peeling behavior of a viscoelastic thin film. The authors agreed that there is a close relationship between the peel-off force and the tuber peeling rate. The peeling rate is also theoretically related with the peeling efficiency of the machine, the higher the peeling rate, the higher the peeling efficiency. This means that the amount of the peels obtained from the cassava, cocoyam and potatoes tubers will decrease significantly with an increase in the residence time of machine operation. A similar result was reported by Liu *et al.* [32] in their work on the effect of particles on the surface cleaning of dry ice. The authors opined that theoretical analysis of the moments of forces caused by particle impact and aerodynamic drag showed that particle impact is primarily responsible for the peeling.

3.3 Independent model validation

The results of the independent validation of the models for predicting the cassava, sweet potatoes, and cocoyam tubers, from the Weibull and Jennings theories are shown in Figures 7-9, respectively. The values obtained from the models were very close to the actual data obtained from an independent experiment, with mean square error generally less than 10% as shown in Tables 2 and 3. Irrespective of the speed and the residence time differences, the models were able to predict the peeling rate and the amount of peels well within acceptable limits. Previous studies have shown that most models used for describing the peeling rate and the amount of peels are influenced by various

Table 2. Weibull model parameters for tuber peeling

Product	-(R-1)	ln (R/T)	R^2	MSE	Speed (rpm)
Cassava	0.5060	0.7946	0.9802	0.014039	750
	0.4269	0.8398	0.9336	0.020462	550
	0.3996	0.7969	0.8759	0.058424	350
Sweet potato	0.2726	-0.4615	0.9086	0.339939	750
	0.3459	-0.5346	0.8925	0.033261	350
	0.3509	-0.3253	0.7329	0.019684	550
Cocoyam	0.2658	-0.6249	0.9529	0.820625	750
	0.4770	0.2560	0.9505	0.991292	550
	0.6254	0.8583	0.9942	0.794371	350

Table 3. Jennings model parameters for tuber peeling

Product	- K_R	c	R^2	MSE	Speed (rpm)
Cassava	0.0201	1.7600	0.9203	0.047496	750
	0.0215	2.0183	0.7694	0.024448	550
	0.0225	2.0309	0.7539	0.047385	350
Sweet potato	0.0285	0.9930	0.8636	0.458236	750
	0.0272	0.7241	0.9505	0.126436	550
	0.0286	0.8724	0.9953	0.713663	350
Cocoyam	0.0213	0.8273	0.9005	0.967158	750
	0.0219	1.2518	0.9558	0.993578	550
	0.0151	1.5943	0.9100	0.805114	350

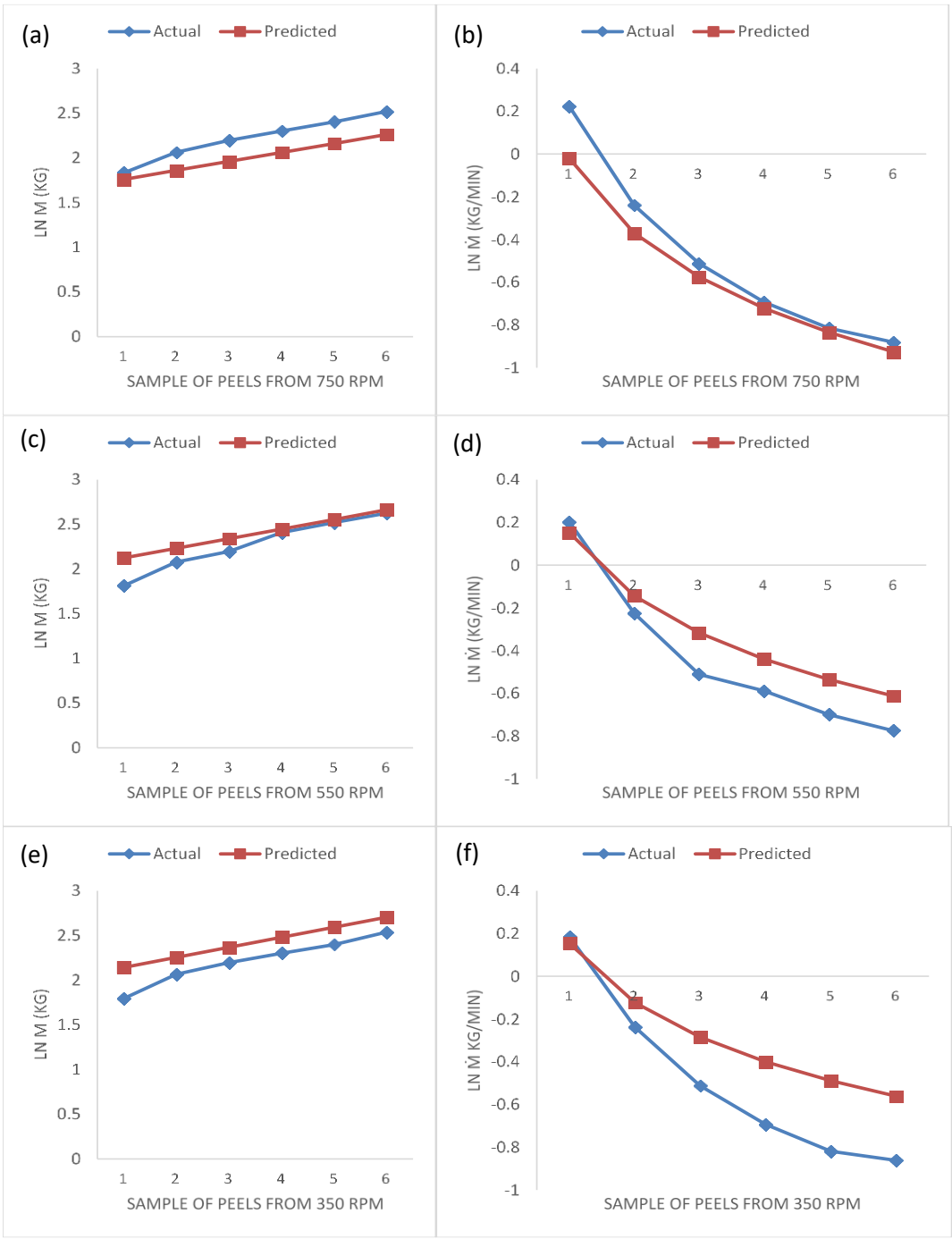

Figure 7. Independent validation of models for predicting cassava peeling rate using (a) Weibull model at 750 rpm, (b) Jennings model at 750 rpm, (c) Weibull model at 550 rpm, (d) Jennings model at 550 rpm, (e) Weibull model at 350 rpm, and (f) Jennings model at 350 rpm

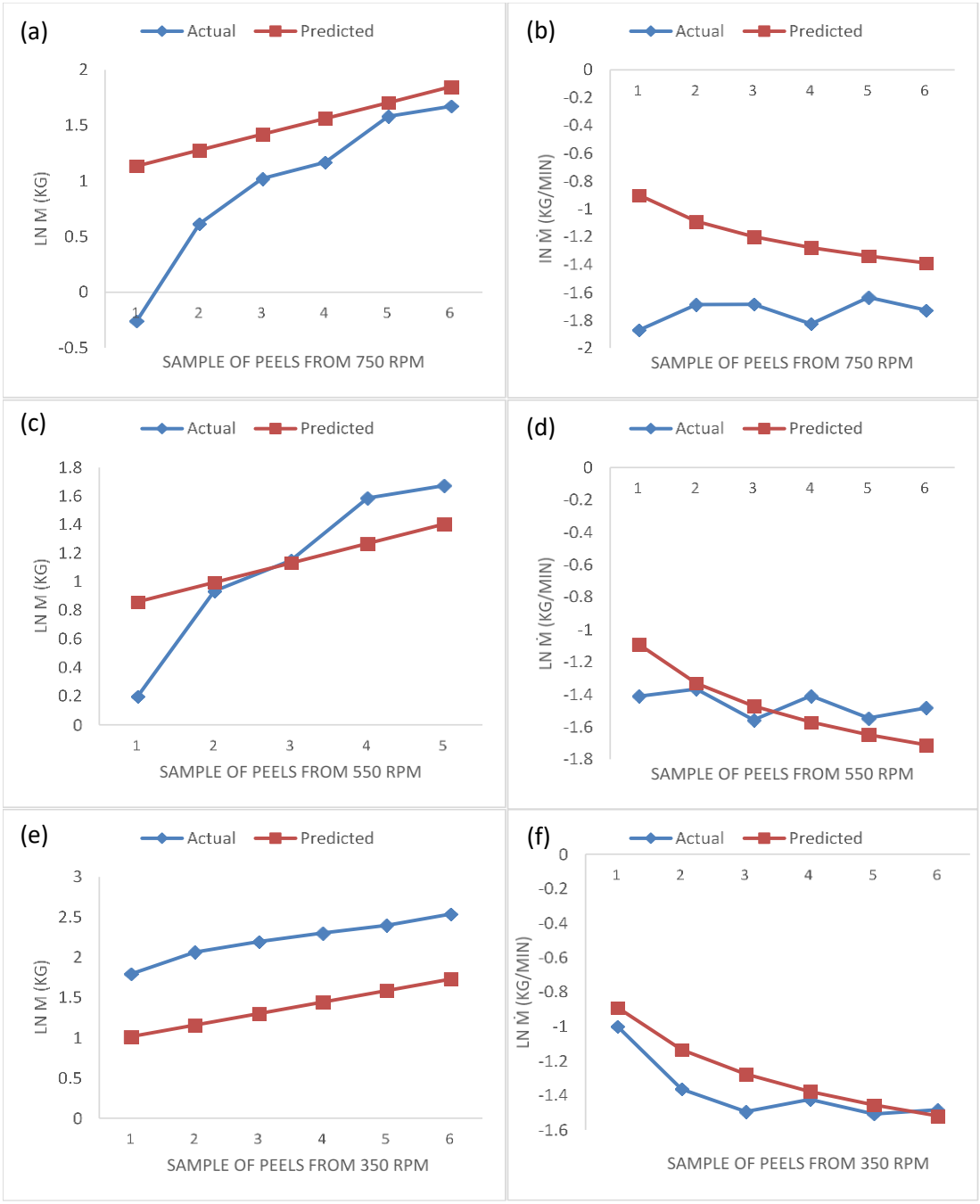

Figure 8. Independent validation of models for predicting sweet potatoes peeling rate using (a) Weibull model at 750 rpm, (b) Jennings model at 750 rpm, (c) Weibull model at 550 rpm, (d) Jennings model at 550 rpm, (e) Weibull model at 350 rpm, and (f) Jennings model at 350 rpm

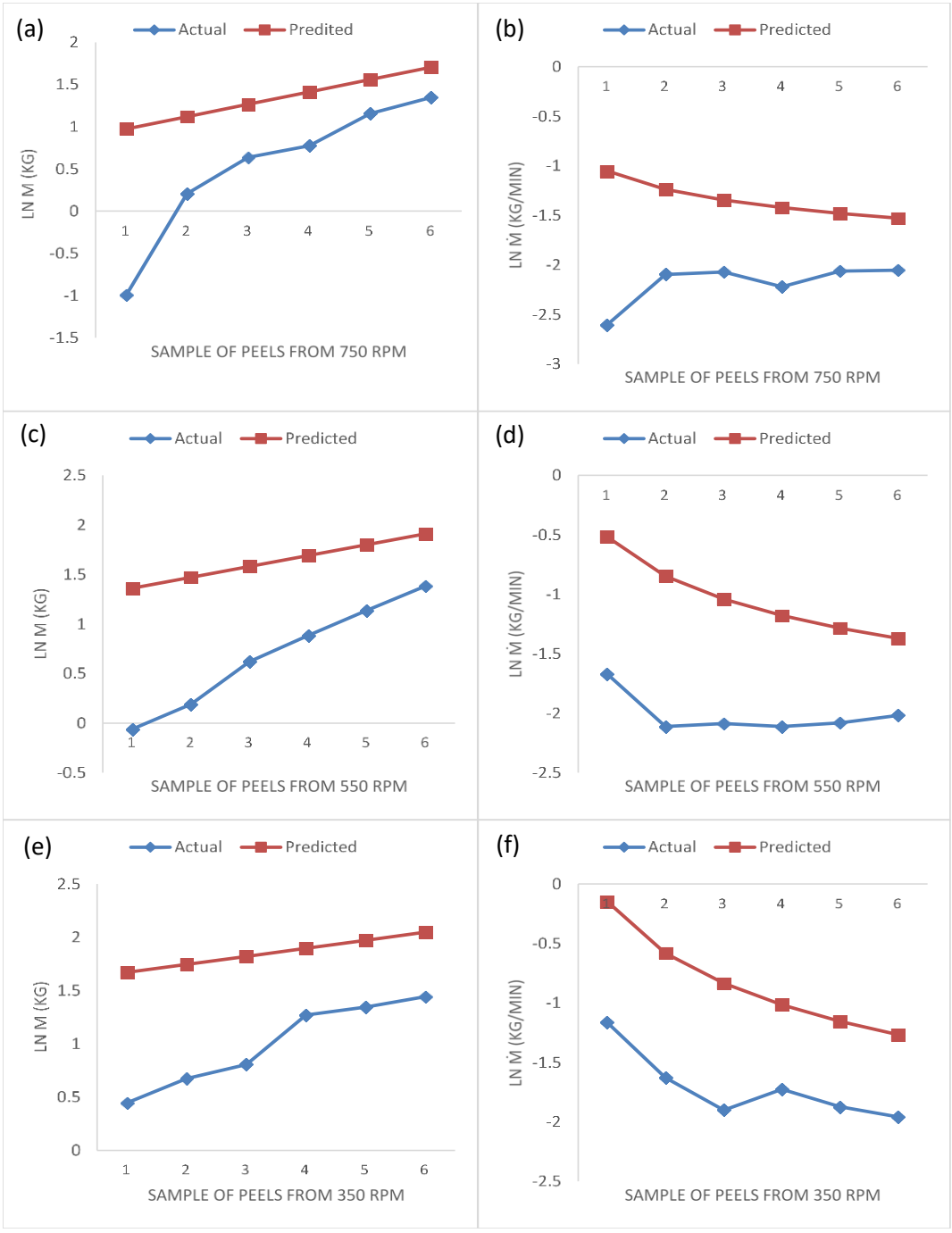

Figure 9. Independent validation of models for predicting cocoyam peeling rate using (a) Weibull model at 750 rpm, (b) Jennings model at 750 rpm, (c) Weibull model at 550 rpm, (d) Jennings model at 550 rpm, (e) Weibull model at 350 rpm, and (f) Jennings model at 350 rpm

model parameters, including the peeling angle, thickness, and other intrinsic property [33-37]. Also, Kutzbach [38] shows similar results in his work on the mathematical modelling of grain separation. Thus, in this investigation, the model parameters can be used for predicting the response variables with very close margin of errors.

4. Conclusions

This research predicted the peeling rate of an existing multi-tuber peeling machine using classical particle removal theories. The machine was designed to peel fresh cassava, sweet potatoes, and cocoyam tubers at a speed range of 350-750 rpm. The tuber peeling rate were determined for 1 h at intervals of 5 min. The models were developed based on the Weibull and Jennings theories. The peeling rate of the machine increases with an increase in the residence time and the speed of the machine operation ($p< 0.05$). Also, the relative weight of the tuber peels increases with an increase in the residence time irrespective of the speed of operation of the peeling machine. The values obtained from the models were very close to the actual data obtained from an independent experiment, with mean square error generally less than 10%. The Weibull model parameters were better estimators of the peeling rate with $R^2 > 95\%$ and mean square error (MSE) < 10%, irrespective of the speed and residence time of machine operation.

5. Acknowledgements

The authors acknowledge the technical assistance provided by the technologists in the crop processing and storage laboratory, Department of Agricultural and Biosystems Engineering of the Landmark University, Omuaran, Kwara State, Nigeria.

References

[1] Ohwovoriole, E.N., Obi, S. and Mgbeke, A.C.C., 1988. Studies and preliminary design for a cassava tuber peeling machine. *Transactions of the American Society of Agricultural Engineers*, 31(2), 380-385.

[2] Fadeyibi, A. and Ajao, O.F., 2020. Design and performance evaluation of a multi-tuber peeling machine. *AgriEngineering*, 2 (1), 55-71.

[3] Ale, M.O. and Manuwa, S.I., 2020. Design and fabrication of a semi-automatic cassava planter. *IOP Conference Series: Earth and Environmental Science*, 445(1), https://doi.org//10.1088/1755-1315/445/1/012002

[4] Kumar, G.P., Khobragade, C.B., Gupta, R.K. and Raza, K., 2019. Development and performance evaluation of an electric motor-powered ginger washing-cum-peeling machine. *International Journal of Current Microbiology and Applied Sci*ences, 8(2), 722-737.

[5] Alli, O.D. and Abolarin, M.S., 2019. Design modification of a cassava attrition peeling machine. *Journal of Physics: Conference Series*, 1378(3), https://doi.org/10.1088/1742-6596/1378/3/032029

[6] Tobiloba, O., Oluwaseun, K. and Leramo, R.O., 2019, December. Performance of cassava peeling machines in Nigeria: A review of literature. *Journal of Physics: Conference Series*, 1378 (1), https://doi.org/10.1088/1742-6596/1378/2/022084

[7] Samuel, O.C. and Emmanuel, I., 2019. Design of a modernized cassava peeling machine. *International Journal of Innovative Science and Research Technology*, 4(10), 1-10.

[8] Edeh, J.C., Nwankwojike, B.N. and Abam, F., 2020. Design modification and comparative analysis of cassava attrition peeling machine. *Agricultural Mechanization in Asia, Africa, and Latin America*, 51(1), 63- 69.
[9] Ezekwe, G.O., 1976. A feature for achieving a constant depth of peel in the mechanical peeling of cassava. *Nigerian Journal of Engineering*, 1(3), 174-181.
[10] Picket, L.K. and West, N.L., 1988. Agricultural machinery-functional elements-threshing, separating and cleaning. In: R.H. Brown, 1st ed. *Handbook of Engineering in Agriculture*. Boca Raton: CRC Press, pp. 65-85.
[11] Ali, N.M., Muhammad, S.S., Salim, F. and Majid, A.A., 2019. Design and development of potato processing machine. *Politeknik and Kolej Komuniti Journal of Engineering and Technology*, 1(1), 121-130.
[12] Adetan, D.A., Adekoya, L.O. and Aluko, O.B., 2006. Theory of a mechanical method of peeling cassava tubers with knives. *International Agrophysics*, 20(4), 269-274.
[13] Seth, O., 2020. A review on the performance of some cassava peeling machines developed. *North American Academic and Research Journal*, 3(2), 97-162.
[14] Olukunle, O.J. and Akinnuli, B.O., 2013. Theory of an automated cassava peeling system. *International Journal of Engineering and Innovative Technology (IJEIT)*, 2(8), 177-184.
[15] Asonye, G.U., Asoegwu, S.N., Maduako, J.N. and Madubuike, C.N., 2019. A mathematical model for predicting the cutting energy of cocoyam (*Colocasia esculenta*). *Arid Zone Journal of Engineering, Technology and Environment*, 15(1), 174-189.
[16] Mohammed, I.K., Charalambides, M.N. and Kinloch, A.J., 2016. Modeling the effect of rate and geometry on peeling and tack of pressure-sensitive adhesives. *Journal of Non-Newtonian Fluid Mechanics*, 233(1), 85-94.
[17] Aguirre, R. and Garray, A.E., 1999. Continuous flowing portable separator for cleaning and upgrading beans seeds and grains. *Agricultural Mechanization in Asia, Latin America and Africa*, 30(1), 59-63.
[18] Calabria, R. and Pulcini, G., 2000. Inference and test in modelling the failure/repair process of repairable mechanical equipment. *Reliability Engineering and System Safety*, 67(1), 41-53.
[19] Murthy, D.P., Xie, M. and Jiang, R., 2004. *Weibull Models*. 2nd ed. New York: John Wiley and Sons.
[20] Bjarnason, H. and Hougaard, P., 2000. Fisher information for two gamma frailty bivariate Weibull models. *Lifetime Data Analysis*, 6(1), 59-71.
[21] Costa, A.F.B. and Rahim, M.A., 2000. Economic design of X and R charts under Weibull Shock Models. *Quality and Reliability Engineering International*, 16(1), 143-156.
[22] Davison, A.C. and Louzada-Neto, F., 2000. Inference for the Poly-Weibull Model. *Journal of the Royal Statistical Society-Series D: The Statistician*, 49(1), 189-196.
[23] Ogunlowo, A.S. and Adesuyi, S.A., 1999. A low-cost rice cleaning and destoning machine. *Agricultural Mechanization in Asia, Africa, and Latin America*, 30(1), 20-24.
[24] Dürr, H. and Graßhoff, A., 1999. Milk heat exchanger cleaning: modelling of deposit removal. *Food and Bioproducts Processing*, 77(2), 114-118.
[25] Simonyan, K.J., Yiljep, Y.D. and Mudiare, O.J., 2006. Modeling the grain cleaning process of a stationary sorghum thresher. *Agricultural Engineering International: CIGR Journal*, 8(1), 1-17.
[26] Dasman, A., Arifin, N.S., Kasim, A.R.M. and Yacob, N.A., 2019. Formulation of dusty micropolar fluid mathematical model. *Journal of Physics: Conference Series*, 1366(1), https://doi.org/10.1088/1742-6596/1366/1/012032
[27] Zhang, H., Xu, Y., Gan, Y., Chang, Z., Schlangen, E. and Šavija, B., 2020. Microstructure informed micromechanical modelling of hydrated cement paste: Techniques and

challenges. *Construction and Building Materials*, 25(1), https://doi.org/10.1016/j.conbuildmat.2020.118983

[28] Rothaug, S., Wacker, P., Yin, W. and Kutzbach, H.D., 2003. Capacity increase of cleaning units by circular oscillation. *Proceedings of the International Conference on Crop Harvesting and Processing*, Kentucky, Michigan, USA, February 9-11, 2003, 109-118.

[29] Ferraz, A.C.O., Mittal, G.S., Bilanski, W.K. and Abdullah, H.A., 2007. Mathematical modeling of laser-based potato cutting and peeling. *Bio Systems*, 90 (3), 602-613.

[30] Simonyan, J.K. and Yiljep, D.Y., 2008. Investigating grain separation and cleaning efficiency distribution of a conventional stationary Rasp-Bar sorghum thresher. *Agricultural Engineering International: CIGR Journal*, 10(1), 1-13.

[31] Peng, Z., Wang, C., Chen, L. and Chen, S., 2014. Peeling behavior of a Viscoelastic thin film on a rigid substrate. *International Journal of Solids and Structures*, 51(25-26), 4596-4603.

[32] Liu, Y.H., Maruyama, H. and Matsusaka, S., 2011. Effect of particle impact on surface cleaning using dry ice jet. *Aerosol Science and Technology*, 45(12), 1519-1527.

[33] Benyahia, L., Verdier, C. and Piau, J.M., 1997. The mechanisms of peeling of uncross-linked pressure sensitive adhesives. *The Journal of Adhesion*, 62(1-4), 45-73.

[34] Du, J., Lindeman, D.D. and Yarusso, D.J., 2004. Modeling the peel performance of pressure-sensitive adhesives. *The Journal of Adhesion*, 80(7), 601-612.

[35] Marin, G. and Derail, C., 2006. Rheology and adherence of pressure-sensitive adhesives. *The Journal of Adhesion*, 82(5), 469-485.

[36] Xu, D.B., Hui, C.Y. and Kramer, E.J., 1992. Interface fracture and Viscoelastic deformation in Finite size specimens. *Journal of Applied Physics*, 72(8), 3305-3316.

[37] Zhou, M., Tian, Y., Pesika, N., Zeng, H., Wan, J., Meng, Y. and Wen, S., 2011. The extended peel zone model: Effect of peeling velocity. *The Journal of Adhesion*, 87(11), 1045-1058.

[38] Kutzbach, H.D., 2003. Approaches for mathematical modeling of grain separation. *Proceedings of the International Conference on Crop Harvesting and Processing*, Kentucky, Michigan, USA, February 9-11, 2003, 121-130.

Current Applied Science and Technology Vol. 21 No. 2 (April-June 2021)

Content Analysis of Covid-19 and Agriculture News in Bangladesh Using Topic Modeling Algorithm

M Moriom Khatun[1]*, Md Saeed Siddik[2], Md Abdur Rahman[3] and Shah Khaled[4]

[1]Department of Agribusiness and Marketing, Sher-e-Bangla Agricultural University, Bangladesh
[2]Institute of Information Technology, University of Dhaka, Bangladesh
[3]Center for Advanced Research in Science, University of Dhaka, Bangladesh
[4]Waterloo Management of Integrated Manufacturing Systems Lab, University of Waterloo, Canada

Received: 24 June 2020, Revised: 22 September 2020, Accepted: 5 November 2020

Abstract

Covid-19 pandemic is an ongoing global crisis which affects all the economic sectors including the most fundamental sector, agriculture. Bangladesh, a developing country and is home to 2.11% of the world's population, is facing a massive shock in the agricultural sector which is the backbone of the country's economy. In the era of technology and having lockdown in recent pandemic, every person willingly collects information on agriculture and rural economics from publicly available online news articles. To satisfy the readers' demand, not only the online blogs and newspapers, but also printed newspapers have taken a serious look at open access articles. This research analyzed entire online articles related to Covid-19 and Bangladesh agriculture news published during this country wide lockdown after the first case was addressed. Topic modeling algorithm has been used to determine the underlying topics over these textual contents for mitigating the gap between media coverage and actual scenario. This research considered the entire set of English online articles indexed by the most prominent Google search engine to point out diverse topics which are covered by various news sources. The dataset and experimental results were statistically analyzed to define the relationship and significance among different independent variables. Numerous interesting findings have been reported in this research including the fearsome number of female agricultural reporters, high frequency topic of agricultural economics and government spokesman, significance between underlying topics and article sources, etc. It concludes with recommendations to bridge the gap between government policy and actual scenario presented by news sources on Bangladeshi agricultural sector during Covid-19.

Keywords: Covid-19; agriculture news; content analysis; topic modeling; clustering algorithm
DOI 10.14456/cast.2021.26

*Corresponding author: Email: moriom@sau.edu.bd
Tel: +8801520083662

1. Introduction

Covid-19 is an infectious viral disease that has created a global health emergency and a crisis in the agriculture and food sector [1, 2]. It has already grabbed the eyeballs of people all over the planet and changed communication and economic trends throughout the virtual and online systems [3]. Health experts have encouraged paperless communication and transaction during this pandemic to ensure social distancing and sanitization. That is why publicly available online contents become more and more demandable to broadcast precise information to the national and international communities. Furthermore, several newspapers have already stopped their printing operation and started fully online versions because of public demand for them to adapt to the current situation [4]. Since major business operations have been partially or fully closed down for safety reasons, locally grown and based industries e.g., agriculture, crafts, and so on, have become crucial supports for the economies of various countries. News reporters have increasingly become real pillars of democracy as they have tried to focus on the real issues and bridge the gap between policymakers and end-users. By analyzing the media contents, one may gather the real point of view about the current situation.

Bangladesh is a South Asian country. It has the 8th highest number of the global population and has been severely affected by the Covid-19 pandemic. People in Bangladesh have faced severe restrictions on their daily activities during safety lockdown. However, the majority of the country's population is directly or indirectly related to agriculture, and they are continuing with their farming, harvesting, and supplying of food to support demand and thus push along the economic cycle accordingly. However, the actual scenario of agriculture and rural economics is not positively reflected in the news in comparison with other issues, e.g., politics, media, sports, etc. [5]. Hence, rural affairs are often skipped over by policymakers, international aid groups and charities. There are some current works available on agricultural news analysis. However, these are predefined subtopics and not dynamically generated, which cannot ensure the actual underlying topics of those contents to predict the optimal results.

Newspaper contents can be a valuable source and was analyzed for wolf recolonization in France using structural topic modeling [6]. Chandelier *et al*. [6] studied media dissemination of information to detect wolf recovery in France. Since they regarded newspapers as a good source of content, they developed a statistical method for structural topic modeling that allows them to generate topics from a large number of texts about the targeted wolf recovery. They conducted two regional newspaper surveys and found a gap in representations of wolf management between citizens who had directly interacted with the wolf and who favored detailed information content. Another topic modeling application was presented by Gosh and Guha [7] for Twitter data analysis of US healthcare-related issues. The survey data, which was extracted from Twitter.com, came from obesity-related queries about childhood obesity, and intake of desserts and fast food. The data were then analyzed using statistical model and the comparative study between rural and urban areas, northern and southern states, and between coasts and inland states were determined. Bhatia *et al.* [8] presented the role of representations of the human–leopard conflict in Mumbai through media-content analysis. They conducted a content analysis of print media articles on human–leopard conflict in Mumbai, India. That research found that English-language and non-English-language print media differed significantly in their framing of human-wildlife conflicts. Another study demonstrated the coverage of the three most popular Bangladeshi domestic newspapers of the climate change issue from May 2006 to June 2009 [9]. This paper considered newspaper content as the most valuable communication research items and analyzed them to give an overview of Bangladeshi climate change concerns. They collected data in 15 predefined categories and analyzed their significance of data in those categories as observed in three domestic newspapers. It turned out that agricultural issues only featured at 8.3% of content in comparison with other climate issues.

Recently, the effects of Covid-19 on the agriculture sector have been addressed by some researches, where a Canadian Prof. Ellen Goddard presented the impact of Covid-19 on food retail and foodservice in Canada [1]. She put forward an economic model that described the Canadian food sector before the pandemic and the losses that were being incurred due to the impact of the disease. Her paper concluded with some recommended actions that should be taken by the foodservice, food retail, and government in response to remarkably uncertain projections in the future. The effect of the Covid-19 pandemic in agriculture for international trade relations was elaborately presented by Kerr [2]. The author described the short and long-run implications for the food supply chain of this pandemic. He suggested strengthening institutions that govern international trade for mitigating the post effect of this pandemic. The impact of Covid-19 on Iowa State's corn, soybean, ethanol, pork, and beef sectors was depicted by Hart *et al*. [10]. They presented the comparative study of these agricultural products with the estimated price and Covid-19 price damage. This paper was one of the first analyses that showed the slowdown in production and economic damages caused by the pandemic in the United States.

Analysis of agriculture related news only was rarely addressed by some researches, where Narayana and Kumar [5] presented a content analysis of agricultural news coverage in the daily newspapers of India. It was a study of five local daily newspapers of India and found that agriculture news was just 4.61%, where as political news was 27.3%. Ogessa and Sife [11] presented content analysis of the coverage of agricultural information in Tanzanian newspapers. They found that the prominence of agricultural information was as low as 4.9% in all the newspapers, which was too low to have any impact on and appeal to readers. They recommended that the government formulate policies to increase the coverage of development and agriculture-related news in the newspapers. Newspaper reportage and its effect on promoting agricultural development in Nigeria were presented by Okorie and Oyedepo [12], who analyzed three different domestic newspapers. They focused on 12 predefined agricultural sub-sectors and searched for related news in the newspapers. Since those sub-sectors were predefined and fixed, some relevant content may have been incorrectly assigned or missed out. In contrast, dynamic sub-sectors may increase the acceptance of relevant news information. Local and global brand food and beverages in Jamaican newspaper were analyzed to determine standardized strategies [13]. Newspaper contents were automatically analyzed to demonstrate the current views of climate change in India [14]. The researchers used a topic modeling algorithm to classify the contents into four overarching themes. Another newspaper analysis was used to determine the impact of Covid-19 on the tourism sector in China [15], which is an excellent work but its scope was limited to the tourism sector only.

Based on the analysis of the above literature, this paper presents dynamically generated underlying discussed keywords on Covid-19 and Bangladesh Agriculture using a topic modeling algorithm to predict a better view of the current situation on the agriculture sector of Bangladesh. This research also helps to find out the topics that need to be emphasized for better communication. We have collected a dataset from publicly available online news sources, including newspapers (printed and online), organizational portal, blogs, and forums. Then, the dataset is filtered and cleaned for observation using a topic modeling algorithm, which is widely used for textual data analysis. Finally, identified underlying topics, keywords, and contents are statistically analyzed with independent variables. This paper selects six research questions to determine the scenario presented by open access news sources about agriculture in Bangladesh during Covid-19, which will be helpful to bridge the gap between policymakers and the agriculture sector.

RQ1: What are the underlying topics that can be identified in articles related to the impact of Covid-19 on the agriculture sector in Bangladesh?

RQ2: What is the distribution of article sources and writers?

RQ3: What is the relationship between identified topics across the source types and content?

RQ4: Does the proportion of author type differ across the online news source types?

RQ5: Does the content length significantly relate to the type of content writer?

RQ6: Does the proportion of author types differ with identified topics and news source types?

By addressing those research questions, this paper visualizes the current point of views on the Covid-19 and Bangladesh Agriculture sector that occur in newspapers or online portals. Some important findings were also addressed in this paper including the low number of female writers, high proportion of government-related content, and the correlation between content size and source type. This paper concluded with some appropriate guidelines and suggestions for communication concerned with the agricultural sector during Covid-19 pandemic, and it is hoped that these will assist policy makers and international aid groups.

2. Materials and Methods

This research presents an analysis of open access online articles on the Covid-19 and Bangladesh agriculture using topic modeling algorithms in order to uncover the underlying discussed issues. A detailed description of methods, dataset collection and other materials are presented in this section.

2.1 Dataset

Data were collected from open access publicly available online English articles that were concerned with the effects of Covid-19 on Bangladesh Agriculture. The articles were published in local and international newspapers, organizational portals, blogs or forums. These articles selected were sampled from the date of the first Covid-19 patient confirmed in Bangladesh (March, 2020) until the date that the country reported 75,000 cumulative patients (June 10, 2020). All articles that were available online and indexed by the Google search engine were considered. The Google search engine was selected as it had the highest search engine market share worldwide (92.06%) and its market share in Bangladesh was 98.34% [16]. We used four search queries (Q) in Google with specific settings that are given below.

Q1: "Bangladesh agriculture covid-19"

Q2: "Bangladesh agriculture pandemic"

Q3: "Bangladesh agriculture coronavirus"

Q4: "Bangladesh farmer covid-19"

Tool: Country: Bangladesh; Time: Any time; Result: All result;

Setting: Region Settings: Bangladesh; Private results: Use private results.

The collected and filtered dataset was publicly available at online for further usages (https://sites.google.com/view/moriomrima/research). Four source types were categorized from the dataset: Blog & Forum (5%), Organizational Portal (18%), Online Newspaper (20%) and Printed Newspaper online version (57%). An overview of the observation data is listed in Table 1. It should be mentioned that the observation sample size is not that large because most of the news sources did not cover agriculture issues frequently. On the other hand, a large number of printed newspapers did not have an online version, which was a major barrier to information sharing in the recent digital world. However, people in Covid-19 lockdown have been increasing their online activities in order to maintain social distancing and safety issues. So, to cover maximum reachable articles we exclusively consider online version content for data analysis.

Table 1. Overview of survey data

Source Type	Source Name	Observation	(%)	Cumulative
Blog and Forum	City Farmer	1	5%	5%
	Fish Tank	1		
	Techlife	1		
	East Asia Forum	1		
Organization Portal	Aesa Network	1	18%	23%
	Anadolu Agency	1		
	Atlanta Council	1		
	BAEN BD	1		
	Bangladesh Awami League	2		
	BRAC	1		
	Databd	1		
	Fish Tank	1		
	Green Watch BD	1		
	Int. Finance Corporation	1		
	KMPG	1		
	Light Castle	1		
	Relief Web	1		
	US Embassy	1		
	USAID	1		
Online Newspaper	Bangladesh Monitor	1	20%	43%
	bd24live	1		
	bdnews24	6		
	Channel News Asia	1		
	Daily Industry	1		
	En Prothom Alo	1		
	IPS News	1		
	Somoy News	2		
	UCA News	1		
	United News Bangladesh	2		
	World Economic Forum	1		
Printed Newspaper	Arab News	4	57%	100%
	Bangladesh Post	5		
	Business Standard	3		
	Daily Asian Age	2		
	Daily Star	16		
	Dhaka Tribune	5		
	Financial Express	10		
	Independent	1		
	New Age	4		
Total		88	100%	

2.2 Topic modeling algorithm for textual data classification

Topic modeling is a classic solution to information retrieval problems from textual documents [17]. Such problems are closely related to the problem presented in this paper named textual article

classification problems on Covid-19 and Bangladesh Agriculture. Topic modeling imagines a fixed set of topics, where each topic represents a set of words. One of the popular topic modeling techniques, known as Latent Dirichlet Allocation (LDA) [18], has been used for selecting the topics from the dataset of Covid-19 in Bangladesh Agriculture articles. The goal of LDA is to map all the articles to the topics in a way such that the words in each article are mostly captured by those pre-determined topics.

The textual data was scrolled from various sources with title, author, contents, date and source name. Then stop words were removed from the contents, and data were finally processed by lemmatization and word stemming. Then, the filtered words were transformed into bags of words and a probabilistic model was executed to distribute the words into different prominent topics as output. The overall process of this experiment is depicted in Figure 1 and the steps are described below.

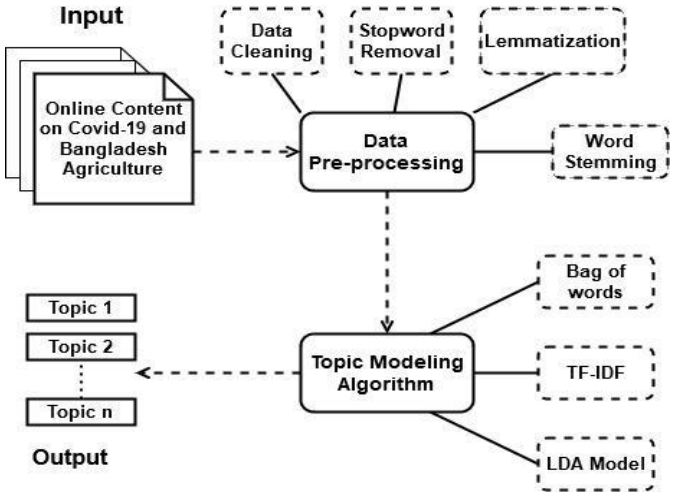

Figure 1. Overview of topic modeling algorithm

Data cleaning:
Only Covid-19 and Bangladesh Agriculture-related online content are allowed for the next phase of data pre-processing. Others irrelevant data are erased from the dataset in the process of data cleaning.

Stop word removal:
Stop words, which are words that have no specific meaning in the sentence, including prepositions, conjunctions and others are removed for better data modeling.

Lemmatization:
Lemmatization is the process of grouping together the various forms of a word so all of them can be analyzed as a single item [19]. Filtered words are lemmatized when words having the third person form in the sentence are changed to first person and verbs in past and future tenses are changed into present tense format.

Word stemming:
The lemmatized words which are basically verbs need to be stemmed, and this refers to the conversion to their root form. Finally, a set of purified and filtered words are ready for processing in the topic modeling algorithms.

Bag of words:
A 'Bag of words' is a special type of dictionary containing the words related to respective articles in 'Covid-19 and Bangladesh Agriculture'. After stemming, the purified words are counted and stored in a dictionary containing the number of times a word appears in a single article. Those frequencies will be used to determine the influential words for modeling the topics.
TF-IDF:
TF-IDF is a numerical statistic which is used to reflect how important a word is to an article in the collection dataset on 'Covid-19 and Bangladesh Agriculture'. TF-IDF is a very popular approach in information retrieval systems. It is the product of two statistics, Term Frequency and Inverse Document Frequency [20]. The processes for calculating TF-IDF are presented in equations (1), (2), and (3) as follows:

$$tf(t,a) = \frac{f_{t,a}}{\sum_{t' \in a} f_{t',a}} \quad (1)$$

In the above equation (1), term frequency *tf(t,a)* = 1 if *t* occurs in *a* and 0 otherwise, and $\sum_{t' \in a} f_{t',a}$ is the summation of the number of words in article *a*.

$$idf\ (t,A) = log\ log \frac{N}{|\ a \in A : t \in a\ |} \quad (2)$$

In the above equation (2), the inverse document frequency is depicted as *idf (t,A)*. Where N is the total number of articles in the dataset N = | A | and$|\ a \in A : t \in a\ |$ is the number of articles where the term t appears. If the term is not in the database, this will lead to a division-by-zero, hence it is therefore common to adjust the denominator to $1 + |\ a \in A : t \in a\ |$.

$$tfidf\ (t,a,A) = tf(t,a) \times idf(t,A) \quad (3)$$

Then TF-IDF is calculated by the mathematical product of TF and IDF, which is depicted in equation (3). A high weight of TF-IDF is reached by a high term frequency (in the given article); the weights hence tend to filter out common terms from the dataset on Covid-19 and Bangladesh Agriculture.
LDA model:
Latent Dirichlet Allocation (LDA) is a probabilistic model for analyzing the underlying probable topics based on the collection of textual articles [18]. Blei *et al.* [18] presented LDA as random mixtures over latent topics, where each topic is characterized by a distribution over words in textual dataset. It has been assumed that a generative process for each document ***w*** in a dataset ***D*** for LDA is used to implement topic modeling algorithm. The details of that are listed below.

i. Choose **N** ~ Poisson (**ξ**).
ii. Choose **θ** ~ Dir (**α**).
iii. For each of the ***N*** words w_n:
    a. Choose a topic z_n ~ Multinomial (**θ**).
    b. Choose a word w_n from $p(w_n \mid z_n, \beta)$, a multinomial probability conditioned on topic z_n

2.3 Implementation

One of the world's most popular data analytics based programming languages named Python version 3.8 (https://www.python.org/) was used for data interpretation in this research. Several programming library modules were also used in the experiment, and included were pandas (https://pandas.pydata.org/) for data handle, Python nltk (https://www.nltk.org/) for data preprocessing, genism (https://pypi.org/project/gensim/) for LDA modeling, and matplotlib (https://matplotlib.org/) for result visualization. The IBM SPSS 26 and Microsoft Excel 2013 were also used for statistical data analysis.

3. Results and Discussion

Textual newspaper content was collected and analyzed to pull up actual scenarios in the Bangladeshi agriculture sector during Covid-19 pandemic. The findings with discussion are presented in this section.

3.1 Research questions

This paper addresses six different research questions to present its findings. The results and their discussion with feedback are described below.

RQ1: What are those topics to visualize the contents of Covid-19 and Agriculture in Bangladesh?

The topic modeling algorithm dynamically created a total of 6 of the most prominent agricultural topics for presenting Covid-19 and Bangladesh Agriculture. The overviews of those topics with their relevant information are listed in Table 2, in which topic-wise article distribution, frequent terms, keywords, number of words and probable meanings are presented accordingly. The terms of the entire dataset are visualized in Figure 2(a), where several prominent terms are located with different color and size. The descriptions of six individual topics are listed below.

Topic 1 contains 20.5% of the total articles including the keywords related to supply chain management. The probable title of this topic is the economic impact on food and agricultural products supply chain during Covid-19. It has only 485(8.25%) times social media share which indicates readers' low level of interest. The term visualization of Topic 1 is presented in Figure 2(b).

Topic 2 contains only 5.7% of the total article and features keywords in the area of Agribusiness and Product Harvesting. The tentative title of this topic is Crisis in harvesting seasonal fruits and boro paddy by farmers during Covid-19. The automatically tagged terms under this topic are visualized at Figure 2(c). However, the social media share is 507 (8.62%) times which is also low.

Topic 3 contains the second highest percentage of the total articles (27.3%), with keywords of Agricultural Economics and Government. The potential title of this topic is Million dollar Government support for the country's SME, agriculture and fish sector. It must be mentioned that Bangladesh Government announced a stimulus package known as Taka 5000 Crore to offer financial assistance to the farmers. A large number of news portals presented this topic positively and its social media share is 942 (16.02%) time, which is high. Term visualization of topic 3 is presented at Figure 2(d).

Topic 4 contains the highest number of articles which is 34.1% of total. The keywords of this topic are Production Loss, Natural Disaster, and Government. This topic is related to the catastrophe of super cyclone Ampan and Covid-19 pandemic. The probable title of this topic is Government initiatives to mitigate district-wise production loss in Covid19 lockdown and Ampan cyclone. Since it has a direct effect on the country's agriculture sector, the social media share is also the highest at 2816(47.89%) time, which indicates that people are conscious of the combine natural disaster and pandemic issue. The underlying terms of Topic 4 are represented at Figure 2(e).

Topic 5 contains only 6.8% of the total articles with the keywords of Farmers' safety and Rural Economic. This topic is closely related to the pandemic health issue and the agricultural sector. However, as part of this topic is already covered by topic 3, its coverage and level of peoples' interest are relatively low, which is indicated by the social media share value (1.52%). The underlying terms covered by this topic is presented at Figure 2(f).

Table 2. Topic wise term distribution and probable meaning with article frequency

Topic	Arti-cle (%)	# of terms	Keywords	Probable description of topic	Top 20 words for this topic	Social media share
1	20.50	8003	Supply Chain Management	Economic impact of food and agricultural products supply chain during Covid-19	['market', 'inputs', 'prices', 'demand', 'country', 'food', 'vulnerable', 'income', 'impact', 'sector', 'supply', 'production', 'crisis', 'government', 'economic', 'people', 'farmers', 'Bangladesh', 'covid19', 'agricultural',]	8.25%
2	5.70	5009	Agribusiness, Product Harvest	Crisis for harvesting seasonal fruits and boro paddy by farmers during Covid-19.	['farmer', 'budget', 'mango', 'paddy ', 'pandemic', 'covid19', 'agricultural', 'food', 'vegetables', 'rice', 'seasonal', 'meeting', 'government', 'ministry', 'harvest', 'relief', 'crop', 'production', 'fruits', 'agriculture']	8.62%
3	27.30	15914	Agricultural Economics, Government	Million dollar Govt. support for country's SME, agriculture and fish sector	['farmer, 'food', 'sme', 'year', 'stimulus', 'lockdown', 'poor', 'fish', 'minister', 'banks', 'bank', 'coronavirus', 'Bangladesh', 'package', 'people', 'farmer', 'million', 'workers', 'government', 'April']	16.02%
4	34.10	12523	Production loss, Natural Disaster, Government	Government initiatives to mitigate district wise production loss in covid19 lockdown and Ampan cyclone	['income', 'support', 'agriculture', 'covid19', 'hospitals', 'package', 'damaged', 'amphan', 'people', 'district', 'prime', 'farmers', 'district', 'health', 'country', 'minister', 'cyclone', 'government', 'hectares', 'taka']	47.89%
5	6.80	1086	Farmers safety, Rural Economy	Prime minister announced motivational packages for farmer, health workers and victims.	['assistance', 'coronavirus', 'minister', 'production', 'world', 'need', 'economy', 'people', 'pandemic', 'food', 'crisis', 'Bangladesh', 'agriculture', 'country', 'prime', 'health', 'sector', 'farmers', 'fish', 'government']	1.52%
6	5.70	2585	Product Purchase, post-harvest storage, Government	Ministry of Bangladesh government said the collection and harvesting target of agricultural food and boro paddy.	['ministry', 'crop', 'food', '$589m', 'price', 'haor', 'percent', 'harvesting', 'farmers', 'country', 'taka', 'harvest', 'rice', 'Bangladesh', 'government', 'boro', 'agricultural', 'paddy', 'loan', 'impact']	17.7%

(a) textual visualization of entire article

(b) textual visualization of Topic 1

(c) textual visualization of Topic 2

(d) textual visualization of Topic 3

(e) textual visualization of Topic 4

(f) textual visualization of Topic 5

(g) textual visualization of Topic 6

Figure 2. Topic wise article visualization for Covid-19 and Agriculture in Bangladesh

Topic 6 contains only 5.7% of the total articles having keywords Product Purchase, Post-Harvest Storage, and Government. This topic covers the Government's crop purchasing policy and its implication on farmers' perception. It should be mentioned that the agricultural ministry of Bangladesh fixed the purchasing price and harvesting target of several agricultural food and boro paddy to support the farmers during pandemic. As it is concerned with one of the vital decisions on

rural economics, its social media share is the second highest at 1041(17.70%) time. The underlying terms of topic 6 are visualized in Figure 2(g).

RQ2: What is the distribution of article sources and writers for the content of Covid-19 and Agriculture in Bangladesh?

The articles concerned with Covid-19 and Agriculture in Bangladesh were collected from various sources that were categorized under four types, named as Blog & Forum, Online Newspaper, Organizational Portal and Printed Newspaper, and these had distributions of 4.5%, 20.5%, 18.2% and 56.8%, respectively. The results are presented in Table 3 and Figure 3. It can be seen that online and printed newspapers cover two-third of the dataset. It can be predicted that people are not willing to discuss about agricultural issues on their own in blogs or forums. Individual source-based content distribution is depicted as a pie chart in Figure 4.

Table 3. Statistical analysis of article source type

Source Type	Frequency	%	Valid %	Cumulative %
Blog & Forum	4	4.5	4.5%	4.5
Online Newspaper	18	20.5	20.5	25.0
Organizational Portal	16	18.2	18.2	43.2
Printed Newspaper	50	56.8	56.8	100.0
Total	88	100	100.0	

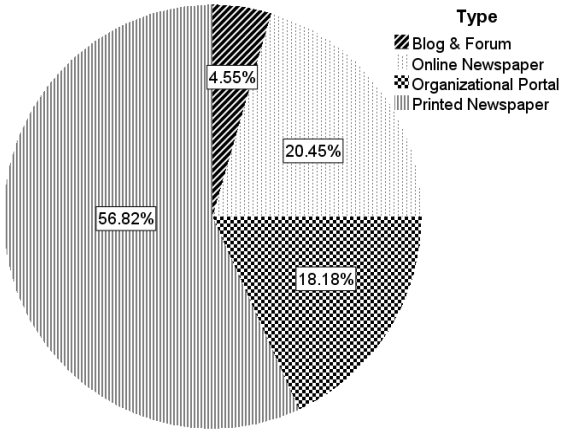

Figure 3. A pie chart showing statistical analysis of article source types

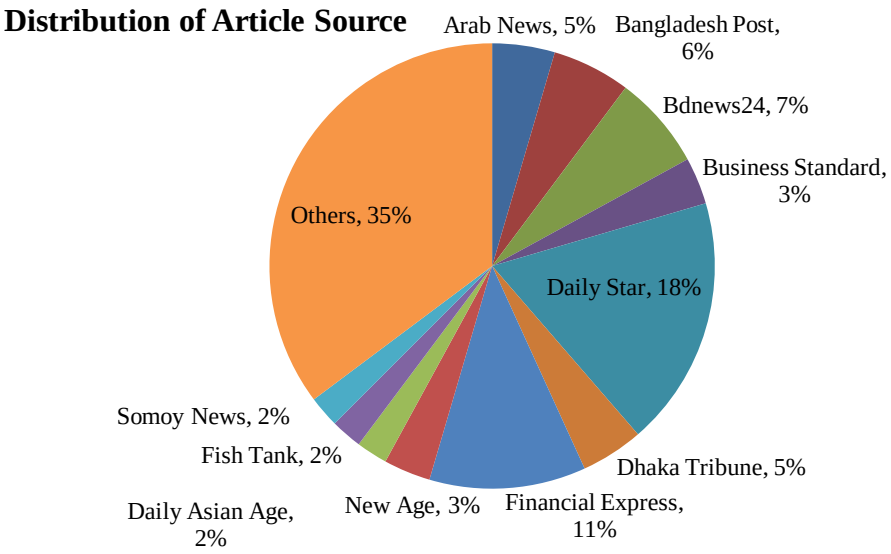

Figure 4. Visualization of article source names

Moreover, more than 60% of the content writers are corresponding editors, which means the ordinary agricultural events are covered by responsible person. A notable observation was that concerned with female content writers in agriculture. Only 2.3% of the articles were written by female agricultural reporters, which should be increased. The other 36% of individual reporters are male in gender. The details of article writer statistics are presented at Table 4 and Figure 5.

Table 4 shows that corresponding editors wrote the highest number of agricultural articles, and these writers may have been of either gender. However, the publicly gender-specific reporters are not equal to males and females in the agriculture sector during this Covid-19 pandemic.

Table 4. Statistical analysis of content writers

Writer	Frequency	%	Valid %
Corresponding Editor	54	61.4	61.4
Female	2	**2.3**	2.3
Male	32	36.4	36.4
Total	88	100	100.0

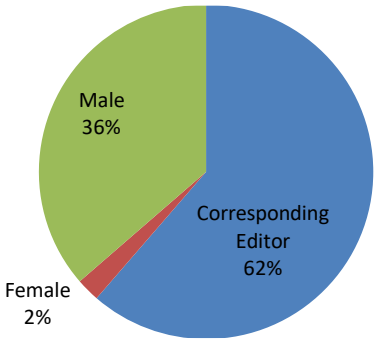

Figure 5. A pie chart showing statistical analysis of content writers

A publishing date-wise article frequency histogram can be seen in Figure 6. It shows that the date range for article consideration was March 01, 2020, to June 10, 2020. It can be seen that May 24 2020 was the day on which the maximum number of articles (11 articles) was published, and the mean publishing date was May 01, 2020. The majority of the Covid-19 and Bangladeshi agriculture-related articles were published within April and May 2020 with some outliers on June 07 and March 02, 2020. Not only were those two months peak times for the outbreak of Covid-19 in Bangladesh, they were also significant because the Government subsidiary package announcements, super cyclone Ampan stroke, and other agriculture-related issues occurred then.

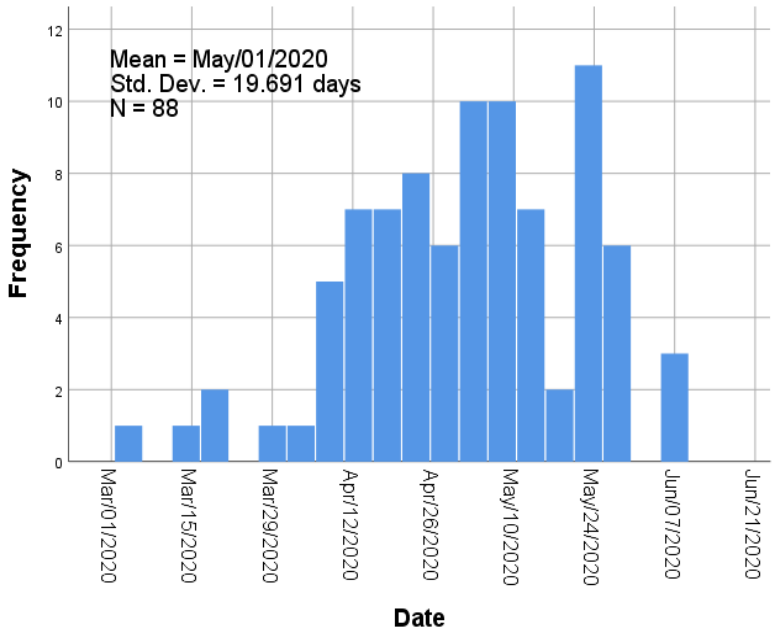

Figure 6. Histogram of published articles based on date

RQ3: What are the relations with identified topics across the source types and content?

Research question 3 can be split in two different sub questions. The first one is about the relationship between identified topics and content. Figure 7 presents the relationship between identified topics and content variables, where content variables have two forms named as content length and content frequency. Our analysis found that topic 4 has the maximum number of articles but their lengths are below average. It means this type was related to typical media reports only. The maximum number of article lengths is in topic 2, but its frequency is the lowest. Our observation found that these types of articles are basically detailed observations from the reporter. It was also found that topic 3 has the optimal coverage based on frequency and length, which covers the country's agricultural economics and Government issues.

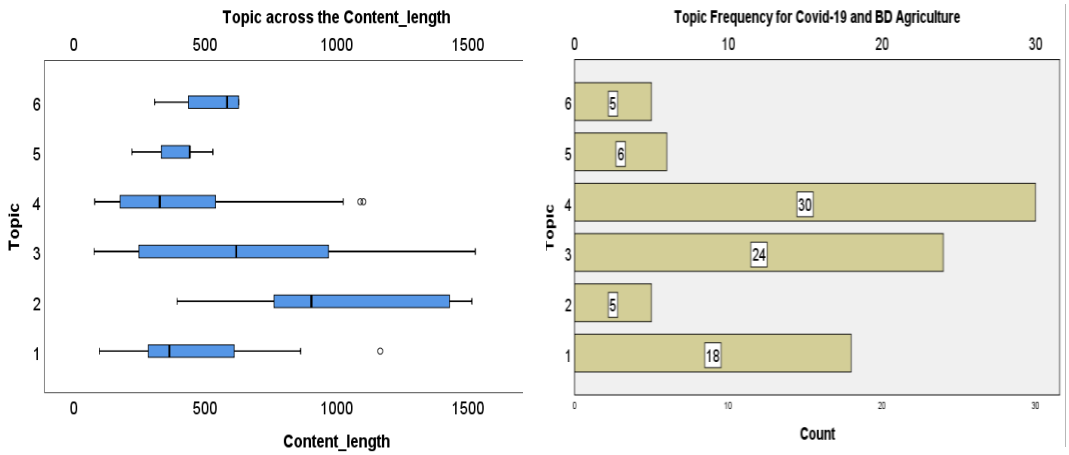

Figure 7. Relationship between identified topics and content

The second part of research question 3 is about the relationship between identified topic and source type, which confirms the topic coverage source. Figure 8 presents the relationship between article source and topics. It shows that printed newspapers covered the highest number of articles and obviously topic 4 has the highest frequency count. An interesting finding that can be reported from the graph is that the organizational portal covers the highest number of the country's agricultural economic issues, which is a type of investigation and R&D report. It was also found that newspapers (both online and printed) cover the maximum number of typical media issues e.g. super cyclone Ampan, product pricing, etc.

RQ4: Does the proportion of author type differ across the online news source types?

Research question 4 is related to the relationship between content writer and source type. We selected the hypotheses shown below for this experiment.

H0 = Author types are independent across the online news source categories.

H1 = Author types are dependent across the online news source categories.

Table 5 presents the statistical analysis of content writer and source type, where the significance of Pearson chi-square and likelihood ratio is also shown. The fact that the *p* value of chi-square is 0.862, which is far larger than 0.05, means that the null hypothesis is accepted and it can be concluded that author types are independent across the article source categories

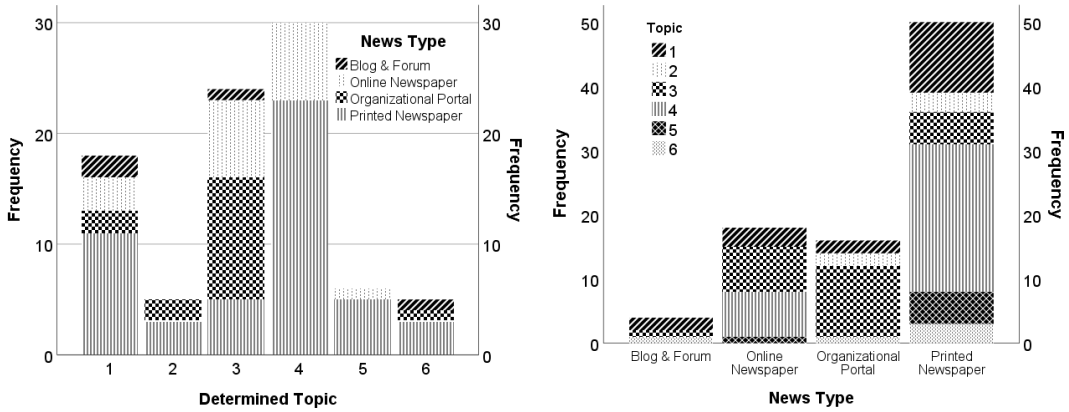

Figure 8. Identified topic and type of article relation

Table 5. Relationship between content writer and source type

		Source Type				Total
		Blog & Forum	Online Newspaper	Organizational Portal	Printed Newspaper	
Author	Corresponding Editor	2	10	10	32	54
	Female	0	0	0	2	2
	Male	2	8	6	16	32
	Total	4	18	16	50	88

Chi-Square Tests			
	Value	**df**	**Asymptotic Significance (2-sided)**
Pearson Chi-Square	2.558[a]	6	.862
Likelihood Ratio	3.276	6	.774
N of Valid Cases	88		

[a]6 cells (50.0%) have expected count less than 5. The minimum expected count is .09.

RQ5: Does content length significantly relate to the type of content writer?

Research question 5 deals with the relationship between content writer and content length. We selected various hypotheses for this experiment. It can be clearly seen that female writer frequency is ferociously low. To measure the significance of article length and writer type, the following hypotheses were used.

H0: There is no relationship between the two variables, content length and content writer.

H1: There is a significant relationship between content length and content writer type.

Table 6 presents the statistical results of the above hypotheses via Pearson chi-square and likelihood ratio. Since the *p* value 6 is 0.011, which is less than level of significance, the null hypothesis is rejected. It can therefore be determined that content length is significantly related to content writer type.

Table 6. Content length and content writer cross tabulation

		Content Writer Type			Total
		Corresponding Editor	Female	Male	
Content Length	<300	25	0	5	30
	300-599	17	0	10	27
	600-899	6	2	10	18
	900-1199	3	0	5	8
	>1200	3	0	2	5
Total		54	2	32	88

Chi-Square Tests			
	Value	**df**	**Asymptotic Significance (2-sided)**
Pearson Chi-Square	19.746[a]	8	0.011
Likelihood Ratio	18.950	8	0.015
Linear-by-Linear Association	7.912	1	0.005
N of Valid Cases	88		

[a]9 cells (60.0%) have expected counts less than 5. The minimum expected count is .11.

RQ6: Does the proportion of author type differ with identified topics and news source types?

Research question 6 focuses on the difference between identified topics and news source types. To evaluate their difference, the hypotheses below were selected.

H0: There is no relationship between variables news source category and newly identified topics.

H1: There is a significant relationship between the categorical variable topic and source type.

Table 7 presents the statistical analysis of the above hypotheses to measure the differences. Based on this Table, the *p* value is .002 which is less than 0.05, and this means the null hypothesis is rejected and source types and identified topics are not independent. It can be concluded that there is a significant correlation between content source type and determined topic.

Table 7. Identified topics and source type cross tabulation

		Topic						Total
		1	**2**	**3**	**4**	**5**	**6**	
Source Type	Blog & Forum	2	0	1	0	0	1	4
	Online Newspaper	3	0	7	7	1	0	18
	Organizational Portal	2	2	11	0	0	1	16
	Printed Newspaper	11	3	5	23	5	3	50
Total		18	5	24	30	6	5	88

Chi-Square Tests			
	Value	**df**	**Asymptotic Significance (2-sided)**
Pearson Chi-Square	36.251[a]	15	.002
Likelihood Ratio	43.088	15	.000
Linear-by-Linear Association	2.018	1	0.155
N of Valid Cases	88		

[a]19 cells (79.2%) have expected count less than 5. The minimum expected count is .23.

3.2 Performance evaluation

A pool of experts blindly evaluated the results found from the topic modeling algorithms. That pool consisted of five members, including two agricultural academicians, two agriculture service providers, and one agriculture expert policymaker. The review process was blind, and no one shares their scores with others. The reviews were collected on three categories, named as accepted, neutral, and rejected. Then, we use the majority voting on those topics generated by our work. It was found that the experts dismissed none of the items and the keywords. In contrast, more than eighty percent of outcomes were accepted, which confirmed the model's accuracy.

3.3 Recommendations

This paper presents some recommendations based on the experiment and data analysis which depicted a proper view of online news articles on Covid-19 and Bangladesh Agriculture. These recommendations can also be used for creating agriculture policy and decision support. The recommendations for the agriculture section in Bangladesh during Covid-19 are listed below.

1) Too much government-related news in the agriculture sector was found. It needs to be amalgamated with detailed investigation and creative news related to actual farmers' issues during this pandemic.
2) National newspapers and publicly available news portals did not put agriculture at the top of their news priorities. However, Bangladesh is predominantly an agricultural country, and agricultural news should be prioritized to grab the eyeballs of policymakers.
3) Personal experience or opinions inside blogs related to agriculture were alarmingly low and should be increased to publicize more actual views of the current problems.
4) The numbers of female authors that reported on agriculture news articles was chronically low. This imbalance needs to be corrected by government subsidiary or other relevant actions.

4. Conclusions

This research dealt with English articles on Covid-19 and agriculture in Bangladesh to figure out which sections were communicated enough and which needed more emphasis. This analysis was conducted using topic modeling algorithms to determine the underlying topics of the articles. Then, several statistical analyses were performed to answer six different research questions. It was found that there is a significant correlation between article source type and determined topics. Furthermore, the correlation between content length and writer is significant. It is also reported that newspapers did not cover enough detailed investigation of the current problems of agriculture in the Covid-19 issue. On the other hand, several organizations did the opposite, because most of the articles in organizational portals focused on the agricultural problematic issues.

Finally, this paper recommends that newspapers should focus more on problems with an internal investigation and engage more female writers to cover agricultural matters in Bangladesh. This research can be extended to other prominent topics such as education, labor, and social service. Comparing the articles among other countries' newspapers and publicly available online news sources may also be a future direction of this work to determine a broader view of the agriculture sector during this pandemic.

References

[1] Goddard, E., 2020. The impact of COVID-19 on food retail and food service in Canada: Preliminary assessment. *Canadian Journal of Agricultural Economics*, https://dx.doi.org/10.1111/cjag.12243

[2] Kerr, W.A., 2020. The COVID-19 pandemic and agriculture: Short- and long-run implications for international trade relations. *Canadian Journal of Agricultural Economics*, https://dx.doi.org/10.1111/cjag.12230

[3] Irvine, M. 2020. *How COVID-19 Is Shaping Google Search Trends & Patterns.* [Online] Available at: https://www.wordstream.com/blog/ws/2020/03/30/covid-19-google-search trends

[4] Bangkok Post, 2020. *Sixty Australian Newspapers to Stop Printing.* [Online] Available at: https://www.bangkokpost.com/world/1890915/sixty-australian-newspapers-to-stop-printing

[5] Narayana, U. and Kumar, S. 2009. Content analysis of agricultural news coverage in leading language dailies of India-A study of Kannada language dailies of Karnataka State. *University Journal of Communication*, 3(1), 1-14.

[6] Chandelier, M., Steuckardt, A., Mathevet, R., Diwersy, S. and Gimenez, O., 2018. Content analysis of newspaper coverage of wolf recolonization in France using structural topic modeling. *Biological Conservation*, 220(1), 254-261.

[7] Ghosh, D. and Guha, R., 2013. What are we 'tweeting' about obesity? Mapping tweets with topic modeling and Geographic Information System. *Cartography and Geographic Information Science*, 40(2), 90-102.

[8] Bhatia, S., Athreya, V., Grenyer, R. and Macdonald, D.W., 2013. Understanding the role of representations of human-leopard conflict in Mumbai through media-content analysis. *Conservation Biology*, 27(3), 588-594.

[9] Miah, M.D., Kabir, M.H., Koike, M. and Akther, S., 2011. Major climate-change issues covered by the daily newspapers of Bangladesh. *The Environmentalist*, 31(1), 67-73.

[10] Hart, C.E., Hayes, D.J., Jacobs, K.L., Schulz, L.L. and Crespi, J.M., 2020. The Impact of COVID-19 on Iowa's Corn, Soybean, Ethanol, Pork, and Beef Sectors. [online] Available at: https://www.card.iastate.edu/products/policy-briefs/display/?n=1301

[11] Ogessa, C.M. and Sife, A.S., 2017. Newspaper coverage of agricultural information in Tanzania. *University of Dar es Salaam Library Journal*, 12(1), 12-26.

[12] Okorie, N. and Oyedepo, T., 2011. Newspaper reportage and its effect towards promoting agricultural development in Nigeria. *Journal of Media and Communication Studies*, 3(2), 27-32.

[13] Ahn, R.J., Nelson, M.R. and Ferguson, G.M., 2020. Local and standardized strategies: A content analysis of newspaper food and beverage advertising in Jamaica. *Newspaper Research Journal*, 41(2), 179-203.

[14] Keller, T.R., Hase, V., Thaker, J., Mahl, D. and Schäfer, M.S., 2020. News media coverage of climate change in India 1997-2016: Using automated content analysis to assess themes and topics. *Environmental Communication*, 14(2), 219-235.

[15] Chen, H., Huang, X. and Li, Z., 2020. A content analysis of Chinese news coverage on COVID-19 and tourism. *Current Issues in Tourism*, https://doi.org/10.1080/13683500.2020.1763269

[16] Stat Counter Global Stats, 2020.*Search Engine Market Share Worldwide*. [Online] Available at: https://gs.statcounter.com/search-engine-market-share

[17] Wallach, H.M., 2006. Topic modeling: beyond bag-of-words, *Proceedings of the 23rd International Conference on Machine Learning*, New York, United States, 2006, pp. 977-984.

[18] Blei, D.M., Ng, A.Y. and Jordan, M.I., 2003. Latent dirichlet allocation. *Journal of Machine Learning Research*, 3(1), 993-1022.
[19] Manning, C.D., Raghavan, P. and Schütze, H., 2009. An Introduction to Information Retrieval. Cambridge:*Cambridge University Press*.
[20] Jones, K.S., 1972. A statistical interpretation of term specificity and its application in retrieval, *Journal of Documentation*, 28(1), 11-21.

Dong Ra Nang National Forest Change Detection using Multi-temporal LANDSAT 7 ETM$^+$ Imagery by Using CART Classification: Object-Oriented Approach

Sopholwit Khamphilung*

Department of Geoinformatics, Faculty of Informatics, Mahasarakham University, Maha Sarakham, Thailand

Received: 25 May 2020, Revised: 8 September 2020, Accepted: 12 November 2020

Abstract

This study presents change detection analysis using object-based image analysis in Dong Ra Nang national forest, Kalasin province. This national forest was previously cleared and used for agricultural purposes for an extended period of time according to media reports published between 2007-2015. In order to perform a LU/LC examination, a time series of LANDSAT 7 ETM$^+$ images acquired from 3 dates (25/11/1999, 28/11/2007 and 21/11/2015) were used for image segmentation and LU/LC classification. Furthermore, a CART algorithm and crucial image band ratios, such as MSAVI and NDVI, including mean of image layer bands, were used to improve image classification of degradation of the forest. The information from three thematic layers sampling points that had been derived from visual interpretations was used for CART training, applying and classifying the satellite images into 6 LU/LC classes, namely, (1) dense forest, (2) light forest, (3) bare land, (4) agricultural area, (5) plantation area, and (6) bodies of water on hierarchical image networks. Prior to the deforestation detection analysis, each image scene was classified individually using a CART algorithm. Then, the classified images were synchronized with the main map for performing land use/ land cover changes analysis focused on deforestation using image hierarchical image network by relation to image objects in vertical and horizontal aspects. The results indicated that the forest areas decreased dramatically by 50% from 1999-2007. On the other hand, there was a slight increase in bare land by an area of 38.68 sq.km. The majority of the area was used for farm land according to the report of the Forest Management Office, Khon Kaen province. The vegetation area emerged in the central area surrounding by bare land and agricultural area. In 2007-2015, the vegetation rapidly decreased by 30.89 sq.km., and the area tended to be bare land and agricultural area.

Keywords: OBIA; remote sensing; classification and regression tree; CART
DOI 10.14456/cast.2021.27

*Corresponding author: Tel.: (+66) 85-5503-666, Fax: (+66) 43-3547-59
E-mail: sopholwit.c@msu.ac.th

1. Introduction

National forests play an important role in social and economic aspects of the country. Dong Ra Nang is a well-known national forest located in the rural districts of Kalasin Province, Northeast, Thailand. There are issues of forest encroachment by villagers who live around the forest area. Their searching for subsistence plants, farming and logging have led to deforestation in the forest. The rainforest has the potential to develop a significant biodiversity. Therefore, the forest should be protected from unexpected phenomena, especially illegal natural resources over-exploitation. Interestingly, the forest is home to many important economic trees, such as Teak wood, Agar wood, and Yang. In terms of land use/land cover change detection, various processes can be used to study land use/land changes, particularly the process of remote sensing classification techniques or field surveying. Earth Observation Satellites (EOS) are emerging in various systems and image resolution; such as LANDSAT satellite imagery. The researcher was able to compare those imageries in the same area from past to present based on existing temporal resolution from selected data sources. In image classification; however, satellite imagery is characterized by two types of classification procedures, namely, pixel-based and object-based image analysis [1, 2]. The similarity of this methodology is that some advantage of spectral information derived from various sensors, can comply with statistical analysis tools (i.e. Parallelepiped, Maximum likelihood classifier) [3, 4]. Pixel-based image analysis has the disadvantage that it cannot take the spatial relations among target pixels, for example, the distance between objects, sizes, and shape information aimed at integrating to the target classes [5]. Such crucial information can be the criteria that make image classification more accurate. Object-based image analysis, on other hand, is more likely to overcome some of the drawbacks from the previously-mentioned image classification approach. In addition, pixel-based image analysis also shows a classification result error called the salt and pepper effect. Since pixel-based image classification is focused on individual pixels without considering the spatial relationships among the image objects, one pixel can be classified in more than one class. Generally, objects on the Earth's surface are categorized into two main types. i.e., man-made and natural features observing from satellite imageries. Visual interpretation and digital image processing can be used to distinguish image features. Some land covering objects, such as bodies of water, agricultural areas are involved not only because of their spectral information but also because of their shape characteristics (e.g., compactness, rectangular fit and roundness). These shape properties are derived from the image segmentation from the pixel homogeneity values by comparison with size and shape [6, 7]. However, these objects can be discriminated by an experienced user who can recognize some emerged shape, such as geometry of natural bodies of water, and man-made bodies of water with different shapes. In term of digital satellite image analysis, object-based image analysis is able to involve spectral and geometric information for classification procedures that increase classification quality. Moreover, object-oriented analysis comprises optimal tools and algorithms that can increase the accuracy and precision of image classification more than any other classifier paradigms can. For this research, a CART Algorithm was applied to identify the changes in LU/ LC classification focusing on forest changes [6-8]. Obviously, object-based image analysis applied to VHR imagery [9], and modification of LU/LC change detection by utilizing object-oriented approach have become more and more popular approaches for satellite image classification. Furthermore, pixel-based and object-based image analysis for change detection were also compared to see which could provide the best solution in a particular area [10].

2. Materials and Methods

2.1 Study area and data

This study utilized LANDSAT 7 ETM$^+$ images that were acquired on November 25, 1999 / Nov 28, 2007/ and November 21, 2015 which had spatial resolution 30 x 30 meters by the use of the object-oriented approach (Figure 1). Prior to classification, pre-processing of the data was performed, such as image subset creation, image filtering and geo-referencing for data quality improvement. Based on the various satellite image bands; set-relevant and appropriate bands were selected for data analysis. The utilized multispectral bands revealed the target objects reflectance, e.g., near infrared (NIR), which has the characteristic of reflecting the vegetation information. It can be used for performing of image band ratios, such as Normalized Difference Vegetation Index (NDVI). This research employed 4 bands of LANDSAT 7 ETM$^+$ images, namely, ETM$^+$ band 1 (Blue band: 0.450-0.515 μm), ETM$^+$ band 2 (Green band: 0.525-0.605 μm), ETM$^+$ band 3 (Red band: 0.630-0.69 μm), and ETM$^+$ band 4 (NIR band: 0.775-0.900 μm), respectively (Table 1).

2.2 Image segmentation

Image segmentation is one the most important processes aimed at creating image objects from various pixel values. Optimal scale parameters were derived from multiresolution segmentation algorithm evaluated using ESP Tools (Estimate Scale Parameter) [11, 12]. This algorithm merges candidate adjacent pixels to the best fit image objects from user defined criterion. The process starts by searching an image pixel and merging a nearest neighbor repeatedly creating image objects based on spectral and shape homogeneity criterion defined by the user [13, 14]. Each image was segmented for creating image objects using scale parameter = 15, shape = 0.2, and compactness = 0.7, respectively (Table 2). Hierarchical image object level L1T1 represents the initial image object level 1 derived from LANDSAT 7 ETM$^+$ imagery acquired on November 25, 1999. Hierarchical image object levels L1T2 and L1T3 refer to the next two years of dynamic circumstances in the preservation area, i.e. year 2007 and 2015. Image layer weight was used to emphasize the most important target values assigned to NIR band with a layer weighted value of 3, which was aimed at the emphasis of vegetative reflectance, while other image bands weighted with value of 1. The appropriate factors for determination for image object level 1 were derived by computing a statistical value algorithm to obtain the optimal correlation values. Each image was copied to create new image object level that represents dynamic time series for possibility changes, including image hierarchical network properties applying to each image year. There are 3 new image object levels containing processed data that are prepared for individual LU/LC classification by CART classifier.

2.3 Feature analysis and selection

Prior to creating the rule set for classification, feature analysis is performed from various spectral and contextual information [15]. Spectral information; for example, image mean layers (mean Blue, mean Green, maen Red and mean NIR) are used as the image objects reflectance from certain classes. Contextual information describes shape characteristics and spatial relations of image objects related to man-made and natural features. Thus, this paper considers crucial integration factors to discriminate forest and non-forest area without considering social factors. Moreover, the modified

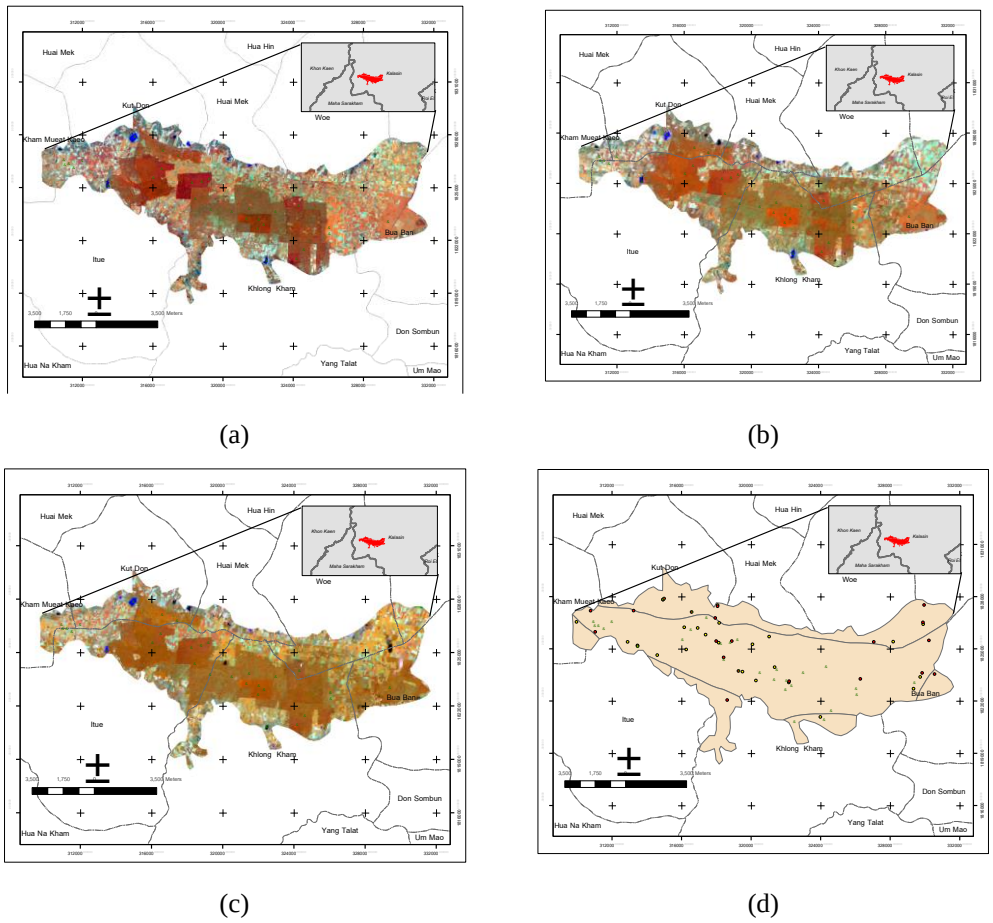

Figure 1. (a) LANDSAT 7 ETM$^+$ R,G,B 4,5,3 acquired on 25/11/1999, (b) LANDSAT 7 ETM$^+$, R,G,B 4,5,3 acquired on 28/11/2007, (c) LANDSAT 7 ETM$^+$, R,G,B 4,5,3 acquired on 21/11/2015, and (d) sampling plots from visual interpretation

Table 1. Image bands selection and alias names

Date	Bands	Alias Names
25/11/1999	Mean Blue, Mean Green, Mean Red, Mean NIR	1999_Blue, 1999_Green, 1999_Red, 1999_NIR
28/11/2007	Mean Blue, Mean Green, Mean Red, Mean NIR	2004_Blue, 2007_Green, 2007_Red, 1999_NIR
21/11/2015	Mean Blue, Mean Green, Mean Red, Mean NIR	2015_Blue, 2015_Green, 2015_Red, 2015_NIR

Table 2. Multiresolution image segmentation properties

Date	Scale parameter	Shape	Compactness	Image Layer weight	Image Object Level	Image objects
25/11/1999	15	0.2	0.7	Blue=1,	L1T1	2,383
28/11/2007	15	0.2	0.7	Green=1,	L1T2	1,576
21/11/2015	15	0.2	0.7	Red =1, NIR=3	L1T3	4,212

soil-adjusted vegetation index (MSAVI) was used for improving forest area and soil reflectance classification in areas that some indices were not able to carry out an appropriate result. This index seeks to address the limitations of NDVI and has been applied to areas with high reflectance of soil surface [16]. The output of MSAVI is a new image layer represents vegetation greenness with values ranging from -1 to +1 (equation 1).

$$\boldsymbol{MSAVI} = \frac{(\boldsymbol{NIR} - \boldsymbol{RED})(\mathbf{1}+\boldsymbol{L})}{\mathbf{NIR}+\mathbf{RED}+\mathbf{L}} \quad (1)$$

More interestingly, when apply this index, L value is the soil-brightness correction factor that needs to be input to the equation. L value is usually calculated from NIR and RED bands from selected data multiplied by 2 and s factors. However, users are able to choose the default value of 0.5 instead of using the calculation equation (equation 2).

$$\boldsymbol{L} = \frac{\mathbf{2}*\mathbf{s}*(\mathbf{NIR}-\mathbf{RED})*(\mathbf{NIR}-\mathbf{s}*\mathbf{RED})}{\mathbf{NIR}+\mathbf{RED}} \quad (2)$$

The results of the CART classification were derived from the multi-temporal imageries, and then these were examined by combining several processes to figure out the increase and decrease of forest and non-forest area. Fields surveys were verified using GPS, including the reference points and the relevant reference image objects collected from well-known target area. In order to determine the percentage of post-classification accuracy, the goal of overall accuracy should be 80 percent or higher.

2.4 Classification and regression tree (CART)

In this paper, satellite imageries were classified by using CART algorithm [17, 18]. Prior to that achievement, 3 points sample data sets were derived from visual interpretation which represented training areas for each LU/LC class by cognition domain input to the algorithm. Each point layer was created individually based on the target LU/LC classes that emerged from the study area. The vector data contained spatial and attribute information in point data representation model. There were 31 visual interpretation classified points corresponding with 6 classes in 1999, 20 points for 2007, and 25 points in 2015. The image objects data inherited image objects information from image segmentation and image selected bands, such as mean image band information and some image band ratios, such as NDVI, etc. The CART classifier comprises training, applying, querying, and authentication after classified. The training process as described above is based on classified points defined by visual interpretation, including the selected image features information. The CART (classification and regression tree) is non-parametric classification rule [19, 20]. The algorithm begins with creating a non-terminal binary tree node for each single input variable (x), and then splits this node with max purity with Gini index recursive process creating next two child nodes. The leaf nodes of the tree contain an output variable (y) which is used to make a prediction. The

process continues dividing tree branches until every aspect of the dataset is classified and visible in tree leaf nodes. For example, a classification node t_1 is a starting node for dividing dataset on x-y plane into two groups, i.e., t_2 and t_3. Then, t_2 and t_3 can represent the next terminal nodes for the classification possible class until a suitable tree is constructed.

2.5 Image classification

2.5.1 Data preparation

Prior to image classification by CART algorithm, there were 3 point vector layers created from visual interpretation for LU/LC data input into the model as described above. Each layer covered all of the target land use/land cover classes in 3 specific time series used for training CART, including spectral information and contextual information of selected classes.

2.5.2 Applying CART algorithm

There are 4 processes of decision tree classification, namely, vector to sample, training, applying and querying from unknown image objects to the target classes [21, 22]. Each imagery is input to the algorithm for creating the new classes from the visual interpreted point data using the assign class by thematic layer and vector to sample algorithms. The target class classified from the thematic layer 1 inherits attribute information from the attribute data (field name *Class_name)*, which maintain corresponding LU/LC classes for hierarchical image network level L1T1. Then, this classified layer was input to training process employing image object properties and selected features to determine what nodes, branches and child nodes should be constructed on the decision tree diagram. There were 7 object features used in the multiple features selection on image object level L1T1 and on the mapT1 (1999), namely, MSVI, NDVI and layer mean Green, mean Blue, mean Red, and mean NIR derived from each year. In the classification process, the system requirements properties were set for creating classification tree nodes and branches to achieve the optimum results. The maximum tree depth was set to 9, the minimum number of samples per node = 2, possible cluster values of a categorical variable = 16, and performance of cross validation = 3. Then, these properties were applied to the mapT2 (2007), and the mapT3 (2015) for creating and classifying the image object layers L2T2 and L3T3, respectively. The 3 image time series were analyzed in the same environment using CNL (Cognition Network Language) employed in object-based image analysis workflow creating the classification rule set [23]. The query process illustrates CNL tree on the specific location enabled branches and nodes classified from above described properties. The results show both LU/LC maps and arcs/nodes generated from CART algorithm.

2.5.3 Accuracy assessment

This process was performed from individual data examined from points, image objects and field random check points and verified by GPS in the study area. The existing collected points were compared with the visual classified images, including the existing maps as described above. This process was performed on each year's data based on existing and training information, including sample image objects derived from visual interpretation used as TTA masks. The target classes were evaluated from error matrix focused on user's accuracy and producer's accuracy and calculated for overall accuracy and kappa statistics. This research set a goal for overall accuracy of the image classification in each year at more than 80%.

2.5.4 Land use/land cover change evaluation using hierarchical image network

The classified images were evaluated using image object hierarchical networks from vertical and horizontal aspects [24, 25]. Each independent classified map was synchronized to the main map that represented the initial state for all analytical tasks [26]. Change detection was evaluated using image objects correlation from all directions based on existing classified image objects from image temporal resolution, including class descriptions from the class hierarchy approach [27]. The main map stands for the start and end points from the first step of the study till the achievement of changes evaluation [28]. This map layer comprises 3 maps collected from all transformative results from the classified independent maps, i.e. mapT1, mapT2 and mapT3 [29]. Change detection technique utilized the hierarchical image network to compare by relation to image objects on the horizontal X-axis, and by correlation to sub-objects on the vertical aspect (Y-axis) [30, 31]. The analytical processes are illustrated in Figure 2.

3. Results and Discussion

3.1 Image classification

The Landsat 7 ETM^+ imageries were classified using object-oriented approach in Dong Ranang national forest, Kalasin province, Thailand from 1999-2015, as described above. The 1999 image classification results show that the 6 target classes were spread throughout the area (Figures 3 and 4). The initial node had a 100% brightness value (<64.82), and in the next two child nodes, the brightness was divided into 59.3% of mean 1999_blue layer classified as light forest, and brightness of 48%.1% was classified as light forest. MSVIT1 information inherited at 37% was separated into 18.5% classified as dense forest, and the next node still had MSVIT1 of less than 0.783, which was classified as light forest (7.4%) and dense forest (11.1%). On the first right node classified to brightness and mean 1999_blue spectral information. The brightness < 76.76 divided to plantation area and agricultural area, and the 1999_blue < 79.81 was classified as bare land and body of water. The largest area identified was plantation area, which occupied 50.57 sq.km, followed by agricultural area at 17.54 sq.km, and body of water at 4.32 sq.km. (Table 3).

In 2007, the mean layer of blue band value was the initial point with a value of <73.93 (100%). The next two branches inherited brightness with < 60.38 (50%) and 50% of mean 2007 NIR (< 52.41). The brightness value divided into a 2007_green value node, classified as plantation area (Figures 5 and 6). The 2007_green information classified to dense and light forest. The mean 2007_NIR information scored <51.41 (50%) and classified to body of water at the first right node, and the next node displayed mean brightness value of < 74.45, and classified to agricultural area and bare land with mean brightness of 15% and 25%, respectively. Dense forest was absent in this year. Agricultural area was the main land cover class by 46.97 sq.km., followed by light forest 20.14, plantation area 11.86, and 0.77 sq.km was body of water (Table 4).

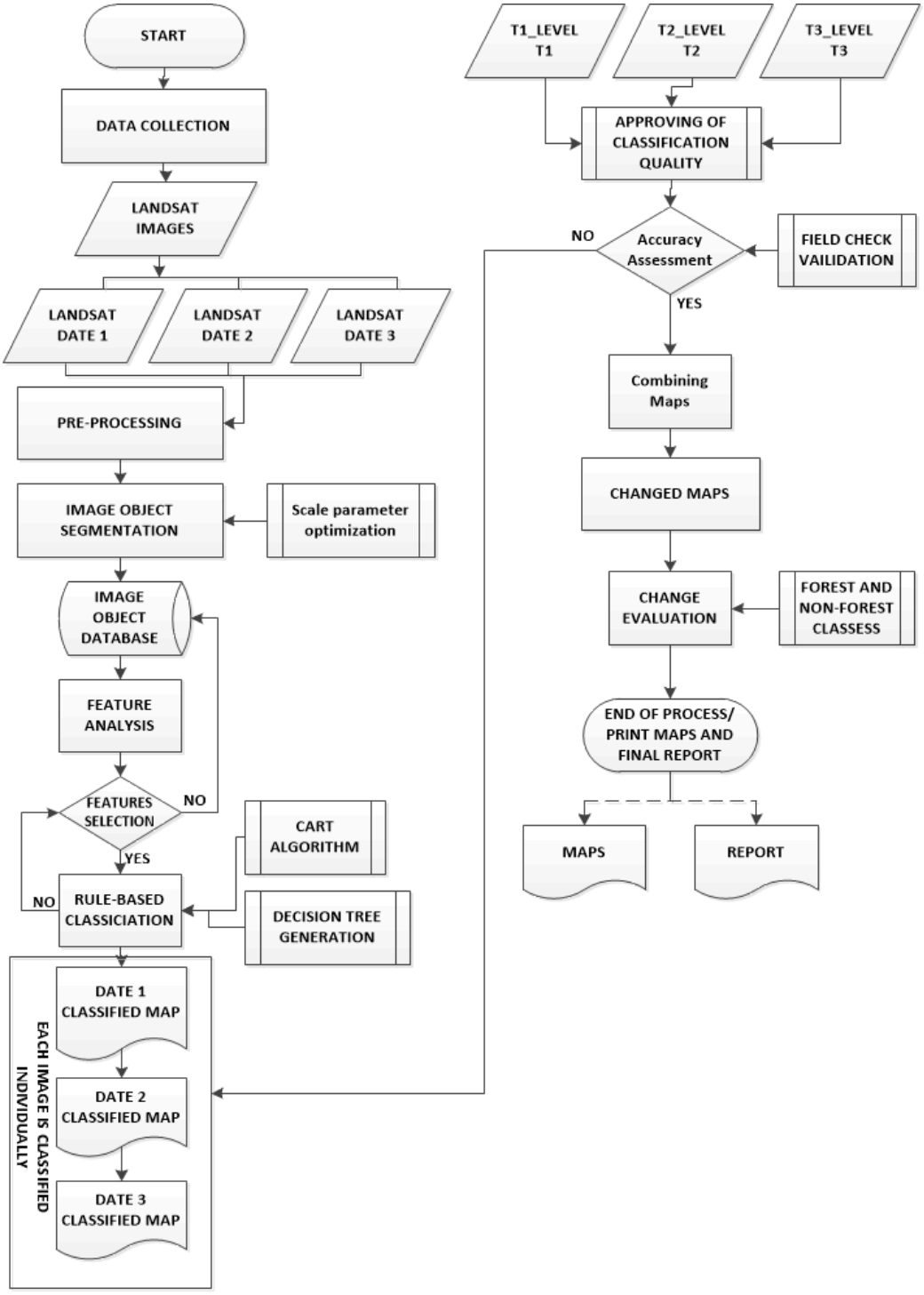

Figure 2. Workflow diagram of Dong Ranang change detection analysis

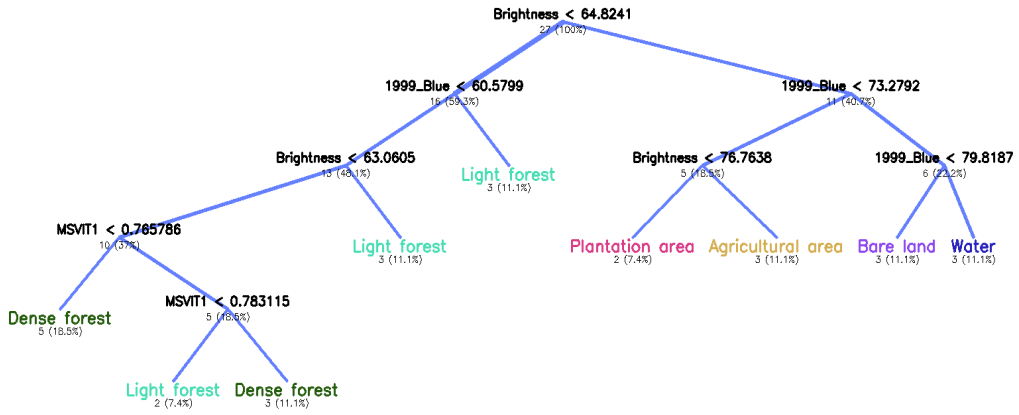

Figure 3. CART parent and child nodes in 1999

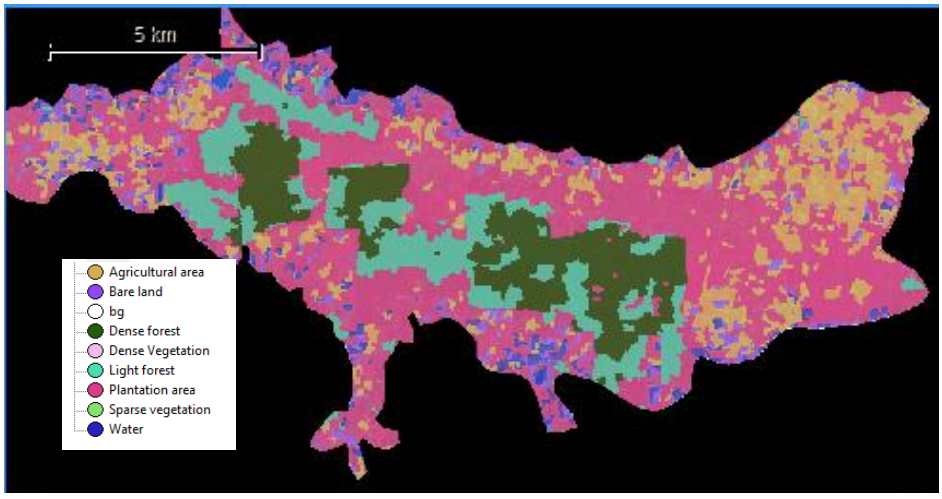

Figure 4. LANDSAT 7 ETM^{+} imagery classification result in 1999

Table 3. The classification area in 1999

Class name	Area (sq.km)
Dense forest	13.88
Light forest	14.70
Agricultural area	17.54
Bare land	5.88
Plantation area	50.57
Water body	4.325
Total	**106.89**

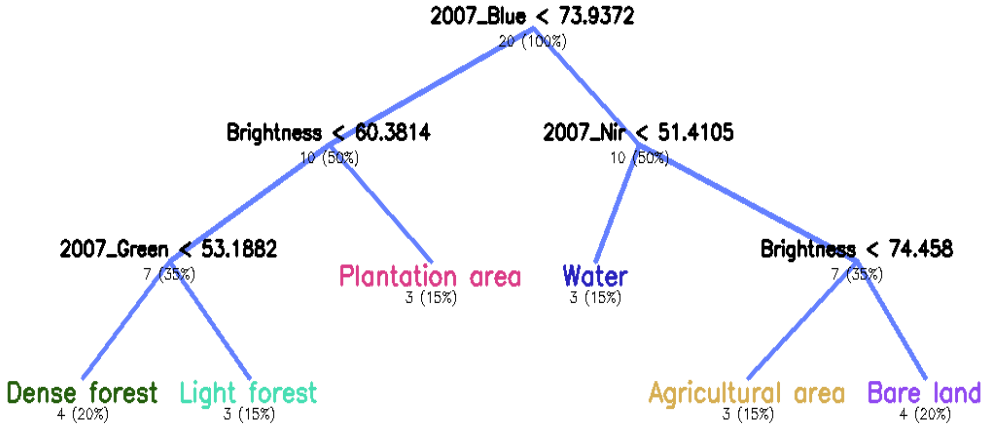

Figure 5. CART parent and child nodes in 2007

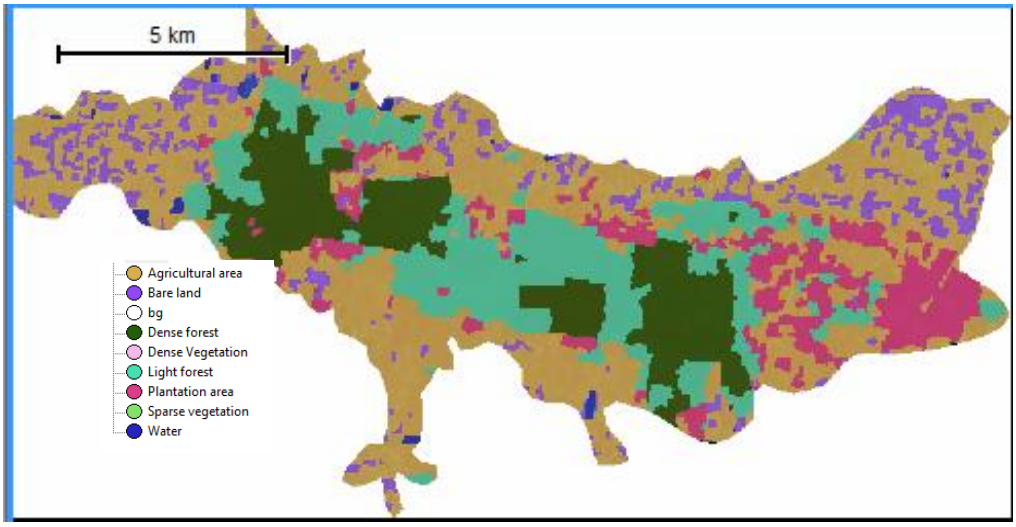

Figure 6. Landsat 7 ETM^{+} imagery classification result in 2007

Table 4. The classification area in 2007

Class name	Area (sq.km.)
Dense forest	0
Light forest	20.14
Agricultural area	46.97
Bare land	9.99
Plantation area	11.86
Water body	0.77
Total	**89.73**

In 2015, the algorithm created 2015_mean blue information by 100% (<62.71) for the first starting node (Figures 7 and 8). The next two nodes, MSVIT3 < 0.44 and 2015_mean blue < 65.20 were generated. The MSVIT3 (52.2%) was light forest and the other node still divided to dense forest and plantation area with 21.7% and 17.4% of the mean blue information derived in 2015. Moreover, 47.8% of the mean blue was classified to agricultural area and the next one node was classified to body of water and bare land from NIR information in 2015 at 13% and 17.4%, respectively. The largest area class covered was bare land, trending due to deforestation having an area at 48.66 sq.km., followed in decreasing order by dense forest 18.13 sq.km, agricultural area 16.08 sq.km, and body of water 0.29 sq.km, respectively (Table 5).

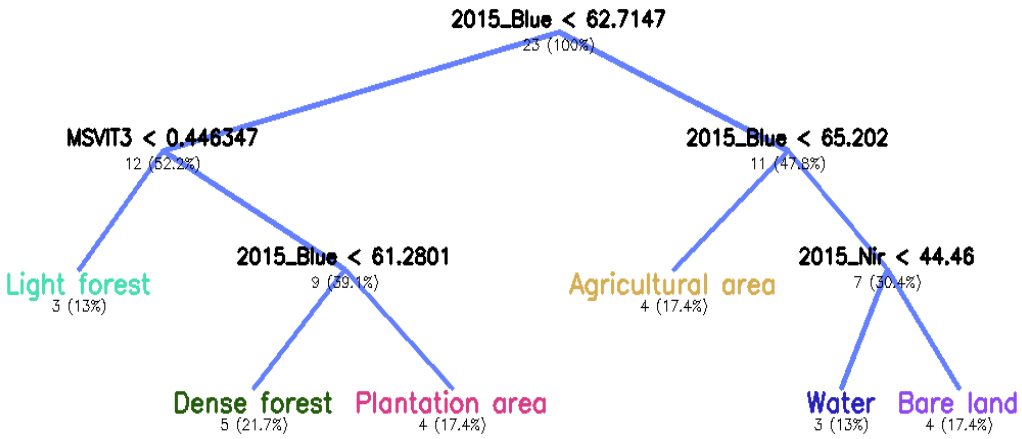

Figure 7. CART parent and child nodes in 2015

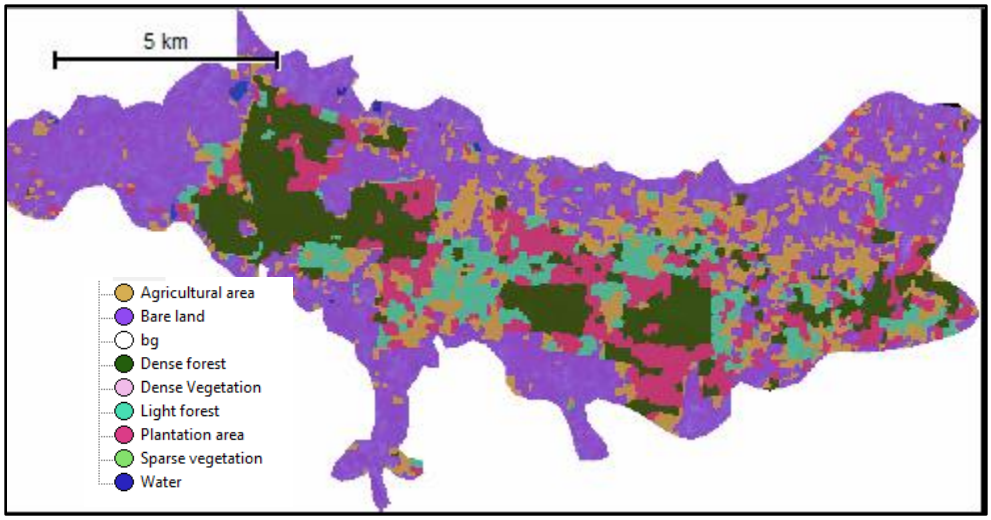

Figure 8. Landsat 7 ETM^{+} imagery classification result in 2015

Table 5. The classification area in 2015

Class names	Area (sq.km.)
Dense forest	18.13
Light forest	9.32
Agricultural area	16.08
Bare land	48.66
Plantation area	14.05
Water body	0.29
Total	**106.53**

3.2 Accuracy assessment

In the accuracy assessment process, the classified maps were compared with reference objects and collected points data from field surveying in Dong Ranang national forest. The reference data were the same data set as the data used as the sample points. These data, derived from 3 acquiring dates, were converted from the point data format to TTA Mask utilizing a process called Error matrix which was based on TTA Mask for performing and comparing with classified images. In 1999, for dense forest, the user accuracy was 85%, for light forest 70%, plantation area 86%, and overall accuracy was 87.33%. Moreover, in 2007, the overall accuracy was 88.17%, the user accuracy for dense forest was 87%, for light forest 71%, and plantation area scored 88%. Lastly, the overall accuracy in 2015 was 89.63%, dense forest had user accuracy of 91%, light forest 46%, plantation area 91%, and agricultural area 8%.

3.3 Change detection

Change detection analysis deployed the image hierarchical image network described above. Image classified by date, date 1 (1999), date 2 (2007) and date 3 (2015) were synchronized to the main map. The main map refers to the output window which the classification images were synchronized to this panel for changes evaluation and perform final discussion approach.

3.4 Map synchronization

Map synchronization is the process used for transferring the classification results in each year to the main map. However, the operation under the eCognition environment is a multi-tasking one in which the analyst can create more than one map. This makes it possible to send results from different maps over different time periods through various processes in order to obtain specific results. For example, this paper used these features to examine LU/LC changes. In addition, under the same environment, data can be analyzed using the same classification rules, which means it is unnecessary to create a new rule set for each satellite image from different specific time frames.

3.5 Image hierarchical network

The synchronized algorithm enabled the transfer of the classified maps to the main map. The classification results for 1999 data were synchronized to the main map. At the same time, on the main map, the data layer L1T1 was copied for creating the upper image object hierarchy network which represented the classification results in 1999. The data layer L1T2 was used to maintain the classification results in 2007. Then, change detection analysis from 1999-2007 was begun by using the relational to sub-objects approach. The results of land use analysis for each period were sent to

the main map. The main map data layer consisted of L1T1 classification results for 1999, L1T2 classification results for 2007, and L1T3 classification results for 2015. These classification results were arranged in the structural relationships of hierarchical image objects in horizontal and vertical aspects. This is called change detection analysis using a subtractive approach. Therefore, the conversion to sub-objects algorithm was used to perform this task, which was to 'cookie-cut' the outlines for the images that had been classified in all 3 periods. After that, the classification results L1T2 (Level_changeT1_T2: 1999-2007) and L1T3 (Level_changeT2_T3: 2007-2015) were copied to the upper layer data.

3.6 Class description creation

In order to evaluate hierarchical network of image objects on changes level, class descriptions were created to define target classes properties, and to analyze changes by defining class definitions and class-related features (relation to sub objects). The top most layer was 2007, and an image object at Level 1 maintaining the first hierarchical relationship with classified data in 1999 (Level 2) shows the vertical distance of the hierarchy image objects. The L2 level related to the level L1, is the lowest level of hierarchical mage object. However, by comparing with overlay analysis derived in GIS, which was not able to draw structure relationships, both horizontal and vertical directions are used as the supporting tools when preparing in the object-based image analysis approach.

The changes layer (Change_level_T1_T2) in 1999 indicated that the image object in the red area was classified as sparse forest after considering the NDVI and MSAVI2 values as described above. This was to evaluate the result of the transition layer in 1999, that is to see if it had changed or not. For example, the sparse forest tree tops can be changed to other land cover types. Changes in land use from light forest in 1999 to 2007 can be determined that it changed if the hierarchical image object distance on the data layer Change_level_T1_T1 related to the image object level L1T1 (2) by the distance = 1 (100%), and associated with L1T2 (1) = 0 (not related). This process is called class description achieved by using class relations to sub object features creating a class description for each target class (Figure 9).

3.7 Change detection analysis in 2007-2015 using relational to sub-objects

At this stage, there were the same conceptual routine tasks concerned with the study of land use changes during 1999-2007. The results from 1999-2007 were input to the top most changes level. The L1T3 layer was duplicated to the sub-object level by performing the subtractive approach to changes image objects. The analytical process that considered the overlapping of two-time series of land use was done by analyzing all cross validation aspects (Figures 10 and 11).

3.8 Land use land cover changes detection

Then, above, we have described the methodology of image classification in each year using CART and LU/LC change detection via the image hierarchical subtractive approach. There were 6 LU/LC classes classified in this area, namely, (1) dense forest, (2) light forest, (3) agricultural area, (4) bare land, (5) plantation area, and (6) body of water. The LU/LC change evaluation from 1999-2007 found that the dense forest showed a dramatically decrease in the area of -13.88 sq.km. The highest increase in area was plantation area (+38.68 sq.km), followed by agricultural area increased +29.43 sq.km, and plantation area increased +38.68 sq.km, respectively. Additionally, the evaluation from 2007-2015 indicated that the most decreased LU/LC class was agricultural area with -30.89 sq.km compared with 1999-2007, followed by the most increasing area which was bare land (+38.67 sq.km), and dense forest showed a slight increase of 18.13 sq.km (Table 6).

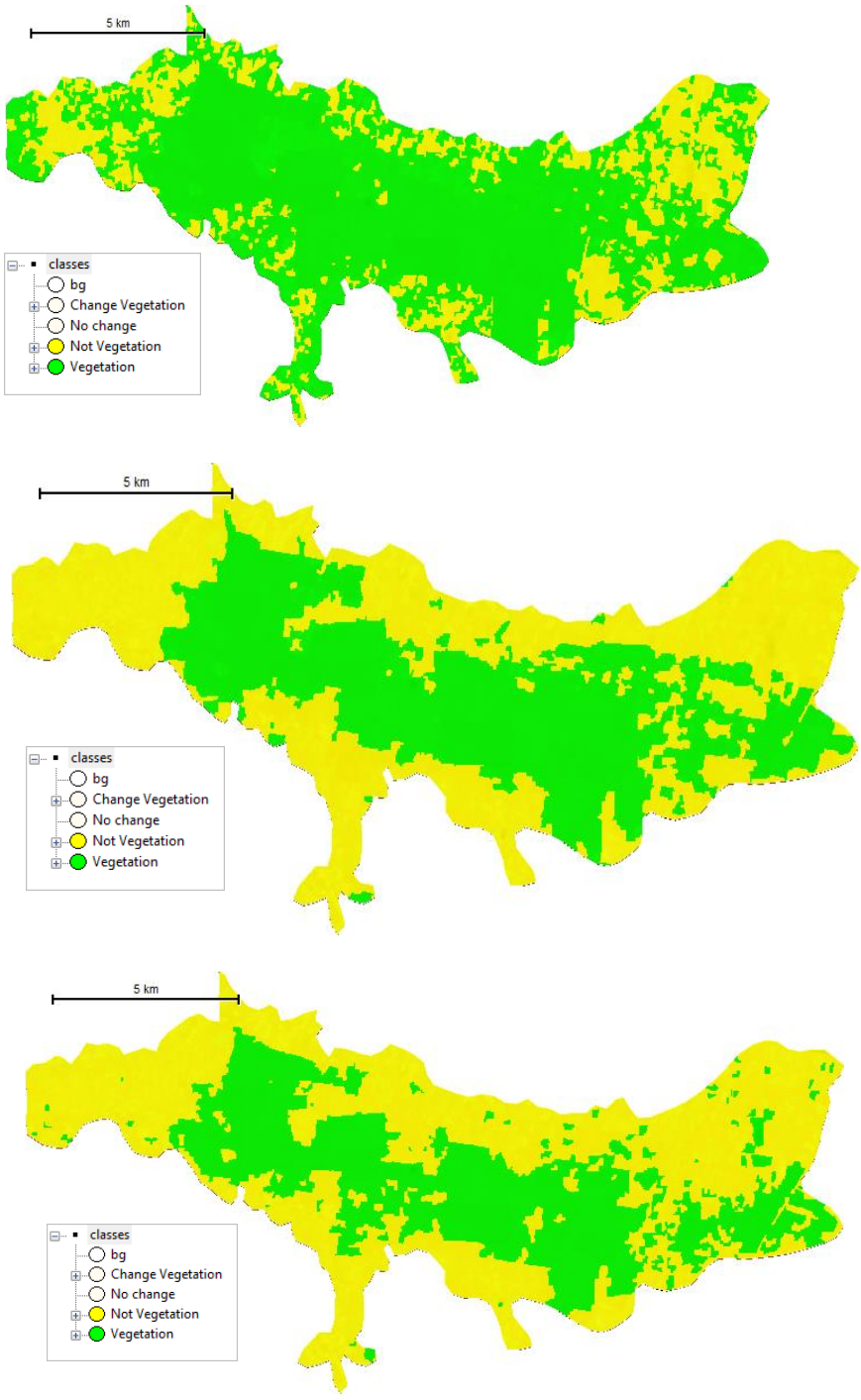

Figure 9. Forest and non-forest areas grouped by corresponding classes (a) 1999, (b) 2007, and (c) 2015

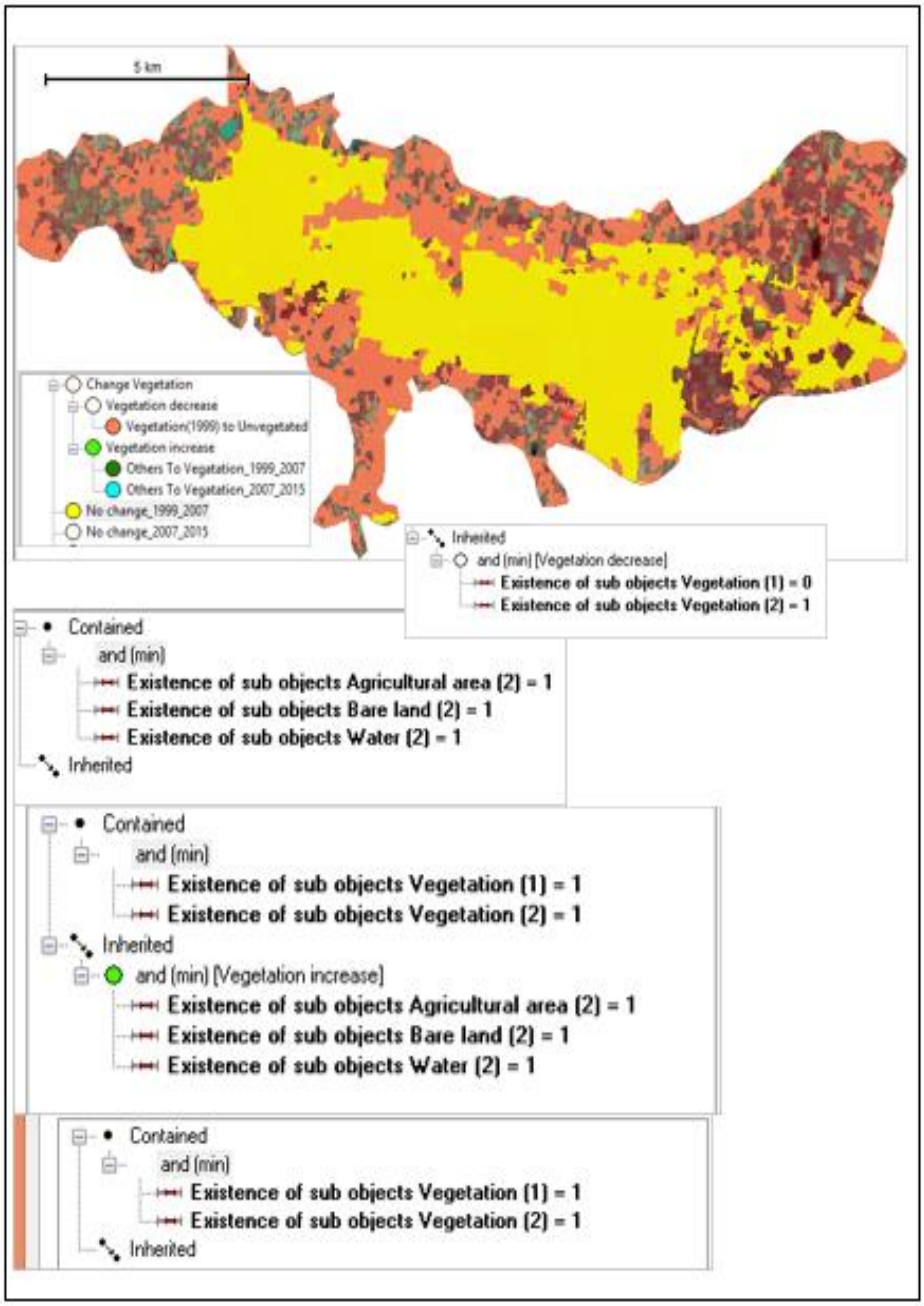

Figure 10. Land use change evaluation using hierarchical image network from 1999-2007

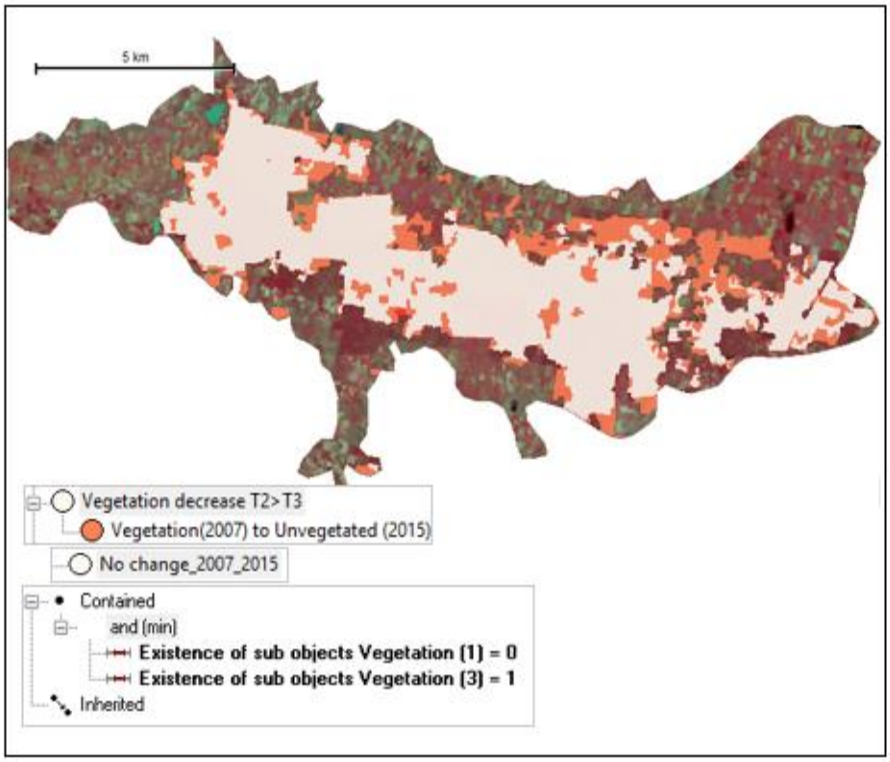

Figure 11. Land use change evaluation by using hierarchical image network from 2007-2015

Table 6. Land use land cover changes in Dong Ranang national forest from 1999-2015

Class name	1999 (km^2)	2007 (km^2	2015 (km^2)	Changing rate from 1999-2007	Changing rate from 2007-2015
Dense forest	13.88	0	18.13	-13.88	+18.13
Light forest	14.70	20.14	9.32	+6.14	-3.18
Agricultural area	17.54	46.97	16.08	+29.43	-30.89
Bare land	5.88	9.99	48.66	-4.11	+38.67
Plantation area	50.57	11.86	14.05	+38.68	+2.19
Water body	4.325	0.77	0.29	-3.555	0.48
Total	**106.89**	**89.73**	**106.53**		

4. Conclusions

This paper identifies forest changes in Dong Ranang National Forest using object-based image analysis applying CART classifier to classify images from the three-time series of LANDSAT 7 ETM^+, namely 1999, 2007, and 2015. The data of these images underwent image pre-processing in order to import to the object-oriented analytical tool effectively.

The LANDSAT 7 ETM$^+$ images from 1999-2007 were used for LU/LC changes detection analysis. Each image was classified individually using CART, including the integration of sampling points that represented LU/LC classes derived from visual interpretation. The classification stratification was composed of six classes, namely, (1) dense forest (2) light forest (3) agricultural lands (4) bare land (5) plantation this area, and (6) body of water. Under the object-oriented environment tool, the classification rule set was defined for the classification of processes using Cognition Network Language (CNL). This is consistent with image object properties and inherited information from image segmentation process. The segmentation process begins with pixel values, which are used to create image objects, each of which has its own reflectance properties, such as mean values of chosen bands, including spatial information among image objects. To increase the accuracy of the classification effectively, CART algorithm was used for classifying the three dates of Landsat imageries. In order to achieve the appropriation of the classification results, the processes began with vector sampling in order to train the data. These samples were brought into the process as the training data, creating LU/LC classes representative from known to uncertain classes. The vector to sample approach comprises training, applying and querying. The training is a process that lets the system know that the user has now determined that the selected sample is the data set used for the classification. The system assesses the various statistical correlations that were selected with the characteristics of the data that has been used. Applying CART is the process by which the selected tool is completely used in the system, the last step that analysts have chosen. Query decision tree making is a rendering process of tree network to show the results of the selection of factors responding to selection for use in satellite image analysis. The branches showed the diagram of the proportion of each selected classification factor.

Accuracy assessment was performed separately by year. The reference data obtained from the point data was derived from visual interpretation. After importing point sample data, the researchers exported the image objects that had been classified by visual interpretation, and then converted from sample point data into TTA mask used for comparing classified image objects with correct reference data. The overall accuracy in 1999 was 87.33%, in 2007 was 88.17% and in 2015 was 89.63, respectively.

Change detection in Dong Ranang National forest deployed an object-oriented image analysis for classifying the 3 time series described above. The results indicated that the forest area in 1999 was still abundant, and spread over the whole area with a total forest area of 79.15 sq.km. Some vegetation indices were used for image classification, including class description and image object hierarchical network. In 2007, the forest area had decreased significantly, and showed an area of 32 sq.km, which was a drop of 47.15 sq.km from 1999. More interestingly, the 2007 data showed that some areas of forest had changed to unexpected area type. It was found that the agricultural area covered an area of 46.97 sq.km in 2015. The forest area had still not rebounded significantly. In 2007, most of this area was still empty spaces, which was because forest area had changed to bare land. However, the Office of Forest Resources Management No. 7 (Khon Kaen province-based office) has developed reforestation projects aimed at restoring the state of the forest, which had been over exploited.

5. Acknowledgements

I would like to express gratitude to Geoinformatics Research Unit, Faculty of Informatics, Mahasarakham University for the research fund support.

References

[1] Blaschke, T., 2013. Object based image analysis: a new paradigm in remote sensing? *American Society for Photogrammetry and Remote Sensing Annual Conference*, March, 2013, 24-28.

[2] Lang, S., 2008. Object-based image analysis for remote sensing applications: modeling reality - dealing with complexity. In: T. Blaschke, S. Lang and G.J. Hay, eds. Object-Based Image Analysis: Spatial Concepts for Knowledge-Driven Remote Sensing Applications. Heidelberg: Springer; pp. 3-27.

[3] Karimi, H., Jafarnezhad, J. and Kakhani, A., 2020. Landsat time-series for land use change detection using support vector machine: Case study of Javanrud District, Iran. In: *2020 International Conference on Computer Science and Software Engineering (CSASE)*, 2020. 12831.

[4] Martha, T.R., Kerle, N., van Westen, C.J., Jetten, V. and Kumar, K.V., 2011. Segment optimization and data-driven thresholding for knowledge-based landslide detection by object-based image analysis. *IEEE Transactions on Geoscience and Remote Sensing*, 49(12), 4928-4943.

[5] Heumann, B.W., 2011. An object-based classification of mangroves using a hybrid decision tree-support vector machine approach. *Remote Sensing*, 3(11), 2440-2460.

[6] Hussain, M., Chen, D., Cheng, A., Wei, H. and Stanley, D., 2013. Change detection from remotely sensed images: From pixel-based to object-based approaches. *ISPRS Journal of Photogrammetry and Remote Sensing*, 80, 91-106.

[7] Ma, C., Ai, B., Zhao, J., Xu, X. and Huang, W., 2019. Change detection of mangrove forests in coastal Guangdong during the past three decades based on remote sensing data. *Remote Sensing*, 11(8), 921, https://doi.org/10.3390/rs11080921 https://doi.org/10.3390/rs11080921

[8] Liu, X., Chen, Y., Li, S., Cheng, L. and Li, M., 2019. Hierarchical classification of urban ALS data by using geometry and intensity information. *Sensors*, 19(20), 4583, https://doi.org/10.3390/s19204583

[9] Song, A., Kim, Y. and Han, Y. 2020. Uncertainty analysis for object-based change detection in very high-resolution satellite images using deep learning network. *Remote Sensing*, 12(15), 2345, https://doi.org/10.3390/rs12152345

[10] Pereira-Pires, J.E., Aubard, V., Silva, J.M.N., Ribeiro, R.A., Pereira, J.M.C., Fonseca, J.M. and Andre, M., 2020. Pixel-based and object-based change detection methods for assessing fuel break maintenance. In: *2020 International Young Engineers Forum (YEF-ECE)*, July, 2020, 49-54.

[11] Drăguţ, L., Eisank, C. and Strasser, T., 2011. Local variance for multi-scale analysis in geomorphometry. *Geomorphology*, 130(3), 162-172.

[12] Qin, R., Huang, X., Gruen, A. and Schmitt, G., 2015. Object-based 3-D building change detection on multitemporal stereo images. *IEEE Journal of Selected Topics in Applied Earth Observations and Remote Sensing*, 8(5), 2125-2137.

[13] Zhang, H., Eziz, A., Xiao, J., Tao, S., Wang, S., Tang, Z., Zhu, J. and Fang, J., 2019. High-resolution vegetation mapping using extreme gradient boosting based on extensive features. *Remote Sensing*, 11(12), 1505, https://doi.org/10.3390/rs11121505

[14] Qi, J., Chehbouni, A., Huete, A.R., Kerr, Y.H. and Sorooshian, S. 1994. A modified soil adjusted vegetation index. *Remote Sensing of Environment*, 48(2), 119, https//doi.org/10.1016/0034-4257(94)90134-1

[15] Ren, H. and Feng, G., 2014. Are soil-adjusted vegetation indices better than soil-unadjusted vegetation indices for above-ground green biomass estimation in arid and semi-arid grasslands? *Grass and Forage Science*, 70(4), https//:doi.org/10.1111/gfs.12152

[16] Huo, L.-Z., Boschetti, L. and Sparks, A.M., 2019. Object-based classification of forest disturbance types in the conterminous United States. *Remote Sensing*, 11(5), 477, https://doi.org/10.3390/rs11050477

[17] Zhan, Q., Molenaar, M. and Tempfli, K., 2002. Hierarchical image object-based structural analysis toward urban land use classification using high-resolution imagery and airborne LIDAR data. In: *Proceedings of the 3rd International Symposium on Remote Sensing of Urban Area's 2002*, pp. 251-258.

[18] Shao, Y. and Lunetta, R.S. 2012. Comparison of support vector machine, neural network, and CART algorithms for the land-cover classification using limited training data points. ISPRS *Journal of Photogrammetry and Remote Sensing*, 70, 78-87.

[19] Denison, D.G.T., Mallick, B.K. and Smith, A.F.M., 1998. A Bayesian CART algorithm | *Biometrika*, 85(2), 363-377.

[20] Ma, H., Liu, Y., Ren, Y., Wang. D., Yu, L. and Yu, J., 2020. Improved CNN classification method for groups of buildings damaged by earthquake, based on high resolution remote sensing images. *Remote Sensing*, 12(2), 260, https//doi.org/10.3390/rs12020260

[21] Hong, L. and Zhang, M., 2020. Object-oriented multiscale deep features for hyperspectral image classification. *International Journal of Remote Sensing*, 41(14), 5549-5572.

[22] Rahimizadeh, N., Kafaky, S.B., Sahebi, M.R. and Mataji, A. 2019. Forest structure parameter extraction using SPOT-7 satellite data by object- and pixel-based classification methods. *Environmental Monitoring and Assessment*, 192(1), 43, https://doi.org/10.1007/s10661-019-8015-x

[23] Fallatah, A., Jones, S. and Mitchell, D. 2020. Object-based random forest classification for informal settlements identification in the Middle East: Jeddah a case study. *International Journal of Remote Sensing*, 41(11), 4421-445.

[24] Ghasemain, B., Asl, D.T., Pham, B.T., Avand, M., Nguyen, H.D. and Janizadeh, S., 2020. Shallow landslide susceptibility mapping: A comparison between classification and regression tree and reduced error pruning tree algorithms. *Vietnam Journal of Earth Sciences*, 42(3), 208-227.

[25] Benedetti, A., Picchiani, M., Del Frate, F., 2018. Sentinel-1 and sentinel-2 data fusion for urban change detection. *IGARSS 2018-2018 IEEE International Geoscience and Remote Sensing Symposium*, Valencia, 2018, 1962-1965.

[26] Lin, Y., Zhang, L., Wang, N., Zhang, X., Cen, Y. and Sun, X., 2020. A change detection method using spatial-temporal-spectral information from Landsat images. *International Journal of Remote Sensing*, 41(2), 772-793.

[27] Ai, J., Zhang, C., Chen, L. and Li, D., 2020. Mapping annual land use and land cover changes in the Yangtze estuary region using an object-based classification framework and landsat time series data. *Sustainability*, 12(2), 659, https://doi.org/10.3390/su12020659

[28] Zhang, X., Xiao, P. and Feng, X. 2020. Object-specific optimization of hierarchical multiscale segmentations for high-spatial resolution remote sensing images. *ISPRS Journal of Photogrammetry and Remote Sensing*, 159, 308-321.

[29] Krauß, T. and Tian, J., 2020. Automatic change detection from high-resolution satellite imagery. In: D.G. Hadjimitsis, K. Themistocleous, B. Cuca, A. Agapiou, V. Lysandrou, R. Lasaponara, N. Masini and G. Schreier, eds. *Remote Sensing for Archaeology and Cultural Landscapes: Best Practices and Perspectives Across Europe and the Middle East*. Cham: Springer International Publishing, pp. 47-58.

[30] Ghosh, D. and Chakravortty, S., 2020. Change detection of tropical mangrove ecosystem with subpixel classification of time series hyperspectral imagery. In: D.J. Hemanth, ed. *Artificial Intelligence Techniques for Satellite Image Analysis*. Cham: Springer International Publishing, pp. 189-211.

[31] Tejenaki, S.A., Ebadi, H. and Mohammadzadeh, A. 2020. Automatic road detection and extraction from MultiSpectral images using a new hierarchical object-based method. *Journal of Geomatics Science and Technology*, 9(3), 13-27.

Assessment of the Effects of Land Use/Land Cover Changes on Soil Loss and Sediment Yield Using WaTEM/SEDEM Model: Case Study of Ziz Upper Watershed in SE-Morocco

Fenjiro Imad[1], Zouagui Anis[2] and Manaouch Mohamed[1]*

[1]Laboratory of Environment, Societies and Territories, Department of Geography, Faculty of Letters and Human Sciences, Ibn Tofail University, Kenitra, Morocco
[2]Research Unit of Water and Soil Management and Conservation, National Energy Center for Nuclear Science and Technology, Rabat, Morocco

Received: 19 July 2020, Revised: 15 October 2020, Accepted: 13 November 2020

Abstract

Water erosion and sediment production rates are closely related to land use and land cover (LULC). A spatially distributed soil erosion and sediment delivery model can be used as a good tool to assess the effects of changes in land use/land cover on erosion processes. However, the calibration of such a model requires a lot of data, which is sometimes non-existent. In this work, WaTEM/SEDEM model of spatial distribution of sediments and their delivery to rivers was applied to the large Ziz basin (4,435 km^2) in south-eastern Morocco. Model calibration and validation were carried out based on recorded sediment yield during the period from 1973 to 2009 at Hassan Eddakhil dam in the catchment outlet. Thereafter, three LULC scenarios were modeled by reproducing land use/land cover in 1936 and in 1957 and then a hypothetical future scenario. The results of LULC dynamics revealed that degraded forest drastically declined while rangeland substantially increased between 1936 and 2017. These changes in LULC can be explained by the interactions between bioclimatic factors and ecologically inadequate and ultimately destructive human interventions (overgrazing, deforestation). The comparison of WaTEM/SEDEM simulations for these scenarios with the current situation of LULC shows that sediment yield has increased from 1.5 million to 2.2 million ton/year and an increase in specific sediment yield from 3.37 to 5.6 t/ha/year. For soil erosion classes, the results show a trend of slight to moderate class from 1936 to current situation. The present study has shown that the great anthropogenic pressure on the natural resources of the Ziz upper watershed ended by the outcropping of pavements of soils exposed directly to the erosive processes.

Keywords: LULC change; WaTEM/SEDEM; GIS; sediment yield; Ziz; SE Morocco
DOI 10.14456/cast.2021.28

*Corresponding author: Tel.: (+212) 672561079 Fax: (+212) 672561079
E-mail: mmanaouch@gmail.com

1. Introduction

The world's population is projected to reach10 billion by 2056, and this increase will lead to substantial increases in demand for natural resources (water, air, soil) [1]. For soil resources, research did not start until the middle of the 20th century, and it was focused on the physico-chemical and biological properties, the genesis, and the geographic distribution of soils [2].The degradation of the soil resource has had a negative impact on the well-being of at least 3.2 billion people and caused a massive extinction affecting one sixth of all species on the planet [3]. The United Nations Sustainable Development Goals explicitly identify soil resources as being of crucial importance and promote soil resources' protection in order to achieve the ambitious goal of Zero Land Degradation by 2030 [4]. These goals provide good opportunities for soil erosion modelers to respond with more specific assessments and solutions on how to reach these goals.

In Europe, water erosion is the most serious danger to soils [5]. Accelerated water erosion affects one sixth of land surface [6] and mountainous regions are among the high-risk areas due to steep slopes that increase soil erosion and sediment redistribution rates [7].

Recently, many studies have demonstrated that land cover/land use (LULC) is among the main drivers of soil erosion intensity, and historical LULC changes have affected soil erosion rates and sediment yields in many watersheds around the world [7].

A quantitative assessment of the impact of LULC changes on soil loss and sediment export can be conducted in various ways: in the field by suspended sediment measurement, and in experimental watershed by long-term monitoring. Nowadays, geographic information systems (GIS) techniques and remote sensing data (RS) can be used successfully to enable rapid and detailed soil erosion assessment. Thus, these useful techniques provide effective methods of measuring, analyzing and managing soil erosion from the scale of the plot to the regional. Therefore, spatial and quantitative information on soil erosion at the watershed scale can contribute significantly to soil conservation planning.

In Morocco, according to the national watershed management plan [8], soil erosion has affected a large part of the national territory (75%). The cumulative annual soil losses are estimated at 100 million tones [9], with 50 million m^3 of water loss each year by siltation in large dams. These results have triggered alerts for urgent intervention and monitoring of soil losses for better decision-making with regard to the conservation of soil and water resources.

To assess and predict soil erosion under different conditions and to develop management plans, soil erosion models are good tools for assessing soil erosion rates for the current LULC conditions with a number of alternative LULC scenarios. Spatially distributed erosion and sediment transport models allow the assessment of both the differences in total sediment yield, differences in sediment sources, and the existence of sedimentation traps within catchments. Empirical models such as USLE (Universal Soil Loss Equation) were the first introduced, followed by physical models. Among these models, there was WaTEM/SEDEM (Water and Tillage Erosion Model [10] and SEdiment DElivery Model [11]), a spatially-distributed soil redistribution rates and sediment delivery model, based on RUSLE (Revised Universal Soil Loss Equation) and equipped with a sediment transport equation to predict sediment supply in a drainage network at regional scale [7]. The first modelling of soil erosion on European scale using WaTEM/SEDEM model indicates that sediments delivery towards fluvial system were 15.3% of total eroded soils [6].

The main objective of the present study was to assess soil redistribution rates and sediment supply to a stream network under current, past and future conditions of LULC in a semi-arid context using WaTEM/SEDEM model, calibrated and validated by recorded sediment yields at the catchment outlet. The study area (Ziz upper watershed in southeast Morocco) is a large catchment with poorly developed soils [12] for which a good amount of sediment yield data was recorded during 1973 to 2009 at the Hassan Eddakhil dam, the only hydraulic structure built in 1971 with an

initial water capacity of 380.10^6 m^3 [13]. It was built with two objectives: to protect the Tafilalet plain against floods and to provide the water needs for irrigation and for the use of the population.

2. Materials and Methods

2.1 Study area

Ziz upper watershed is located in the oriental region of Moroccan High Atlas (Figure 1). It is a large mountainous watershed in Ziz at Draa-Tafilalet region and covers a total area of approximately 4,435 km^2. It borders central High Atlas to the West, upper Moulouya to the North and Anti Atlas to the south. Ziz upper watershed topography is very rugged, and the altitude varies from 1,023 m a.s.l. (above sea level) to 3,687 m a.s.l. in the north-west part with an average altitude of 1,812 m. The dominant slope class that occupies more than 80% of the Ziz upper watershed area is between 0 and 15°.

This basin experiences a semi-arid climate characterized by a harsh winter and a moderate summer with mean annual temperatures ranging from 10.2°C to 19.2°C [2]. The annual rainfall ranges from 119 mm to 377 mm and falls in spring and autumn. The Ziz catchment is crossed by national road 13 and regional road 706, which connect the center of Imilchil to the center of Er-Rich. The 2014 census reported the population of Draa-Tafilalet region at 1,635,008, compared to 149,580 in 2004 [14]. Most people live in rural areas on the banks of Oued Ziz where they predominantly practice subsistence farming of cereals and legumes, and their farms are concentrated along the riverbanks. The center of Er-Rich is the largest agglomeration located at the point where two major Oueds branches, that drain the upstream western and northern parts of Ziz valley, meet. The soils represented are poorly developed, and are alluvial or colluvial contributions in the deposition areas, or even raw minerals have not yet developed [15].

According to the geological map [16, 17] of the study area, Jurassic formations largely dominate and occur in two main levels of limestone: The Upper Aalenian and the Dogger. Triassic formations occur in small areas and include marls and dolomitic clays with salt levels and basalts [15]. The dominant LULC features include: poorly vegetated areas or rangelands (64%), degraded forest (25%), agricultural fields (10.1%), and water bodies (0.6%).

2.2 WaTEM/SEDEM model

In this work, we used WaTEM/SEDEM model to estimate soil loss and sediment transport in a large mountain watershed, under current, past and future conditions. This model has been applied in different conditions including Spanish catchments [18-20], Australian catchments [21], Slovenian landscapes [22], European scale [23] and recently in Czech watersheds [24].

WaTEM/SEDEM model is based on RUSLE equation and a transport capacity equation (TC) to predict sediment delivery in a drainage network [10, 11, 25]. This model comprises three components; the first is used to calculate annual soil erosion using the RUSLE approach as shown in equation 1 [26].

$$A = \mathrm{R} * \mathrm{K} * \mathrm{LS}_{2\mathrm{D}} * \mathrm{C} * \mathrm{P} \quad (1)$$

Where A is the mean annual soil loss (kg/m^2/year), R is a rainfall erosivity factor (MJ mm/m^2/h/year), K is a soil erodibility factor (kg h/MJ/mm), C is a dimensionless cover and management factor, P is a dimensionless erosion control practice factor, and LS_{2D} is a slope-length factor [27]. The second is used to estimate sediment flux from slopes to the stream network (equation 2) [11].

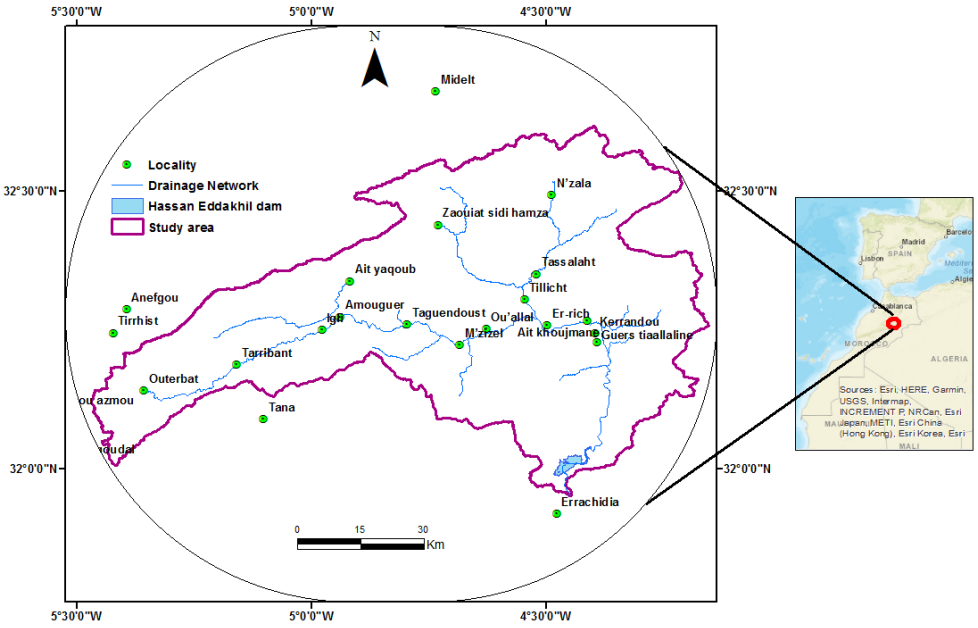

Figure 1. Location of the Ziz upper watershed in southeast Morocco

$$TC = ktc * R * K * (LS_{2D} - 4{,}1s^{0,8}) \quad (2)$$

Where TC is the annual transport capacity (kg/m/year) and R, K, and LS factors are the same as in equation 1, s is the local slope (m/m) and ktc is a transport capacity parameter (m). The third is tillage erosion which represents the net soil flux caused by tillage on a hillslope of infinitesimal length and unit width and is proportional to the local slope gradient (equation 3) [28]:

$$Qs,t = ktill\ s = -ktill\ dh/dx \quad (3)$$

Where Qs,t is the net downslope flux due to tillage translocation (kg/m/year), ktill is the tillage transport coefficient (kg/m/year), s is the local slope gradient (m/m), h is the height at a given point of the hillslope (m) and x is the horizontal distance (m)[28].

2.2.1 Model inputs

WaTEM/SEDEM model requires that input parameter files must have the same resolution. The topographic data and the river topology/flow were derived from SRTM-DEM (main input). The C factor was estimated using the regression relation of Van der Knijff [29], The K factor was estimated using the Wischmeier monogram and the results of soil studies of the national watershed management plan for the adjacent Assif Melloul watershed [15]. The R factor was calculated using rainfall data available from meteorological stations. Road and ponds maps were produced using satellite images and available topographic maps of the study area.

The inputs layers were generated in IDRISI GIS software (Clark Labs, Clark University) with a horizontal resolution of 30 * 30m. This resolution was choosed to keep the same DEM's resolution. The input layers consisted of R factor, K factor, C factor and Parcel map. The P factor was fixed to be 1 in WaTEM/SEDEM.

2.2.2 Model calibration

WaTEM/SEDEM calibration was conducted by adjusting its parameters (ktc and ktill). Then, the simulation results were compared with observed results in the Hassan Eddakhil dam. Recorded sediment data from 1973 to 1990 were used for model calibration and those recorded from 1991 to 2009 were used for model validation. To assess model results efficiency, we used The Nash–Sutcliffe equation 4 [30].

$$NS = 1 - \frac{\sum_{i=1}^{n}(Oi-Pi)^2}{\sum_{i=1}^{n}(Oi-Omean)^2} \quad (4)$$

Additionally, the relative root mean square error (RRMSE) was used as an estimate of the model accuracy according to equation 5.

$$RRMSE = \frac{\sqrt{\frac{1}{n}\sum_{i=1}^{n}(Oi-Pi)^2}}{\frac{1}{n}\sum_{i=1}^{n}Oi} \quad (5)$$

Where n is the number of observations, Oi is the observed value, Omean is the mean observed value, and Pi is the predicted value. The closer the value of NS is to 1, the more efficient is the model. Details of the calibration procedure are given in the studies of Mohamed *et al.* [31].

2.3 LULC change detection

The detection of LULC changes in the Ziz upper watershed was carried out using the overlay operation of three parcel maps obtained from georeferenced maps (1936 and 1957) and from the Landsat 8 images acquired in March 2017 for the same geographical area. LULC change was very pronounced during the period from 1936 to 2017. Figures 2 and 3 present LULC dynamics in the study area and a probable future situation.

During the period of 1936 to 2017, the Ziz upper watershed was dominated by degraded forest and followed by poorly vegetated areas. Meanwhile, agricultural fields and water bodies were the least land use types. The results show that degraded forest consistently underwent serious decrease. On the contrary, poorly vegetated areas kept on increasing. The decrease of degraded forest from 1936 to 2017 reflected the great pressure of deforestation and overgrazing undertaken by the population. Figure 3 shows more details about the dynamic LULC change in the Ziz upper watershed.

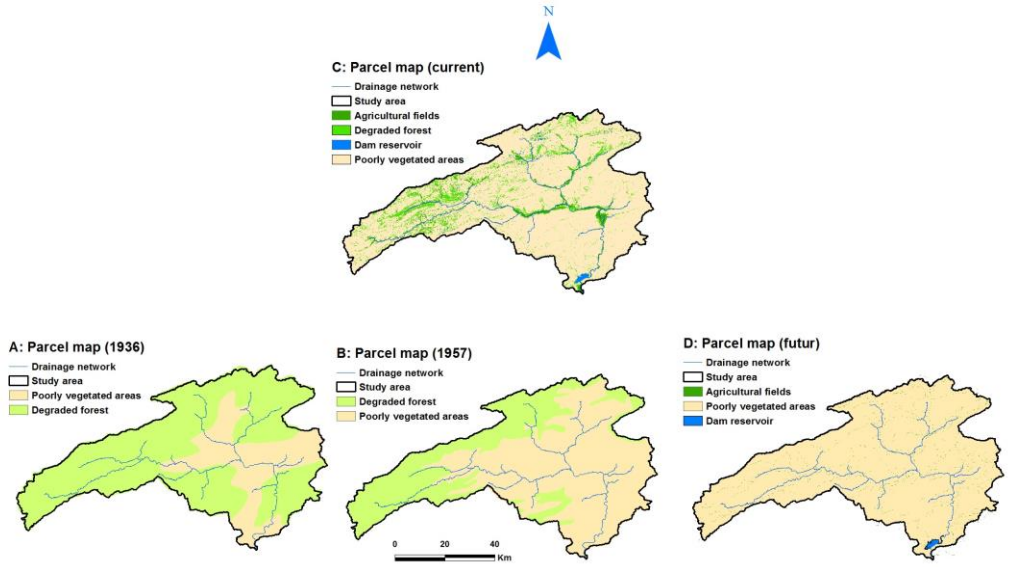

Figure 2. Dynamic change of parcel maps of the Ziz upper watershed under past (A:1936, B:1957), current (C) and likely future conditions (D)

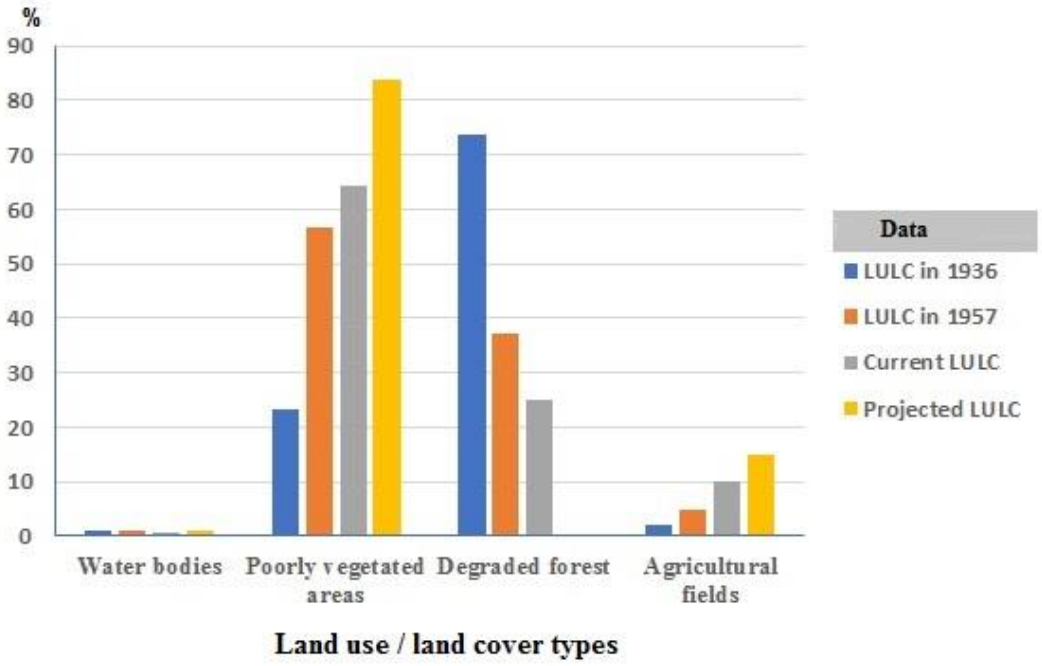

Figure 3. Diagram of Land Use/Land Cover (LULC) dynamic in the Ziz upper watershed under past, current and future conditions

3. Results and Discussions

3.1 WaTEM/SEDEM calibration and validation

Optimal parameters found in the model calibration were ktcmax = 477m and ktill = 0m. This ktcmax seems at first to be high in comparison with those found by Verstraeten [32] in Belgium watersheds (ktcmax = 250m), by Haregweyen *et al.* [33] in Ethiopian catchments (ktcmax = 110m), by Syahli [34] in Merawu watershed in Indonesia (ktcmax = 297m), and by Konecna *et al.* [24] in Czech watershed (ktcmax = 55m). These comparisons should be taken very carefully since the environmental conditions are not similar and the resolution of the Digital Elevation Models (DEMs) used is different in all these studies. With reference to the tillage transport coefficient (ktill) that controls the intensity of tillage erosion, in the case of our study: agricultural fields which occupy 10% of the total area in the Ziz upper watershed, are very narrow and distributed along the banks of the Ziz valley. They are generally small flat areas and plowing there is done by conventional tools such as the wood plow. So, the contribution of tillage to soil redistribution was almost negligible. Also, in comparison with the WaTEM/SEDEM application made by Quijano *et al*. [20], ktill was fixed at the value of 0 knowing that in their study area (Ebro basin, NE Spain) the plowing was done by modern mechanical tools. The application of the WaTEM/SEDEM model using optimal parameters allowed us to predict the annual sediment yield and the predicted soil loss map. The comparison of simulated results with those measured at the catchment outlet shows a good correlation (65%). The Relative Root Mean Square Error (RRMSE) of the model's accuracy found in this simulation was approximately 2.6%. For more details, we refer to the studies of Mohamed *et al*. [31].

3.2 Sediment main sources and deposition areas

To simplify the reading of the predicted soil loss map, the Ziz upper catchment was subdivided into 27 sub-basins (Figure 4A and Table 1). In all the pixels of each sub-basin, GIS Idrisi calculates soil losses and deposits. If the losses are greater than the deposits, we have a negative balance which means erosion and if the losses are less than the deposits, we will have a positive balance, which means deposition. The results show that the sub-basins n° 1, 20, 21, 22, 23 and 24 display positive values, which means that they are intermediate locations of sedimentation. The other sub-basins show negative values, which means that they are hotsspot of sediment generation.

The sub-basins n°3, 4 and 5 are the most sediment producing. However, n° 22 is the site receiving the highest sediment deposit. For other LULC situations, Figure 4 and Table 2 illustrate the spatial distribution of soil erosion and deposition in the Ziz upper watershed.

Table 2 showed that soil erosion affected about 9/10 of the study area under different LULC situations, and it was only approximately 1/10 of the catchment area that experienced deposition. The areas affected by erosion increased slowly. On the contrary, those where the deposition occurred decreased slightly. Figure 4 shows that the steeply sloped parts were the areas that experienced the worse erosion. However, deposition occurred in the southern parts of the catchment and in the areas where the topography was relatively flat.

3.3 Results of WaTEM/SEDEM application for different LULC situations

LULC change dynamic from 1937 to 2017 indicates a reduced area occupied by degraded forest at the expense of poorly vegetated areas (rangelands). The results show a reduction of about 2/3 in degraded forest (73.6% to 25%) over the last decades. This occurred as a result of the deforestation

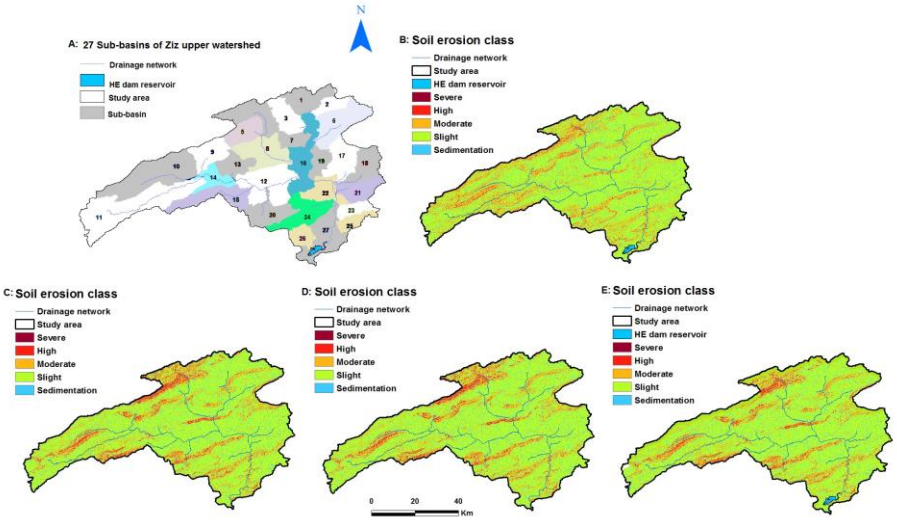

Figure 4. The 27 sub-basins (A) and predicted soil loss map of the Ziz upper watershed under past (C:1936, D:1957), current (B) and a likely future Land Use/Land Cover (E)

Table 1. Distribution of sediment budgets and water erosion factors values by sub-basin in the Ziz upper watershed for the current LULC conditions

Sub-basin	Area (ha)	Area (%)	R factor	K factor	LS factor	C factor	Sediment budget (t/year)
1	14457.7	3.3	0.0038	0.072	12.2	0.79	347.52
2	6547.1	1.5	0.0037	0.080	11.7	0.82	-6010.53
3	13244.4	3.0	0.0037	0.077	13.7	0.83	-37205.12
4	17442.8	4.0	0.0039	0.107	24.7	0.84	-46342.52
5	11812.1	2.7	0.0038	0.116	26.0	0.83	-31054.55
6	22775.2	5.2	0.0036	0.108	11.0	0.83	-3722.84
7	6915.7	1.6	0.0035	0.115	10.3	0.84	-745.65
8	21023.7	4.8	0.0036	0.094	12.6	0.83	-5460.84
9	13725.4	3.2	0.0038	0.101	20.3	0.84	-24213.46
10	38278.8	8.8	0.0044	0.072	20.5	0.80	-20352.4
11	46372.6	10.7	0.0050	0.069	18.9	0.82	-7749.95
12	27139.6	6.2	0.0036	0.080	9.3	0.83	-436.52
13	10869.1	2.5	0.0038	0.067	11.4	0.86	-6640.84
14	8994.3	2.1	0.0038	0.061	15.6	0.84	-4651.29
15	8254.7	1.9	0.0034	0.068	10.3	0.87	-912.82
16	21920.5	5.0	0.0034	0.091	10.2	0.83	-4485.32
17	16244.8	3.7	0.0034	0.086	11.6	0.86	-1595.33
18	13752.5	3.2	0.0034	0.066	8.9	0.87	-2214.26
19	17608.7	4.0	0.0039	0.115	14.1	0.86	-21532.94
20	15649.9	3.6	0.0036	0.080	20.1	0.81	284.53
21	12206.1	2.8	0.0033	0.094	10.1	0.84	179.94
22	12465.9	2.9	0.0033	0.087	11.6	0.79	3243.93
23	18098.8	4.2	0.0033	0.110	16.9	0.83	450.66
24	6831.7	1.6	0.0033	0.059	14.3	0.81	102.42
25	6641.9	1.5	0.0032	0.053	15.9	0.79	-37.87
26	7469.8	1.7	0.0031	0.072	22.8	0.80	-655.62
27	18238.7	4.2	0.0030	0.077	21.4	0.82	-25418.36

Table 2. Spatial distribution of soil erosion and deposition in the study area under past, current and future condition of Land Use/Land Cover (LULC)

Year	1936 (%)	1957 (%)	Current (%)	Projected (%)
Erosion	88.12	88.54	90.5	91.2
Deposition	11.47	11.45	9.5	8.2

(to ensure the wood used for heating and cooking) and overgrazing (mostly herds of goats). As a result, the increase of poorly vegetated areas (rangelands) caused the appearance of bare soil that were exposed directly to erosive agents that increased water erosion rates and sediment yields. The WATEM/SEDEM model allowed the prediction of sediment delivery maps for the three LULC scenarios, which was interesting for comparing the effect of LULC changes on soil erosion and sediment yields. Table 3 provides more details.

Table 3. Summary of the WaTEM / SEDEM model results for different LULCs scenarios in the Ziz upper watershed

WaTEM/SEDEM results	For 1936	For 1957	Current	Projected
Total sediment production (t/year)	52831150.3	44772374.3	23135015.6	37125431.9
Total sediment deposition (t/year)	51328083.7	43257181.9	21105686.6	34885858.6
Total river export (t/year)	1495651.6	1507824.3	2027095.5	2229264.9
Sediment yield (t/year)	1503066.6	1515192.4	2029328.9	2239573.3
Specific sediment yield (t/ha/year)	3.37	3.57	4.58	5.6

For the current LULC situation, the specific sediment yield is 4.58 t/ha/year, while for 1936, 1957 and a likely future condition the specific sediment yields are 3.37, 3.57 and 5.6 t/ha/year, respectively. These results show that the transition of degraded forest areas from steeply sloped to poorly vegetated areas caused high rate of soil loss and sediment yield. These results revealed that sediment yield at the catchment outlet of the Ziz upper watershed follows the LULC change.

According to the predicted map of soil erosion classes, the results show an increasing trend from slight to moderate (from 1936 to current situation) and slight erosion classes increased slowly while areas in the high soil severity class decreased. Meanwhile, other soil erosion classes had mix increase and decrease trends, such as high class that increased from 1936 to 1957 and decreased from 1957 to 2017. Table 4 presents more details about the dynamic of erosion classes.

Table 4. Distribution of soil erosion classes in the Ziz upper watershed under current, past and future conditions

Soil loss (t/ha/year)	Erosion class	Area (%) for 1936	Area (%) for 1957	Area (%) for current	Area (%) for future
>70	Severe	0.17	0.16	0.18	0.14
20 to 70	High	5	5.1	1.9	4.6
7 to 20	Moderate	17.6	17.6	19.4	16.8
0 to 7	Slight	77.1	77	78.5	78.3

The results of the spatial distribution of soil erosion classes showed that the highest rate of slight erosion class occured in the current situation (78.5%) and the lowest occured in 1936 and 1957. Meanwhile, the lowest high class and the highest moderate class are occured in the current LULC. İn 1936 and 1957 conditions, the spatial distribution of soil erosion classes looked similar. The diagram in Figure 5 gives a description of the distribution of erosion classes and depositions in (ha) for the different scenarios.

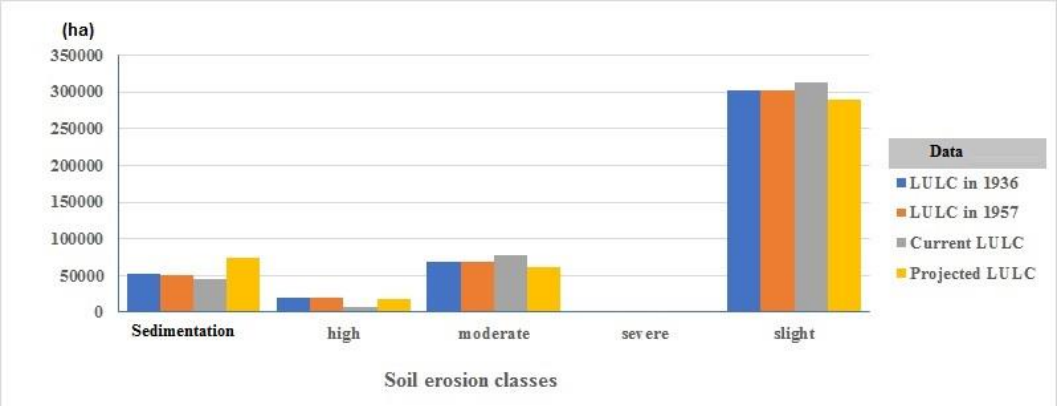

Figure 5. Diagram of soil erosion classes composition in the Ziz upper watershed under past, current and future conditions of LULC

3.4 Sediment yield at the Hassan Eddakhil dam

For the current LULC situation, the total sediment production is 23,135,015.6 ton/year, which represents significant soil erosion, and this quantity is directly linked to the effect of soil erosion on-site. However, during the transportation process, the amount of eroded soil available as suspended sediment that can reach the catchment outlet called "sediment yield" is about 2,029,328.9 ton/year. This large quantity of suspended sediment leads to off-site problems related to the supply of sediment to the rivers which lead to the early siltation of the Hassan Eddakhil dam, the only hydraulic infrastructure in the study area. On the other hand, based on Ghorbel and Claude's work [35] for converting sediment densities, it was found that "one cubic meter of mud with an apparent density (da) = 1.7 contains 1.2 tons of solids (sediments)". So, considering this average value, the sediment load arriving at the Hassan Eddakhil dam can as well be expressed as 1,691,107.4 m^3/year.

Given that the dam reservoir has an initial water capacity of 380 million cubic meters, the sediment yield calculated according to the WaTEM/SEDEM model contributes annually 4% of the dam siltation, which gives the dam an estimated lifespan of 22.7 years. This estimate omits other sediment sources (river bank erosion, permanent gully erosion and fluvial transport) and assumes that suspended sediment does not leave the dam during dredging operations and flood evacuation.

The results showed that the sediment delivery ratio has increased from past to current LULC situation. Moreover, it is expected to decrease under future LULC conditions. Table 5 presents more details about the dam siltation rate and lifespan for the differents LULCs scenarios.

Table 5. Simulated gross erosion, sediment yield (SY), sediment delivery ratio (SDR), dam siltation (%) and dam lifespan (year) under current and three LULCs scenarios (1936, 1957 and future) in the Ziz upper watershed

Period	Gross erosion (Mt/year)	SY (Mt/year)	SY (Mm^3/year)	SDR (%)	Dam siltation (%)	Dam life time (year)
LULC in 1936	52.8	1.5	1.25	2.84	-	-
LULC in 1957	44.8	1.5	1.26	3.34	-	-
Current LULC	23.1	2.03	1.69	8.79	4.4	22.7
Projected LULC	37.1	2.24	1.87	6.04	4.9	20.4

3.5 Impact of each factor on water erosion according to the WaTEM / SEDEM model

To identify the factors most pertinent to water erosion in the study area, we used the principal component analysis (PCA). The results presented in Figure 6 show that for the current LULC situation, there are negative correlations varying from 66 to 91% between water erosion and most factors: R^2 = 82.95% for the topographic factor (LS); R^2 = 91.6% for the crop managment factor (C); R^2 = 89.7% for the rainfall erosivity factor (R) and finally R^2 = 66.12% for the soil erodibility factor (K).

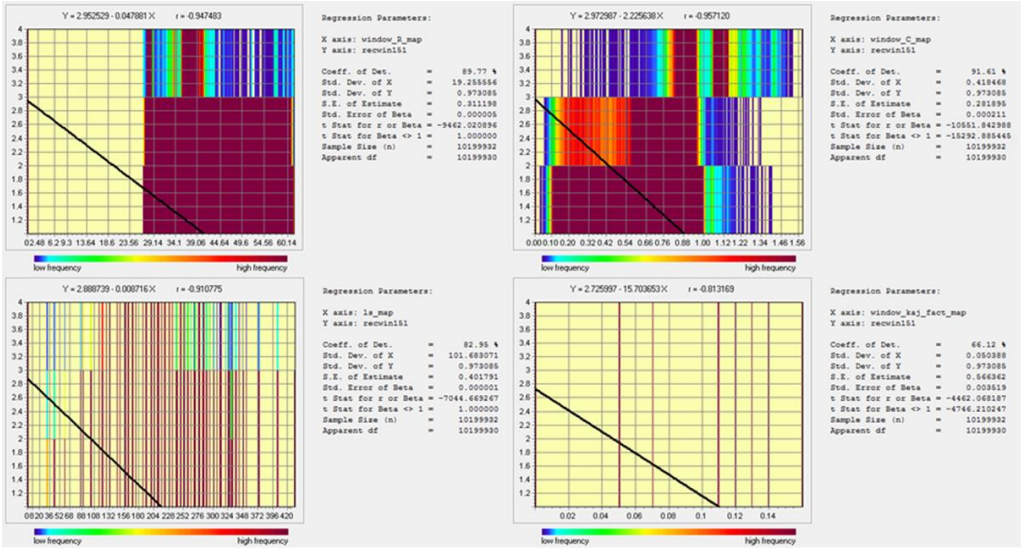

Figure 6. Statistical analysis of erosion production factors according to WaTEM/SEDEM model

The PCA results show that we must grant more importance to the two factors (C) and (LS). Suggested actions might involve more reforestation to protect land surface and to improve land cover, and the adoption of land conservation practices such as limiting the lengths of slopes so they generate less runoff. Spatially, we recommend these actions firstly, in sub-basins n°3, 4 and 5, where the (LS) factor is very important and conservation practices are rare, and secondly, in sub-basin n°27, an area which generates most of the sediment contributing to the dam siltation.

4. Conclusions

In this work, sediment yield data derived from the bathymetrical surveys conducted over 37 years (1973 to 2009) of suspended sediments at the Hassan Eddakhil dam in the Ziz upper catchment outlet were used to calibrate and validate WaTEM/SEDEM model. Model simulations for both the sediment yield (SY) and the specific sediment yield (SSY) were in good agreement with measured data. The NS and RRMSE were 0.65 and 0.026, respectively.

Based on the WaTEM / SEDEM results for the current LULC situation in the Ziz upper watershed, the sediment yield is 1.6 million ton/year and the specific sediment yield is 4.58 t/ha/year. A large proportion of the sediment comes from the sub-basins n°3, 4 and 5 in the northern upstream parts and hilly landscape (steep slopes) of the Ziz watershed. The sediment budget results

showed that these three sub-basins contributed approximately 46% of sediment production. Application of the calibrated WaTEM/SEDEM model to the Ziz upper watershed under past and future condition of LULC enabled an estimation of the impact of LULC change on soil erosion and sediment yield. The results revealed that soil erosion rates and sediment yield are influenced by LULC change. Furthermore, the decrease in degraded forest and corresponding increase in poorly vegetated areas (barren land) led to increased soil erosion rates and sediment yield. Mean sediment yields were 3.37, 3.57, 4.58 and 5.6 t/ha/year for the LULCs scenarios in 1936, 1957, current and future conditions, respectively.

This study has demonstrated that the WaTEM/SEDM model can be used for assessing sediment budget under current and alternative LULC scenarios. We evaluated changes in the sediment yield and changes in the main sediment sources and sedimentation areas as a result of past and future condition of LULC. So, these results can be used to implement some measures to prevent soil erosion.

The spatial-temporal distribution of soil erosion classes under different scenarios show the trend of slight to moderate class over the period of 1936 to 2017. For performing a good calibration of the WaTEM/SEDEM model, the use of recorded sediment yield at the catchment outlet and soil redistribution rates is required for further application of such models. The use of isotopic techniques such as the 137 Cs can also provide a robust model calibration.

5. Acknowledgements

The authors would like to thank the National Energy Center for Nuclear Science and Technology in Rabat, the agency for the Guir-Ziz-Ghris hydraulic basin in Errachidia and the laboratory of the Environment, Societies and Territories of the Faculty of Letters and Humanities from Ibn Tofail University of Kénitra.

References

[1] Ferreira, C.S., Pereira, P. and Kalantari, Z., 2018. Human impacts on soil. *Science of the Total Environment*, 644, 830-834.

[2] Navas, A., Machin, J., Gaspar, L., Sadiki, A., Kabiri, L. and Faleh, A., 2013. *Les sols dans le pays du Ziz (Sud-est marocain) Caractéristiques et aspects de dégradation*. Fes: Info-Print.

[3] IPBES, 2018. Summary for policymakers of the thematic assessment report on land degradation and restoration of the Intergovernmental Science-Policy Platform on Biodiversity and Ecosystem Services. In: R. Scholes, L. Montanarella, A. Brainich, N. Barger, B. ten Brink, M. Cantele, B. Erasmus, J. Fisher, T. Gardner, T.G. Holland, F. Kohler, J.S. Kotiaho, G. Von Maltitz, G. Nangendo, R, Pandit, J. Parrotta, M.D. Potts, S. Prince, M. Sankaran and L. Willemen, eds. *Intergovernmental Platform on Biodiversity and Ecosystems Services Secretariat*, Bonn: IPBES, pp. 1-31.

[4] Panagos, P. and Katsoyiannis, A., 2019. Soil erosion modelling: the new challenges as the result of policy developments in Europe. *Environmental Research*, 172, 470-474.

[5] Kirkby, M.J., Irvine, B.J., Jones, R.J.A., Govers, G. and PESERA Team, 2008. The PESERA coarse scale erosion model for Europe. I.–Model rationale and implementation. *European Journal of Soil Science*, 59(6), 1293-1306.

[6] Schroter, D., Cramer, W., Leemans, R., Prwntice, I.C., Araujo, M.B., Arnell, N.W., Bondeau, A., Bugmann, H., Carter, T.R., Gracia, C.A., de la Vega-Leinert, A.C., Erhard, M., Ewert, F., Glendining, M., House, J.I., Kankaanpaa, S., Klein, R.J.T., Lavorel, S., Lindner, M., Metzger, M.J., Meyer, J., Mitchell, T.D., Reginster, I., Rounsevell, M., Sabate, S., Sitch, S., Smith, B., Smith, J., Smith, P., Sykes, M.T., Thonicke, K., Thuiller, W., Tuck, G., Zaehle, S. and Zierl, B., 2005. Ecosystem service supply and vulnerability to global change in Europe. *Science*, 310, 1333-1337.

[7] Alatorre, L.C., Beguería, S., Lana-Renault, N., Navas, A. and García-Ruiz, J.M., 2012. Soil erosion and sediment delivery in a mountain catchment under scenarios of land use change using a spatially distributed numerical model. *Hydrology and Earth System Sciences*, 16(5), 1321-1334.

[8] PNABV, 1995. *Plan national d'aménagement des bassins versants au Maroc*. [Online] Available at: www.eauxetforets.gov.ma

[9] Heusch, B., 1970. L'érosion du Prérif. *Annales de la Recherche Forestière au Maroc*, 12, 9-179.

[10] Van Oost, K., Govers, G. and Desmet, P.J.J., 2000. Evaluating the effects of landscape structure on soil erosion by water and tillage. *Landscape Ecology*, 15(6), 579-591.

[11] Van Rompaey, A.J.J., Verstraeten, G., Van Oost, K., Govers, G. and Poesen, J., 2001. Modelling mean annual sediment yield using a distributed approach. *Earth Surface Processes and Landforms*, 26(11), 1221-1236.

[12] Billaux, P. and Bryssine, G., 1967. Les sols du Maroc. In : Congrès de pédologie méditerranéenne: Excursion au Maroc. *Cahiers de la Recherche Agronomique*, 1, 59-101.

[13] ABH-GZR, 2019. *Agence du Bassin Hydraulique de Guir-Ziz-Ghris*. [Online] Available at: http://www.abhgzr.ma.

[14] HCP, 2015. *Haut-Commissariat au Plan du Maroc : Centre National de Documentation*. [Online] Available at: https://www.hcp.ma.

[15] PNABV, 2014. *Plan National d'Aménagement des Bassins Versants : Étude d'aménagement du bassin versant d'Assif Melloul, Agence du Bassin Hydraulique de l'Oum Er-Rbia*. [Online] Available at: www.eauxetforets.gov.ma

[16] Gonzague, D. and Despujols, M., 1939. Carte géologique de Midelt au 1: /200 000. *Service Géologique du Maroc*.

[17] Lyazidi, M., Eyssautier, L., Marcais, J., Choubert, G. and Faillot P., 1956. Carte géologique de Rich et Boudnib au 1/200 000. *Service Géologique du Maroc*.

[18] de Vente, J., Poesen, J., Verstraeten, G., Van Rompaey, A. and Govers, G., 2008. Spatially distributed modelling of soil erosion and sediment yield at regional scales in Spain. *Global Planetary Change*, 60, 393-415.

[19] Alatorre, L.C., Begueria, S. and Garcıa-Ruiz, J.M., 2010. Regional scale modeling of hillslope sediment delivery: a case study in Barasona reservoir watershed (Spain) using WATEM/ SEDEM. *Journal of Hydrology*, 391, 109-123.

[20] Quijano, L., Begueria, S., Gaspar, L. and Navas, A., 2016. Estimating erosion rates using 137Cs measurements and WATEM/SEDEM in a Mediterranean cultivated field. *Catena*, 138, 38-51.

[21] Verstraeten, G., Prosser, I. P. and Fogarty, P., 2007. Predicting the spatial patterns of hillslope sediment delivery to river channels in the Murrumbidgee catchment, Australia. *Journal of Hydrology*, 334, 440-454.

[22] Bezak, N., Rusjan, S., Petan, S., Sodnik, J. and Mikos, M., 2015. Estimation of soil loss by the WATEM/SEDEM model using an automatic parameter estimation procedure. *Environmental Earth Sciences*, 74(6), 5245-5261.

[23] Borrelli, P., Van Oost, K., Meusburger, K., Alewell, C., Lugato, E. and Panagos, P., 2018. A step towards a holistic assessment of soil degradation in Europe: Coupling on-site erosion with sediment transfer and carbon fluxes. *Environmental Research*, 161, 291-298.

[24] Konecna, J., Karásek, P., Beitlerová, H., Fučík, P., Kapička, J., Podhrázská, J. and Kvítek, T., 2019. Using WaTEM/SEDEM and HEC-HMS models for the simulation of episodic hydrological and erosion events in a small agricultural catchment, *Soil and Water Research*, 15, 18-29.

[25] Verstraeten, G., Van Oost, K., Van Rompaey, A., Poesen, J. and Govers, G., 2002. Evaluating an integrated approach to catchment management to reduce soil loss and sediment pollution through modelling. *Soil Use and Management*, 18(4), 386-394.

[26] Renard, K.G., Foster, G.R., Weesies, G.A., and Porter, J.P., 1991. RUSLE-revised universal soil loss equation. *Journal of Soil and Water Conservation*, 46(1), 30-33.

[27] Desmet, P.J.J. and Govers, G., 1996. A GIS procedure for automatically calculating the USLE LS factor on topographically complex landscape units. *Journal of Soil and Water Conservation*, 51(5), 427-433.

[28] Govers, G., Vandaele, K., Desmet, P., Poesen, J. and Bunte, K., 1994. The role of tillage in soil redistribution on hillslopes. *European Journal of Soil Science*, 45(4), 469-478.

[29] van der Knijff, J.M., Jones, R.J.A. and Montanarella, L., 1999. *Soil Erosion Risk Assessment in Italy*. European Soil Bureau: Joint Research Center of the European Commission.

[30] Nash, J.E. and Sutcliffe, J.V., 1970. River flow forecasting through conceptual models: Part 1: a discussion of principles. *Journal of Hydrology*, 10(3), 282-290.

[31] Mohamed, M., Anis, Z. and Imed, F., 2020. Regional-scale modeling of water erosion and sediment yield in a semi-arid context: A case study of Ziz upper watershed in south-eastern Morocco. *GEOIT4W-2020: Proceedings of the 4th Edition of International Conference on Geo-IT and Water Resources 2020*, Al-Hoceima, Morocco, March 11-12, 2020, http://doi.org/10.1145/3399205.3399209

[32] Verstraeten, G., 2006. Regional scale modelling of hillslope sediment delivery with SRTM elevation data. *Geomorphology*, 81, 128-140.

[33] Haregweyen, N., Poesen, J., Verstraeten, G., Govers, G., de Vente, J., Nyssen, J., Deckers, J. and Moeyersons, J., 2013. Assessing the performance of a spatially distributed soil erosion and sediment delivery model (WATEM/SEDEM) in Northern Ethiopia. *Land Degradation & Development*, 24(2), 188-204.

[34] Syahli, F., 2015. *The impact of Land Use Change on Soil Erosion in Serayu Watershed, Case Study Merawu Watershed, Banjarnegara, Central Java*. MSc., University of Twente.

[35] Ghorbel, A. and Claude, J., 1977. Mesure de l'envasement dans les retenues de sept barrages en Tunisie: Estimation des transports solides. In: *Erosion and Solid Matter Transport in Inland Waters*, July 1977, 219-232.

Global Stability of the Transmission of Hand-Foot-Mouth Disease According to the Age Structure of the Population

Jiraporn Lamwong[1], Napasool Wongvanich[2], I-Ming Tang[3], Thurdkwun Changpuek[4] and Puntani Pongsumpun[4]*

[1]Department of Applied Basic Subjects, Thatphanom College, Nakhon Phanom University, Nakhon Phanom, Thailand
[2]Department of Instrumentation and Control Engineering, Faculty of Engineering, King Mongkut's Institute of Technology Ladkrabang, Bangkok, Thailand
[3]Computational and Applied Science for Smart Innovation Cluster (CLASSIC), Faculty of Science, King Mongkut's University of Technology Thonburi, Bangkok, Thailand
[4]Department of Mathematics, Faculty of Science, King Mongkut's Institute of Technology Ladkrabang, Bangkok, Thailand

Received: 5 June 2020, Revised: 26 October 2020, Accepted: 23 November 2020

Abstract

This study investigates a transmission model of Hand-Foot-Mouth disease (HFMD) where the age structure of the population is taken into account. Most infections in Thailand occur among children below the age of 10 years, whose immunity to HFMD is lower than people of age greater than 10 years. Therefore, a mathematical model was developed in which the population was separated into two groups with respect to age: one comprised of children aged less than 10 years, and another comprised of the rest of the population. The reproductive number was obtained by the next-generation matrix approach. Global asymptotical stability of the developed model was assured using Lyapunov's direct method. The model was validated by showing that the 2D and 3D trajectories of the numerical solutions for the different sub-population groups converged to the endemic equilibrium states when the reproduction number was greater than one, thus supporting the theoretical conclusions. Results show that the time series behaviors of the different normalized populations groups converge to the disease-free state when the values of the parameters are such that the basic reproductive number is 0.591481 (i.e., less than one) and to an endemic state when the values of the parameters are such that $R_0 = 54.4523$ and $R_0 = 192.575$ (i.e. greater than one). The results of this study can suggest ways for reducing the outbreak of this disease.

Keywords: Hand-Foot-Mouth Disease (HFMD); SEIR model; mathematical model; stability; age structure
DOI 10.14456/cast.2021.29

*Corresponding author: Tel.: 662-329-8000 Ext. 6196 Fax: 662-329-8412
E-mail: puntani.po@kmitl.ac.th

1. Introduction

Hand-Foot-Mouth Disease (HFMD) is a disease caused by enteroviruses, Coxsackie virus groups A and B [1-4]. The disease often is found in children because children have lower immunity. The disease only infects humans. The symptoms appear 3-7 days after the exposure to the virus [2, 5]. Most infected people exhibit only asymptomatic symptoms or a slight fever which is called Exanthematous fever. Some, however, will develop blisters in the mouth. When this happens, the sick person is said to be infected with Herpangina Hand-Foot-Mouth Disease, a viral haemorrhagic conjunctivitis disease. As we mentioned, most infected people do not show any symptoms. However, children of age less than 10 years are more susceptible to contract the disease than those older than 10 years of age since they may not have developed the immunity obtained from the asymptomatic infections. HFMD is transmitted through direct contact between the mouth and a hand or shared object such as spoon, glass or toy that has been contaminated with the mucus or saliva from the blister of an infected person. Most of this contact and spread occurs among children in nurseries or lower grades at schools. Children in higher grades and adults would have developed the immunity to the virus through exposure to it that they were unaware of [6]. HFMD became an important public health problem in Thailand in 1997, and outbreaks of Enterovirus 71 infections were reported in other countries in the Asia-Pacific region, such as Malaysia and Brunei [7]. In 1998 and 2000, outbreaks were reported in Taiwan and Singapore. Thailand reported outbreak beginning in 2003, and these have continued until the present [8-10]. Figure 1 shows the outbreaks of HFMD in Thailand over the period 2003-2018. The age distribution of the patients in 2020 was reported to be 93.37% for patients aged between 0-10 years, and 6.63% for patients older than 10 year of age [11]. As we see, the younger the child is, the higher the incidence of infection is. This is because they have not yet been exposed to the virus. If they had been exposed, they would have developed immunity to the disease. According to Figure 2, the study of HFMD divides participants into 2 groups; the first group is people between 0-10 years and the other group is people older than 10 years, because two groups have distinctly different infections.

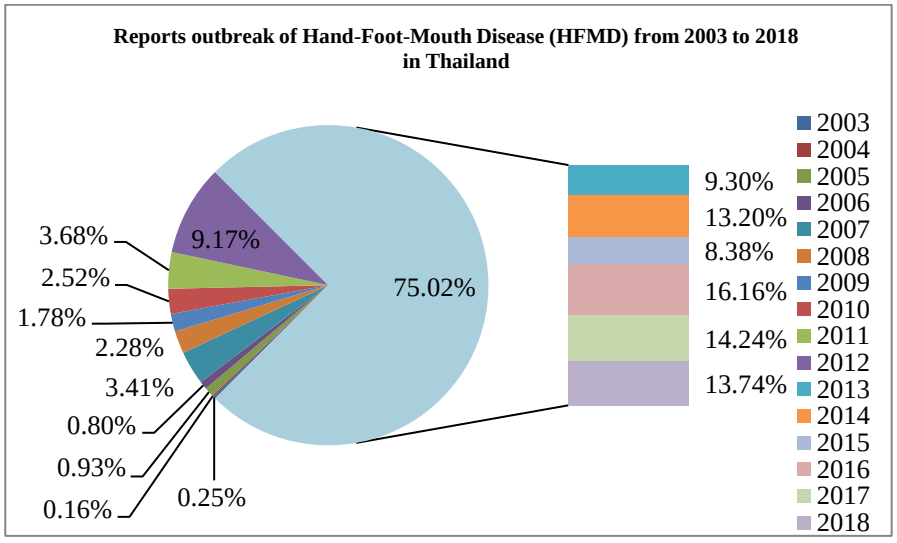

Figure 1. Reports on outbreaks of Hand-Foot-Mouth Disease (HFMD) from 2003 to 2018 in Thailand [12]

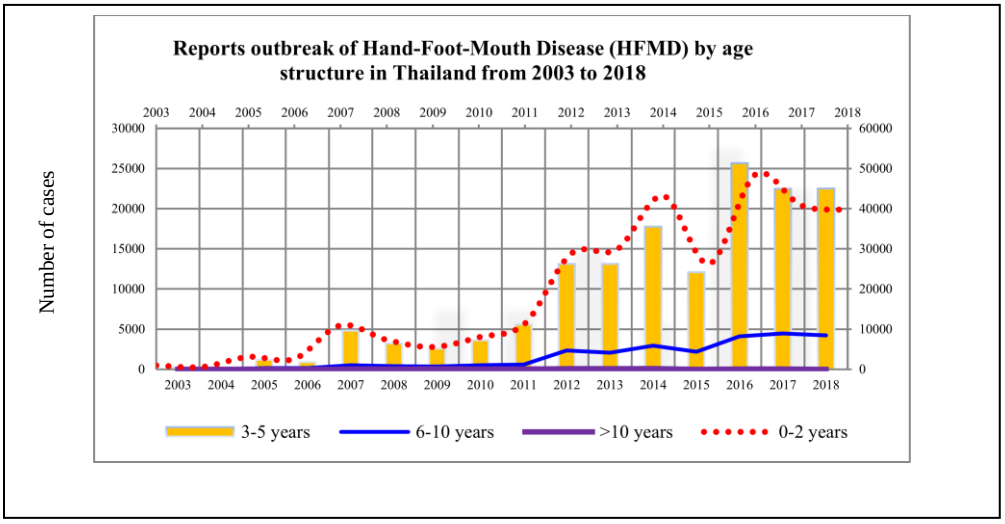

Figure 2. Reports on outbreaks of Hand-Foot-Mouth Disease (HFMD) by age structure in Thailand from 2003 to 2018 [13]

Several mathematical models to describe HFMD have been developed in the literature. In 2016, Li *et al.* [14] developed a SEIHR (S = Susceptible, E = Infected but not infectious, I = Infectious (clinical and subclinical), H = Hospitalized and R = Recovered) model to study HFMD in China. In their model, like ours, the population was divided in two groups; children (0-16 years) and adults (older than 16 years) and applied to the HFMD data for China from 2009 to 2014. Earlier, Wang *et al*. [3] conducted a time series analysis on its relationship with weather. They looked at the links between the admission of HFDM patients in the public hospitals in Hong Kong between 2008 and 2011 and the weather. In 2018, Tan and Cao [2] studied a dynamic model of HFMD which included the effects of vaccination in some children. They only considered children of age below 10 years since their immune systems were relatively intact (i.e. the antibodies to the HFMD virus were not present because of the unaware exposure to the asymptomatic form of the infections). Chadsuthi and Wichapeng [1] developed a mathematical model to study the effects of the contaminated environments in Bangkok and used it to understand the course of the HFMD from the reported information of individuals hospitalized with this disease. A number of age-structured models in the literature have also been developed, albeit for other diseases such as tuberculosis (TB) [15], Chikungunya [16] and HIV [17]. These models are based on the premise that the susceptibility of individuals varies with time, and consequently, involves the need for partial differential equations models. In this paper, the model of Pongsumpun and Wongvanich [18] is further developed. An assumption is that the susceptibility of individuals is quantized. In other words, the total population is divided into two groups, each with different finite susceptibility. The first group comprises population of children between 0-10 years, while the second group comprises a population of all other ages. The developed model is easier to analyze and interpret, and allows for global stability analysis to be conducted, which was not conducted in the previous works of Li *et al.* [14] and Pongsumpun and Wongvanich [18].

The structure of this paper is as follows: Section 2 formulates the mathematical model in which the population groups are normalized and determines the positivity of solutions for the disease-free and endemic steady state. We used the next generation matrix method to find the basic reproductive number and used the Lyapounov function method to establish the global stability of the equilibrium point. Section 3 then shows the numerical simulation including some discussions. The paper is concluded in Section 4.

2. Materials and Methods

In this study, we use the Susceptible-Exposed-Infected-Recovered (SEIR) model to describe the dynamic transmission of Hand-Foot-Mouth Disease in Thailand. We assume that the human population is divided into two groups; group one consists of children in the age group between 0-10 years and group two is consists of people of age greater than 10 years. Each age group is divided into four subcategories; susceptible, exposed, infected and recovered. In this section, we used mathematical programs to help obtain the equilibrium point and basic reproductive number.

2.1 Parameter and Equations of the model

We suppose that N_h is the total human population at time t. At time t, there are susceptible children between 0-10 years old S_a, E_a are exposed children of ages between 0-10 years, I_a are the infected children in this age group and R_a are the recovered children in this age group. S_b, E_b, I_b and R_b are populations of the corresponding human population groups above the age of 10 years. The descriptions of the changes in the different groups within each population class are given as:

- To begin, rate of change in the total human populations is due to the birth rate times the total human population (ΛN_h). The rate of change in the number of susceptible children (S_a) depends upon the infection of a susceptible child when the child is exposed to an infected child (the exposure can be either direct or indirect). The rate of change is given by $\beta_1 S_a I_a$ where β_1 is the infection rate for human population of ages between 0-10 years, or by $\beta_2 S_b I_b$ where β_2 is the infection rate for human population of ages greater than 10 years. The number of susceptible children also decrease when they become 11 years old or when they die of natural causes. The rates of changes for these two factors are σS_a and μS_a, respectively. The rate of change in the number of exposed children E_a depends on the rate of exposure of a susceptible child to infected population regardless of which population the infected person belongs to, the rate at which the exposed child becomes an infected child (εE_a), ε being the incubation rate, the rate at which a child becomes 11 years (σE_a) and natural death of the exposed child (μE_a). The rate of change in the number of infected children (I_a) depends on the incubation rate of the child, the rate at which the child recovers from the infected (ϕI_a), the rate at which the infected child becomes 11 years (σE_a) and the natural death of the infected child (μI_a). The rate of change in the number of recovered children (R_a) depends on the rate of recovery, the natural death of recovered child (μR_a) and the rate at which the recovered child becomes 11 years (σR_a).
- Regarding the second group, the rate of change in the number of susceptible adults (people older than 10 years) S_b depends on the rate at which children (humans younger than 10 years old) become 11 years old, the rate at which any susceptible adult is exposed to an infected adult $(\beta_2 S_b I_b)$ and the death of the susceptible person. The rate of change in the number of exposed human population (E_b) depends on the rate at which infected human population are

exposed to the virus, the incubation rate (εE_b) and natural death rate human of exposed human (μE_b). The rate of change in the number of infected human populations (I_b) depends on the incubation rate (εE_b), the number of adults who recovered from the infected (ϕI_b) where ϕ is the rate of recovery and the death rate of infected adults (μI_b) who die of natural causes. The rate of change in the number of recovered human population (R_b) depends on the recovery rate from the infected and natural death rate of recovered human populations (μR_b). Definition of parameters in our model is shown in Table 1.

Table 1. Definition of parameters

Parameter	Biological meaning
Λ	Birth rate
β_1	Infected rate for human populations when the ages are between 0-10 years
ε	Incubation rate
ϕ	Recovery rate
σ	Rate at which the ages between 0-10 years changed to child above the age of 10 years
β_2	Infection rate for the human population whose age is greater than 10 years
μ	Natural death rate of human
N_h	Total human population

The mathematical description of the transmission of Hand-Food-Mouth Disease, which includes the age structure in Thailand, is given by the following systems of ordinary differential equations;

$$S_a'(t) = \Lambda N_h - \beta_1 S_a I_a - (\mu + \sigma) S_a \quad (1)$$

$$E_a'(t) = \beta_1 S_a I_a - (\mu + \varepsilon + \sigma) E_a \quad (2)$$

$$I_a'(t) = \varepsilon E_a - (\mu + \phi + \sigma) I_a \quad (3)$$

$$R_a'(t) = \phi I_a - (\mu + \sigma) R_a \quad (4)$$

$$S_b'(t) = \sigma(S_a + E_a + I_a + R_a) - \beta_2 S_b I_b - \mu S_b \quad (5)$$

$$E_b'(t) = \beta_2 S_b I_b - (\mu + \varepsilon) E_b \quad (6)$$

$$I_b'(t) = \varepsilon E_b - (\mu + \phi) I_b \quad (7)$$

$$R_b'(t) = \phi I_b - \mu R_b \quad (8)$$

The total population condition is also given by:

$$N_h'(t) = S_a'(t) + E_a'(t) + I_a'(t) + R_a'(t) + S_b'(t) + E_b'(t) + I_b'(t) + R_b'(t).$$

2.2 Positivity invariant sets of solutions of SEIR model

Proposition 1. Let $S_a(t)$, $E_a(t)$, $I_a(t)$, $R_a(t)$, $S_b(t)$, $E_b(t)$, $I_b(t)$, $R_b(t)$ be the trajectories of the respective functions of equations (1)-(8) with the initial conditions:

$S_a(0),\ E_a(0),\ I_a(0),\ R_a(0),\ S_b(0),\ E_b(0),\ I_b(0),\ R_b(0)$, and also invariant set

$\omega = \left\{ S_a(\mathrm{t}), E_a(\mathrm{t}), I_a(\mathrm{t}), R_a(\mathrm{t}), S_b(\mathrm{t}), E_b(\mathrm{t}), I_b(\mathrm{t}), R_b(\mathrm{t}) \in R_+^8; W_1 \le \Lambda N_h / (\mu+\sigma), W_2 \le \sigma W_1 / \mu. \right\}$

and ω is a positively invariant set for equations (1)-(8).

Proof. Combining by equations (1)-(8) by

$$W(\mathrm{t}) = \left(W_1(\mathrm{t}), W_2(\mathrm{t})\right)$$
$$= \left(S_a(\mathrm{t}) + E_a(\mathrm{t}) + I_a(\mathrm{t}) + R_a(\mathrm{t}),\ \ S_b(\mathrm{t}) + E_b(\mathrm{t}) + I_b(\mathrm{t}) + R_b(\mathrm{t})\right)$$

we have

$$W'(\mathrm{t}) = \left(W_1'(\mathrm{t}), W_2'(\mathrm{t})\right)$$
$$= \begin{pmatrix} \Lambda N_h - \beta_1 S_a I_a - (\mu+\sigma)S_a + \beta_1 S_a I_a - (\mu+\varepsilon+\sigma)E_a + \varepsilon E_a - (\mu+\phi+\sigma)I_a + \phi I_a - (\mu+\sigma)R_a, \\ \sigma(S_a + E_a + I_a + R_a) - \beta_2 S_b I_b - \mu S_b + \beta_2 S_b I_b - (\mu+\varepsilon)E_b + \varepsilon E_b - (\mu+\phi)I_b + \phi I_b - \mu R_b \end{pmatrix}$$
$$= \begin{pmatrix} \Lambda N_h - (\mu+\sigma)S_a - (\mu+\sigma)E_a - (\mu+\sigma)I_a - (\mu+\sigma)R_a, \\ \sigma(S_a + E_a + I_a + R_a) - \mu S_b - \mu E_b - \mu I_b - \mu R_b \end{pmatrix}$$
$$= \left(\Lambda N_h - (\mu+\sigma)W_1,\ \sigma W_1 - \mu W_2\right)$$

Hence, $W_1'(\mathrm{t}) = \Lambda N_h - (\mu+\sigma)W_1 \le 0 \quad$ for $\quad W_1 \ge \dfrac{\Lambda N_h}{(\mu+\sigma)}$ (9)

$$W_2'(\mathrm{t}) = \sigma W_1 - \mu W_2 \le 0 \quad \text{for} \quad W_2 \ge \frac{\sigma W_1}{\mu} \tag{10}$$

From the above equations (9)-(10), $W'(\mathrm{t}) \le 0$ whenever $W_1 \ge \dfrac{\Lambda N_h}{(\mu+\sigma)}$ and $W_2 \ge \dfrac{\sigma W_1}{\mu}$. Using an integrating factor, we have $0 \le \left(W_1(\mathrm{t}), W_2(\mathrm{t})\right) \le \left(\dfrac{\Lambda N_h}{(\mu+\sigma)} + W_1(0)\,\mathrm{e}^{-(\mu+\sigma)t}, \dfrac{\sigma W_1}{\mu} + W_2(0)\,\mathrm{e}^{-\mu t} \right)$.

As $t \to \infty$, and hence $0 \le \left(W_1(\mathrm{t}), W_2(\mathrm{t})\right) \le \left(\dfrac{\Lambda N_h}{(\mu+\sigma)}, \dfrac{\sigma W_1}{\mu} \right)$. The other case is similar. Thus ω is a positively invariant set. We can see that all equations described by equations (1)-(8) in the non-negative octant R_+^8 are positively invariant [19].

Note that the infection rate does not introduce exogenous mortality in the population, and the latter is assumed to be constant in size at any given time. Therefore the rate of change of the total human populations is zero, and consequently the birth and death rates are equivalent. Then we have $\Lambda = \mu$.

We introduce the normalized variables:

$$s_a = \frac{S_a}{N_h}, e_a = \frac{E_a}{N_h}, i_a = \frac{I_a}{N_h}, r_a = \frac{R_a}{N_h},\ s_b = \frac{S_b}{N_h}, e_b = \frac{E_b}{N_h}, i_b = \frac{I_b}{N_h}, r_b = \frac{R_b}{N_h}.$$

Then we have the reduced equations as follows:

$$s_a'(\mathrm{t}) = \Lambda - \beta_1 N_h s_a i_a - (\mu+\sigma)s_a \tag{11}$$

$$e_a'(\mathrm{t}) = \beta_1 N_h s_a i_a - (\mu+\varepsilon+\sigma)e_a \tag{12}$$

$$i_a'(\mathrm{t}) = \varepsilon e_a - (\mu+\phi+\sigma)i_a \tag{13}$$

$$r_a'(\mathrm{t}) = \phi i_a - (\mu+\sigma)r_a \tag{14}$$

$$s_b^{'}(t) = \sigma(s_a + e_a + i_a + r_a) - \beta_2 N_h s_b i_b - \mu s_b \quad (15)$$

$$e_b^{'}(t) = \beta_2 N_h s_b i_b - (\mu + \varepsilon) e_b \quad (16)$$

$$i_b^{'}(t) = \varepsilon e_b - (\mu + \phi) i_b \quad (17)$$

$$r_b^{'}(t) = \phi i_b - \mu r_b \quad (18)$$

where we have the conditions $s_a + e_a + i_a + r_a + s_b + e_b + i_b + r_b = 1.$

2.3 Equilibrium points

Equations (11)-(18) are the reduced equations. Equilibrium points are obtained by setting the right hand side of equation (11)-(18) to zero. Then we have two equilibriums:

i) The disease-free steady state:

$$T^* = (s_a^{0^*}, e_a^{0^*}, i_a^{0^*}, r_a^{0^*}, s_b^{0^*}, e_b^{0^*}, i_b^{0^*}, r_b^{0^*}) = \left(\frac{\Lambda}{\mu + \sigma}, 0, 0, 0, \frac{\Lambda\sigma}{\mu(\mu + \sigma)}, 0, 0, 0 \right)$$

when $R_0 < 1.$

ii) Endemic steady state: $Q^* = (s_a^{1^*}, e_a^{1^*}, i_a^{1^*}, r_a^{1^*}, s_b^{1^*}, e_b^{1^*}, i_b^{1^*}, r_b^{1^*})$

where

$$s_a^{1^*} = \frac{(\varepsilon + \mu + \sigma)(\mu + \sigma + \phi)}{\beta_1 \varepsilon N_h},$$

$$e_a^{1^*} = \frac{\Lambda\beta_1\varepsilon N_h - (\mu + \sigma)(\varepsilon + \mu + \sigma)(\mu + \sigma + \phi)}{(\varepsilon + \mu + \sigma)\beta_1 \varepsilon N_h},$$

$$i_a^{1^*} = \frac{\Lambda\varepsilon}{(\varepsilon + \mu + \sigma)(\mu + \sigma + \phi)} - \frac{(\mu + \sigma)}{\beta_1 N_h},$$

$$r_a^{1^*} = \frac{\Lambda\phi\varepsilon}{(\mu + \sigma)(\varepsilon + \mu + \sigma)(\mu + \sigma + \phi)} - \frac{\phi}{\beta_1 N_h},$$

$$s_b^{1^*} = \frac{(\mu + \varepsilon)(\mu + \phi)}{\beta_2 \varepsilon N_h},$$

$$e_b^{1^*} = \frac{\varepsilon(\alpha\beta_2\sigma N_h - \mu(\mu + \sigma)(\mu + \phi)) - \mu^2(\mu + \sigma)(\mu + \phi)}{\beta_2 \varepsilon N_h (\mu + \varepsilon)(\mu + \sigma)},$$

$$i_b^{1^*} = \frac{\Lambda\varepsilon\sigma}{(\mu + \varepsilon)(\mu + \sigma)(\mu + \phi)} - \frac{\mu}{\beta_2 N_h},$$

$$r_b^{1^*} = \frac{\Lambda\varepsilon\sigma\phi}{\mu(\mu + \varepsilon)(\mu + \sigma)(\mu + \phi)} - \frac{\phi}{\beta_2 N_h}$$

when $R_0 > 1.$

2.4 Basic reproductive number

The basic reproductive number (R_0) is calculated by the next-generation matrix [20, 21]. We can write the right-hand side of equations (11)-(18) as F and V. Then we have gains and losses:

$$\begin{vmatrix} Gains\,to\,e_a: & \beta_1 N_h s_a i_a \\ Gains\,to\,i_a: & 0 \\ Gains\,to\,e_b: & \beta_2 N_h s_b i_b \\ Gains\,to\,i_b: & 0 \end{vmatrix}, \quad \begin{vmatrix} Losses\ from\,e_a: & (\mu+\varepsilon+\sigma)e_a \\ Losses\ from\,i_a: & -\varepsilon e_a + (\mu+\phi+\sigma)i_a \\ Losses\ from\,e_b: & (\mu+\varepsilon)e_b \\ Losses\ from\,i_b: & -\varepsilon e_b + (\mu+\phi)i_b \end{vmatrix}.$$

Where F is the Jacobian matrix of the gains matrix and V is the Jacobian matrix of the losses matrix,

$$F = \begin{bmatrix} 0 & \beta_1 N_h s_a & 0 & 0 \\ 0 & 0 & 0 & 0 \\ 0 & 0 & 0 & \beta_2 N_h s_b \\ 0 & 0 & 0 & 0 \end{bmatrix}, \quad V = \begin{bmatrix} \mu+\varepsilon+\sigma & 0 & 0 & 0 \\ -\varepsilon & \mu+\phi+\sigma & 0 & 0 \\ 0 & 0 & \mu+\varepsilon & 0 \\ 0 & 0 & -\varepsilon & \mu+\phi \end{bmatrix}.$$

When the disease-free steady state is

$T^* = (s_a^{0^*}, e_a^{0^*}, i_a^{0^*}, r_a^{0^*}, s_b^{0^*}, e_b^{0^*}, i_b^{0^*}, r_b^{0^*}) = \left(\frac{\Lambda}{\mu+\sigma}, 0, 0, 0, \frac{\Lambda\sigma}{\mu(\mu+\sigma)}, 0, 0, 0 \right)$ and substitute T^* in F and V above and determine $H = FV^{-1}$, we have

$$H = \begin{bmatrix} \frac{\Lambda\beta_1 N_h(\varepsilon^2+\varepsilon\mu)}{(\mu+\varepsilon)(\mu+\sigma)(\mu+\varepsilon+\sigma)(\mu+\phi+\sigma)} & \frac{\Lambda\beta_1 N_h}{(\mu+\sigma)(\mu+\phi+\sigma)} & 0 & 0 \\ 0 & 0 & 0 & 0 \\ 0 & 0 & \frac{\Lambda\beta_2 N_h \varepsilon\sigma}{\mu(\mu+\varepsilon)(\mu+\sigma)(\mu+\phi)} & \frac{\Lambda\beta_2 N_h \sigma}{\mu(\mu+\phi)(\mu+\sigma)} \\ 0 & 0 & 0 & 0 \end{bmatrix}$$

R_0 is the eigenvalues of the matrix $H = FV^{-1}$.

We have $R_0 = \max\left\{ \frac{\Lambda\beta_1\varepsilon N_h}{(\mu+\sigma)(\mu+\varepsilon+\sigma)(\mu+\phi+\sigma)}, \frac{\Lambda\beta_2\varepsilon\sigma N_h}{\mu(\mu+\varepsilon)(\mu+\sigma)(\mu+\phi)} \right\}$. (19)

2.5 Global stability of the equilibrium states

Theorem 1. If $R_0 < 1$, then the disease-free equilibrium point $T^* = (s_a^{0^*}, e_a^{0^*}, i_a^{0^*}, r_a^{0^*}, s_b^{0^*}, e_b^{0^*}, i_b^{0^*}, r_b^{0^*}) = \left(\frac{\Lambda}{\mu+\sigma}, 0, 0, 0, \frac{\Lambda\sigma}{\mu(\mu+\sigma)}, 0, 0, 0 \right)$ of equations (11)-(18) is globally asymptotically stable in the ω. We assume that

$$\begin{cases} \beta_1 = \frac{(\mu+\sigma)}{N_h s_a^{0^*}} \\ \beta_2 = \frac{\mu}{N_h s_b^{0^*}} \\ \Lambda = (s_a + e_a + i_a + r_a)(\mu+\sigma) \end{cases}. \quad (20)$$

Proof. We consider the Lyapunov function

$$\mathrm{L(t)} = (s_a - s_a^{0^*} \ln s_a) + e_a + i_a + r_a + (s_b - s_b^{0^*} \ln s_b) + e_b + i_b + r_b$$

$$
\begin{aligned}
L^{'}(\mathrm{t}) &= s^{'}_{a}\left(1-\frac{s^{0*}_{a}}{s_a}\right)+e^{'}_{a}+i^{'}_{a}+r^{'}_{a}+s^{'}_{b}\left(1-\frac{s^{0*}_{b}}{s_b}\right)+e^{'}_{b}+i^{'}_{b}+r^{'}_{b} \\
&= \left(\Lambda-\beta_1 N_h s_a i_a-(\mu+\sigma)s_a\right)\left(1-\frac{s^{0*}_{a}}{s_a}\right)+\left(\beta_1 N_h s_a i_a-(\mu+\varepsilon+\sigma)e_a\right)+\left(\varepsilon e_a-(\mu+\phi+\sigma)i_a\right) \\
&\quad +\left(\phi i_a-(\mu+\sigma)r_a\right)+\left(\sigma(s_a+e_a+i_a+r_a)-\beta_2 N_h s_b i_b-\mu s_b\right)\left(1-\frac{s^{0*}_{b}}{s_b}\right)+\left(\beta_2 N_h s_b i_b-(\mu+\varepsilon)e_a\right) \\
&\quad +\left(\varepsilon e_b-(\mu+\phi)i_b\right)+\left(\phi i_b-\mu r_b\right) \\
&= \Lambda\left(1-\frac{s^{0*}_{a}}{s_a}\right)-\beta_1 N_h s_a i_a+\beta_1 N_h s^{0*}_{a} i_a-(\mu+\sigma)s_a+(\mu+\sigma)s^{0*}_{a}+\beta_1 N_h s_a i_a-(\mu+\varepsilon+\sigma)e_a+\varepsilon e_a \\
&\quad -(\mu+\phi+\sigma)i_a+\phi i_a-(\mu+\sigma)r_a+\sigma(s_a+e_a+i_a+r_a)\left(1-\frac{s^{0*}_{b}}{s_b}\right)-\beta_2 N_h s_b i_b+\beta_2 N_h s^{0*}_{b} i_b-\mu s_b \\
&\quad +\mu s^{0*}_{b}+\beta_2 N_h s_b i_b-(\mu+\varepsilon)e_b+\varepsilon e_b-(\mu+\phi)i_b+\phi i_b-\mu r_b \\
&= \Lambda\left(1-\frac{s^{0*}_{a}}{s_a}\right)-(\mu+\sigma)s_a+(\mu+\sigma)s^{0*}_{a}+\beta_1 N_h s^{0*}_{a} i_a-(\mu+\sigma)e_a-(\mu+\sigma)i_a-(\mu+\sigma)r_a \\
&\quad +\sigma(s_a+e_a+i_a+r_a)\left(1-\frac{s^{0*}_{b}}{s_b}\right)-\mu s_b+\mu s^{0*}_{b}+\beta_2 N_h s^{0*}_{b} i_b-\mu e_b-\mu i_b-\mu r_b \\
&= \Lambda\left(1-\frac{s^{0*}_{a}}{s_a}\right)+(\mu+\sigma)s^{0*}_{a}\left(1-\frac{s_a}{s^{0*}_{a}}\right)+\beta_1 N_h s^{0*}_{a} i_a-(\mu+\sigma)e_a-(\mu+\sigma)i_a-(\mu+\sigma)r_a \\
&\quad +\sigma(s_a+e_a+i_a+r_a)\left(1-\frac{s^{0*}_{b}}{s_b}\right)+\mu s^{0*}_{b}\left(1-\frac{s_b}{s^{0*}_{b}}\right)+\beta_2 N_h s^{0*}_{b} i_b-\mu e_b-\mu \mathrm{i}_b-\mu r_b \\
&= \Lambda\left(1-\frac{s^{0*}_{a}}{s_a}\right)+(\mu+\sigma)s^{0*}_{a}\left(1-\frac{s_a}{s^{0*}_{a}}\right)+i_a(\beta_1 N_h s^{0*}_{a}-(\mu+\sigma))-(\mu+\sigma)e_a-(\mu+\sigma)r_a \\
&\quad +\sigma(s_a+e_a+i_a+r_a)\left(1-\frac{s^{0*}_{b}}{s_b}\right)+\mu s^{0*}_{b}\left(1-\frac{s_b}{s^{0*}_{b}}\right)+i_b(\beta_2 N_h s^{0*}_{b}-\mu)-\mu e_b-\mu r_b.
\end{aligned}
$$

From equation (20), we have

$$
\begin{aligned}
L^{'}(\mathrm{t}) &= \Lambda\left(1-\frac{s^{0*}_{a}}{s_a}\right)+(\mu+\sigma)s^{0*}_{a}\left(1-\frac{s_a}{s^{0*}_{a}}\right)+\sigma(s_a+e_a+i_a+r_a)\left(1-\frac{s^{0*}_{b}}{s_b}\right)+\mu s^{0*}_{b}\left(1-\frac{s_b}{s^{0*}_{b}}\right) \\
&\quad -(\mu+\sigma)e_a-(\mu+\sigma)r_a-\mu e_b-\mu r_b.
\end{aligned}
$$

From $s^{0*}_{a}=\dfrac{\Lambda}{(\mu+\sigma)}$, $s^{0*}_{b}=\dfrac{\Lambda\sigma}{\mu(\mu+\sigma)}$, we have

$$
\begin{aligned}
L^{'}(\mathrm{t}) &= \Lambda\left(1-\frac{s^{0*}_{a}}{s_a}\right)+(\mu+\sigma)\frac{\Lambda}{(\mu+\sigma)}\left(1-\frac{s_a}{s^{0*}_{a}}\right)+\sigma(s_a+e_a+i_a+r_a)\left(1-\frac{s^{0*}_{b}}{s_b}\right)+\mu\frac{\Lambda\sigma}{\mu(\mu+\sigma)}\left(1-\frac{s_b}{s^{0*}_{b}}\right) \\
&\quad -(\mu+\sigma)e_a-(\mu+\sigma)r_a-\mu e_b-\mu r_b.
\end{aligned}
$$

And we have assumed that $\Lambda=(s_a+e_a+i_a+r_a)(\mu+\sigma)$, thus

$$
\begin{aligned}
L^{'}(\mathrm{t}) &= \Lambda\left(1-\frac{s_a^{0*}}{\mathrm{s}_a}\right)+\Lambda\left(1-\frac{s_a}{s_a^{0*}}\right)+\sigma(s_a+e_a+i_a+r_a)\left(1-\frac{s_b^{0*}}{\mathrm{s}_b}\right)+\sigma(s_a+e_a+i_a+r_a)\left(1-\frac{s_b}{s_b^{0*}}\right)-(\mu+\sigma)e_a \\
&\quad -(\mu+\sigma)r_a-\mu e_b-\mu r_b \\
&= \Lambda\left(2-\frac{s_a^{0*}}{\mathrm{s}_a}-\frac{s_a}{s_a^{0*}}\right)+\sigma(s_a+e_a+i_a+r_a)\left(2-\frac{s_b^{0*}}{\mathrm{s}_b}-\frac{s_b}{s_b^{0*}}\right)-(\mu+\sigma)e_a-(\mu+\sigma)r_a-\mu e_b-\mu r_b \\
&= -\Lambda\left(\frac{\left(s_a^{0*}-\mathrm{s}_a\right)^2}{s_a s_a^{0*}}\right)-\sigma(s_a+e_a+i_a+r_a)\left(\frac{\left(s_b^{0*}-\mathrm{s}_b\right)^2}{s_b s_b^{0*}}\right)-(\mu+\sigma)e_a-(\mu+\sigma)r_a-\mu e_b-\mu r_b \\
&= -\left[\Lambda\left(\frac{\left(s_a^{0*}-s_a\right)^2}{s_a s_a^{0*}}\right)+\sigma(s_a+e_a+i_a+r_a)\left(\frac{\left(s_b^{0*}-s_b\right)^2}{s_b s_b^{0*}}\right)+(\mu+\sigma)e_a+(\mu+\sigma)r_a+\mu e_b+\mu r_b\right]\le 0
\end{aligned}
\tag{21}
$$

So, $L^{'}(\mathrm{t})\le 0$ .Using LaSalle's extension to Lyapunov's method [22], if and only if $s_a^{0*}=\mathrm{s}_a$, $e_a=0, i_a=0,\ r_a=0, s_b^{0*}=\mathrm{s}_b,\ e_b=0, i_b=0, r_b=0$. Then the equilibrium steady state $T^*=(s_a^{0*},e_a^{0*},i_a^{0*},r_a^{0*},s_b^{0*},e_b^{0*},i_b^{0*},r_b^{0*})=\left(\frac{\Lambda}{\mu+\sigma},0,0,0,\frac{\Lambda\sigma}{\mu(\mu+\sigma)},0,0,0\right)$ is globally asymptotically stable in the ω .

Theorem 2. If $R_0>1$, then the positive endemic equilibrium point $Q^*=(s_a^{1*},e_a^{1*},i_a^{1*},r_a^{1*},s_b^{1*},e_b^{1*},i_b^{1*},r_b^{1*})$ of equations (9)-(16) is globally asymptotically stable in the ω. Assume that

$$
\begin{cases}
M=\dfrac{\mu}{\varepsilon} \\
\Lambda=\dfrac{(\mu+\sigma)(\varepsilon+\mu+\sigma)(\mu+\sigma+\phi)}{\beta_1\varepsilon N_h} \\
\mu=\dfrac{\sigma(\mathrm{s}_a+e_a+i_a+\mathrm{r}_a)}{s_b^{1*}} \\
\beta_1=\dfrac{\mu}{N_h s_a^{1*}} \\
\beta_2=\dfrac{M\phi}{N_h s_b^{1*}}
\end{cases}
\quad .
\tag{22}
$$

Proof We consider the Lyapunov function:

$$K=(s_a-s_a^{1*}\ln s_a)+e_a+i_a+(s_b-s_b^{1*}\ln s_b)+e_b+Mi_b$$

$$K^{'}(\mathrm{t})=s_a^{'}\left(1-\frac{s_a^{1*}}{\mathrm{s}_a}\right)+e^{'}_a+i^{'}_a+s^{'}_b\left(1-\frac{s_b^{1*}}{s_b}\right)+e^{'}_b+Mi^{'}_b$$

$$K^{'}(\mathrm{t}) = \left(\Lambda - \beta_1 N_h s_a i_a - (\mu+\sigma)s_a\right)\left(1-\frac{s_a^{1^*}}{s_a}\right) + \left(\beta_1 N_h s_a i_a - (\mu+\varepsilon+\sigma)e_a\right) + \left(\varepsilon e_a - (\mu+\phi+\sigma)i_a\right) +$$

$$\left(\sigma(s_a+e_a+i_a+r_a) - \beta_2 N_h s_b i_b - \mu s_b\right)\left(1-\frac{s_b^{1^*}}{s_b}\right) + \left(\beta_2 N_h s_b i_b - (\mu+\varepsilon)e_b\right) + M\left(\varepsilon e_b - (\mu+\phi)i_b\right)$$

$$= \Lambda - \beta_1 N_h s_a i_a - (\mu+\sigma)s_a - \Lambda\frac{s_a^{1^*}}{s_a} + \beta_1 N_h s_a i_a \frac{s_a^{1^*}}{s_a} + (\mu+\sigma)s_a\frac{s_a^{1^*}}{s_a} + \beta_1 N_h s_a i_a - \mu e_a - \varepsilon e_a - \sigma e_a + \varepsilon e_a$$

$$- \mu i_a - \phi i_a - \sigma i_a + \sigma(\mathrm{s}_a + e_a + i_a + r_a) - \beta_2 N_h s_b i_b - \mu s_b - \sigma(s_b + e_a + i_a + r_a)\frac{s_b^{1^*}}{s_b}$$

$$+ \beta_2 N_h s_b i_b \frac{s_b^{1^*}}{s_b} + \mu s_b \frac{s_b^{1^*}}{s_b} + \beta_2 N_h s_b i_b - \mu e_b - \varepsilon e_b + M\varepsilon e_b - M\mu \mathrm{i}_b - M\phi \mathrm{i}_b$$

$$= \Lambda\left(1-\frac{s_a^{1^*}}{s_a}\right) - (\mu+\sigma)s_a\left(1-\frac{s_a^{1^*}}{s_a}\right) - \beta_1 N_h s_a i_a + \beta_1 N_h i_a s_a^{1^*} + \beta_1 N_h s_a i_a - \mu e_a - \sigma e_a - \mu i_a - \phi i_a - \sigma i_a$$

$$+ \sigma(\mathrm{s}_a + e_a + i_a + r_a)\left(1-\frac{s_b^{1^*}}{s_b}\right) - \mu s_b\left(1-\frac{s_b^{1^*}}{s_b}\right) - \beta_2 N_h s_b i_b + \beta_2 N_h i_b s_b^{1^*} + \beta_2 N_h s_b i_b - \mu \mathrm{e}_b - \varepsilon \mathrm{e}_b + M\varepsilon e_b$$

$$- M\mu i_b - M\phi i_b$$

$$= \Lambda\left(1-\frac{s_a^{1^*}}{s_a}\right) + (\mu+\sigma)s_a^{1^*}\left(1-\frac{s_a}{s_a^{1^*}}\right) + \beta_1 N_h i_a s_a^{1^*} - \mu e_a - \sigma e_a - \mu i_a - \phi i_a - \sigma i_a + \sigma(s_a + e_a + i_a + r_a)\left(1-\frac{s_b^{1^*}}{s_b}\right)$$

$$+ \mu s_b^{1^*}\left(1-\frac{s_b}{s_b^{1^*}}\right) + \beta_2 N_h i_b s_b^{1^*} - \mu e_b - \varepsilon e_b + M\varepsilon e_b - M\mu i_b - M\phi i_b.$$

From $s_a^{1^*} = \dfrac{(\varepsilon+\mu+\sigma)(\mu+\sigma+\phi)}{\beta_1 \varepsilon N_h}$, we have

$$K^{'}(\mathrm{t}) = \Lambda\left(1-\frac{s_a^{1^*}}{s_a}\right) + (\mu+\sigma)\frac{(\varepsilon+\mu+\sigma)(\mu+\sigma+\phi)}{\beta_1 \varepsilon N_h}\left(1-\frac{s_a}{s_a^{1^*}}\right) + \beta_1 N_h i_a s_a^{1^*} - \mu e_a - \sigma e_a - \mu i_a - \phi i_a - \sigma i_a$$

$$+ \sigma(s_a + e_a + i_a + r_a)\left(1-\frac{s_b^{1^*}}{s_b}\right) + \mu s_b^{1^*}\left(1-\frac{s_b}{s_b^{1^*}}\right) + \beta_2 N_h i_b s_b^{1^*} - \mu e_b - \varepsilon e_b + M\varepsilon e_b - M\mu i_b - M\phi i_b.$$

Substituting the relations in equations (22), we have $\Lambda = \dfrac{(\mu+\sigma)(\varepsilon+\mu+\sigma)(\mu+\sigma+\phi)}{\beta_1 \varepsilon N_h}$ and

$$\mu = \frac{\sigma(\mathrm{s}_a + e_a + i_a + \mathrm{r}_a)}{s_b^{1^*}}$$

$$K^{'}(\mathrm{t}) = \Lambda\left(1-\frac{s_a^{1^*}}{s_a}\right) + \Lambda\left(1-\frac{s_a}{s_a^{1^*}}\right) + \beta_1 N_h i_a s_a^{1^*} - \mu e_a - \sigma e_a - \mu i_a - \phi i_a - \sigma i_a + \sigma(s_a + e_a + i_a + r_a)\left(1-\frac{s_b^{1^*}}{s_b}\right)$$

$$+ \sigma(s_a + e_a + i_a + r_a)\left(1-\frac{s_b}{s_b^{1^*}}\right) + \beta_2 N_h i_b s_b^{1^*} - \mu e_b - \varepsilon e_b + M\varepsilon e_b - M\mu i_b - M\phi i_b$$

$$= -\Lambda\frac{(s_a^{1^*} - s_a)^2}{s_a s_a^{1^*}} + \beta_1 N_h i_a s_a^{1^*} - \mu e_a - \sigma e_a - \mu i_a - \phi i_a - \sigma i_a - \sigma(s_a + e_a + i_a + r_a)\frac{(s_b^{1^*} - \mathrm{s}_b)^2}{s_b s_b^{1^*}}$$

$$+ \beta_2 N_h i_b s_b^{1^*} - \mu e_b - \varepsilon e_b + M\varepsilon e_b - M\mu i_b - M\phi i_b$$

$$K^{'}(\mathrm{t}) = -\Lambda\frac{(s_a^{1^*}-s_a)^2}{s_a s_a^{1^*}} - \sigma(s_a+e_a+i_a+r_a)\frac{(s_b^{1^*}-s_b)^2}{s_b\, s_b^{1^*}} + i_a(\beta_1 N_h s_a^{1^*}-\mu) + i_b(\beta_2 N_h s_b^{1^*}-M\phi)$$
$$+ e_b(M\varepsilon-\mu) - \mu e_a - \sigma e_a - \phi i_a - \sigma i_a - \varepsilon e_b - M\mu i_b.$$

Substituting the relations in equations (22), we have

$$K^{'}(\mathrm{t}) = -\Lambda\frac{(s_a^{1^*}-s_a)^2}{s_a s_a^{1^*}} - \sigma(s_a+e_a+i_a+r_a)\frac{(s_b^{1^*}-s_b)^2}{s_b s_b^{1^*}} - \mu e_a - \sigma e_a - \phi i_a - \sigma i_a - \varepsilon e_b - M\mu i_b$$
$$= -\left[\Lambda\frac{(s_a^{1^*}-s_a)^2}{s_a s_a^{1^*}} + \sigma(s_a+e_a+i_a+r_a)\frac{(s_b^{1^*}-s_b)^2}{s_b s_b^{1^*}} + \mu e_a + \sigma e_a + \phi i_a + \sigma i_a + \varepsilon e_b + M\mu i_b\right] \le 0 \qquad (23)$$

Hence, the condition (23) show that $K^{'}(\mathrm{t}) \le 0$ of all terms. Then the equilibrium steady state $Q^* = (s_a^{1^*}, e_a^{1^*}, i_a^{1^*}, r_a^{1^*}, s_b^{1^*}, e_b^{1^*}, i_b^{1^*}, r_b^{1^*})$ is globally asymptotically stable in the ω.

3. Results and Discussion

In this section, we simulate the dynamic behavior of HFMD in Thailand by numerically solving the equations (11)-(18),where thevalues of the parameter values are listed in Table 2.

Table 2. Values of the parameter of our HFMD model

Parameter	The disease-free	Endemic (case 1)	Endemic (case 2)	Reference
Λ	$1/(75*365)$	$1/(74*365)$	$1/(74*365)$	[14]
β_1	0.00045	0.0329	0.045	Assumption
ε	$1/5$	$1/5$	$1/5$	[14],[23]
ϕ	$1/14$	$1/14$	$1/14$	[2],[23]
σ	0.0002	0.0002	0.0002	[2]
β_2	0.005	0.0492	0.058	Assumption
μ	$1/(75*365)$	$1/(70*365)$	$1/(70*365)$	[14]
N_h	10	100	300	Estimated
R_0	0.591481	54.4523	192.575	

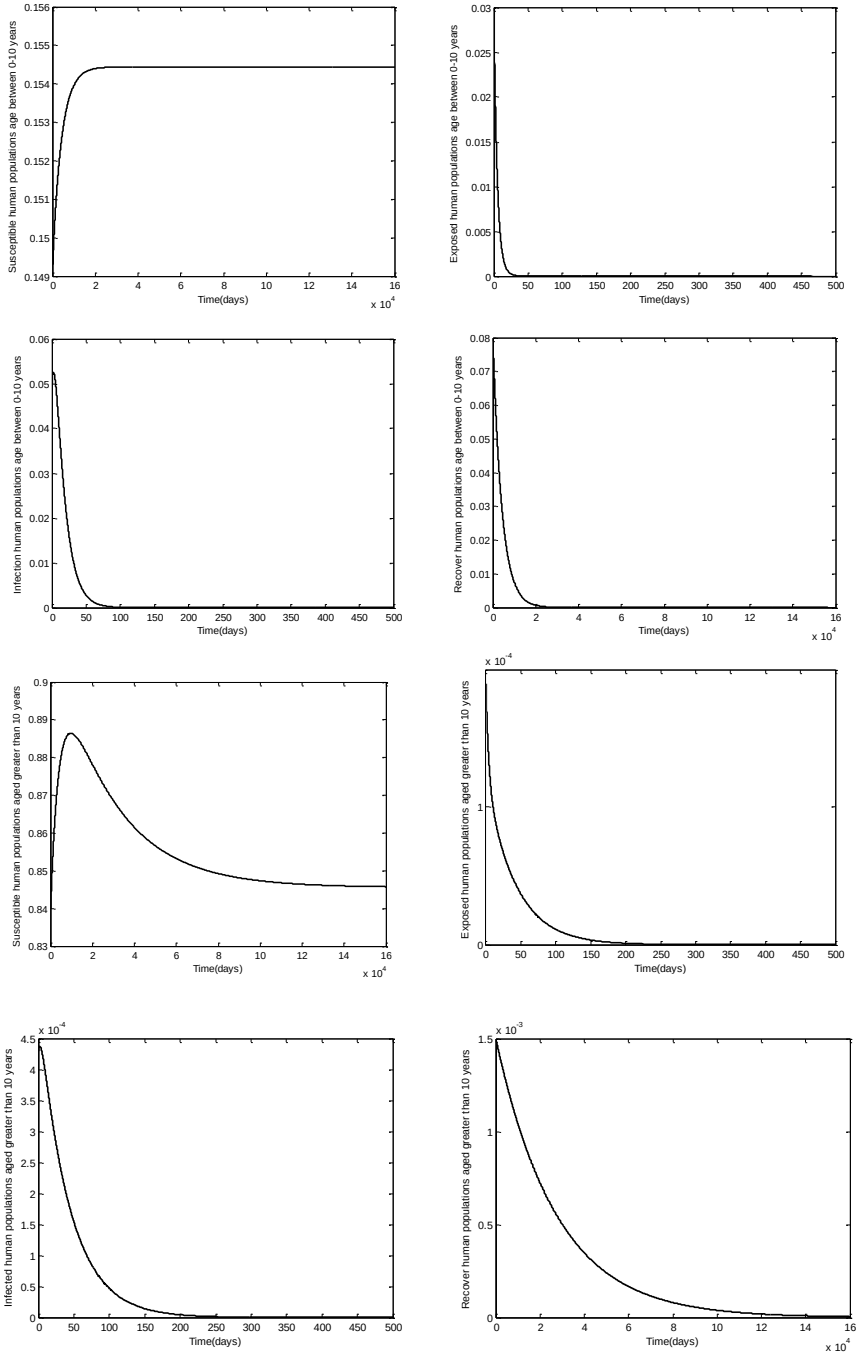

Figure 3. Solutions to the fractional of the global stability of T^* from equations (11)-(18) when $R_0 = 0.591481$

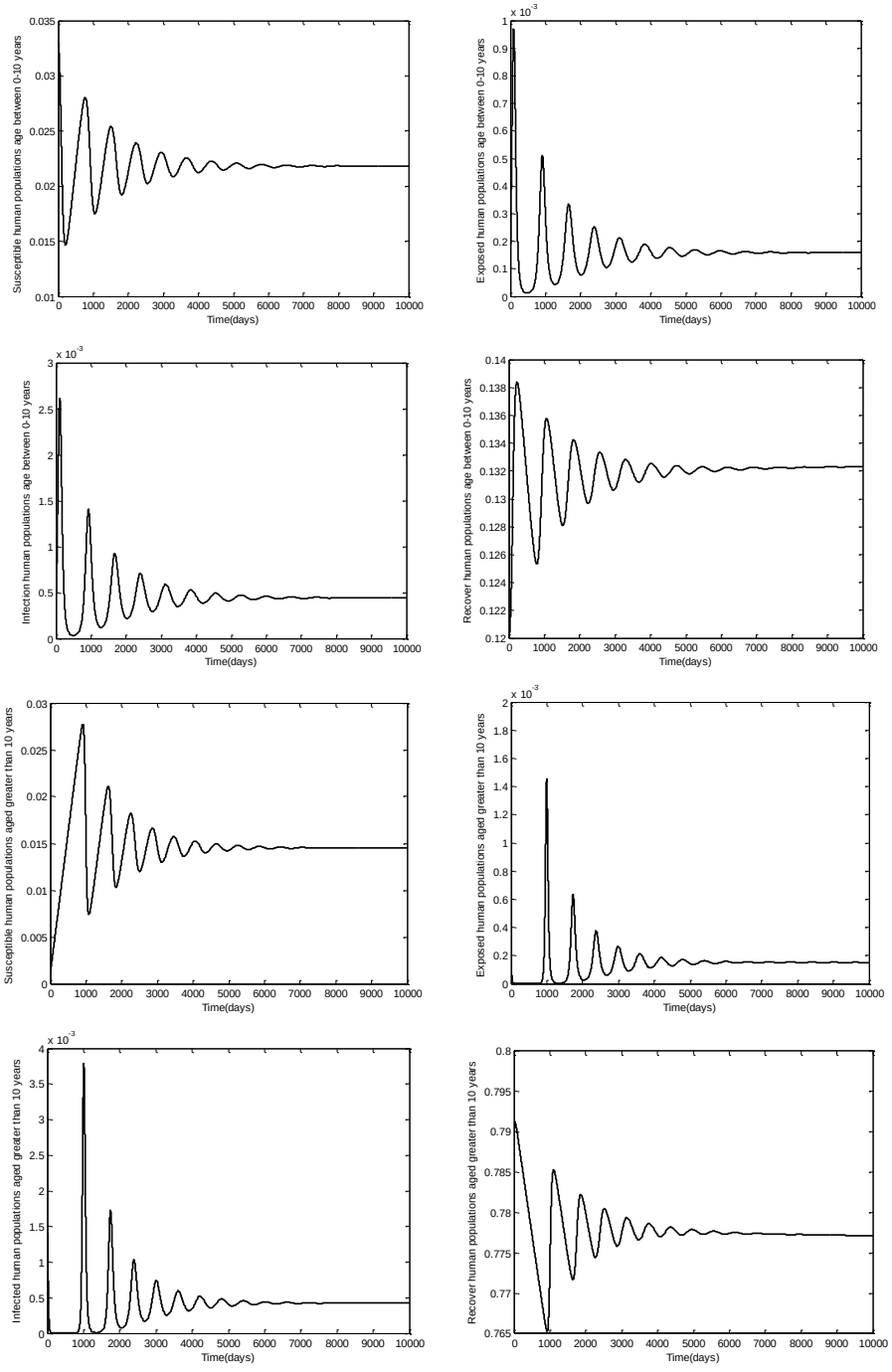

Figure 4. Solutions to the fractional of the global stability of Q^* from equations (11)-(18) when $R_0 = 54.4523$

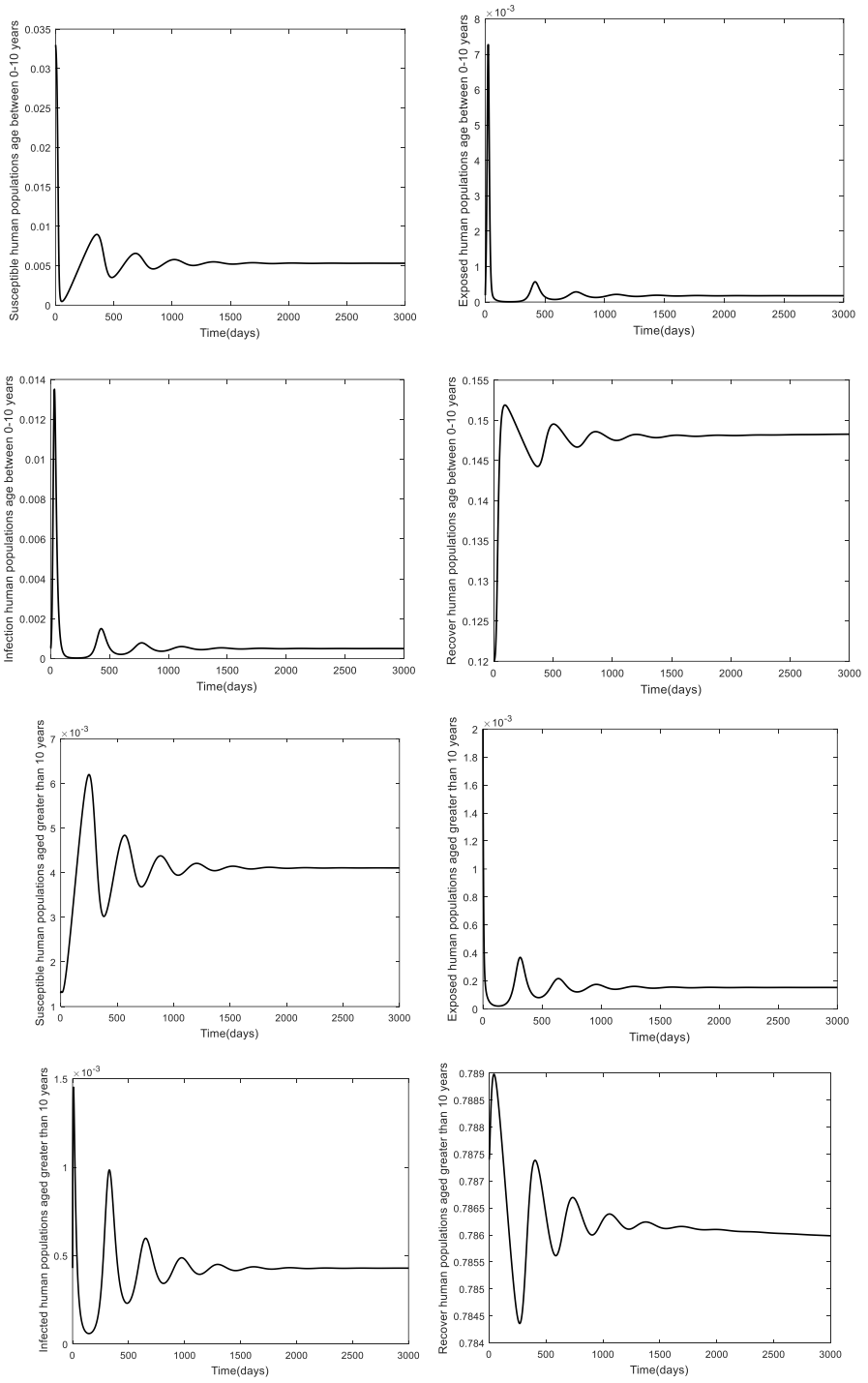

Figure 5. Solutions to the fractional of the global stability of Q^* from equations (11)-(18) when $R_0 = 192.575$

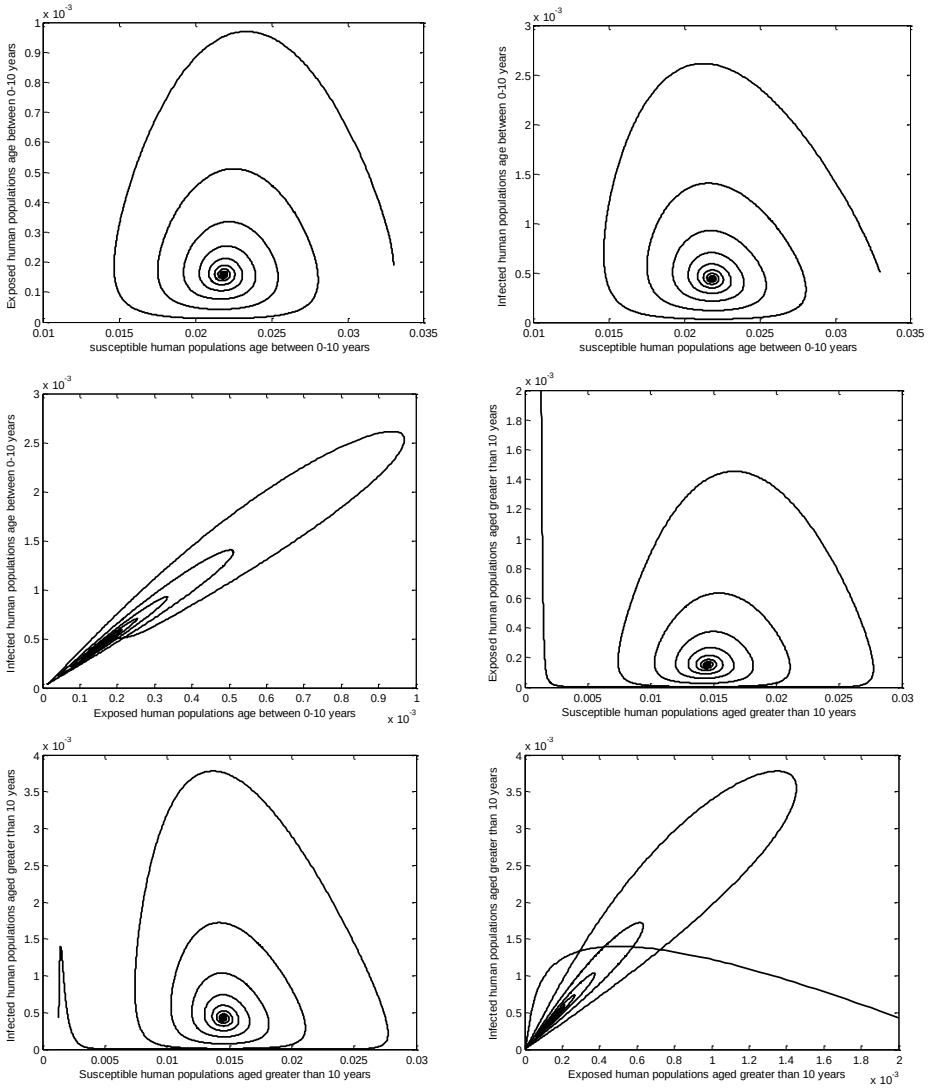

Figure 6. Solutions to the fractional projected onto the 2D of the global stability of Q^* from equations (11)-(18) when $R_0 = 54.4523$

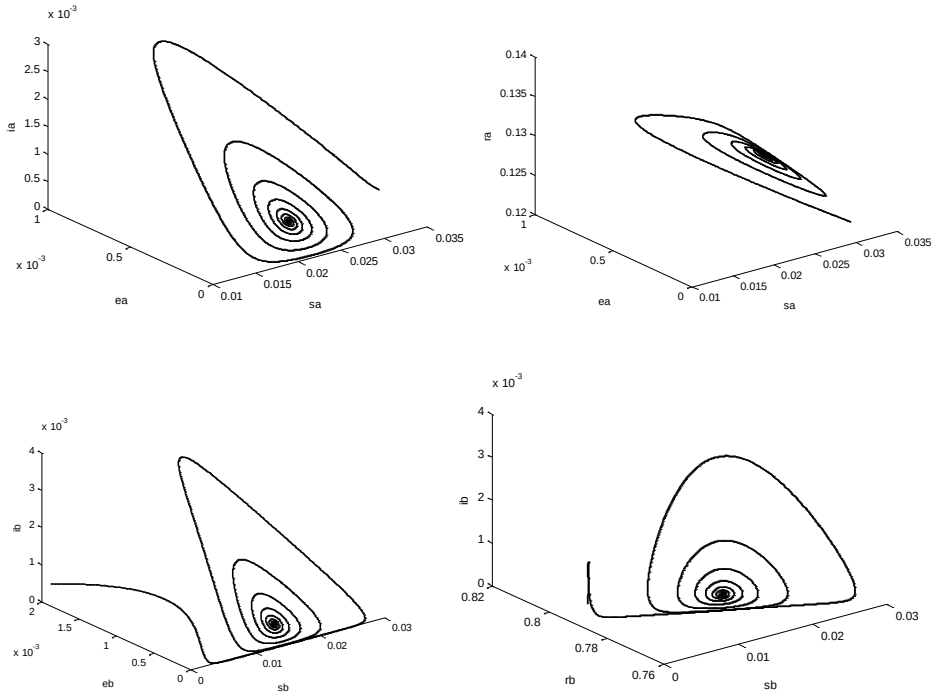

Figure 7. Solutions to the fractional projected onto the 3D of the global stability of Q^* from equations (11)-(18) when $R_0 = 54.4523$

For the numerical results, we used the values of the parameters shown in Table 2. When equilibrium state converge to the disease-free state $T^* = (0.1544, 0, 0, 0, 0.8456, 0, 0, 0)$, it is seen from Figure 3 that the equilibrium point for the susceptible lower age population (between 0-10 years) is lower than that for a larger age (>10 years). This implies that the children's age group is able to control the disease faster when $R_0 < 1$. Figures 4 and 5 then show the numerical trajectories for the global stability of the endemic state at different values of the basic reproductive number $R_0 = 54.45$ for Figure 4 and 192.575 for Figure 5. It is seen that as the basic reproductive number increases, the outbreak converges to the equilibrium point faster than an outbreak with a lower basic reproductive number. Figure 6 presents the 2D phase portrait trajectories of (s_a, e_a), (s_a, i_a), $(e_a, i_a), (s_b, e_b), (s_b, i_b)$ and (e_b, i_b) from the use of Matlab. Figure 7 shows the 3D phase portrait of (s_a, e_a, i_a), $(s_a, e_a, r_a), (s_b, e_b, i_b), (s_b, r_b, i_b)$, again with the use of Matlab. Both of these Figures depict clearly the convergence of the trajectories to the equilibrium when $R_0 > 1$. Note that these stability analyses are important from the control design perspective. In other words, if the system is deemed stable, then a simple controller would be required to track the desired disease trajectory. However, if the system is not stable, then a stabilizing controller must firstly be designed before a suitable controller could be implemented. Such a process is a lot more difficult to implement from the control perspective.

4. Conclusions

In this research, we have studied a transmission model of Hand-Foot-Mouth disease (HFMD) by creating the mathematical model of HFMD according to the data of the disease. We distributed human population into two groups; the first group is the children of ages between 0-10 years and the second group is people who are older than 10 years. Each age group is divided into four subclasses; susceptible, exposed, infected and recovered. From HFMD model, we assume the number of human population is constant. We establish 2 equilibrium states: a disease-free equilibrium state and endemic equilibrium state. The basic reproductive number (R_0) is determined using the next generation method and is denoted R_0. as

$$R_0 = \max\left\{\frac{\alpha\beta_1\varepsilon N_h}{(\mu+\sigma)(\mu+\varepsilon+\sigma)(\mu+\phi+\sigma)}, \frac{\alpha\beta_2\varepsilon\sigma N_h}{\mu(\mu+\varepsilon)(\mu+\sigma)(\mu+\phi)}\right\}.$$

When $R_0 < 1,$ the disease-free steady state is globally asymptotically stable as can be seen in theorem 1 and when $R_0 > 1,$ the endemic steady state is globally asymptotically stable as can be seen in theorem 2. Since Hand-Foot-Mouth Disease is often found in children, we created mathematical model and divided into two groups for the analysis of the disease of each population group. Moreover, our analysis for parameters revealed parameters that affected the outbreak which are the infection rate for human population when the ages are between 0-10 years, the infection rate of a child above the age of 10 years and total human population. The results of this study can suggest ways for reducing the outbreak of this disease. If the importance of the disease is not realized and action taken, outbreaks will continue to occur.

5. Acknowledgements

This work is supported by Thatphanom College, Nakhon Phanom University and King Mongkut's Institute of Technology Ladkrabang grant number (2562-02-05-02).

References

[1] Chadsuthi, S. and Wichapeng, S., 2018. The modelling of hand, foot, and mouth disease in contaminated environments in Bangkok, Thailand. *Computational and Mathematical Methods in Medicine*, 2018(1), 1-8.

[2] Tan, H. and Cao, H., 2018. The dynamics and optimal control of a hand-foot-mouth disease model. *Computational and Mathematical Methods in Medicine*, 2018(2), 1-11.

[3] Wang, P., Goggins, W.B. and Chan, E.Y.Y., 2016. Hand foot and mouth disease in Hong Kong: A time-series analysis on its relationship with weather. *PLOS ONE*, 11, 1-12.

[4] Hii, Y.L., Rocklöv, J. and Ng, N., 2011. Short term effects of weather on hand, foot and mouth disease. *PLOS ONE*, 6, 1-6.

[5] Ma, Y., Liu, M., Hou, Q. and Zhao, J., 2013. Modelling seasonal HFMD with recessive infection in Shangdong, China. *Mathematical Biosciences and Engineering*, 10(4), 1159-1171.

[6] Wang, J., Xiao, Y. and Cheke, R.A., 2019. Modelling the effects of contaminated environments in mainland China on seasonal HFMD infections and the potential benefit of a pulse vaccination strategy. *Discrete and Continuous Dynamical Systems Series B*, 24(11), 5849-5870.
[7] Chua, K.B. and Kasri, A.R., 2011. Hand foot and mouth disease due to enterovirus 71 in Malaysia. *Virologica Sinica*, 26(4), 221-228.
[8] AbuBakar, S., Sam, I.-C., Yusof, J., Lim, M.K., Misbah, S., Mat Rahim, N. and Hooi, P.-S., 2009. Enterovirus 71 outbreak, Brunei. *Emerging Infectious Diseases*, 15(1), 79-82.
[9] Lin, T.Y., Twu, S.-J., Ho, M.-S., Chang, L.-Y. and Lee, C.-Y., 2003. Enterovirus 71 outbreaks, Taiwan: Occurrence and recognitio. *Emerging Infectious Diseases*, 9(3), 291-293.
[10] Chan, K.P., Goh, K.T., Chong, C.Y., Teo, E.S., Lau, G. and Ling, A.E., 2003. Epidemic hand, foot and mouth disease caused by human enterovirus 71, Singapore. *Emerging Infectious Diseases*, 9(1), 78-85.
[11] Department of Disease Control, Ministry of Public Health, 2020. *Hand, Foot and Mouth Disease.* [online] Available at: https://ddc.moph.go.th/brc/news.php?news=11722&deptcode=brc
[12] Department of Disease Control, Ministry of Public Health, 2018. *Hand, Foot and Mouth Disease Situation.* [online] Available at: https://ddc.moph.go.th/uploads/files/85e47349de0c253e4b709db62fb44126.pdf
[13] Department of Disease Control, Ministry of Public Health, 2018. *Hand, Foot and Mouth Disease Situation*. [online] Available at: https://ddc.moph.go.th/uploads/files/333f54af3da87cf66599a0def2c30856.pdf
[14] Li, Y., Wang, L., Pang, L. and Sanhong, L., 2016. The data fitting and optimal control of a hand, foot and mouth disease (HFMD) model with stage structure. *Applied Mathematics and Computation*, 276, 61-74.
[15] Cao, H. and Zhou, Y., 2012. The discrete age-structured SEIT model with application to tuberculosis transmission in China. *Mathematical and Computer Modelling*, 55, 385-395.
[16] Agusto, F.B., Easley, S., Freeman, K. and Thomas, M., 2016. Mathematical model of three age-structured transmission dynamics of chikungunya virus. *Computational and Mathematical Methods in Medicine*, 2016, 1-31.
[17] Wang, J., Zhang, R. and Kuniya, T., 2015 . Mathematical analysis for an age-structured HIV infection model with saturation infection rate. *Electronic Journal of Differential Equations*, 2015(33), 1-19.
[18] Pongsumpun, P. and Wongvanich, N., 2018. Age structural model of the hand foot mouth disease in Thailand. *2018 2nd European Conference on Electrical Engineering and Computer Science*, 2018, 134-141.
[19] Pongsumpun, P., Sungchasit, R. and Tang, I. M., 2017. Lyapunov function for a dengue transmission model where two species of mosquitoes are present: Global stability. *American Journal of Applied Sciences*, 14 (10), 994-1004.
[20] van den Driessche, P. and Watmough, J.A., 2002. Reproduction numbers and sub-threshold endemic equilibrium for compartmental models of disease transmission. *Mathematical Biosciences*, 180, 29-48.
[21] Heffernan, J.M., Smith, R.J. and Wahl, L.M., 2005. Perspectives on the basic reproduction ratio. *Journal of the Royal Society Interface*, 2(4), 281-293.
[22] La Salle, J.P., 1976. *The Stability of Dynamical Systems*. Philadelphia: Society for Industrial and Applied Mathematics.
[23] Chan, S.J., Labadin, J. and Podin, Y., 2017. A dynamic SEIPR model for the spread of hand, foot and mouth disease in Sarawak. *Journal of Telecommunication Electronic and Computer Engineering*, 9, 125-129.

Response of Culture Media and Auxin on Growth and Glucosinolate Accumulation in the Hairy Root Cultures of Rocket (*Eruca sativa*)

Sang Un Park[1,2], Nam Su Kim[2], Sun Ju Bong[1] and Sook Young Lee[3]*

[1]Department of Crop Science, Chungnam National University, Yuseong-gu, Daejeon, Korea
[2]Department of Smart Agriculture Systems, Chungnam National University, Yuseong-gu, Daejeon, Korea
[3]Marine Bio Research Center, Chosun University, Sinji-myeon, Wando-gun, Jeollanamdo, Korea

Received: 11 June 2020, Revised: 28 September 2020, Accepted: 25 November 2020

Abstract

Rocket (*Eruca sativa*) is a domesticated plant species that is commonly eaten in salads and known to provide health benefits because of the high levels of glucosinolates, flavonols, and other compounds. Hairy root cultures (HRCs) are effective biotechnological tools for biosynthesis of secondary metabolites under various growing conditions. HRCs of rocket were treated with growth media of half-strength and full-strength Murashige-Skoog (MS) media, Gamborg's B5 medium, and Schenk and Hildebrand (SH) medium and auxins to evaluate the growth response and the accretion of glucosinolate. The growth pattern of the hairy roots varied extensively under the different media and auxin treatments; the highest and the lowest fresh weights were recorded in HRCs grown under full-strength SH and half-strength MS media, respectively. Treatment with NAA at 1.0 mg/l produced the highest hairy root fresh weight, followed by the treatments with IAA 0.1 mg/l and IBA 1.0 mg/l. The MS media induced the highest glucosinolate accumulation, followed by B5; all media enhanced the production of glucosinolates but auxins treatments (exception for glucoerucin) did not positively enhance the production of glucosinolates. Total glucosinolate levels were increased 1.7, 1.68, 1.33, and 1.26 fold in full-strength MS, half-strength MS, half-strength B5, and B5, respectively. These findings indicated that hairy root production and glucosinolate accumulation did not follow the same trend. Although SH media and NAA 1.0 slightly enhanced hairy root production, full-strength MS media induced higher amounts of glucosinolate, and auxin treatments did not increase the accumulation of glucosinolate. We therefore propose that MS media, regardless of additional treatment, provides a valuable alternative approach for the mass production of hairy root cultures and glucosinolates in rocket.

Keywords: glucosinolates; growth media; auxin; hairy root; rocket salad
DOI 10.14456/cast.2021.30

*Corresponding author: Tel.: +82-10-8610-6739; Fax: +82-61-555-1260
E-mail: seedbank@chosun.ac.kr

1. Introduction

Eruca sativa is commonly known as 'salad' or 'cultivated' rocket and is well-known for its hot, peppery, and bitter flavor profile [1]. The crops jointly known as rockets are all members of the family *Brassicaceae* and are native to the regions neighboring the Mediterranean Sea [2]. *Eruca sativa* is cultivated commercially worldwide, particularly in the USA, the UK, Italy, Spain, Morocco, Israel, and Australia [3]. It is also cultivated in some parts of Asia, including Pakistan, Iran, and India, and the leaves are used in salad and as vegetables, or livestock feed [2]. Rocket salad leaves contain glucosinolates, the most abundant of which are glucoerucin, glucoraphanin, and glucosativin [4]. Rocket salad has been reported to have astringent, antiphlogistic, antacid, diuretic, digestive, laxative, stimulative, anti-inflammatory (for colitis), and blood circulation properties [5]. Other studies have shown that rocket salad inhibits cancer [6, 7] and has antioxidant [8, 9], antimicrobial [10], and anti-inflammatory properties [11].

Approximately 200 different glucosinolates occur naturally in plants [12, 13]. Regular intake of vegetables from the family *Brassicaceae* provides benefits to human health [14, 15]. Consumption of vegetables containing glucosinolates (GSLs) and flavonols is associated with reduced risk of numerous cancers [16-18] and with improved cardiovascular health [19]. However, much of the world's populations do not eat sufficient quantities of these vegetables to obtain these benefits [20].

Auxins are a class of phyto-hormones that play a major role in the processes of growth and development in plant life cycles. Auxins influence wound response, axial elongation in the shoot, fruit growth and development, coleoptile growth, initiation of flowering, development of reproductive organs, and ethylene biosynthesis. Auxins are also involved in root growth and development, including the formation of adventitious roots and root re-growth [21]. When the concentration of auxins is decreased by removing the apical meristem, the stimulation of roots is decreased and stem growth is increased. The most common phytohormones, indole-3-acetic acid (IAA), indole-3-butyric acid (IBA) and naphthalic acetic acid (NAA) are transported from the stem to the root, and the overall root development is stimulated. These plant hormones, particularly IBA, IAA, and NAA are generally used to stimulate root growth and development in plant cutting propagation. However, if the concentration of auxin is too high, the elongation of roots is inhibited and the formation of adventitious roots increases. The optimal concentration of auxin is therefore essential.

Plant tissue culture media are used for plant growth and propagation to provide controlled conditions that include the necessary inorganic compounds, adequate pH levels, and sources of carbon [22, 23]. Previous studies investigating the selection of the appropriate basal media for hairy root initiation and growth and the accumulation of desirable natural products have shown that the ideal medium is dependent on the plant species in question [23-27]. HRC is promising biotechnological tool because of the fast growth rate and secondary metabolite production that it induces under controlled conditions [28]. Because of these advantages, HRC has been broadly investigated in many plant species for the mass collection of secondary metabolites used for food additives and by the pharmaceutical industry. Studies have investigated glucosinolate accumulation in response to different treatments in the hairy roots of the plants of Brassicaceae family, including kale [29], watercress [30], mustard [31], Chinese cabbage [32], and broccoli [33].

Few studies have investigated HRC for glucosinolate accumulation in rocket salad [34, 35]. Auxin and media played a vital role in the accumulation of secondary metabolites. However, the use of HRC according to media and auxin concentration in rocket salad has never been studied. Therefore in this study, we investigated the growth and glucosinolate content in rocket salad hairy roots in various culture media and auxin concentrations to determine the optimal culture environment and thereby enhance the production of glucosinolates.

2. Materials and Methods

2.1 Plant Materials

Rocket salad seeds were obtained from a seed company (Asia Seeds Co., Ltd, Seoul, Korea). The seeds were sterilized by immersion in 70 % (v/v) ethanol for 30 s and 2% sodium hypochlorite for 10 min. The seeds were then rinsed five times with sterilized water and maintained on Petri dishes with MS medium consisting of 30 g/l sugar and 0.8 % agar at pH 5.7 with no additional hormones for germination.

2.2 Establishment of hairy roots

Young leaves of 10-day-old old rocket salad were wounded using a scalpel and dipped in a suspended liquid medium of *Agrobacterium rhizogenes* (strain R1000) for 10 min. The seedlings were cleaned with sterilized paper and incubated on antibiotic-free MS (Murashige and Skoog) medium [36], for 2 days under dark conditions at 25°C. Infected leaves were co-cultured for 2 days and then washed using sterilized water and dried with sterilized paper. These were then transferred to 1/2 MS solid medium for 2 to 3 weeks after addition of 250 mg/l cefotaxime and then incubated under dark conditions. The hairy roots that emerged from the wounded parts were separated from the leaves and cultured under the same conditions. One fast-growing clone was selected for the experiment and cultured further.

2.3 Treatment of culture medium and auxins

Liquid growth media of both half-strength and full-strength MS, SH (Schenk and Hildebrandt medium) [37], and B5 (Gamborg B5 medium) [38] were selected as the culture media for the hairy root cultures. To allocate equal weight (2g fresh weight), hairy roots were measured and transferred to each liquid culture medium where 30 ml was maintained in each flask. Treated samples of the different media were collected after a culture period of 4 weeks and kept in liquid nitrogen for glucosinolate analysis. The samples were then ground finely using a pestle and lyophilized for 72 h at -80°C for HPLC analysis of GSL compounds. In addition, the auxins IAA, IBA, and NAA were used in concentrations of 0.1, 0.5, and 1 mg/l using half-strength of MS media as basal media to compare the effects of auxin type and concentration on hairy root cultures. Hairy roots were measured and transferred to each liquid culture medium in equal weight (2g fresh weight). Auxin-treated samples were collected after 4 weeks of culture and immediately frozen in liquid nitrogen for analysis of glucosinolates. The samples were lyophilized for 72 h at -80°C for HPLC analysis of GSL compounds and ground finely using a pestle. All samples were prepared in triplicates.

2.4 Extraction of DS-GSLs and HPLC analysis

Glucosinolates were extracted and desulfated according to the procedure of International Organization for Standardization (ISO) 9167-1 [39] and Kim *et al.* [40]. Glucosinolates were extracted with 70 % MeOH (v/v) and incubated at 70°C for 5 min in a water bath. The extracted samples were centrifuged at 12,000 rpm for 10 min at 4°C. The resulting supernatant was placed into a mini-column packed with DEAE-Sephadex A 25 (40 mg dry weight) and desulfated by the addition of 75 µl aryl sulfatase solution (23 mg/ml). Ultrapure water (1.5 ml) was added to elute the desulfo-glucosinolates samples. An Agilent Technologies 1200 series HPLC system (Palo Alto, CA, USA) was used to analyze the desulfated extracts, and reversed-phase chromatography was performed with an Inertsil ODS-3 column (150 × 3.0 mm i.d., particle size 3 µm; GL Sciences,

Tokyo, Japan) equipped with an E-type cartridge guard column (10 × 2.0 mm i.d., 5 µm). The wavelength for UV detection of glucosinolate was 227 nm, and the column oven temperature and flow rate were 40°C and 0.4 ml/min, respectively. The mobile phase was composed of (A) ultrapure H2O and (B) acetonitrile (HPLC grade). The gradient was as follows: initiation 7% solvent B followed by 7-24% solvent B (18 min), 24% solvent B (14 min), 7% solvent B (0.1 min), and 7 % solvent B for 8 min (total 40 min). The individual desulfo-glucosinolates were quantified based on their HPLC peak area ratios, reference to a desulfo-sinigrin external standard, and response factors (ISO 9167-1, 1992).

2.5 Statistical analysis

All data were measured as the means of three replicates. Three subsamples were randomly generated from each treated sample of rocket salad, and each replicate sample was separately subjected to extraction. Data were analyzed by analysis of variance (ANOVA) with sums of squares partitioned to reflect trial effects, using SAS Software (release 9.2; SAS Institute Inc., Cary, NC, USA), and the means were separated via Duncan's multiple range test($P < 0.05$).

3. Results and Discussion

3.1 Production of hairy root cultures in rocket salad grown with different media

Rocket salad hairy roots were treated in full-strength and half-strength MS medium, B5 medium, and SH medium to investigate the effect of culture medium on hairy root growth and glucosinolate production. The growth pattern of the hairy roots of rocket salad varied greatly under different media conditions (Figure 1). The highest dry weight (309 mg/flask) and the lowest dry weight (185 mg/flask) were recorded from full-strength SH and ½ MS media, respectively. The dry weights of the hairy roots of rocket salad were 67.03%, 57.48%, 49.73%, 43.78%, and 20.90% higher when cultured with SH, B5, ½ SH, 1/ B5, and MS, respectively, as compared to the lowest dry weight producer (½ MS medium).

Several factors increase secondary metabolite production and biomass production, including the type and concentration of salt in the medium, the type and quantity of carbohydrates, nitrate and phosphate, and the levels of growth regulator [22, 23-27]. Different media formulations (including MS, SH, B5, and Linsmaier and Skoog (LS)), have been developed and widely implemented for plant cultures [41]. In this study, different media showed significant effects on hairy root cultures (HRCs) of rocket salad, where the highest and the lowest fresh weights were observed when cultured in full-strength SH and ½ MS media, respectively. Numerous studies reported that different media affect the production of hairy root cultures. For instance, SH medium was reported to be optimal for HRC growth in watercress [42] and Chinese skullcap [27]; our results are consistent with these previous studies. In contrast, the hairy roots of hybrid ginseng [24], gamhar [25], and potato [26] exhibited the greatest growth in B5 media, and MS medium positively affected the growth of hairy root cultures of ginseng [43], cell suspension cultures of *Gymnema sylvestre* [44] and the hairy roots of broccoli [33].

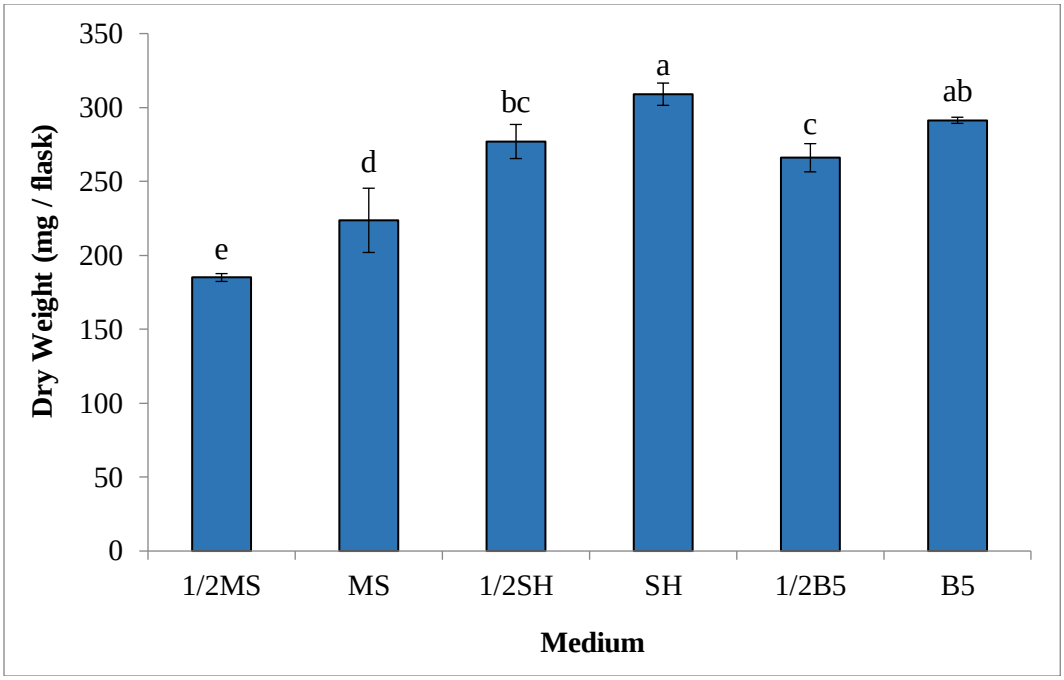

Figure 1. Effects of different media on the dry weight of rocket salad hairy root cultures. Values are means of three independent replicate results. Mean values with different letters were significantly different ($p < 0.05$, ANOVA, DMRT). DMRT: Duncan's multiple range test, MS= Murashige and Skoog, SH=Schenk and Hildebrandt, B5= Gamborg

3.2 Production of hairy root culture in rocket salad grown under conditions of different auxins

The hairy roots of rocket salad were treated with different concentrations of auxins. Three concentrations of the auxins, IAA, IBA, and NAA, were used to determine the effects on hairy root growth in rocket salad. The highest dry weight (331.33 mg/flask) and the lowest dry weight (270.67 mg/flask) were recorded from cultures in NAA 1.0 and from the control (only half-strength MS media), respectively (Figure 2). The dry weights of the hairy roots of rocket salad were not significantly different among the auxin treatments. The dry weights of the hairy roots of rocket salad were 22.41%, 21.18%, 20.44%, 18.59%, 16.75%, 15.76%, 15.15%, 14.16%, and 4.43% higher under treatments of NAA 1.0, IAA 0.1, IBA 1.0, IAA 0.5, IBA 0.5, NAA 0.5, IBA 0.1, IAA 1.0, and NAA 0.1, respectively, compared with the control treatment.

Exogenous growth regulators have been used extensively in plant cell, tissue, and hairy root cultures [41]. Among the various growth enhancers, auxins (particularly IAA, IBA, and NAA) play important roles in root development and promote hairy root induction [45]. Moreover, biomass and metabolite accumulation in media treated with different types and concentrations of auxins differed in plant cell cultures [46]. In this study, the highest fresh weight of HRC of rocket salad was obtained from a medium treated with NAA 1.0, followed by that with IAA 0.1 and IBA 1.0. Our findings support the results of other studies that determined the effects of auxins on higher biomass production in a wide range of plant species, such as tobacco [47], Indian mulberry [48], sorghum [49, 50], broccoli [51], and kale [52].

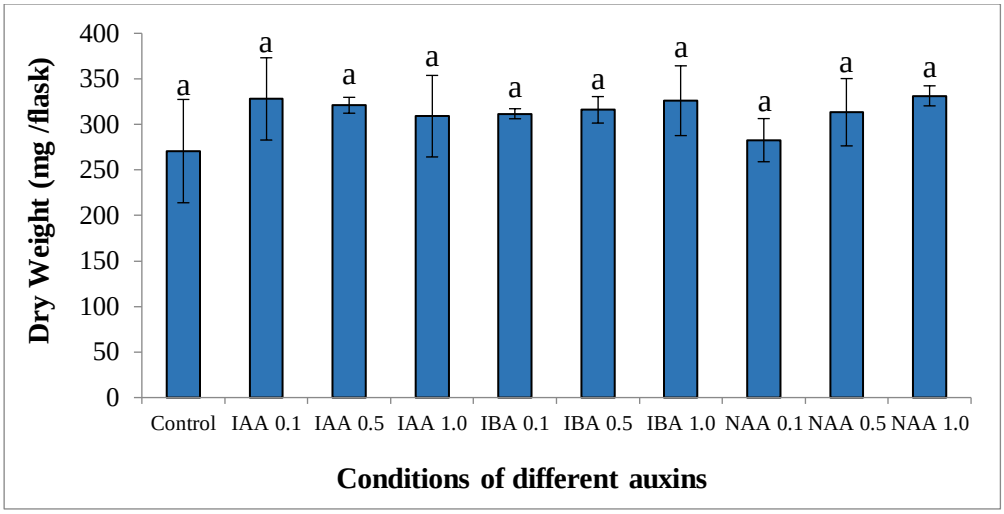

Figure 2. Effects of exogenous auxins on the fresh weight of rocket salad hairy root cultures. Values are means of three independent replicate results. Mean values with different letters were significantly different ($p < 0.05$, ANOVA, DMRT). IAA = indole-3-acetic acid, IBA = indole-3-butyric acid (IBA), and NAA = 1-naphthaleneacetic acid

3.3 Glucosinolates in the hairy root cultures of rocket salad in response to growth media

Based on the analysis of the hairy root cultures of rocket (*Eruca sativa*), the following six glucosinolates: glucoiberin, glucoerucin, glucoraphasatin, glucobrassicin, 4-methoxyglucobrassicin, and glucosativin, were observed at different levels in response to different growth media (Table 1). MS media yielded the greatest total accumulation of glucosinolates, followed by B5, and the lowest total accumulation of glucosinolates was found in the SH media. Total glucosinolate levels were increased by 1.7, 1.68, 1.33, and 1.26 in MS media containing ½ MS, ½ B5, and B5, respectively, compared with the lowest accumulated glucosinolates (from SH medium). The glucosativin level was much higher than that of 4-methoxy glucobrassicin, irrespective of the medium. MS media showed the best results for accumulation of glucoiberin, followed by B5 media, and SH media resulted in the least glucoiberin production. Glucoerucin content also varied widely by medium. MS media at half-strength accumulated the most glucoerucin, which was 2.89 times higher than the lowest (SH medium). Glucoraphasatin content did not vary significantly among the media. Half-strength MS media yielded double the quantity of glucoraphasatin of the least productive medium (MS). Glucobrassicin content was significantly higher in B5 and SH media; for the other media, the accumulation was almost similar. The content of glucobrassicin was 13.33 and 10.67 times higher in B5 and SH media, respectively, compared with the other four media. The quantity of 4-methoxy glucobrassicin was higher than in the control, irrespective of the medium used. Full-strength B5 medium showed the highest accumulation of 4-methoxy glucobrassicin, resulting in levels 4.2, 3.71, 3.58, and 2.56 times greater than those of the lowest (MS medium) for media treated with B5, ½ B5, SH,1/2 B5, and ½ SH, respectively. Glucosativin accumulation was higher at both concentrations of MS media, and the accumulation in other media was also slightly increased. Glucosativin accumulation, as influenced by different media, ranged from 3.48 to 18.85 µmol/g dry wt. Glucosativin accumulation was remarkably higher in MS medium (18.85 µmol/g dry wt) and

Table 1. Glucosinolate content in rocket salad hairy roots in various media

Glucosinolate (μmol/g dry wt)	1/2 MS	MS	1/2 SH	SH	1/2 B5	B5
Glucoiberin	0.15^{a}	0.20^{ab}	0.03^{c}	0.03^{c}	0.09^{b}	0.11^{b}
Glucoerucin	0.52 ^{a}	0.25^{bc}	0.31^{b}	0.18^{c}	0.45^{a}	0.25^{bc}
Glucoraphasatin	0.06 ^{a}	0.03^{b}	0.05^{ab}	0.04^{b}	0.04^{ab}	0.05^{ab}
Glucobrassicin	0.03 ^{c}	0.03^{c}	0.03^{c}	0.32^{b}	0.03^{c}	0.40^{a}
4-Methoxy glucobrassicin	3.24^{d}	2.25^{e}	5.77^{c}	8.35^{b}	8.05^{b}	9.45^{a}
Glucosativin	14.77^{a}	16.00^{a}	4.97 ^{bc}	3.48^{c}	6.14^{b}	3.83^{c}
Total	**18.76^{a}**	**18.85^{a}**	**11.16^{c}**	**12.40^{bc}**	**14.80^{b}**	**14.09^{b}**

Note: The data are presented as means with three replications in each individual sample. Mean values with different letter (s) in the same rows were significantly different ($p < 0.05$, ANOVA, DMRT). B5 = Gamborg B5 medium; 1/2 B5 = half-strength B5; MS = Murashige and Skoog medium; 1/2 MS = half-strength MS; SH = Schenk and Hildebrandt medium; 1/2SH = half-strength SH.

½ MS medium (18.76 μmol/g dry wt). The accumulated glucosativin was 4.6, 4.24, and 1.76 times higher following treatment with MS, ½ MS, and ½ B5 media, respectively.

GSL content in plants varies widely in response to factors including agronomic management, climatic conditions, mineral nutrient availability location, and plant variety [53-55]. In the present study, growth medium significantly influenced the accumulation of glucosinolates. Full-strength MS medium yielded the highest accumulation of total and individual glucosinolates, followed by ½ MS, ½ B5, and B5 media, respectively, whereas the lowest accumulated glucosinolates was found in SH media. These data are supported by a study in which growth medium was shown to significantly influence growth and glucosinolate content in broccoli [33]. In another study, MS basal medium increased the accumulation of glucosinolates over that of tissue grown in 1/2 SH medium [42]. In contrast, half and full-strength B5 and SH media induced the highest accumulations of glucosinolates in the hairy roots of broccoli [33]. Lee *et al*. [52] reported that B5 medium positively affected the production of total glucosinolates in HRCs of kale (*Brassica oleracea* var. *acephala*). B5 medium was optimal for both callus growth and the production of flavonoids. In addition, 1/2 B5 medium supported the highest production of flavones in HRCs of *Scutellaria baicalensis* [27].

3.4 Glucosinolate accumulation in hairy root cultures of rocket (*Eruca sativa*) in response to auxin treatment

The effects of different levels of auxins (IAA, IBA, and NAA) on glucosinolate accumulation in the hairy roots of rocket salad were investigated. The glucosinolates glucoiberin, glucoerucin, glucoraphasatin, glucobrassicin, 4-methoxy glucobrassicin, and glucosativin were observed in different quantities in response to different auxins (Table 2). Treatment with auxins negatively affected the production of glucosinolate in HRCs. The range of total accumulation level of

glucosinolates as influenced by different concentrations of auxins was 6.24 to 11.43 μmol/g dry wt, in which the highest level was found in the control treatment and the lowest in the IBA 1.0 treatment. The accumulation of total glucosinolates in the hairy roots of rocket salad was decreased by 45.41%, 44.88%, and 39.63% by treatment with IBA 1.0, IAA 1.0, and NAA 0.5, respectively, as compared with the control. The decreasing trend for other concentrations was the same but the level of decreasing was lower compared to IBA 1.0, IAA 1.0, and NAA 0.5. The auxin treatment did not increase the level of any glucosinolates, with the exception of glucoerucin. Glucoerucin accumulation level in the hairy roots of rocket salad was increased by 69.57%, 43.48%, and 26.09% on treatments with NAA 1.0, IBA 1.0, and IAA 0.1, respectively, compared to that of the control. The range of glucoiberin accumulation as influenced by different concentrations of auxins was 0.03 to 0.12 μmol/g dry wt, where the highest amount was obtained in the control and the lowest was obtained with IBA 0.5 treatment. Glucoiberin accumulation in the hairy roots of rocket salad was decreased by 75%, 41.67%, and 33.33% on the treatment with IBA 0.5, 0.1 and 0.5 IAA, and NAA 0.5, respectively, compared with the control. Gucoraphasatin content affected by different concentrations of auxins ranged from 0.02 to 0.04 μmol/g dry wt, with the highest value being in the control, and the lowest values were observed with IAA and IBA treatments. Glucoraphasatin accumulation in the hairy roots of rocket salad was decreased by 50%, 50%, and 25% on treatment with all IAA, IBA 1.0, and all NAA, respectively, as compared with the control. The difference in glucobrassicin content was very close among the treatments; the highest value was obtained from the control and IBA 0.05 treatments, and the values were equivalent for the rest of the treatments. The accumulation of 4-methoxyglucobrassicin was the highest, irrespective of auxin treatment. The range of accumulation levels of 4-methoxyglucobrassicin affected by the concentration of auxins was 3.96 to 6.66 μmol/g dry wt, with the highest level being obtained with the control treatment and the lowest level being obtained with the IAA 0.5 treatment. Glucoiberin accumulation in the hairy roots of rocket salad was decreased by 40.54%, 31.98 %, and 27.33% on treatment with IAA 0.5, NAA 0.5, and IBA 1.0, respectively, compared with the control. The second highest accumulated glucosinolate was glucosativin, irrespective of auxin treatment. The highest level was detected in the control treatment and the lowest level was detected in the NAA 1.0 treatment. Glucoiberin accumulation in the hairy roots of rocket salad was decreased by 81.38%, 79.77%, and 78.16% on treatments with NAA 1.0, IAA 1.0, and IBA 1.0, respectively, compared with the control.

Secondary metabolite accumulation in any part of the mother plants or transformed plants is dependent upon the organs or parts of the plants [5]. Accumulation of any product can be affected by external treatments such as phytohormones and elicitors, as well as by environmental factors [47-50]. Auxins are known to play important roles in plant growth, root development, and variation in the accumulation of secondary metabolites. The improvement in hairy root culture observed in this study is consistent with earlier reports on enhanced growth following treatment with exogenous auxin in hairy root cultures of *Lippia dulcis* [48], *Lobelia inflata* [56], *Panax hybrid* [57], and *S. baicalensis* [27].

Auxin treatment did not induce an increase in the level of any glucosinolates in this study, with the exception of glucoerucin. Only glucoerucin accumulation in the hairy roots of rocket salad was increased by 69.57%, 43.48%, and 26.09% on treatments with NAA 1.0, IBA 1.0, and IAA 0.1, respectively. The accumulation of any secondary metabolites in response to any treatment, particularly for auxin, can vary depending upon the plant species. From several previous studies, it was revealed that glucosinolate accumulation was enhanced at 0.5 to 1.0 mg/l of auxins particularly in the hairy roots of broccoli [33, 51], in Chinese cabbage [32], and in kale [52]. In other studies, it was reported that auxins treatments boosted the accumulation of sorgoleone in the root hairs of sorghum [49, 50]. In this study, media composition and auxin enhanced the production of hairy root cultures of rocket salad, although auxin had little effect on the accumulation of glucosinolates. Nevertheless, the effects of auxins can differ across different plant species.

Table 2. Glucosinolate content in rocket salad hairy roots under various auxin concentrations (μmol/g dry wt)

Treatment	Control	IAA 0.1	IAA 0.5	IAA 1.0	IBA 0.1	IBA 0.5	IBA 1.0	NAA 0.1	NAA 0.5	NAA 1.0
Glucoiberin	0.12^{a}	0.07^{b}	0.07^{bc}	0.08^{ab}	0.08^{ab}	0.03^{c}	0.08^{ab}	0.10^{ab}	0.08^{ab}	0.09^{ab}
Glucoerucin	0.23^{cd}	0.29^{bc}	0.28^{bc}	0.20^{d}	0.24^{cd}	0.23^{cd}	0.33^{ab}	0.24^{cd}	0.33^{ab}	0.39^{a}
Glucoraphasatin	0.04^{a}	0.02^{ab}	0.02 ^{ab}	0.02^{b}	0.03 ^{ab}	0.03 ^{ab}	0.02 ^{ab}	0.03 ^{ab}	0.03 ^{ab}	0.03^{ab}
Glucobrassicin	0.03^{a}	0.02^{cd}	0.02 ^{cd}	0.02 ^{cd}	0.02 ^{cd}	0.03 ^{ab}	0.02d	0.02 ^{cd}	0.00^{e}	0.02^{bc}
4-Methoxy Glucobrassicin	6.66^{a}	4.99^{cd}	3.96^{e}	5.10 ^{cd}	5.42^{bcd}	5.62^{bc}	4.84^{cde}	5.01 ^{cd}	4.53^{de}	6.17 ^{ab}
Glucosativin	4.35^{a}	1.33^{def}	2.38^{b}	0.88^{f}	1.05^{ef}	1.57^{cde}	0.95^{f}	2.00^{bc}	1.93^{bcd}	0.81^{f}
Total	**11.43^{a}**	**6.72^{b}**	**6.72 ^{b}**	**6.30 ^{b}**	**6.83 ^{b}**	**7.51 ^{b}**	**6.24 ^{b}**	**7.40 ^{b}**	**6.90 ^{b}**	**7.51 ^{b}**

Note: The data are presented as mean ± SD with three replications in each individual sample. Mean values with different letters in the same rows were significantly different ($p < 0.05$, ANOVA, DMRT). IAA, indole-3-acetic acid; IBA, indole-3-butyric acid; NAA, 1-naphthaleneacetic acid

4. Conclusions

The growth of rocket salad hairy roots was increased by treatment with SH media, and the auxin NAA at 1.0 concentration and MS medium induced greater accumulation of glucosinolates. No single auxin treatment enhanced the accumulation of any glucosinolate except for glucoerucin. Our findings indicate that hairy roots are a viable option for obtaining glucosinolate compounds from rocket salad, and that MS medium provides an alternative approach for mass production of hairy roots and glucosinolates in rocket salad, regardless of additional treatment. These findings support our current laboratory endeavors to enhance glucosinolate compound accumulation in hairy root cultures of rocket salad.

5. Acknowledgements

This study was supported by research fund from Chosun University, 2019.

References

[1] Pasini, F., Verardo, V., Cerretani, L., Caboni, M.F. and D'Antuono, L.F., 2011. Rocket salad (*Diplotaxis* and *Eruca* spp.) sensory analysis and relation with glucosinolate and phenolic content. *Journal of the Science of Food and Agriculture*, 91(15), 2858-2864.

[2] Martinez-Sanchez, A., Marin, A., Llorach, R., Ferreres, F. and Gil, M.I., 2006. Controlled atmosphere preserves quality and phytonutrients in wild rocket (*Diplotaxis tenuifolia*). *Postharvest Biology and Technology*, 40(1), 26-33.

[3] Bozokalfa, K.M., Esiyok, D. and Yagmur, B., 2011. Use of multivariate analysis in mineral accumulation of rocket (*Eruca sativa*) accessions. *Genetika-Belgrade*, 43(3), 437-448.

[4] Sahoo, R.K., Kumar, M., Sukla, L.B. and Subudhi, E., 2017. Bioprospecting hot spring metagenome: lipase for the production of biodiesel. *Environmental Science and Pollution Research*, 24(4), 3802-3809.

[5] Bennett, R.N., Rosa, E.A.S., Mellon, F.A. and Kroon, P.A., 2006. Ontogenic profiling of glucosinolates, flavonoids, and other secondary metabolites in *Eruca sativa* (salad rocket), *Diplotaxis erucoides* (wall rocket), *Diplotaxis tenuifolia* (wild rocket), and *Bunias orientalis* (Turkish rocket). *Journal of Agricultural and Food Chemistry*, 54(11), 4005-4015.

[6] Azarenko, O., Jordan, M.A. and Wilson, L., 2014. Erucin, the major isothiocyanate in arugula (*Eruca sativa*), inhibits proliferation of MCF7 tumor cells by suppressing microtubule dynamics. *PloS One*, 9(6), e100599, https://doi.org/10.137/journal.pone.0100599

[7] Michael, H.N., Shafik, R.E. and Rasmy, G.E., 2011. Studies on the chemical constituents of fresh leaf of *Eruca sativa* extract and its biological activity as anticancer agent in vitro. *Journal of Medicinal Plants Research*, 5, 1184-1191.

[8] Alam, M.S., Kaur, G., Jabbar, Z., Javed, K. and Athar, M., 2007. *Eruca sativa* seeds possess antioxidant activity and exert a protective effect on mercuric chloride induced renal toxicity. *Food and Chemical Toxicology*, 45(6), 910-920.

[9] Koubaa, M., Driss, D., Bouaziz, F., Ghorbel, R.E. and Chaabouni, S.E., 2015. Antioxidant and antimicrobial activities of solvent extract obtained from rocket (*Eruca sativa* L.) flowers. *Free Radicals and Antioxidants*, 5(1), 29-34.

[10] Khoobchandani, M., Ojeswi, B.K., Ganesh, N., Srivastava, M.M., Gabbanini, S., Matera, R., Iori, R. and Valgimigli, L., 2010. Antimicrobial properties and analytical profile of traditional

Eruca sativa seed oil: Comparison with various aerial and root plant extracts. *Food Chemistry*, 120(1), 217-224.

[11] Yehuda, H., Khatib, S., Sussan, I., Musa, R., Vaya, J. and Tamir, S., 2009. Potential skin antiinflammatory effects of 4-methylthiobutylisothiocyanate (MTBI) isolated from rocket (*Eruca sativa*) seeds. *Biofactors*, 35(3), 295-305.

[12] Clarke, D.B., 2010. Glucosinolates, structures and analysis in food. *Analytical Methods*, 2(4), 310-325.

[13] Jørgensen, M.E., Nour-Eldin, H.H. and Halkier, B.A., 2015. Transport of defense compounds from source to sink: lessons learned from glucosinolates. *Trends Plant Science*, 20(8), 508-514.

[14] Holst, B. and Williamson, G., 2004. A critical review of the bioavailability of glucosinolates and related compounds. *Natural Product Reports*, 21(3), 425-447.

[15] D'Antuono, L.F., Elementi, S. and Neri, R., 2009. Exploring new potential health-promoting vegetables: glucosinolates and sensory attributes of rocket salads and related *Diplotaxis* and *Eruca* species. *Journal of the Science of Food and Agriculture*, 89(4), 713-722.

[16] Higdon, J.V., Delage, B., Williams, D.E. and Dashwood, R.H., 2007. Cruciferous vegetables and human cancer risk: epidemiologic evidence and mechanistic basis. *Pharmacological Research*, 55(3), 224-236.

[17] Herr, I. and Büchler, M.W., 2010. Dietary constituents of broccoli and other cruciferous vegetables: implications for prevention and therapy of cancer. *Cancer Treatment Reviews*, 36(5), 377-383.

[18] Krzyzanowska, J., Czubacka, A. and Oleszek, W., 2010. Dietary phytochemicals and human health. *Advances in Experimental Medicine and Biology*, 698, 74-98.

[19] Podsedek, A., 2007. Natural antioxidants and antioxidant capacity of *Brassica* vegetables: A review. *LWT-Food Science and Technology*, 40(1), 1-11.

[20] Casagrande, S.S., Wang, Y., Anderson, C. and Gary, T.L., 2007. Have Americans increased their fruit and vegetable intake? The trends between 1988 and 2002. *American Journal of Preventive Medicine*, 32(4), 257-263.

[21] Woodward, A.W. and Bartel, B., 2005. Auxin: regulation, action, and interaction. *Annals of Botany*, 95(5), 707-735.

[22] George, E.F., Hall, M.A. and De Klerk, G.-J., 2008. The components of plant tissue culture media I: macro-and micro-nutrients. In: E.F. George, M.A. Hall and G.-J. De Klerk, eds. *Plant Propagation by Tissue Culture: Volume 1. The Background*. 3rd ed. Dordrecht: Springer, pp. 65-113.

[23] Saad, A.I.M. and Elshahed, A.M., 2012. Plant tissue culture media. In: A. Leva and L.M.R. Rinaldi, eds. *Recent Advances in Plant In Vitro Culture*. Winchester: In Tech, 29-40.

[24] Washida, D., Shimomura, K., Nakajima, Y., Takido, M. and Kitanaka, S., 1998. Ginsenosides in hairy roots of a *Panax* hybrid. *Phytochemistry*, 49(8), 2331-2335.

[25] Dhakulkar, S., Ganapathi, T.R. Bhargava, S. and Bapat, V.A., 2005. Induction of hairy roots in *Gmelina arborea* Roxb. and production of verbascoside in hairy roots. *Plant Science*, 169(5), 812-818.

[26] Kumar, G.B.S., Ganapathi, T.R., Srinivas, L., Revathi, C.J. and Bapat, V.A., 2006. Expression of hepatitis B surface antigen in potato hairy roots, *Plant Science*, 170(5), 918-925.

[27] Kim, Y.S., Li, X., Park, W.T., Uddin, M.R., Park, N.I., Kim, Y.B., Lee, M.Y. and Park, S.U., 2012. Influence of media and auxins on growth and falvone production in hairy root cultures of baikal skullcap, *Scutellaria baicalensis*. *Plant Omics Journal*, 5(1), 24-27.

[28] Georgiev, M.I., Agostini, E., Ludwig-Müller, J. and Xu, J., 2012. Genetically transformed roots: from plant disease to biotechnological resource. *Trends in Biotechnology*, 30(10), 528-537.

[29] Cuong, D.M., Park, S.U., Park, C.H., Kim, N.S., Bong, S.J. and Lee S.Y., 2019. Comparative analysis of glucosinolate production in hairy roots of green and red kale (*Brassica oleracea* var. *acephala*). *Preparative Biochemistry and Biotechnology*, 49(8), 775-782.

[30] Cuong, D.M., Park, C.H., Bong, S.J., Kim, N.S., Kim, J.K. and Park, S.U., 2019. Enhancement of glucosinolate production in watercress (*Nasturtium officinale*) hairy roots by overexpressing cabbage transcription factors. *Journal of Agricultural and Food Chemistry*, 67(17), 4860-4867.

[31] Cuong, D.M., Kim, J.K., Bong, S.J., Baek, S.A., Jeon, J., Park, J.S. and Park, S.U., 2018. Comparative analysis of glucosinolates and metabolite profiling of green and red mustard (*Brassica juncea*) hairy roots. *3 Biotech*, 8, 382, https://doi.org/10.1007/s13205-018-1393-x

[32] Bong, S.J., Uddin, M.R., Kim, S.-J., Park, J.S. and Park, S.U., 2015. Influence of auxins and wounding on glucosinolate biosynthesis in hairy root cultures of Chinese cabbage (*Brassica rapa* ssp. *pekinensis*). *Biosciences Biotechnology Research Asia*, 12(2), 1041-1046.

[33] Kim, S.-J., Park, W.T., Uddin, M.R., Kim, Y.B., Nam, S.-Y., Jho, K.H. and Park, S.U., 2013a. Glucosinolate biosynthesis in hairy root cultures of broccoli (*Brassica oleracea* var. italica). *Natural Product Communications*, 8(2), 217-220.

[34] Xue, S.-H., Luo, X.-J., Wu, Z.-H., Zhang, H.-L. and Wang, X.-Y., 2008. Cold storage and cryopreservation of hairy root cultures of medicinal plant *Eruca sativa* Mill., *Astragalusmembranaceus* and *Gentianamacrophylla* Pall. *Plant Cell, Tissue and Organ Culture*, 92(3), 251-260.

[35] Kastell, A., Schreiner, M., Knorr, D., Ulrichs, C. and Mewis, I., 2018. Influence of nutrient supply and elicitors on glucosinolate production in *E. sativa* hairy root cultures. *Plant Cell, Tissue and Organ Culture*, 132(3), 561-572.

[36] Murashige, T. and Skoog, F., 1962. A revised medium for rapid growth and bio assays with tobacco tissue cultures. *Physiologia Plantarum*, 15(3), 473-497.

[37] Schenk, R.U. and Hildebrandt, A.C., 1972. Medium and techniques for induction and growth of monocotyledonous and dicotyledonous plant cell cultures. *Canadian Journal of Botany*, 50(1), 199-204.

[38] Gamborg, O. L., Miller, R. and Ojima, K., 1968. Nutrient requirements of suspension cultures of soybean root cells. *Experimental Cell Research*, 50(1), 151-158.

[39] International Organization of Standardization, 1992. *Rapeseed - Determination of Glucosinolates Content- Part 1, Method Using High-Performance Liquid Chromatography*. *(ISO 9167-1:1992).* Geneva: International Organization of Standardization.

[40] Kim, S.J., Kawaharada, C., Jin, S., Hashimoto, M., Ishii, G. and Yamauchi, H., 2007. Structural elucidation of 4-(cystein-S-yl) butyl glucosinolate from the leaves of *Eruca sativa*. *Bioscience, Biotechnology, and Biochemistry*, 71(1), 114-121.

[41] Murthy, H.N., Lee, E.-J. and Paek, K.-Y., 2014. Production of secondary metabolites from cell and organ cultures: strategies and approaches for biomass improvement and metabolite accumulation. *Plant Cell, Tissue and Organ Culture*, 118(1), 1-16.

[42] Park, C.H, Kim, N.S., Yeo, H.J., Bong, S.J., Park, J.S., Park, N.I. and Park, S.U., 2019. Effects of culture medium on growth and glucosinolate accumulation in the hairy root cultures of watercress (*Nasturtium officinale*). *Research Journal of Biotechnology*, 14(2), 61-66.

[43] Sivakumar, G., Yu, K.W., Hahn, E.J. and Paek, K.Y., 2005. Optimization of organic nutrients for ginseng hairy roots production in large-scale bioreactors. *Current Science*, 89(4), 641-649.

[44] Nagella, P., Chung, I.-M. and Murthy, H.N., 2011. In vitro production of gymnemic acid from cell suspension cultures of *Gymnema sylvestre* R. Br. *Engineering in Life Sciences*, 11(5), 537-540.

[45] Cheruvathur, M.K. and Thomas, T.D., 2014. Effect of plant growth regulators and elicitors on rhinacanthin accumulation in hairy root cultures of *Rhinacanthus nasutus* (L.) Kurz. *Plant Cell, Tissue and Organ Culture*, 118(1), 169-177.

[46] Mantell, S.H. and Smith, H., 1983. Cultural factors that influence secondary metabolite accumulations in plant cell and tissue cultures. In: S.H. Mantell and H. Smith, eds. *Plant Biotechnology*. Cambridge: Cambridge University Press, pp. 75-108.
[47] Sahai, O. and Shuler, M., 1984. Environmental parameters influencing phenolics production by batch cultures of *Nicotiana tabacum*. *Biotechnology and Bioengineering*, 26(2), 111-120.
[48] Sauerwein, M., Yamazaki, T. and Shimomura, K., 1991. Hernandulcin in hairy root cultures of Lippia dulcis. *Plant Cell Reports*, 9(10), 579-581.
[49] Uddin, M.R., Park, K.W., Kim, Y.K., Park, S.U. and Pyon, J.Y., 2010. Enhancing sorgoleone levels in grain sorghum root exudates. *Journal of Chemical Ecology*, 36(8), 914-922.
[50] Uddin, M.R., Park, W.T., Kim, Y.K., Pyon, J.Y. and Park, S.-U., 2011. Effects of auxins on sorgoleone accumulation and genes for sorgoleone biosynthesis in sorghum roots. *Journal of Agricultural and Food Chemistry*, 59(24), 12948-12953.
[51] Kim, H.H, Kwon, D.Y., Bae, H., Kim, S.J., Kim, Y.B., Uddin, M.R. and Park, S.U., 2013. Influence of auxins on glucosinolate biosynthesis in hairy root cultures of broccoli (*Brassica oleracea* var. *italica*). *Asian Journal of Chemistry*, 25(11), 6099-6101.
[52] Lee, S.Y., Bong, S.J., Kim, J.K. and Park, S.U., 2016. Glucosinolate biosynthesis as influenced by growth media and auxin in hairy root cultures of kale (*Brassica oleracea* var. *acephala*). *Emirates Journal of Food and Agriculture*, 28(4), 277-282.
[53] Brown, A.F., Yousef, G.G., Jeffery, E.H., Klein, B.P., Wallig, M.A., Kushad, M.M. and Juvik, J.A., 2002. Glucosinolate profiles in broccoli: Variation in levels and implications in breeding for cancer chemoprotection. *Journal of the American Society for Horticultural Science*, 127(5), 807-813.
[54] Vallejo, F., Tomas-Barberán, F.A., Gonzalez Benavente-García, A. and García-Viguera, C., 2003. Total and individual glucosinolate contents in inflorescences of eight broccoli cultivars grown under various climatic and fertilization conditions. *Journal of the Science of Food and Agriculture*, 83(4), 307-313.
[55] Kumar, S. and Andy, A., 2012. Health promoting bioactive phytochemicals from *Brassica*. *International Food Research Journal*, 19(1), 141-152.
[56] Bálványos, I., Kursinszki, L. and Szõke, E., 2001. The effect of plant growth regulators on biomass formation and lobeline production of *Lobelia inflata* L. hairy root culture. *Plant Growth Regulator*, 34(3), 339-345.
[57] Washida, D., Shimomura, K., Takido, M. and Kitanaka, S., 2004. Auxins affected ginsenoside production and growth of hairy roots in *Panax hybrid*. *Biological and Pharmaceutical Bulletin*, 27(5), 657-660.

Current Applied Science and Technology Vol. 21 No. 2 (April-June 2021)

Improvement in Biomass Production of a Microalga *Chlorella* sp. S2 Using Starch Processing Wastewater

Siriporn Yossan[1]* and Wannakorn Kitcha[2]

[1]Division of Environmental Science, Faculty of Liberal Arts and Science, Sisaket Rajabhat University, Sisaket, Thailand
[2]Division of Biology, Faculty of Science and Technology, Bansomdejchaopraya Rajabhat University, Bangkok, Thailand

Received: 18 April 2020, Revised: 5 November 2020, Accepted: 9 December 2020

Abstract

Microalgae are promising resources for high-quality dietary supplements, pharmaceutical and biofuel production. This study attempted to improve the biomass of a microalga by cultivation in starch processing wastewater. A microalga identified as *Chlorella* sp. S2 by morphological criterion was isolated from the facultative pond of a noodle making plant. It was able to grow in the starch processing wastewater without addition of nutrients. To increase the biomass productivity of *Chlorella* sp. S2, inorganic nitrogen sources ($NaNO_3$, NH_4Cl and KNO_3) were added into the starch processing wastewater. The optimum nitrogen source was potassium nitrate at 7.5 mM of nitrogen, which increased the number of *Chlorella* sp. S2 up to 1.41×10^7 cells/ml and the specific growth rate was 0.351 d^{-1}. Under sunlight, the microalga *Chlorella* sp. S2 also produced high biomass concentration (2.23±0.04 g/l). It means that microalgal cultivation using starch processing wastewater is a great process to produce biomass. In addition, it is able to reduce organic carbon in the wastewater and reduce cost.

Keywords: microalgae; *Chlorella*; cultivation; starch processing wastewater; biomass production
DOI 10.14456/cast.2021.32

1. Introduction

Nowadays, microalgae are used as dietary supplements, pharmaceuticals, biofuels and in other applications. Microalgae are mixotrophic organisms that are able to be both autotrophs and heterotrophs. Microalgae can fix and transform CO_2 into starch, oilgae, carotenoids and other compounds in similar way to plants and they also release O_2 in autotrophic cultures [1-3]. In addition, organic carbon sources (such as glucose, glycerol, molasses, whey permeate, acetic acid etc.) are used to increase the biomass of microalgae in heterotrophic cultures [4-9].

*Corresponding author: Tel.: (+66) 866395551
E-mail: siripornyos@hotmail.com

Microalgae can be cultivated in ponds and fermenters using wastewater as organic carbon sources [1]. Wastewater consists of nutrients (phosphorus, nitrogen, organic carbon, etc.) which are required by microalgae for growth and biomass production [10]. The use of wastewater can reduce the cost of biomass production because microalgae can grow in it without adding any extra nutrients [1]. In addition, biomass production of microalgae in wastewater can reduce organic carbon, which is an environmentally friendly process.

Chlorella is able to grow mixotrophically in a short time and has simple growth requirements [11, 12]. *Chlorella* contains abundant nutrients, especially high protein content, which are beneficial to human and animal health [13]. In addition, *Chlorella* can be used to remove the colour and COD of textile wastewater effluent [14, 15]. It also removes nitrogen, phosphorus and carbon from water to reduce eutrophication in an aquatic environments, and it tolerates untreated wastewater [16, 17].

In this study, to save the cost of microalgal biomass production, starch processing wastewater was used as organic carbon and nutrient sources for cultivation. The microalga *Chlorella* sp. was chosen to investigate the optimal conditions for increasing biomass concentration in mixotrophic culture.

2. Materials and methods

2.1 Isolation and purification

The microalga was isolated from wastewater treatment ponds (oxidation ponds) at a noodle making plant in Sisaket Province, Thailand, with a plankton net (10 µm × 7 µm in size). The microalga *Chlorella*-like green colonies were separated using a sterile micropipette washing method [18] and cultivated in a modified Chu13 [19]. The microalga *Chlorella* was subjected to purification by serial dilution followed by plating. The single colony was isolated and cultured in liquid modified Chu13 medium at room temperature (28-30ºC), with a light intensity of 3,000 lux using cool-white fluorescent lamps (16 h) for 7 days. The isolated microalga was approximately identified as the genus *Chlorella* according to morphological properties [20].

2.2 Microalgal cultures

The microalga *Chlorella* sp. S2 was grown in starch processing wastewater. The waste water samples were obtained from an anaerobic pond (No.1), facultative pond (No.2) and aerobic ponds (No.3 and No.4) of a noodle making plant in Sisaket Province, Thailand. The pH values of the wastewater samples were acid and neutral pH (5.44-7.13) in ponds No.1-4. The values of phosphorus, nitrogen and potassium in the wastewater samples were determined following AWWA/APHA protocols [21]. The starch processing wastewater was dark because it contained some suspended solids. Therefore, the suspended solids were removed by filtration with absorbent cotton and sterilized with chlorine (calcium hypochlorite; $Ca(OCl)_2$) at a concentration of 15 ppm for 30 min. Chlorine was able to reduce the problems associated with light-shading and the mass transfer of oxygen. To reduce the effect of chlorine on the microalga growth, chlorine was removed by filtered air bubbles from an air pump (0.5 l/min) for 1 h.

The cultivation of the microalga *Chlorella* sp. S2 was attempted by adding 10% (v/v) of seed culture (5×10^6 cells/ml) in 400 ml of starch processing wastewater medium. The culture was incubated with 0.03% CO_2 (0.02 l/min) at room temperature, with a light intensity of 3,000 lux using cool-white fluorescent lamps (light intensity with 16:8 h light photoperiod) for 7 days.

Nitrogen sources ($NaNO_3$, NH_4Cl and KNO_3) at 7.5 mM of nitrogen were added to the starch processing wastewater medium samples to increase the biomass of microalga *Chlorella* sp. S2. Then, the optimal concentration of nitrogen at 3.7, 7.5 and 15.0 mM were tested. The effect of sunlight was also tested in order to save cost on biomass production.

2.3 Analytical methods

All wastewater samples were analyzed for phosphorus, nitrogen and potassium. The pH values of culture broths were measured by pH meter (pH 900, Amtast Industry, USA). Cell concentrations of microalga *Chlorella* sp. S2 were determined using a hemocytometer. Flocculation of microalga was attempted by adding Alum (0.3 g/l at pH 6.0) [22]. Next, sedimentation was allowed to occur under gravity for 10 min and supernatant was removed and precipitate was dried at 60ºC until constant weight was observed for microalgal biomass. The specific growth rate (μ) was calculated using data in the exponential phase using the following equation:

$$\mu\ (d^{-1}) = \frac{ln\frac{x_2}{x_1}}{t_2 - t_1}$$

where x_1 and x_2 are the concentrations of microalgal cells (g/l) at time t_1 and t_2, respectively [23].

All experiments were performed in triplicate. Analysis of variance was performed to calculate significant differences in treatment means, and the least significant difference ($p \leq 0.05$) was used to separate means, using SPSS software.

3. Results and Discussion

3.1 Growth of microalga in the starch processing wastewater

Under the microscope, the isolated S2 showed a spherical shape with no flagellum (Figure 1). It was identified as *Chlorella* sp. S2 by morphological criterion. The microalga *Chlorella* sp. S2 was cultivated in starch processing wastewater collected from oxidation ponds (No.1-4) in the noodle making plant. The algal biomass concentration from pond No.2 increased faster and to a higher level compared with other ponds (No. 1, 3 and 4) (Figure 2). It provided the highest biomass of 2.26×0.12 g/l on the 7th day and also provided the highest cell number of 5.6×10^6 cells/ml on the day 5th while entering the steady stage until the 7th day. It was interesting that biomass was cultivated from microalga *Chlorella* sp. S2 without addition of any nutrients in the starch processing wastewater yielded high biomass. This might have been because there were organic carbon and nutrient elements (phosphorus 230.96 mg/l, nitrogen 7.9 mg/l and potassium 55.97 mg/l) for the growth of microalga *Chlorella* sp. S2 in the mixotrophic condition. This might be the reason of cost saving for biomass production of *Chlorella* sp. S2. There were lower biomass and cell number in the starch

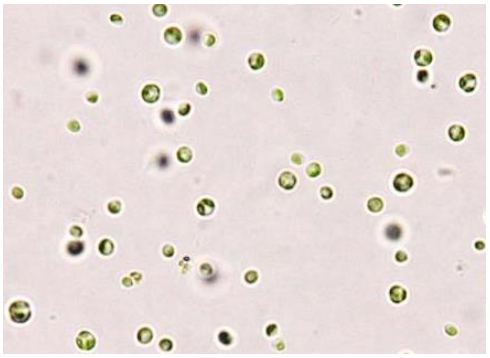

Figure 1. The microalga *Chlorella* sp. S2 under the microscope (40×)

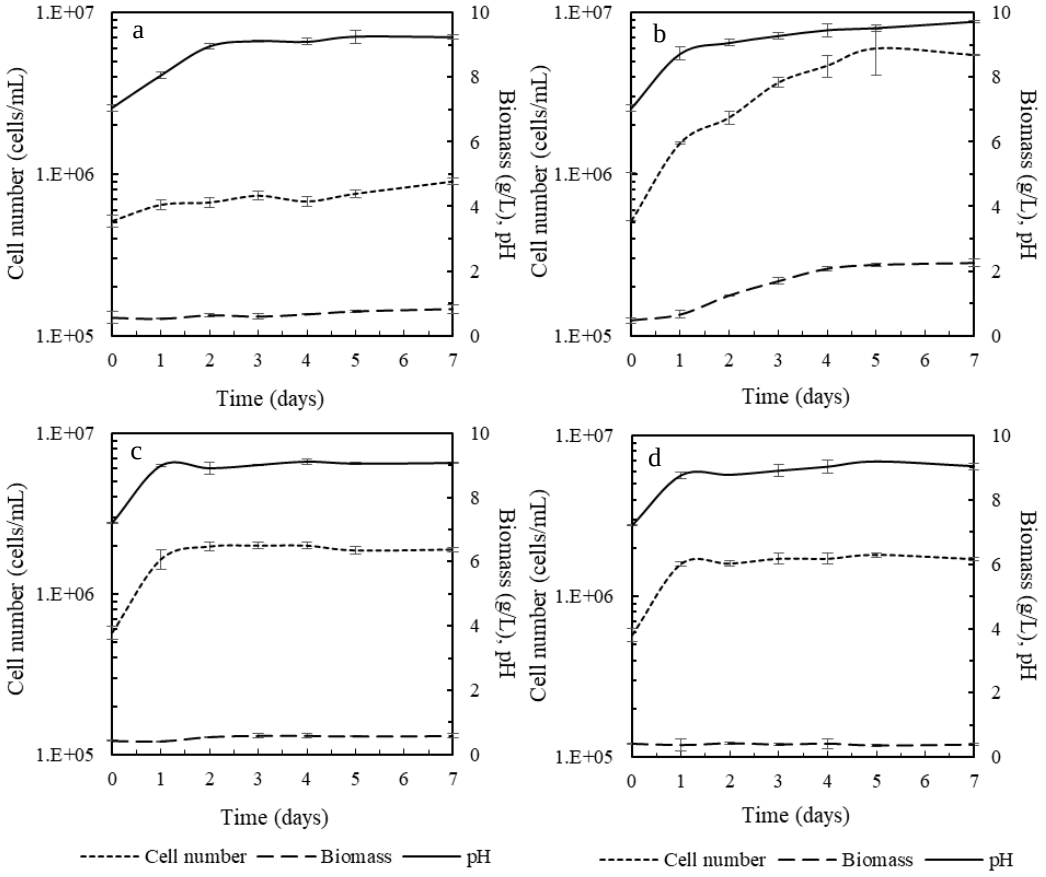

Figure 2. Comparison of growth of *Chlorella* sp. S2 in the starch processing wastewater from wastewater treatment pond No.1 (a), No.2 (b), No.3 (c) and No.4 (d)

processing wastewater from wastewater treatment ponds No. 1, 3 and 4, a result which might have been influenced from the depletion of nitrogen in the culture medium used. There was a nitrogen concentration of only 7.9 mg/l in the starch processing wastewater medium. An increase in microalgal biomass was found under nitrogen-rich conditions [24]. On the other hand, microalga *Chlorella protothecoides* grew well using glucose as a carbon source on the heterotrophic condition [25]. In all cultivations, pH increased from 6.8 to 9.5 because CO_2 dissolves in the culture medium as bicarbonate form (HCO_3^-). When microalgae consumes CO_2, the OH^- is formed and makes the culture medium more alkaline [26].

3.2 Effect of nitrogen sources on growth

There was a low nitrogen concentration (7.9 mg/l) in the starch processing wastewater from wastewater treatment pond No.2. Hence, the biomass production of microalga *Chlorella* sp. S2 was enhanced by addition of nitrogen sources. The influence of $NaNO_3$, NH_4Cl, KNO_3 (7.5 mM nitrogen) was investigated as shown in Figure 3. The biomass of microalga *Chlorella* sp. S2 increased rapidly in the starch processing wastewater with the addition of KNO_3 (2.57±0.18 g/l), Na_2NO_3 (2.27±0.08 g/l) and NH_4Cl (2.42±0.21 g/l), respectively. The addition of nitrogen sources provided the highest biomass on the 4th day, whereas cell number increased steadily until the day 5th (Figure 3b) but the biomass did not increase. However, without addition of nitrogen sources, the biomass developed later, on the 5th day. Microalgae cultivation should have suitable nitrogen concentration because they require nitrogen to synthesize proteins [27]. Thus KNO_3, which showed a rapid increase of biomass and cell number, was chosen as a suitable nitrogen source. This was similar to previous research with *Chlorella protothecoides*, where biomass concentration increased with the addition of both inorganic and organic nitrogen sources (nitrate, ammonium and urea) [25]. The highest biomass concentration of *Chlorella sorokiniana* occurred when glycine was used as the nitrogen source [28].

3.3 Effect of nitrogen source concentration on growth

The optimum levels of nitrogen (KNO_3) concentration for the biomass production of *Chlorella* sp. S2 were varied from 3.7 to 15.0 mM as demonstrated in Figure 4. The effect of nitrogen (KNO_3) concentration on growth was observed. When the concentration of KNO_3 was increased, the biomass and cell number of *Chlorella* sp. S2 also increased steadily until the 5th day of cultivation. It was interesting that the biomass and cell number of *Chlorella* sp. S2 grew slightly faster and provided the highest specific growth rate of 0.351 d^{-1} at KNO_3 of 7.5 mM (Figure 4b). However, there was no significant difference between 7.5 and 15.0 mM of KNO_3. The biomass concentration in the starch processing wastewater without addition of nitrogen was similar to the addition of 3.7 mM of KNO_3 (Figure 4a), but with the addition of KNO_3, *Chlorella* sp. S2 grew slightly faster. In addition, the broth culture medium of *Chlorella* sp. S2 presented dark green at 7.5 and 15.0 mM of KNO_3 as shown in Figures 5c and 5d, respectively. The biomass of microalga *Nannochlolis* also increased when the nitrate concentration was increased from 0.9-9.9 mM of nitrate [29] while *Scenedesmus dimorphus* provided high biomass at 0.06 M of nitrate [30]. At the low concentration of KNO_3 (3.7 mM), it was yellow-green (Figure 5b) and without addition of nitrogen source it was bright yellow-green (Figure 5a). This means there was not enough nitrogen concentration in the starch processing wastewater for microalgal growth. Furthermore, the biomass production of *Scenedesmus dimorphus* and *Chlorella photothecoides* increased in medium which had high a concentration of nitrogen [30] while the biomass production of *Chlorella vulgaris* decreased in the medium with a limit nitrogen concentration [31].

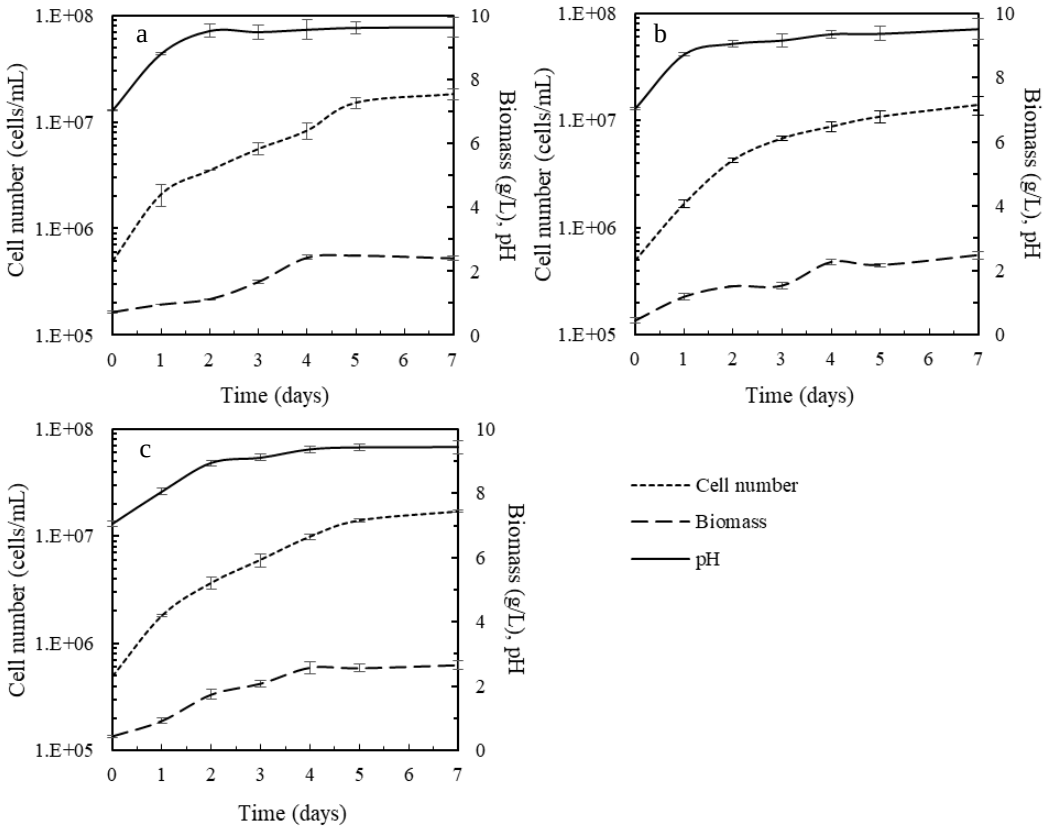

Figure 3. Effect of nitrogen sources on cell number, biomass and pH of *Chlorella* sp. S2 in the starch processing wastewater from wastewater treatment pond No.2: $NaNO_3$ (a), NH_4Cl (b) and KNO_3 (c)

3.4 Effect of sunlight

Microalgae are autotrophic organisms, therefore, light is the most important factor which affects growth and storage of products [32]. To reduce the cost of microalgal cultivation, the effects of lighting sources were observed as shown in Figure 6. The microalga *Chlorella* sp. S2 was grown in the starch processing wastewater medium with the addition of KNO_3 (7.5 mM). It was found that *Chlorella* sp. S2 grew well and provided the highest biomass and cell number of 2.23±0.04 g/l and 6.18 ± 10^6 cells/ml, respectively on the 5th day of cultivation. It showed a specific growth rate of 0.328 d^{-1}. The specific growth rate of the microalga *Chlorella* sp. S2 under sunlight conditions slightly decreased compared to that of culture using cool-white fluorescent lamps (16 h) (0.351 d^{-1}). That might have been influenced by the high light intensity of the sunlight (3,000-6,000 lux), which was not suitable for growth of the microalga *Chlorella* sp. S2.

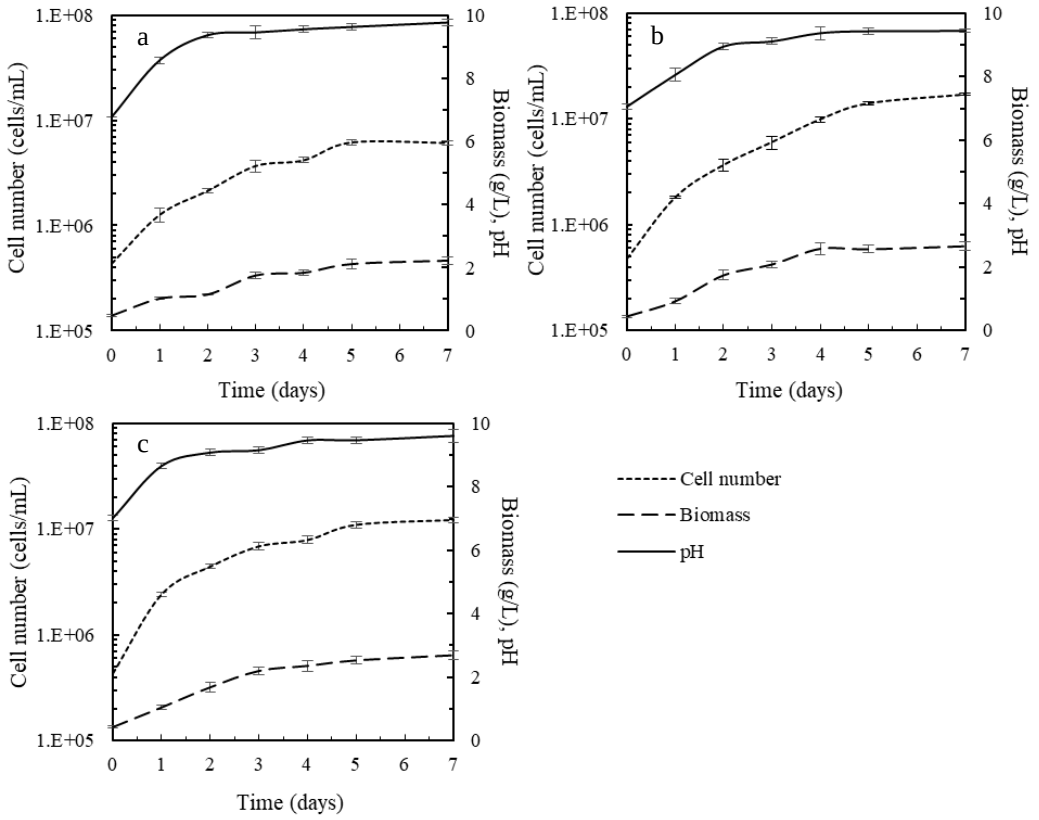

Figure 4. Effect of nitrogen concentration at 3.7 mM (a), 7.5 mM (b), and 15.0 mM (c), on cell number, biomass and pH of *Chlorella* sp. S2 in the starch processing wastewater from wastewater treatment pond No.2

Figure 5. The microalga *Chlorella* sp. S2 cultures after cultivation in the effluent without addition of nitrogen (a), with addition of nitrogen at 3.7 mM (b), 7.5 mM (c) and 15.0 mM (d) of KNO_3 on 7^{th} day

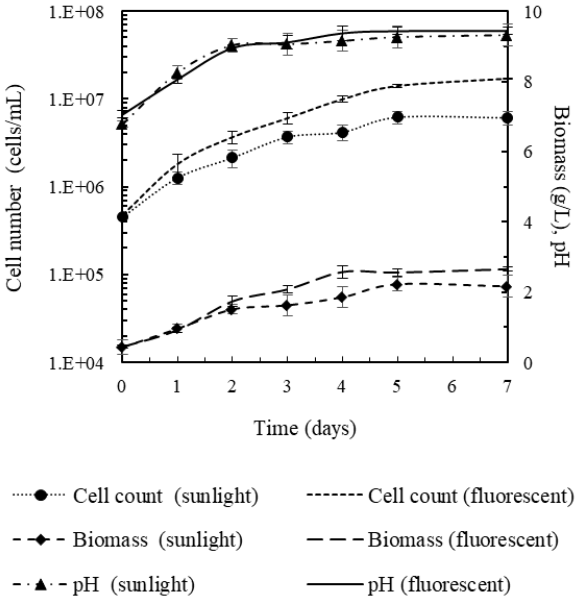

Figure 6. Effect of sunlight and fluorescent lamps at 3,000 lux light intensity with 16:8 h light photoperiod on cell number, biomass and pH of *Chlorella* sp. S2 in the starch processing wastewater with the addition of 7.5 mM KNO_3

4. Conclusions

The microalga *Chlorella* sp. S2, isolated from the starch processing wastewater in the noodle making plant, grew well in the starch processing wastewater from wastewater treatment pond No.2. It provided high biomass concentration and cell number with and without the addition of nitrogen. When the starch processing wastewater medium with added KNO_3 at 7.5 mM, the highest specific growth rate occurred and the biomass of the microalga *Chlorella* sp. S2 increased slightly faster. The microalga *Chlorella* sp. S2 also grew well under sunlight. This study has shown that the starch processing wastewater from the noodle making plant under the sunlight was able to cultivate the microalga *Chlorella* sp. S2.

5. Acknowledgements

This work was financially supported by the Department of Research and Development and the Faculty of Liberal Arts and Science, Sisaket Rajabhat University.

References

[1] Hodaifa, G., Sanchez, S., Martinez, E. and Orpez, R., 2013. Biomass production of *Scenedesmus bliquus* from mixtures of urban and olive-oil mill wastewaters used as culture medium. *Applied Energy*, 104, 345-352.

[2] Lam, M.K. and Lee, K.T., 2013. Effect of carbon source towards the growth of Chlorella vulgaris for CO2 bio-mitigation and biodiesel production. *International Journal of Greenhouse Gas Control*, 14, 169-176.

[3] Takeshita, T., Ota, T., Yamazaki, T., Hirata, A., Zachleder, V. and Kawano, S., 2014. Starch and lipid accumulation in eight strains of six *Chlorella* species under comparatively high light intensity and aeration culture conditions. *Bioresource Technology*, 158, 127-134.

[4] Li, X., Xu, H. and Wu, Q., 2007. Large-scale biodiesel production from microalga *Chlorella protothecoides* through heterotrophic cultivation in bioreactors. *Biotechnology and Bioengineering*, 98, 764-771.

[5] Katiyar, R., Gurjar, B.R., Bharti, R.K., Kumar, A., Biswas, S. and Pruthi, V., 2017. Heterotrophic cultivation of microalgae in photobioreactor using low cost crude glycerol for enhanced biodiesel production. *Renewable Energy*, 113, 1359-1365.

[6] Ende, S.S.W. and Noke, A., 2019. Heterotrophic microalgae production on food waste and by-products. *Journal of Applied Phycology*, 31, 1565-1571.

[7] Endo, H., Nakajima, K., Chino, R. and Shirota, M., 2014. Growth characteristics and cellular components of *Chlorella regularis*, heterotrophic fast growing strain. *Agrcultural and Biological Chemistry*, 38, 9-18.

[8] Gonzalez, I.E., Parashar, A. and Bressler, D., 2014. Heterotrophic growth and lipid accumulation of *Chlorella protothecoides* in whey permeate, a dairy by-product stream, for biofuel production. *Bioresource Technology*, 155, 170-176.

[9] Xie, Z., Lin, W., Liu, J. and Luo, J., 2020. Mixotrophic cultivation of *Chlorella* for biomass production by using pH-stat culture medium: Glucose-Acetate-Phosphorus (GAP). *Bioresource Technology*, 313, https://doi.org/10.1016/j.biortech.2020.123506

[10] Mahapatra, D.M., Chanakya, H.N. and Ramachandra, T.V., 2013. *Euglena* sp. as a suitable source of lipids for potential use as biofuel and sustainable wastewater treatment. *Journal of Applied Phycology*, 25, 855-865.

[11] Nakanishi, K. and Deuchi, K., 2014. Culture of a high-chlorophyll-producing and halotolerant *Chlorella vulgaris*. *Journal of Bioscience and Bioengineering*, 117, 617-619.

[12] Heredia, A.T., Wei, W., Ruan, R. and Hu, B., 2011. Mixotrophic cultivation of *Chlorella vulgaris* and its potential application for the oil accumulation from non-sugar materials. *Biomass and Bioenergy*, 35, 2245-2253.

[13] Yeh, K.L., Chang, J.S. and Chen, W., 2010. Effect of light supply and carbon source on cell growth and cellular composition of a newly isolated microalga *Chlorella vulgaris* ESP-31. *Engineering in Life Sciences*, 10, 201-208.

[14] Kassas, H.Y. and Mohamed., L.A., 2014. Bioremediation of the textile waste effluent by *Chlorella vulgaris*. *The Egyptian Journal of Aquatic Research*, 40, 301-308.

[15] Kumar, P.K., Krishna, S.V., Naidu, S.S., Verma, K., Bhagawan, D. and Himabindu, V., 2019. Biomass production from microalgae *Chlorella* grown in sewage, kitchen wastewater using industrial CO_2 emissions: Comparative study. *Carbon Resources Conversion*, 2, 126-133.

[16] Ruiz, J., Alvarez, P., Arbib, Z., Garrido, C., Barragan, J. and Perales, J.A., 2011. Effect of nitrogen and phosphorus concentration on their removal kinetic in treated urban wastewater by *Chlorella vulgaris*. *International Journal of Phytoremediation*, 13, 884-896.

[17] Chen, C.-Y., Kuo, E.-W., Nagarajan, D., Ho, S.-H., Dong, C.-D., Lee, D.-J. and Chang, J.-S., 2020. Cultivating *Chlorella sorokiniana* AK-1 with swine wastewater for simultaneous

wastewater treatment and algal biomass production. *Bioresource Technology*, 302, https://doi:10.1016/ j.biortech.2020.122814

[18] Stein, J.R., 1973. *Handbook of Phycological Methods: Culture Methods and Growth Measurements*. London: Cambridge University Press.

[19] Tansakul, P., Savaddiraksa, Y., Prasertsan, P. and Tongurai, C., 2005. Cultivation of the hydrocarbon-rich alga, *Botyococcus braunii* in secondary treated effluent from a sea food processing plant. *Thai Journal of Agricultural Science*, 38, 71-76.

[20] Chaichalerm, S., Pokethitiyook, P., Yuan, W., Meetam, M., Sritong, K., Pugkaew, W., Kungvansaichol, K., Kruatrachue, M. and Damrongphol, P., 2012. Culture of microalgal strains isolated from natural habitats in Thailand in various enriched media. *Applied Energy*, 89, 296-302.

[21] APHA, AWWA & WPCF, 2005, *Standard Methods for the Examination of Water and Wastewater*. Washington D.C.: American Public Health Association.

[22] Chen, L., Wang, C., Wang, W. and Wei, J., 2013. Optimal conditions of different flocculation methods for harvesting *Scenedesmus* sp. cultivated in an open-pond system. *Bioresource Technology*, 133, 9-15.

[23] Srinuanpan, S., Cheirsilp, B., Kitcha, W. and Prasertsan, P., 2017. Strategies to improve methane content in biogas by cultivation of oleaginous microalgae and the evaluation of fuel properties of the microalgal lipids. *Renewable Energy*, 113, 1229-1241.

[24] Yeesang, C. and Cheirsilp, B., 2011. Effect of nitrogen, salt, and iron content in the growth medium and light intensity on lipid production by microalgae isolated from freshwater sources in Thailand. *Bioresource Technology*, 102, 3034-3040.

[25] Shi, X.M., Zhang, X.W. and Chen, F., 2000. Heterotrophic production of biomass and lutein by *Chlorella protothecoides* on various nitrogen sources. *Enzyme and Microbial Technology*, 27, 312-318.

[26] Richmond, A., 1986. *Handbook of Microalgal Mass Culture*. London: CRC Press.

[27] Chu, F.F., Chu, P.N., Shen, X.F., Lam, P.K. and Zeng, R.J., 2014. Effect of phosphorus on biodiesel production from *Scenedesmus obliquus* under nitrogen-deficiency stress. *Bioresource Technology*, 152, 241-246.

[28] Xie, M., Qiu, Y., Song, C., Qi, Y., Li, Y. and Kitamura, Y., 2018. Optimization of *Chlorella sorokiniana* cultivation condition for simultaneous enhanced biomass and lipid production via CO_2 fixation. *Bioresource Technology Report*, 2, 15-20.

[29] Miyamoto, K., 1997. *Renewable Biological Systems for Alternative Sustainable Energy Production*. Rome: Food and Agricultural Organization of the United Nations.

[30] Shen, Y., Pei, Z., Yuan, W. and Mao, E., 2009. Effect of nitrogen and extraction method on algae lipid yield. *International Journal of Agricultureal and Biological Engineering*, 2, 51-57.

[31] Converti, A., Casazza, A.A, Ortiz, E.Y., Perego, P. and Borghi, M.D., 2009. Effect of temperature and nitrogen concentration on the growth and lipid content of *Nannochloropsis oculata* and *Chlorella vulgaris* for biodiesel production. *Chemical Engineering and Processing: Process Intensification*, 48, 1146-1151.

[32] Ruangsomboon, S., 2012. Effect of light, nutrient, cultivation time and salinity on lipid production of newly isolated strain of the green microalga, *Botryococcus braunii* KMITL 2. *Bioresource Technology*, 109, 261-265.

Current Applied Science and Technology Vol. 21 No. 2 (April-June 2021)

Classification Model Development Based on Cluster-to-Class Distance Mapping for Tourism Form Prediction of Inbound Tourism Market in Thailand

Unnadathorn Moonpen[1], Surasak Mungsing[1] and Thepparit Banditwattanawong[2]*

[1]Faculty of Information Technology, Sripatum University, Bangkok, Thailand
[2]Department of Computer Science, Faculty of Science, Kasetsart University, Bangkok, Thailand

Received: 16 July 2020, Revised: 9 November 2020, Accepted: 27 December 2020

Abstract

This paper describes the classification model development of inbound tourism form in Thailand. The models utilized both labeled and originally unlabeled data sets. The latter data set, which was obtained from the Ministry of Tourism and Sports of Thailand that regularly collects unlabeled data, mandated the synthesis of tourism form labels to be usable for classification. To achieve such a label synthesis, we proposed a cluster-to-class mapping algorithm that consisted of three steps. First, searching the best tourist clustering model among the unlabeled tourist data set by comparing the results of K-means, hierarchical cluster analysis, random clustering, and DBSCAN techniques. Second, mapping the clusters to the classes of the labeled data set based on Euclidean similarity to reveal the tourism form labels for the clusters. Finally, searching the best tourism-form classification model based on the data sets with real and synthesized labels by engaging Naïve Bayes, support vector machine, linear regression, and decision tree techniques. Experimental results show that our algorithm effectively generated the tourism form labels since, when using them, we obtained a neutral network model that was capable of predicting the inbound tourism forms of an unseen tourist data set with an F-measure value as high as 98.99%.

Keywords: tourism form; classification algorithm; clustering algorithm; cluster-to-class mapping
DOI 10.14456/cast.2021.31

1. Introduction

Tourism industry plays a leading role in Thailand's economy as domestic and international tourism contributes 2.01 trillion baht per annum by average to the Thai national Gross Domestic Product (GDP) or 15% of total GDP. Moreover, the tourism industry has in recent years employed 4,129,382 people per year or 10.82% of national employment by average. Specifically, income from inbound tourism averaged as high as 10% of the national tourism direct gross domestic products (TDGDP) [1]. It was expected that a tourism situation in Thailand in 2020 would gain a contribution by 37 million foreign tourists or 1.73 trillion baht, which has declined from the 2019 report on the number of 39.8 million foreign tourists who contributed 1.88 trillion baht.

*Corresponding author: Tel: +66(0)2942 8200-45
E-mail: thepparit.b@ku.th

To stimulate the tourism industry's resiliency in the second half of the year after the end of COVID-19 pandemic is deemed important [2]. One strategy that can be used to boost Thailand tourism is to exploit technology and digital platform to meet the personal needs and lifestyles of tourists in terms of tourism forms [3]. Therefore, relevant marketing analysts and entrepreneurs must understand and adapt to such needs [4] although tourism planning and developing is large-scaled and requires highly accurate forecasting to reduce potential risk in a decision making process [5]. The forecasting can be conducted by utilizing recorded tourist data that is collected regularly by Office of the Permanent Secretary of Ministry of Tourism and Sports. Unfortunately, such data is totally unlabeled and inbound tourist data has no label of tourism forms because the data collection has been done without the awareness of the tourism forms's benefits. The unlabeled data cannot be used to enable both tourism-relevant public and private sectors to discover and respond to the lifestyle of inbound tourists. To solve such a problem, the unlabeled data must be processed to synthesize tourism form labels that are useful for the forecasting of the needs of inbound tourists to advocate the inbound tourism market in Thailand.

In Panawong *et al*. [6], classification model of tourism forms, synthesized by latent semantic analysis and machine learning, was created based on 10,250 places of data and 11 types of tourism places. The results were that support vector machine (SVM)- and back propagation neural network (BPNN)-based models using such latent semantic analysis were effectively accurate by 77.82% and 75.96%, respectively. In Chatcharaporn *et al*. [7], Naïve Bayes was used to classify Thailand tourism websites based on a lightweight tourism ontology into 6 types from totally 475 websites. It showed that classification model was effectively accurate to 97.39%. Market segmentation of inbound tourism for foreign tourists in Thailand revealed that the most accurate classification model of tourists was Naïve Bayes [8]. Liu *et al*. [9] created a cluster of new entry tourists and analyzed the main features of tourism packages and seasonal tourism development that defined the identity of tourism packages and gave effective recommendation to individual tourist tourism packages. Types of travelling residents at destinations were analyzed from tourist behaviors and the tagging period of photos taken by the tourists along their roaming places [10]. Empirical analysis system based on neural network for tourism resources appraisal showed that ecosystem and culture values were effectively able to build up the values of recreational resources [11]. The unsupervised machine learning of the market segmentation of leading international tourism businesses in Thailand [8] reported that the best method was the K-means technique that clustered into 5 segments. The segmentation of local tourists in Thailand based on a correlation-based weighting algorithm, self-organizing map (SOM), K-means, and Fuzzy C-Mean revealed that the weighting algorithm performed best [12]. Cufoglu [13] found that hierarchical clustering both forward and backward of tourists yielded a precision of 85.51% for recommending tourism services to individuals. Rodríguez *et al*. [14] developed a hierarchical clustering approach for smartphone geo-localized data to detect meaningful tourism-related market segments. Clustering results were divided into two main clusters and four sub-clusters that could be interpreted according to tourists' temporary spatial patterns and the repetition of visiting patterns. Based on these related works, there is no method for transforming unlabeled tourism data into labeled data. Therefore, a process for the generation of labels for tourism forms facilitating effective classification is needed.

For the above reason, we propose in this paper a novel algorithm for tourism-form label synthesis based on Euclidian distance to create effective forecasting models of tourism forms for Thailand's inbound tourism market.

2. Methodology

Figure 1 portrays the conceptual framework of our research and is described as follows. There are two input data sets: data set 1 contains tourism form labels whereas data set 2 has no tourism form labels. Data set 2 is initially clustered by using the most efficient clustering model that emerges from the experiments of K-mean, hierarchical clustering, random clustering, and density-based spatial clustering of applications with noise (DBSCAN) algorithms. The best model is measured based on a metric called Davies-Bouldin index. Then, the resulting clusters together with data set 1 is exploited by our proposed cluster-to-class mapping algorithm to generate tourism form labels for all records in data set 2. Subsequently, data set 2 with labels and data set 1 are used to train and test classification models to seek the most effective one based on Naïve Bayes, neural network, support vector machine, linear regression, and decision tree algorithms. The performance of the classification models are measured in terms of accuracy, precision, and recall as well as F-measure. By comparing such models' performance values, the effectiveness of our algorithm is finally revealed.

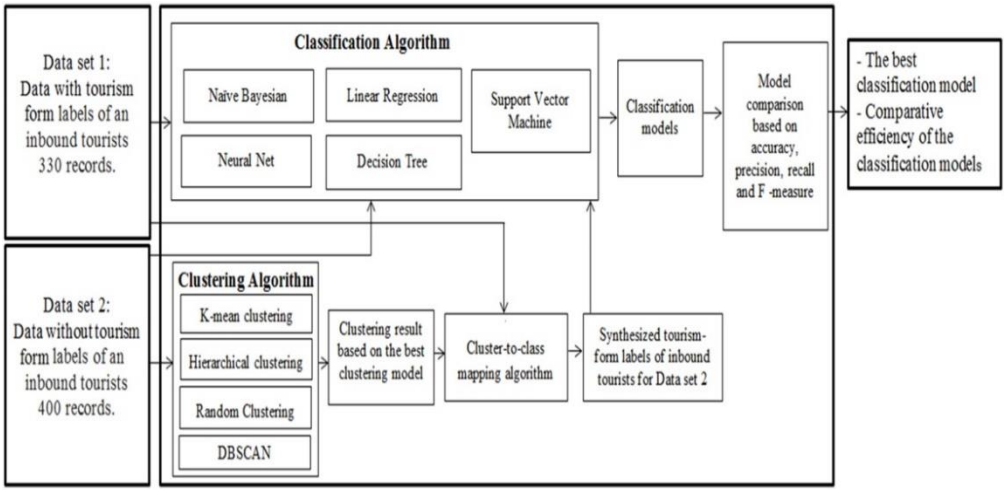

Figure 1. Conceptual framework

2.1 Definition of tourism forms in Thailand

Since we utilized Thailand's tourism forms as classification labels throughout this paper, it is important to understand what they mean. Tourism authority of Thailand (TAT) has classified the inbound tourism forms into 10 forms as follows [15].

1) Eco-tourism is a tourism form that is exclusively concerned with local natural feature having environment management and local cooperative tourism focusing on building conscious mind toward sustainable ecosystem preservation.

2) Arts and science educational attraction standard is defined as a tourism form related to the visiting places of special interest, for example, exclusive museum, educational tourism places including science, industry, technology, and meeting, and seminar.

3) Historical attraction is a tourism form that focused on places with historical values such as archaeological sites, religion, and ancient places, or those with historical parks, fortifications, museums, temples, and places of worship.

4) Natural attraction is a tourism form with the sightseeing of nature such as geographical landscapes, waterfalls, and the mighty symbols of local areas.

5) Recreational attraction is a tourism form focuses on recreation, amusement, entertainment, and education such as entertainment, zoo, amusement park, and the places of Thai culinary experience.

6) Cultural attraction is a tourism form involved with the values of art and culture that are legacies from generation to generation, for example, festivals, lifestyle, art exhibition, culture, local products, dress code, language, and tribal groups.

7) Health tourism is a tourism form with the purposes of medical treatment, hot spring, spa, and health massage.

8) Sea and beach attractions consist of sea and beach as the natural locations that offer activities for visitors, for example, swimming, sun-bathing, diving, water sports, and beachside recreation.

9) Sport tourism focuses on sport activities for tourists or sport competition.

10) Adventure tourism is a form with extreme activities such as hiking and mountain biking.

2.2 Data gathering and engineering

We collected data set 1 at Suvarnabhumi airport in 2019 from the questionnaire surveys of 330 inbound tourists traveling back to their countries. The data set included the tourists' tourism forms according to Section 2.1. Data set 2 was obtained via an official data acquisition process from the Ministry of Tourism and Sports of Thailand in 2017. The data set was collected from 400 tourists. This data set was totally unlabeled in terms of tourism forms unlike data set 1. However, both data sets contained the same 26 basic attributes: tourist ID, gender, age, marital status, region, nationality, occupation, income, tour purpose (e.g., business, conference, studying, sightseeing), sea and beach, eco-tourism, adventure, historical city tour, learn local resident, medical treatment, spa and wellness, Thai food, night life, theme park entertainment, nation special event festival, diving snorkeling, golfing, shopping, Thai boxing, Thai cooking class, and other activities. The values of the 10^{th} to the last attributes were binary (i.e., yes or no) while the other attributes had nonnegative integer values. Tourist ID represented the seasonal behavior of tourists. Tourist ID was actually the ID of questionnaire taken by each tourist. The questionnaires were collected in every quarter throughout the year. Therefore, tourists with nearby tourist ID values might favor similar tourism forms. As for data set 1, tourism type was additionally the 27^{th} attribute whose possible values were of the 10 tourism forms and served as the labels. All attribute values in both data sets were also converted to integers, and fortunately both data sets had no missing values.

2.3 Algorithm and model development

This section describes the formulation of our tourism-form-label synthesis algorithm, which was used to unlock the benefits of data set 2. The steps are explained below while their corresponding results will be reported in Section 3. As for experimental tools, we employed RStudio version 3.6.1 [16] and RapidMiner version 9.5 [17].

2.3.1 Clustering unlabeled data

We experimented four well-known clustering algorithms to construct the best clustering results based on data set 2 to be used in the next step. Clustering is unsupervised learning for grouping

data [18] based on partitioning, hierarchy, density, or grids [19]. We shortly describe such algorithms below, which are the basis of our proposed algorithm.

K-mean clustering [18] performs data partitioning based on the predefined number of clusters that is called k. Let a data set $T = \{x_1, x_2, \dots, x_{|T|}\}$ and an attribute set $x_i = \{x_{i1}, x_{i2}, \dots, x_{in}\}$ where n is the number of dimensions. Let $C = \{c_1, c_2, \dots, c_k\}$ be k clusters, each of which has a member set $c_j = \{x'_{j1}, \dots, x'_{j|c_j|}\}$ where c_j is a member of C, and x_i is a member of T. The formal description of K-means can be described in equation (1)

$$d(\mathrm{x_i}, \mathrm{c'_j}) = |\mathrm{x_i} - \mathrm{c'_j}|, \mathrm{c'_j} = \frac{1}{|\mathrm{c_j}|}\sum_{\mathrm{k=1}}^{|\mathrm{c_j}|} \mathrm{x'_{jk}} \quad (1)$$

where d represents the distance from x_i to c'_j. x_i is represented by an *n*-dimensional attribute vector. c'_j represents the centroid of each cluster. x'_{jk} dictates the member object of c_j dimensions. x_i is assigned to c'_j if their $d(\mathrm{x_i}, \mathrm{c'_j})$ is minimal. To calculate d, Euclidean distance is engaged in this paper.

Hierarchical clustering [18] relies on a tree structure called a dendrogram. This approach groups data into a tree of clusters without a predefined number of clusters by merging the similar objects or object groups and splitting dissimilar objects or object groups. There are two types of hierarchical clustering methods, agglomerative and divisive, depending on whether the hierarchical structure (tree) is formed in either bottom-up (merging) or top-down (splitting) style. The agglomerative hierarchical clustering starts with having each object in its own cluster and then merges these atomic clusters into larger and larger clusters, until all of the objects are included in a single cluster or until some certain termination conditions are satisfied. On the other hand, the divisive hierarchical clustering performs the reverse of agglomerative hierarchical clustering by starting with all objects in one cluster and subdivides it into smaller and smaller pieces, until each object forms a cluster on its own or until satisfying certain termination conditions, such as a desired number of clusters is obtained or the diameter of each cluster is within a certain threshold. Four widely used measures of distance between two clusters are single linkage, complete linkage, centroid comparison, and element comparison. In this research, agglomerative hierarchical clustering and the criteria for the single linkage (minimum distance) defined in equation (2) were utilized. Single linkage (minimum distance) is

$$d_{min}(C_i C_j) = min_{p \in C_i, p' \in C_j} |p - p'| \quad (2)$$

where C_i is cluster i and C_j is cluster j, p is distance between objects in C_i, p' is distance between objects in C_j and $|p - p'|$ is distance from C_i to C_j [20].

Random clustering was generated by shuffling the elements between the fixed clusters. A prevailing assumption for the random clustering ensemble is the permutation model in which the number and sizes of clusters are fixed [21]. If ball 1, ..., ball k are thrown to form a partition $A \in A_k$, then ball $k+1$ is put into an empty urn with probability p_k and into an urn with j balls with probability $(1 - p_k)j/k$. This ball throwing is continued for $k = 1, 2\ 3, \dots$. Mathematically, the clusters at the n[th] step form a partition of the finite set $u_n = \{1, 2, \dots, n\}$, i.e., the set of labeling numbers on balls up to ball n. The family of all partitions of u_n is denoted by A_n. If a partition $A \in A_n$ has s_j subsets of cardinality j (i.e., s_j clusters of size j or s_j urns with j balls), $j = 1, \dots, n$. At the n[th] step of the random clustering process mentioned above, the probability that ball 1, ..., ball n form a partition $A \in A_n$, as shown in equation (3) [22].

$$P(A; A_n) = f_n(s) = f_n(s; p) = \frac{\propto^u}{\propto^{[n]}} \prod_{j=1}^{n} ((j-1)!)^{s_j}, \ 0 < p < 1, \ 0 < \alpha < \infty, \quad (3)$$

$$\text{Define } s = S(A) \in s_n, u = \sum_{j=1}^{n} s_j \text{ , and } \propto^{[n]} = \propto (\propto +1) \cdots (\propto +n-1), \qquad \propto = p/(1-p).$$

where $P(A; A_n)$ is independent of the order of n balls thrown in, and is invariant with respect to the permutation of the indices of the balls. $S(A)$is the size index of A. $f_n(s)$ is the invariance with respect to the indexing of balls in $S(A)$, $f_n(s; p)$ is the invariance with respect to the indexing of the probability of $S(A)$, u is the number of cycles of $A \in A_n$, $\propto$ is the Poisson approximation, p is the probability of an event in sample space A_n. n is thrown to form a partition $A \in A_n$.

Density-based spatial clustering of applications with noise (DBSCAN) is a density-based clustering algorithm that finds the regions of objects with sufficiently high density into cluster. By this nature, it discovers clusters of arbitrary shape in spatial databases with noise. In this method, a cluster is defined as a maximal set of density-connected points. Neighborhood objects within a radius ε of a given object is called the $\varepsilon - neighborhood$ of the object. Each core object has a *minimum number* called *MinObjs*. Given a set of objects D, an object p is directly density-reachable from the object q if p is within the $\varepsilon - neghborhood$ of q, and q is core object. An object p is density-reachable from object q within respect to ε and *MinObjs* in a set of objects, D, if there is a chain of objects $p_1, \ldots, p_n$, where $p_1 = q$ and $p_n = p$ such that p_{i+1} is directly density-reachable form p_i with respect to ε and *MinObjs*, for $1 \leq i \leq n$, $p_i \in D$. An object p is density-connected to object q with respect to ε and *MinObjs* in a set of object, D, if there is an object $o \in D$ such that both p and q are density-reachable from o with respect to ε and *MinObjs*. Finally, a density-based cluster is a set of density-connected objects that is maximal with respect to density-reachability. Every object not contained in any cluster is considered to be noise [18, 23].

Besides the clustering algorithms, a clustering performance metric enlisted in our experiments was Davies–Bouldin index (DBI). DBI value is high when data within the same cluster has high similarity and data between clusters has low similarity. DBI can be calculated by the following formula [24]:

$$DBI = \frac{1}{\mathrm{n}} \sum_{\mathrm{i}=1}^{\mathrm{n}} \max_{\mathrm{i} \neq \mathrm{j}} \left(\frac{\sigma_\mathrm{i} + \sigma_\mathrm{j}}{d(c_i, c_j)} \right) \tag{4}$$

where n is the number of clusters, c_x is the centroid of cluster x, σ_x is the average distance of all elements in cluster x to centroid c_x, and $d(c_i, c_j)$ is the distance between centroids c_i and c_j. Since algorithms that produce clusters with low intra-cluster distances (high intra-cluster similarity) and high inter-cluster distances (low inter-cluster similarity) will have a low DBI, a clustering model that yields the smallest DBI is considered the best. Table 1 lists the parameter values of experimented clustering algorithms.

Table 1. Optimal parameter for each classification model

Algorithm	**Parameter configuration**
K-mean clustering	k=10, max runs=30, Euclidean Distance, Numerical Measure, max optimization steps =100
Hierarchical clustering	k=10, max runs=30, Euclidean Distance, max optimization steps =100, Single Link
Random clustering	k=10, max runs=30, Euclidean Distance, Numerical Measure, max optimization steps =100
DBSCAN	k=10, max runs=30, Euclidean Distance, Numerical Measure, epsilon=0.25, Min point=0.5

As the result of this step, 10 optimal clusters produced by the lowest DBI model will be engaged in the next Section.

2.3.2 Cluster to class mapping

This section describes our cluster-to-class mapping approach that consists of 4 steps as follows.

1) The 10 optimal clusters had their centroids calculated. Similarly, 10 data classes (according to data labels) of data set 1 had their centroids figured out as if each class was a cluster. The calculation was done by averaging the 26 attribute vectors of all records belonging to the same cluster or class as in equation (5) [18, 25].

$$c'_i = \frac{1}{|c_i|}\sum_{k=1}^{|c_i|} x'_{ik} \tag{5}$$

where c'_i is the centroid vector of cluster or class c_i, x'_{ik} represents each element of c_i and has 26 dimensions.

2) In this step, we calculated the Euclidean distance between the centroids of each possible pair of cluster and class. Since there were 10 clusters and 10 classes, there were totally 100 possible distances in total to compute. The formula of Euclidean distance simply follows equation (6):

$$d(i,j) = \sqrt{(C_{i1-}C_{j1})^2 + (C_{i2-}C_{j2})^2 + \cdots + (C_{ip-}C_{jp})^2} \tag{6}$$

where $d(i,j) \geq 0$ is a distance from object i to object j. The strength of this algorithm was a non-variable to the interpretation and rotation of featured area [26] that is suitable for our mapping purpose.

The ideas of the first two steps are clearly illustrated in Figure 2. The centroid vectors of 10 classes and the centroid vectors of 10 clusters are paired to compute 100 possible Euclidian distances. The distances of these pairs are represented as a 10 x 10 matrix with its rows representing 10 tourism forms (i.e., 10 classes) and its columns representing 10 clusters. Each element in the matrix notates each of the calculated Euclidian distance.

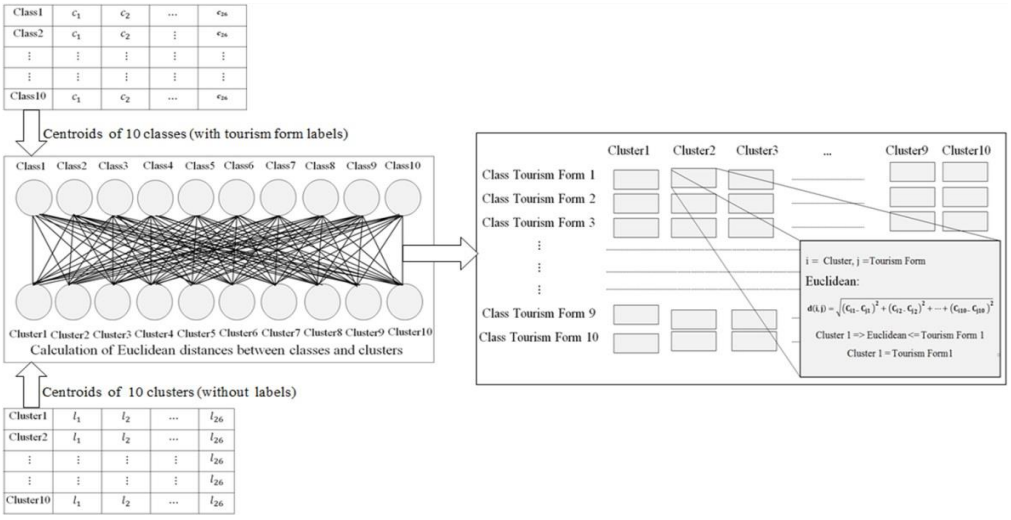

Figure 2. Euclidean distance-based cluster-to-class mapping

3) The 100 Euclidean distance values are sorted to find out 10 class-cluster pairs whose distances were shortest and classes were unique. The 10 classes served as tourism forms associated with the 10 clusters. In this way, tourism form labels were synthesized for each record of data set 2.

All these three steps are described as our proposed algorithm in Table 2. Input variables are C1 (the vector of 10 tourism form classes x_1 to x_{10}) and C2 (the vector of 10 tourist clusters y_1 to y_{10}). Output variable L is the vector of 10 tourism forms, each of which is associated with each member of C2 (i.e., l_1 is tourism form of y_1, l_2 is tourism form of y_2, and so on). Line (1) to line (6) calculate Euclidean distances between 10 tourist clusters and 10 tourism form classes. The result is stored in 10 x 10 sized distance matrix, EDmatrix, (i.e., the 10 x 10 matrix in Figure 2) in line (3). Line (7) transforms EDmatrix to a vector of 100 Euclidean distance values. The 100 values are then sorted on line (8). Vector L in line (9) is initialized to nulls. The loop on line (10) repeats until unique labels are associated with all 10 clusters in C2 and saved into L. Line (11) to line (13) search for the shortest Euclidean distance with respect to each class.

2.3.3 Classification performance comparison

At this point, both data set 1 and data set 2 have been labeled. We deployed them as training and test sets in combination to construct four classification models: the first model was trained and tested by using data set 1 based on a hold-out technique, the second model was trained and tested by using data set 2 based on a hold-out technique, the third model was trained by data set 1 and tested by using data set 2, and the last model was trained by using data set 2 and tested by using data set 1. The performances of these models are compared to conclude research findings.

Table 2. Thailand-inbound-tourism-form label synthesis algorithm by mapping 10 clusters to 10 classes based on Euclidean distances

Algorithm: Tourism form label synthesis

Input C1 is vector of 10 tourism form classes, ($x_1, x_2, \ldots, x_{10}$) where x_i has centroid vector ($x_{i1}, x_{i2}, \ldots, x_{i26}$)
C2 is vector of 10 tourist clusters, ($y_1, y_2, \ldots, y_{10}$) where y_i has centroid vector ($y_{i1}, y_{i2}, \ldots, y_{i26}$)
Output L = ($l_1, l_2, \ldots, l_{10}$) is vector of tourism forms associated with members of C2
Begin
(1) For (i ← 1; i=i+1; i<=10) do
(2) For (j ← 1; j=j+1; i<=10) do
(3) EDmatrix ← $\text{sqrt}(\sum_{k=1}^{26}(x_{ik} - y_{ijk})^2)$ // Euclidean distance vector between C1& C2 is stored in 10 x 10
(4) // distance matrix. EDmatrix's rows represent 10 tourism type classes. Matrix1's columns represent 10 clusters.
(5) End for
(6) End for
(7) M ← convertMatrixToRowVector(EDmatrix) // convert EDmatrix to row vector
(8) S ← sort (M)
(9) L ← (null, …, null)
(10) While (countNotNullMembersOf(L) < 10) // while not all 10 tourism types are assigned as clusters' labels
(11) u ← min(S) // assign minimum element of S to u
(12) S ← S-u // remove u from S
(13) z ← getClassFromRowIndexInEDmatrixOf(u) // assign class name associated with u in EDmatrix to z
(14) If (z ∉ L) // if z has not been assigned as label
(15) L[getColumnIndexOf(u)] ← z //Assign z as label by storing it in L at the same column as that of u in
(16) // EDmatrix
(17) End while
(18) Return(L)
End.

To create the models, we employed five well-known classification algorithms as follows. Classification refers to a supervised machine learning technique used to find objects of relevant

class to help with human decision making such as forecasting unexpected events based on presented input data [18, 27].

Naïve Bayes is possible to presume that all attributes are independent of each other. The values of the attributes are conditionally independent of one another, given the class label of the object, the formula as shown in equation (7):

$$c(x) = \underset{c_i \in C}{argmax} P(c_i) P(a_1(x)|c_i) P(a_2(x)|c_i) \dots P(a_n(x)|c_i) \tag{7}$$

In this formula, each term, except the first term, is the probability to obtain the attribute value, given only the class value. Assume that $a_3(x)$ is dependent on $a_2(x)$, $a_4(x)$ is dependent on $a_1(x)$ and $a_3(x)$, and others are independent of each other. $P(c_i)$ is the prior probability of c_i. $P(a_1(x)|c_i)$ is the first number of objects classes c_i in the training data set. $P(a_2(x)|c_i)$ $P(a_n(x)|c_i)$ is the second number of the number of objects classes c_i in the training data set.

Support vector machine (SVMs) determines a decision boundary to be as far away from the data of two classes as possible. Given the training data $\{x_i, y_i\}$, $i = 1, \dots n$, $\mathrm{x_i} \in \mathrm{R}^d$, $y_i \in \{-1,1\}$ as shown in equation (8):

$$\begin{aligned} &\text{minimize} \quad \frac{1}{2}||\mathrm{w}||^2 \\ &\text{subject to} \quad y_i(w^T x_i + b) - 1 \geq 0 \text{ for all } i \end{aligned} \tag{8}$$

where w is the Euclidean distance, x_i is datum, represented as a vector of d dimension, y is the binary class of -1 or +1, the support vector machine finds the best hyperplane which separates the positive from the negative examples. The point x_i on the hyperplane satisfies the formula $w^T x_i + b = 0$, where w is a normal vector that is perpendicular to the hyperplane. $|b|/||\mathrm{w}||$ is the perpendicular distance from the hyperplane to the origin.

A neural network that was employed in this paper was specifically a multilayer feed-forward neural network consisting of an input layer, one or more hidden layers, and an output layer. Neural networks operate by requiring cooperation through different nodes in the layers to forecast a result as shown in equation (9):

$$\mathrm{y_i} = \int\left(\sum_{\mathrm{i=0}}^{\mathrm{N}} \mathrm{w_{ij}} \mathrm{x_i} + \theta_\mathrm{j}\right) \tag{9}$$

where y_i is the output layer, x_i is the input layer, N is the total number hidden layers, w_{ij} is a weight for node i to node j, and θ_j is the bias associated with j.

Linear regression uses a straight line to approximate correlation between predictor variables and responsive variables as shown in equation (10):

$$w_0 = \bar{y} - w_1 \bar{x} \tag{10}$$

where w_0 and w_1 are regression coefficients or weights, $\bar{x}$ is the mean of $x^{(1)}, x^{(2)}, \dots, x^{(|s|)}$, and $\bar{y}$ is the mean of $y^{(1)}, y^{(2)}, \dots, y^{(|s|)}$, x is predictor variable of presented data, y is responsive variable for coefficient. |s| is a rule of sample of test data set s from $\left(x^{(1)}, y^{(1)}\right), \left(x^{(2)}, y^{(2)}\right), \dots, \left(x^{(|s|)}, y^{(|s|)}\right)$.

A decision tree is a tree-like graph consisting of three components: (1) leaf nodes (rectangular), (2) decision criterion nodes (ovals), and (3) decision branches (lines). The leaf nodes represent classification (decision) outcomes, the root and the intermediate nodes express decision criteria. Given a trained set of object and their associated class label, denoted by $T = \{x_1, x_2, \dots, x_{|\mathrm{T}|}\}$, each object x_i is represented by an n–dimensional attribute vector, $x_i = \left(x_{t1}, x_{t2}, \dots, x_{\mathrm{tn},}, c_t\right)$, depicting the measure values of n attributes, $A_1, \dots, A_n$, of the object with its

class $c_i \in C$, one form m possible class, $C = \{c_1, c_2, \dots, c_{\mathrm{m}}\}$. Here, suppose that A_i has n_i possible values $\{a_{i1}, a_{i2}, \dots, a_{\mathrm{i}(n_i)}\}$. That is, $x_{it} \in \{a_{i1}, a_{i2}, \dots, a_{\mathrm{i}(n_i)}\}$, a binary partition p divides the values of the attribute A_i. The decision tree selects the best attribute as the first node in order to split the training set into a number of subsets. To select such an attribute, we used the gain ratio defined in equation (11).

Information gain:

$$\mathrm{InfoGain}(\mathrm{T}, \mathrm{A_i}) = \mathrm{Info}(\mathrm{T}) - \sum_{\mathrm{k}=1}^{n_i} \frac{|\mathrm{T_{ij}}|}{|\mathrm{T}|} \mathit{Info}\left(\mathrm{T_{ij}}\right) \tag{11}$$

$$\mathrm{Info}(\mathrm{T}) = \sum_{k=1}^{m} (-1) \cdot p(c_k, T) \cdot \log_2\big(p(c_k, T)\big)$$

$$\mathrm{Info}\big(\mathrm{T_{ij}}\big) = \sum_{k=1}^{m} (-1) \cdot p(c_k, \mathrm{T_{ij}}) \cdot \log_2\Big(p\big(c_k, \mathrm{T_{ij}}\big)\Big)$$

Where $p(c_k, T) = \frac{|\mathrm{T_k}|}{|\mathrm{T}|}$ and $p(c_k, \mathrm{T_{ij}}) = \frac{|\mathrm{T_{ijk}}|}{|\mathrm{T_{ij}}|}$

Gain ratio:

$$\mathrm{GainRatio}(\mathrm{T}, \mathrm{A_i}) = \frac{\mathrm{InfoGain(T,A_i)}}{\mathrm{SplitInfo(T,A_i)}}$$

$$\mathrm{SplitInfo}(\mathrm{T}, \mathrm{A_i}) = \sum_{\mathrm{k}=1}^{\mathrm{m}} (-1) \cdot \mathrm{p}\big(\mathrm{T_{ij}}\big) \cdot \log_2\Big(\mathrm{p}\big(\mathrm{T_{ij}}\big)\Big)$$

$$\text{where } \mathrm{p}\big(\mathrm{T_{ij}}\big) = \frac{|\mathrm{T_{ij}}|}{|\mathrm{T}|}$$

where T is a training set before splitting, node A_i is selected for splitting, c_k is the *k*-th class, T_k is the set of the instances with the class c_k in the set T, T_{ij} is a subset of the training set after splitting, contains the objects which have the value of a_{ij} for the attribute A_i, that is $A_i = a_{ij}$ and T_{ijk} is the set of the instances with the class $\mathrm{c_k}$ in the subset T_{ij}.With this notation, $|T|$ is the total number of instances with the training set before splitting, $|T_k|$ is the number of class-*k* instances in the set T, $|T_{ij}|$ is the number of instances in the subset, and $|T_{ijk}|$ is the number of class-*k* instances in the subset T_{ij}.

To measure the performance of classification models, we employed accuracy, precision, recall, and f-measure defined in equations (12), (13), (14), and (15), respectively.

$$\text{accuracy} = \frac{TP}{\mathrm{TP+FP}} \tag{12}$$

$$\text{precision} = \frac{TP}{\mathrm{TP+FN}} \tag{13}$$

$$\text{recall} = \frac{TP+TN}{\mathrm{TP+TN+FP+FN}} \tag{14}$$

$$\text{f-measure} = \frac{\text{2 x recall x precision}}{\text{recall+precision}} \tag{15}$$

where TP is true positive results expressing the number of objects which are classified to be true correctly, FP is false positive errors representing the number of objects classified wrongly to be true, FN is false negative errors indicating the number of objects to be classified as false but it should have been true, and TN is true negative results indicating the number of objects to be classified as false correctly, the higher all thee four metrics, the better classification model [17].

To conduct classification a training set and a test set are needed. We generated both sets by means of a holdout method [19], in which given data was randomly partitioned into two mutually exclusive sets, a training set and a test set. Typically, two-thirds of the data are used as the training set, and remaining one-third is used as the test set. After that, the training set is used to derive a model, whose performance is estimated with the test set. In our classification experiments, each data set (i.e., data set 1 and data set 2) is split into a training set (70% of the

whole data set) and test set (30% of the remaining data). Table 3 shows our parameter value configuration of each classification algorithm.

Table 3. Optimal parameter configuration for each classification model

Algorithm	Parameter configuration
Naïve Bayes	laplace correction =True
Neural Network	hidden layers =2, training cycles =500, learning rate =0.01, momentum =0.9,decay =False, shuffle =True, normalize =True, use local random seed =False, local random seed =2000
Support Vector Machine	kernel type = polynomial, kernel degree =3.0,kernel cache =200,C =0.0, convergence epsilon =0.01, max iterations=100000, scale =True, L pos =1.0, L neg =1.0
Linear Regression	feature selection =*M5 prime*, eliminate colinear features =True, min tolerance =0.05, use bias =True, ridge =1.0E-8
Decision Tree	criterion = accuracy, maximal depth =20,apply pruning =True, confidence =0.1, apply prepruning =True, minimal gain =0.01, minimal leaf size=2, minimal size for split =4, number of prepruning alternatives =3

3. Results and Discussion

3.1 Clustering result

As described in Section 2.3.1, data set 2 was exclusively processed by different clustering algorithms to generate 4 models with 10 clusters each. The algorithm configuration follows Table 1. The DBI values of the models are shown in Table 4 indicating that the best clustering model was derived from DBSCAN.

Table 4. Effectiveness of clustering models for data set 2

Model	DBI
K-mean clustering	1.833
Hierarchical clustering	1.102
Random clustering	0.982
DBSCAN	0.963

3.2 Label synthesis result

Subsequently, as mentioned in Section 2.3.2, the distance matrix in Figure 2 (i.e., EDmatrix in Table 2) is depicted in Table 5. By enlisting our proposed algorithm in Table 2, the shortest distances with respect to each unique class were identified and mapped each unique class to each unique cluster as portrayed in the X-axis label of Figure 3. The class labels became the labels of the tourist data of the clusters. In this way, we could determine which tourist clusters (i.e., data set 2) had tourism forms conforming to which tourist classes (i.e., data set 1). Cluster 1 is the sea and beach tourism form. Cluster 2 is the sport tourism form. Cluster 3 is the spa & wellness tourism form. Cluster 4 is the cultural tourism form. Cluster 5 is the ecotourism form. Cluster 6 is the

natural tourism form. Cluster 7 is the MICE tourism form. Cluster 8 is the historical tourism form. Cluster 9 is the adventure tourism form. And, cluster 10 is the recreational tourism form.

Table 5. Euclidean distances between clusters and classes

Tourism-form class label	Cluster									
	1	**2**	**3**	**4**	**5**	**6**	**7**	**8**	**9**	**10**
Sea_Beach	2.14	25.70	23.61	19.58	12.22	11.18	13.68	17.60	20.43	13.88
Eco_tourism	3.30	24.95	22.72	19.57	10.98	11.10	14.65	15.96	21.28	12.95
Cultural	3.34	29.57	26.94	16.39	13.68	15.10	9.83	20.73	16.52	17.53
Natural	5.57	21.40	20.39	23.18	11.82	7.75	18.00	13.75	24.69	9.38
Recreational	3.30	23.89	22.40	21.12	11.99	9.71	15.49	15.98	22.21	11.97
Historical	3.34	24.34	22.39	20.88	12.12	9.68	15.08	16.75	21.87	12.74
Adventure	2.67	28.47	26.09	17.26	13.10	14.08	11.02	19.72	17.69	16.46
MICE_tourism	8.11	33.92	30.30	12.15	15.42	19.92	6.90	23.66	12.79	21.66
Sport_tourism	2.77	25.52	24.23	20.20	13.24	11.83	14.14	17.24	20.79	13.22
Health_tourism	7.20	24.14	21.57	22.62	13.14	9.54	17.02	17.77	23.56	13.79

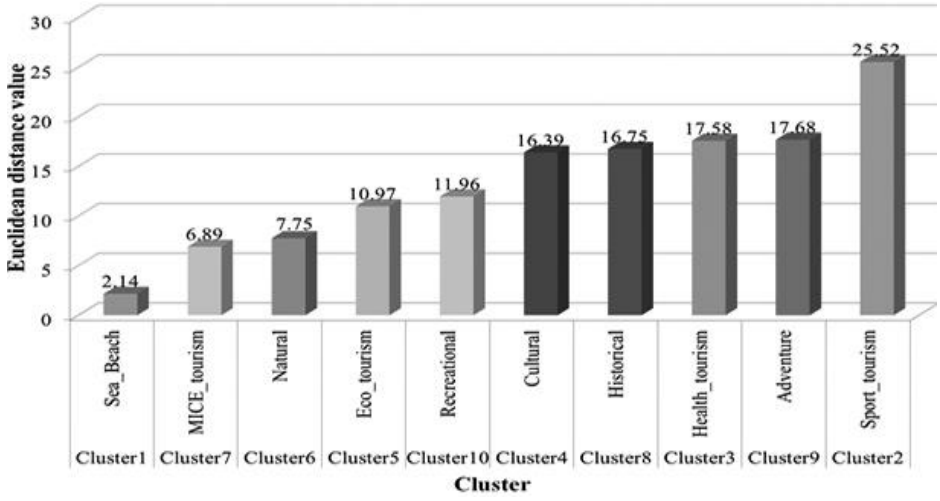

Figure 3. The value of Euclidean distance mapping of clustering and tourism form

3.3 Classification model construction

Based on Section 2.3.3, Table 6 shows the performance of the four classification models trained and tested with the combination of data set 1 and labeled data set 2. When training with data set 1 and testing with labeled data set 2, the neural network model outperformed the other models with F-measure of 94.85%. This means that the synthesized labels reasonably conformed to the labels of data set 1. On the other hand, models that were trained and tested with the same data set 1 and labeled data set 2 using the holdout technique had the best F-measure of 96.08% and 98.99%, respectively. Nevertheless, all of the models trained with labeled data set 2 poorly classified data set 1. In particular, the best of such models was SVM having F-measure of only 27.72%. The reason seems to be that the newer data set (i.e., data set 2) did not cover most patterns existing in the older data set (i.e., data set 1) whereas data set 1 covered most patterns in data set 2 (i.e., tourism behavior changed over the studied time period).

Table 6. Performance comparison of tourism-form classification models

Model	Data set 1 (train 70%, test 30%)				Data set 1 (train) Data set 2 (test)				Data set 2 (train 70%, test 30%)				Data set 2 (train) Data set 1 (test)			
	Accuracy (%)	Precision (%)	Recall (%)	F-measure (%)	Accuracy (%)	Precision (%)	Recall (%)	F-measure (%)	Accuracy (%)	Precision (%)	Recall (%)	F-measure (%)	Accuracy (%)	Precision (%)	Recall (%)	F-measure (%)
Naïve Bayes	22.32	46.98	40.13	43.29	26.43	43.12	61.76	50.78	41.13	64.02	66.67	65.32	16.00	20.52	21.80	21.14
Neural Network	87.98	81.40	85.46	83.38	96.43	95.13	94.57	*94.85*	99.29	98.21	99.78	*98.99*	9.25	14.06	15.98	14.96
Support Vector Machine	93.56	97.53	94.68	*96.08*	61.43	94.11	32.53	48.35	89.72	93.16	92.62	92.88	18.00	34.26	23.27	*27.72*
Linear Regression	58.37	69.52	47.20	56.23	71.07	75.68	45.70	56.99	68.09	73.77	68.67	71.13	10.00	37.84	11.31	17.41
Decision Tree	75.11	75.93	64.51	69.76	65.36	74.38	39.68	51.75	95.39	95.32	97.27	96.29	5.50	25.58	11.27	15.65

Figure 4 comparatively visualizes the models that were optimal (i.e., italized F-measures in Table 6) based on each of four combinations of the data sets. A significant finding is that when classifying unseen and unlabeled tourist data (i.e., data set 2 as a test set), which is regularly collected by the Ministry of Tourism and Sports of Thailand, the synthesized labels of such data set can produce an efficient tourism-form prediction model with F-measure of 98.99%, which surpasses a model trained with data set 1 (F-measure = 94.85%). Therefore, our proposed algorithm serves as a reasonable solution to the research problem stated in Section 1.

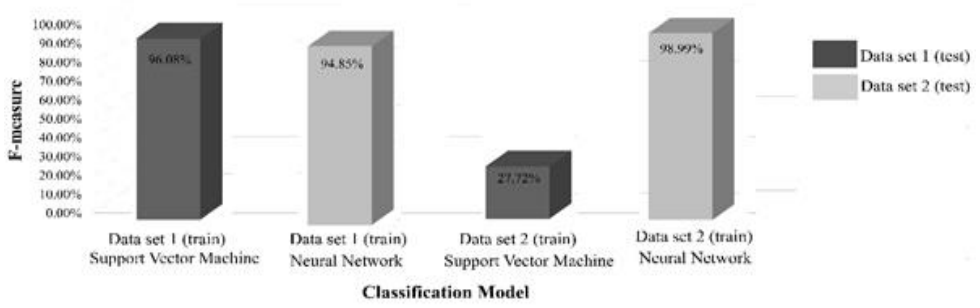

Figure 4. Comparison of effectiveness of the best classification models of each pair of the training data set and the test data set

4. Conclusions

This research proposed an algorithm for generating the tourism form labels of unlabeled Thailand-inbound-tourist data based on Euclidean distance mapping. First, we clustered the unlabeled data set with DBSCAN into 10 clusters. Then the algorithm began with computing the centroids of the clusters and the other labeled data set, containing 10 tourism form classes. Subsequently, the

algorithm calculated Euclidean distances between possible pairs of the classes and the clusters to determine the clusters' labels. The data set with the synthesized labels was used to train a classification model to classify unseen and unlabeled tourist data in an effective manner with F-measure of 98.99%. A possible reason that our cluster-to-class mapping algorithm performed relatively well is the technique of exhaustive search in Figure 2 to evaluate similarity between all possible pairs of classes and clusters. Applying a neural network technique in conjunction with our algorithm yielded the best classification model for forecasting the tourism forms of inbound tourists in Thailand. Tourism entrepreneurs and organization are encouraged to apply our approach to unlabeled tourist data that is available at the Office of the Permanent Secretary of Ministry of Tourism and Sports in order to promote the growth of Thailand's tourism economy.

5. Acknowledgments

We would like to express our sincere gratitude to Office of the Permanent Secretary, Ministry of Tourism and Sports and Suvarnabhumi Airport for kind support in data acquisition.

References

[1] Economic Army of Tourism and Sport, 2020. Thailand tourism situation. *Tourism Economic Review*, 2(1), 11-15.

[2] Office of the National Economic and Social Development Council (NESDC), 2020. *NESDC ECONOMC REPORT*. [Online] Available at: https://www.nesdc.go.th/ewt_dl_link.php?nid=9895&filename=QGDP_report

[3] Department of Tourism, 2018. *The Tourism Development Strategic Plan (2018-2021)*. Bangkok: Department of Tourism.

[4] Tourism Authority of Thailand, 2020. The travel trends to know in 2020. *TAT Review*, 6(1), 17-26.

[5] Mierswa, I., Wurst, M., Klinkenberg, R., Scholz, M. and Euler, T., 2006. YALE: Rapid prototyping for complex data mining tasks. *Proceedings of the 12th ACM SIGKDD International Conference on Knowledge Discovery and Data Mining*, New York, USA., 2006, 935-940.

[6] Panawong, N., Namahoot, C.S. and Brückner, M., 2014. Classification of tourism web with modified Naïve Bayes algorithm. *Advanced Materials Research*, 931-932, 1360-1364.

[7] Chatcharaporn, K., Angskun, J. and Angskun, T., 2014. Tourist attraction categorization using a latent semantic analysis and machine learning techniques. *Information*, 17, 2683-2698.

[8] Srivihok, A. and Yotsawat, W., 2014. Market segmentation of inbound business tourists to Thailand by binding of unsupervised and supervised learning techniques. *Journal of Software*, 9(5), 1334-1341.

[9] Liu, Q., Ge, Y., Li, Z., Chen, E. and Xiong, H., 2011. Personalized travel package recommendation. *IEEE 11th International Conference on Data Mining*, December, 2011, 407-416.

[10] Oender, I., 2017. Classifying multi-destination trips in Austria with big data. *Tourism Management Perspectives*, 21, 54-58.

[11] Zhu, L.N., 2017. Empirical analysis of tourism resources evaluation and promotion based on data mining neural network. *Revista de la Facultad de Ingeniería UCV*, 32(2), 385-389.

[12] Hayamin, P. and Srivihok, A., 2018. Segmentation of domestic tourist in Thailand by combining attribute weight with clustering algorithm. *Journal of Advances in Information Technology*, 9(2), 39-44.
[13] Cufoglu, A., 2014. User profiling- a short review. *International Journal of Computer Applications*, 108(3), 1-9.
[14] Rodríguez, J., Semanjski, I., Gautama, S., de Weghe, N.V. and Ochoa, D., 2018. Unsupervised hierarchical clustering approach for tourism market segmentation based on crowd sourced mobile phone data. *Sensors*, 18(9), https://doi.org./10.3390/s18092972
[15] Department of Tourism in Thailand, 2018. *Tourism Forms*. [online] Available at: https://www.tourismthailand.org
[16] RStudio Team, 2020. *RStudio: Integrated Development for R.* [online] Available at: https://www.rstudio.com
[17] RapidMiner, 2014. *RapidMiner Studio Manual*. [online] Available at: https://docs.rapid miner.com/download/RapidMiner-v6-user-manual.pdf
[18] Theeramunkong, T., 2017. *Introduction to Concepts and Techniques in Data Mining and Application to Text Mining*. 2rd ed. Bangkok: Thammasat University Press.
[19] Jane, E.M. and Raj, E.G.D.P., 2018. Comparative study on partition based clustering algorithms. *International Journal of Research in Advent Technology*, 6(9), 2398-2403.
[20] Han, J. and Kamber, M., 2006. *Data Mining: Concepts and Techniques.* 2nd ed., Illinois: University of Illinois at Urbana-Champaign.
[21] Gates, A.J. and Ahn, Y.-Y., 2017. The impact of random models on clustering similarity. *Journal of Machine Learning Research*, 18, 1-28.
[22] Sibuya, M., 1993. A random clustering process. *Annals of the Institute of Statistical Mathematics*, 45(3), 459-465.
[23] Tran, T.N., Drab, K. and Daszykowski, M., 2013. Revised DBSCAN algorithm to cluster data with dense adjacent clusters. *Chemometrics and Intelligent Laboratory Systems*, 120, 92-96.
[24] Mary, A.V.A. and Jebarajan, T., 2014. Performance metrics of clustering algorithm. *Indian Journal of Applied Research*, 4(8), 165-167.
[25] Witten, I.H., Frank, E. and Hall, M.A., 2005. *Data Mining. Practical Machine Learning Tools and Techniques*. San Francisco: Morgan Kaufmann.
[26] Kumar, V., Chhabra, J.K. and Kumar, D., 2014. Performance evaluation of distance metrics in the clustering algorithms. *INFOCOMP Journal of Computer Science*, 13(1), 38-52.
[27] Mitchell, T.M, 1997. *Machine Learning*. New York: McGraw-Hill.

Review article

Animal Biotechnology and Ethical Issues

Sanu Mahatthanadull[1]* and Dusanee Thanaboripat[2]

[1]International Buddhist Studies College, Mahachulalongkornrajvidayalaya University, Ayutthaya, Thailand
[2]King Mongkut's Institute of Technology Ladkrabang, Bangkok, Thailand

Received: 9 September 2020, Revised: 27 November 2020, Accepted: 30 December 2020

Abstract

Animal biotechnology is one of the main areas of biotechnology which concerns the application of animals, including transgenic animals, in various fields. Even though these transgenic animals can be useful for improving the welfare of humans and animals, the well-being of animals being used in the studies may be negatively affected. Ethical issues relating to experimentation on animals and the production of transgenic animals are discussed in this review, and included here is a consideration of the phenomena of 'conditional ethical blindness'. Finding alternative protocols including the 4 Rs (reduction, refinement, replacement, and responsibility) to minimize the employment of animals in scientific procedures is one way to solve these problematic issues. These strategies can be successively utilized for certain animal biotechnological protocols and can be used to intelligently avoid unethical manipulation of animals.

Keywords: animal; animal biotechnology; transgenic animal; ethical issue; ethics
DOI 10.14456/cast.2021.33

1. Introduction

Nowadays, the advancement of science and technology has become a fundamental part of human's world. Observation and experimentation are the most significant steps in the examination of phenomena. Scientific methodologies lead scientists to consider the truth of things that can only be proven by the 5 senses, i.e. sight-eye, smell-nose, taste-tongue, hearing-ear, and touch-body [1]. However, many scientists are exploring and using the Buddha's teaching to explain about scientific discovery, and there exists a close intellectual bond between Buddhism and modern science [2]. Vast areas of science and technology related to Buddhism are being investigated including quantum physics, biology, modern biotechnology and so on. Biotechnology is a multidisciplinary area which covers the studies of basic sciences such as biochemistry, genetics, microbiology, immunology, chemical engineering, molecular and cell biology, including human, plant and animal physiology.

*Corresponding author: Tel.: +66814079000
E-mail: petchsanu@gmail.com

Applied sciences such as animal biotechnology, plant biotechnology, food biotechnology, agricultural biotechnology, microbial biotechnology, industrial biotechnology, environmental biotechnology and pharmaceutics are also included under the rubric of biotechnology. Smith [3] has concluded that biotechnology implies the application of microorganisms, plant or animal cells, and enzymes to synthesize, transform or even breakdown materials. The areas of health care and medicine, followed by food and agricultural technology are the latest applications of biotechnology. Animal biotechnology is depicted as being one of the most important branches of biotechnology, and the development of animal biotechnology has contributed immensely to human health, nutrition and economy [4].

There are many definitions of "animal biotechnology", and these definitions reflect biotechnology novelty and established practice [5]. For example, it may be routine breeding technologies, e.g., artificial insemination, and some older breeding practices [6, 7]. Straughan [8] defined that "animal biotechnology" covered many well-documented procedures of conventional livestock breeding including the utilization of artificial insemination and performance testing. Animal biotechnology also includes vast developments in reproductive physiology like embryo transfer (surrogacy) and *in vitro* fertilization (test tube babies).

Animal biotechnology has been applied mainly for two purposes: to produce animals that are employed in fundamental biological research for biological development and function, and to create disease models that can mimic human diseases and thus be used for studying diseases (Parkinson's, cystic fibrosis, cancer, etc.) as well as for testing new drugs. The history of animal biotechnology began in the early 1980s with the production of genetically modified animals in which cloned sheep were created by embryonic cell transfer [9]. Somatic cell nuclear transfer was first used in 1996 to create the cloned sheep, Dolly [10]. Although the majority of work within animal biotechnology has been carried out using laboratory mice and sheep, as well as cattle, these technologies have been more recently adapted to other animal species like pigs, cats, goats, and horses. Methodologies and success rates vary from species to species [5]. For example, the success rate of using transgenic animals (pigs, sheep and cattle, and other animals) is only about 1% compared with 2-5% in mice [3].

Recombinant DNA technology (rDNA) is the employment of *in vitro* nucleic acid techniques including recombinant DNA and direct injection of nucleic acids into cells and organelles. It is also the technique that produces hybrid DNA by joining pieces of DNA from different organisms [4, 11]. The transferring of a foreign gene (for growth hormone) from a rat into a mouse by rDNA was the first reported example [11]. Cloning and genetic engineering (genetic modification) are two main techniques used to produce the desired organism. Cloning can be defined as the production of similar populations of genetically identical individuals whereas genetic engineering refers to the modification of DNA in order to create new types of organisms by inserting or deleting genes. Reproductive cloning is the re-creation of a whole organism, and recent advances in biotechnology have made it possible to reproductively clone mammals in the laboratory [12, 13].

1.1 The use of transgenic animals

Although there are some risks associated with the production of genetically modified animals or transgenic animals, such as the fact that an insertion of foreign gene may disturb the genome expression, and that normal reproduction may result in a transgene being released into a wild population, the benefits of cloning techniques are considerable, and some of the key benefits are as follows [14]:

1) Animals may be introduced with desired characteristics that require medical treatments or any feed supplements.

2) A desired characteristic of offspring might be established within one generation.

3) The characteristics needed can be chosen with greater accuracy and specificity.

Furthermore, transgenic animals can be produced to improve the quality of meat, the efficiency of meat and egg production, and the quality and quantity of milk and wool. In addition, transgenic animals may have more disease resistance and can be used for the production of low-cost pharmaceuticals and biologicals. A novel and commercially useful utilization of transgenic animals is the production of pharmaceuticals or human proteins in transgenic lactating animals [3]. Transgenic animals can become bioreactors, producing products like pharmaceuticals that were formerly produced only in a culture of transgenic microorganisms [15]. Singh *et al*. [4] added that the development of transgenic animals was one of the most important advances during the last decades. Transgenic livestock have played a vital role in the large-scale production of novel medications and pharmaceuticals including high valued food for human applications. Numerous recombinant proteins and other pharmaceuticals for humans and livestock therapeutic applications are being produced using transgenic animals [16].

Transgenic technology was originally developed as a research tool for the study of gene function in disease models. The first transgenic mouse was developed in the 1980s using pronuclear microinjection (a process known as transfection, which is a technique that makes use of finely constructed glass needles to inject purified DNA into the fertilized eggs of the selected species) of the exogenous DNA [3]. Moreover, genetic modifications must be achieved in cells if the yield is too low (low rate of random integration and targeted integration via homologous recombination) and this can be done by developing chimeric or transgenic animals [17].

A transgenic organism is an animal or plant that is generated by the introduction of a foreign gene (a transgene) or DNA and the transgene can change the characteristics (phenotype) of the organism [18]. Transgenic animals can be addressed as genetically engineered animals, or genetically manipulated, genetically modified, genetically altered animals, and biotechnology-derived animals. A genetically engineered animal is also defined as “an animal that has had an alteration in its nuclear or mitochondrial DNA (addition, substitution, or deletion of some part of animal’s genetic material or insertion of foreign DNA) accomplished through a deliberate human technological intervention.” In addition, transgenic animals may be animals that have undergone induced mutations, e.g., by radiation or chemicals which is different from mutations that naturally occur in populations. Cloned animals are also considered to be genetically engineered because there is a direct intervention and planning involved in producing these animals [19]. Transgenic animals have been widely used for various purposes but mainly for human health and animal production. Transgenic mammals are significantly used in the areas of biotechnological, agricultural, biological and biomedical sciences including the production of human gene therapy, antibody production, pharmaceuticals, and disease models for the development of new treatments, blood replacement and organ transfer from transgenic animals to humans [20, 21].

Animal models serve as models for understanding certain biological phenomena, with the prospect that discoveries made in organism models will render insights into the biological functions of other organisms [4, 18]. They are also useful for exploring the underlying mechanisms of physiology and disease in humans [18]. Animal models have been used to create new medicines for different diseases. Pig, for instance, shares several anatomical and physiological homologies with human and mimics the human situations in many ways more accurately than other species [22]. Thus, transgenic pigs can be used as an animal model of human diseases such as cancer, cardiovascular diseases, Alzheimer's disease, diabetes mellitus and cystic fibrosis [23]. Furthermore, several types of small mammal models have been developed for cardiovascular abnormalities that occur naturally or that are induced experimentally [24].

Among the mammalian experimental models, transgenic mice are routinely used as mammalian models. Transgenic mice or Omega mice were engineered to carry genes from roundworm that were capable of producing essential omega-3 and omega-6 fatty acids from saturated fats or carbohydrates. These transgenic mice are used as a new animal model in order to

understand the impact of fat on human health [25]. Transgenic fish, birds (poultry) and mammals such as goats, cows, pigs, rabbits, and sheep have been developed as exogenous protein production systems [4]. In particular, preferred ungulates are pigs, sheep, goats, buffaloes, oxen, antelopes, horse, donkeys, deer, mule, elk, caribou, llama, camels and so on. However, working with larger animals, such as cattle, proved to be much more expensive than working with smaller animals such as mice, pigs, goat and sheep. Therefore, some work only focused on breed-early/lactate-early animals like pigs, sheep, and goats [26].

Innovative materials can also be generated by transgenic animals. For instance, transgenic silkworm with chimeric silkworm or spider silk properties has been created by a group of researchers. Another research group produced transgenic silkworms with the ability to produce fluorescent silk by introducing genes (derived from a jellyfish) that coded for green fluorescent protein [27]. In addition, transgenic silkworm that could spin out spider silk, which is a super-tough fiber, was also engineered at Kraig Biocraft Laboratories (KBL), USA. Dragon silk, one of the latest products of this company, was produced from the fibers of these cocoons. This silk is stronger than steel and lighter, tougher, and much more flexible than Kevlar but Kevlar has slightly lower tensile strength than this synthetic fiber. The company is also searching for possible uses of this silk in defensive clothing and other equipment [28].

Recently, rhesus macaques (*Macaca mulatta*), the most widely used monkey model, have been tested for vaccine trial against COVID-19 by injecting a weakened respiratory virus coding of SARS-CoV-2's spike protein in 32 rhesus macaques [29]. Moreover, researchers from Sinovac Biotech, a private Beijing-based company, also introduced two different doses of their COVID-19 vaccine to 8 rhesus macaques. After 3 weeks, SARS-CoV-2, the virus that causes COVID-19, was then introduced into the monkeys' lungs through tubes down their tracheas, and it was found that no monkey developed a full-blown infection [30].

1.2 Ethical issues in animal biotechnology

The use of animals in experimental research has increased due to the advancement of research and development in medical technology. Each year, millions of animals are being experimentally used worldwide and 90% of these animals are mice and rats, including cats, dogs, rabbits and primates [31]. The pain, distress and even death of animals during the experimentation have been a dispute issue for years [32].

Monkeys are one of the most controversial animal models used in experiments because they have a close genetic relationship to humans. However, less than 1% of animals used in European countries (EU) are monkeys. Monkeys are used only if it is not possible to use a non-animal model, or other animal species for the research being undertaken. However, monkeys are frequently used for testing Covid-19 treatments due to their similarity to humans and they are valuable as they provide the most reliable source of information [33].

Modern biotechnology, especially animal biotechnology, has the possibility to draw a wide range of "moral and ethical concerns". This is probably because of basic disagreements about what our behavior and attitudes towards animals ought to be [8]. Definitions of morals and ethics can vary with country, culture, religion, and so on. Different cultures have different moral codes, and many of the practices and attitudes that we may regard as correct or natural are really only cultural products [34]. However, it is debated that the majority of human beings seems to be content that they could benefit from the use of animals, either directly or indirectly. Therefore, the simple use of animals by human beings has not normally been seen as a matter for moral concern [8]. Many different ethical problems concerning cloning and transgenesis depend on people's beliefs. Recently, the number of animals derived from genetic engineering technology has increased significantly, and ethical issues related to this kind of science and animal welfare have grown [35].

Ethical codes, which are sets of principles for human beings to follow, have been created by a number of professional organizations specifically for their respective fields. In Thailand, the Animals for Scientific Purposes Act 2015 (2558 B.E.) has been established with the aim to protect animals, that are used in any research and other scientific procedures, from unnecessary pain, distress, suffering, and lasting harm [36]. Thus, decisions on animal experimentation have often been taken not on the basis of established science-based evidence of environmental risk but rather on ethical grounds.

Singer [37] described "conditional ethical blindness" in terms of a researcher in the area of animal experimentation, who, conditioned by professional rewards, ignores the ethical issues raised by the experiments just like a rat that is conditioned to press a lever in return for a reward of food. It is not only the experimenters themselves who suffer from conditioned ethical blindness but also research institutes can sometimes have conditional ethical blindness. Some researchers who work with animals may want to help solve the problems of human aggression, however, he or she can later find that rewards or professional prestige are more important than ethics.

Lopez [2] claimed that Buddhism is, in fact, the scientific religion best suited for modernity throughout the world. Thus, Buddhism remains significant and necessary for humans [38]. According to Buddhism, humans have to develop wisdom and virtue at the same time. If science goes together with virtue, it will provide more usefulness and convenience to humans.

Transgenic animals arising from intended genetic change can violate animals and sometimes lead to crippling and even death. Thus, the application of genetic modification animals as the models of human disease may cause animals to suffer as they develop the disease [39]. In Buddhism, it is morally wrong to cause harm to animals. An understanding of the Buddhist concept of *kamma* can be very useful for encouraging humans to be more responsible and to improve their moral standards as well as refraining from unwholesome actions [40]. The Buddhist way may help solve problems in a manner that gives the least damaging to all the people involved [41].

Animals are sentient creatures, and they often value their family. On the one hand, human beings are animals; on the other hand, humans define themselves in opposition to all other animals. Through this dualistic interplay, animality has become a fruitful resource for defining what it means to be human [42]. Some people may be against the utilization of animals by humans for any purpose, whereas others may have special concerns about the impacts of genetic engineering and cloning that might affect animal health and welfare. Some people may find it upsetting that industrial terminology like "transgenic animal bioreactors" is used to describe genetically engineered animals that produce human therapeutic or industrial proteins or agricultural products such as food or even as disease model. Mahatthanadull [43] argued against the creation of genetically modified organisms that it intentionally conveys contamination of "alien genes" into the immaculate environment pervasively. Directionless mutation may ultimately affect the biodiversity of the ecosystem in a way that is beyond human control. From this aspect, the ecological equilibrium could be destroyed by just a few scientific equations. A new overwhelming species will infiltrate the original species, and in doing so causing the extinction of the original species. However, animal cloning and transgenic methodologies can surely create welfare concerns. There is always the disturbing possibility that as success rates in animal transgenics get higher, there will be increased demand for the use of animals in this way. Thus, effective and responsible communication among scientific community, industry, and government stakeholders are vital in order to reach a consensus on the acceptability levels of risk for products of animal biotechnology, as well as to identify which set of values should be applied to certain acceptable uses of animal biotechnology [44].

The use of animals in animal biotechnology can cause animals to suffer, therefore, we have a moral obligation to protect them from suffering in every way we can [31]. Based on Buddhism, the killing or harming of all living beings including animals could violate the first precept. To abstain from injury to living creatures is the right action for moral conduct [45]. Mahatthanadull and

Mahatthanadull [46] added that the "penalties for the violation of the Five Precepts" are important as an aim to raise awareness of the consequences of negligently transgressing the precepts. For example, the killing of a small insect such as an ant attracts a lesser penalty than killing a larger animal such as bird or reptile species. The killing of larger animal is a weightier act because it requires a greater degree of intention and force than does the killing of a smaller one, i.e. the larger the animal, the greater the penalty. In fact, the Buddhist commentaries mention four factors that determine the severity of ill-effects that result from killing various kinds of creatures, namely: the degree of virtue (or value) of the animal killed, the size of the animal, the effort made to kill, and the intention with which the killing is done [45]. Therefore, the Buddha makes it clear that the mistreating or killing of larger and more developed animals should be avoided and furthermore that the research-related treatment of animals must be done with well-thought-out and good and upright intention.

According to scientist, all life is classified by hierarchical levels of organization and the cell holds a special place in the hierarchy of life because it is the lowest level of living organisms. Nervous systems distinguish animals from all other kingdoms of life and certain properties of human brains distinguish humans from all other animals. The sizes and shapes of animals affect animals' interactions with external environments. A large animal, such as an elephant, has very different body proportions than a small animal, such as mouse [47] and the perceptual abilities of various animal types (in terms of their senses and brains) vary according to the animal classification. Thus, the physical size of animals and *kamma* are related according to the animal classification designed by scientist [48].

1.3 Alternative methods to animal testing

Technologies related to transgenic and cloned animals might be ethically unacceptable if the animals suffer or are frustrated to a greater degree than that experienced by normal animals of the same species under similar husbandry. However, if there are no adverse effects on individual animals, there is no basis for ethical objections to animal biotechnology. The use of transgenic animals is facing concern of negative impacts on environment because of disrupting ecological balance, food safety concern, ethical and religious concerns. Thus, recommendations by both government and commercial entities are made by supporting of research that helps develop promising bio-therapeutics and biotechnology products. Information and knowledge regarding genetic engineering, production methods, products and regulatory processes should be made available to the public. Education concerning the advantages and challenges related to animal biotechnology is the key to public understanding. In addition, government inadvertence, regulations as well as stringent rules on the research of genetic engineering and transgenic animals should also be considered [49].

In order to overcome the drawbacks of animal experimentation and to avoid unethical procedures, alternatives to animal testing have been proposed [50]. The strategy of 3 Rs, i.e. the reduction, refinement and replacement of laboratory use of animals, can be applied [51]. Three Rs was first described in 1959 by Russell and Burch as the benevolent and ethical way to use animals in research testing and their work was followed worldwide with the establishment of many other research tests [52]. These approaches suggest some ways to make animal experiments more humane by minimizing the numbers of animals so that the numbers of animals used in experiments are reduced, that is by 'reduction'. At the same time the use of animals has to be planned and refined carefully in a way that pain and distress caused during the experiment should be lessen, and this constitutes 'refinement'. For 'replacement', it is described as the use of simpler life forms such as lower vertebrates and invertebrates or the use of non-sentient materials instead of living conscious vertebrates. Two kinds of replacements, i.e. relative and absolute replacement can be applied [53].

These methods can provide an alternative means for drug and chemical testing, up to certain levels. The advantages of these methods are time efficiency, require less man power, and these methods are also cost effectiveness. Doke and Dhawale [32] also suggested alternative methods as follows:

1) *Computer models*: Computers can be used to generate simulations for the prediction of many possibilities of biological and toxic effects of a chemical or potential drug candidate without dissecting animals.

2) *Cells and tissue cultures*: *In vitro* cell and tissue cultures involving the growth of cells in laboratory environment can be used as a considerable alternative for animal experiments. The cells and tissues from animals like brain, kidney, liver, skin can be removed and grown outside the body in a suitable medium for further use. These methodologies are also routinely applied for the preliminary screening of potential drug molecules or chemicals in order to check their efficacy and toxicity [54]. The benefits of these techniques are easy to follow, less time consuming and less expensive when compared to animal tests.

3) *Alternative organisms*: In order to replace experimental animals, different model organisms can be used, e.g., lower vertebrates (zebra fish, *Danio rerio*), invertebrates (fruit fly, *Drosophila melanogaster*, nematode, *Caenorhabditis elegans*) and microorganisms (yeast, *Saccharomyces cerevisiae*).

Because of the advancement and rapid development in biomedical sciences, 'responsibility' is the 4th R added to the basic 3Rs. The addition of 'responsibility' is to let people realize the importance of integrity and honesty in the reasonable and proper use of animals in laboratory because an issue of animal welfare is as important as human welfare [55]. In addition, advanced or sophisticated technologies that are used to replace live animals also include cell-based tests (in vitro); tests that use tissue taken from dead animals or humans (ex vivo); computer-based modelling (in silico); chemical-based analytical tests (in chemico) as well as ethical human studies (in vivo) [56]. However, these alternatives cannot completely eliminate the necessity for the use of animals in the laboratory because intact animals can provide a better model of the complex interaction regarding the physiological process than other alternative techniques [52]. Thus, in order to motivate science to change its paradigm, policies have to be targeted and amplified to reduce animal experimentation as well as to lift regulatory malaise and to provide more funding for development of new approaches [56].

Therefore, these alternative protocols of the 3 Rs plus responsibility can provide dependable outcomes and minimize the use of animals in scientific procedures. Although these strategies can also minimize or in some case nullify the need for ethically-questionable animal experimentation, some studies may still require the use of animals.

2. Conclusions

Animal biotechnology has become an important branch of biotechnology and it is being used in an increasing number of applications in basic science, medical science and agriculture. The core of animal biotechnology is addressed on transgenic animals produced through cloning and genetic engineering techniques which are nowadays becoming extremely advanced and common. There seems to be little doubt that the use of animal biotechnology benefits human welfare. However, whilst using animals as a model, scientific risk assessment and use of the precautionary principle, as well as ethical guidelines have to be highly concerned. Some of the ethical issues are still questionable and responses to them may well depend on individual's opinion, culture and religion. 'Conditional ethical blindness' is also a factor that can determine how individuals, organizations and society see and respond to the main ethical issues. Therefore, one way to solve these problems is the use of alternative protocols such as reduction, refinement, replacement and responsibility to

minimize the use of animals as well as to avoid animal ethical controversies. When experimentation with animals cannot be avoided, they must be treated with as much kindness and compassion as possible. Effective and responsible communication through scientific community, industry and government stakeholders are also required in order to reach a consensus of society on the acceptance of genetic engineering and animal cloning.

References

[1] Phra Dharmakosajarn, 1998. Educating for balance: a Buddhist perspective. *19th General Conference of the World Council for Curriculum and Instruction*, Bangkok, Thailand, July 14, 1998.

[2] Lopez, D.S., 2008. *Buddhism & Science. A Guide for a Perplex*. Chicago and London: The University of Chicago Press.

[3] Smith, J.E., 2009. *Biotechnology*. 5th ed. Cambridge: Cambridge University Press.

[4] Singh, B., Gautam, S.K., Chauhan, M.S. and Singla, S.K., 2015. *Animal Biotechnology*. New Delhi: The Energy and Resources Institute (TERI).

[5] Gjerris, M., Olsson, A. and Sandøe, P., 2006. Animal biotechnology and animal welfare. In: *Ethical Eye: Animal Welfare*. Strasbourg: Council of Europe, pp. 89-110.

[6] American Israeli Cooperative Enterprise (AICE), 2019. *Breakthrough Dividend*. [online] Available at: www.jewishvirtuallibrary.org/jsource/ biotech/ bdcontent.html

[7] National Academy ofSciences (NAS), 2002. *Animal Biotechnology: Science Concerns*. Washington D.C.: National Academy of Science.

[8] Straughan, R., 1999. *Ethics, Morality and Animal Biotechnology*. Swindon: The Biotechnology and Biological Sciences Research Council.

[9] Willadsen, S.M., 1986. Nuclear transplantation in sheep embryos. *Nature*, 320, 63-65.

[10] Wilmut, I., Schnieke, A.E., McWhir, J., Kind, A.J. and Campbell, K.H., 1997. Viable offspring derived from fetal and adult mammalian cells. *Nature*, 385, 810-813.

[11] Smith, J.E., 2004. *Biotechnology.* 4th ed. Cambridge: Cambridge University Press.

[12] Molnar, C. and Gair, J., 2019. *10.1 Cloning and Genetic Engineering*. [online] Available at: https://pressbooks.bccampus.ca/conceptsofbiologymolnarcamosun/chapter/10-1cloning-and-genetic-engineering/.

[13] Twine, R., 2010. *Animal as Biotechnology. Ethics, Sustainability and Critical Animal Studies.* New York: Earthscan.

[14] Singhal, M. and Kansara, N., 2010. Transgenic animals: production and application. *International Journal of Pharmaceutical Sciences and Research*, 1(9), 12-22.

[15] Smith, J.E., 2004. *Biotechnology*. 4th ed. Cambridge: Cambridge University Press.

[16] Houdbine, L.M., 2009. Production of pharmaceutical proteins by transgenic animals, *Comparative Immunology Microbiology and Infectious Diseases*, 32, 1393-1398.

[17] Laible, G., 2018. Production of transgenic livestock: Overview of transgenic technologies. In: H. Niemann and C. Wrenzycki, eds. *Animal Biotechnology 2. Emerging Breeding Technologies.* Cham: Springer, pp. 95-121.

[18] Weitzman, J. and Weitzman, M., 2017. *30-Second Genetics*. London: Ivy Press

[19] Ormandy, E.H., Dale, J. and Griffin, G., 2011. Genetic engineering of animals: Ethical issues, including welfare concerns. *Canadian Veterinary Journal*, 52(5), 544-550.

[20] Wall, R.J. and Seidel, G.E., 1992. Transgenic farm animals, a critical analysis. *Theriogenology*, 38(2), 337-357.

[21] Houdebine, L.-M., 2005. Use of transgenic animals to improve human health and animal production. *Reproduction in Domestic Animals*, 40(4), 269-281.

[22] Rogers, C.S., Abraham, W.M., Brogden, K.A., Engelhardt, J.F., Fisher, J.T., McCray, P.B., McLennan, G., Meyerholz, D.K., Namati, E., Ostedgaard, L.S., Prather, R.S., Sabater, J.R., Stoltz, D.A., Zabner, J. and Welsh, M.J., 2008. The porcine lung as a potential model for cystic fibrosis. *American Journal of Physiology-Lung Cellular and Molecular Physiology*, 295, L240-L263.

[23] Aigner, B.S., Renner, S., Kessler, B., Klymiuk, N., Kurome, M. and Wünsch, A., 2010. Transgenic pigs as models for translational biomedical research. *Journal of Molecular Medicine*, 88(7), 653-664.

[24] Roths, J.B., Foxworth, W.B., McArthur, M.J., Montgomery, C.A. and Kier, A.B., 1999. Spontaneous and engineered mutant mice as models for experimental and comparative pathology: History, comparison, and developmental technology. *Laboratory Animal Science*, 49, 2-34.

[25] Pai, V.J., Wang, B., Li, X., Wu, L. and Kang, J.X., 2018. Transgenic mice convert carbohydrates to essential fatty acids. In: Sarah Lombard, ed. *Animal Biotechnology*. New York: Callisto Reference, pp. 1-6.

[26] Clark, A.J., Ali, S., Archibald, A.L., Bessos, H., Brown, P., Harris, S., McClenaghan, M., Prowse, C., Simons, J.P. and Whitelaw, C.B., 1989. The molecular manipulation of milk composition. *Genome*, 31, 950-955.

[27] Clark, D.P. and Pazdernik, N.J., 2016. Transgenic animals. In: *Biotechnology*, 2nd ed. Amsterdam: Elsevier, pp. 493-521.

[28] Offord, C., 2017. *Meet the Transgenic Silkworms That Are Spinning Out Spider Silk.* [online] Available at: https://www.the-scientist.com/notebook/meet-the-transgenic-silkworms-that-are-spinning-out-spider-silk-30212.

[29] Mercado, N.B., Zahn, R., Wegmann, F., Loos, C., Chandrashekar, A., Yu, J., Liu, J., Peter, L., McMahan, K., Tostanoski, L.H., He, X., Martinez, D.R., Rutten, L., Bos, R., van Manen, D., Vellinga, J., Custers, J., Langedijk, J.P., Kwaks, T., Bakkers, M.J.G., Zuijdgeest, D., Huber, S.K.R., Atyeo, C., Fischinger, S., Burke, J.S., Feldman, J., Hauser, B.M., Caradonna, T.M., Bondzie, E.A., Dagotto, G., Gebre, M.S., Hoffman, E., Jacob-Dolan, C., Kirilova, M., Li, Z., Lin, Z., Mahrokhian, S.H., Maxfield, L.F., Nampanya, F., Nityanandam, R., Nkolola, J.P., Patel, S., Ventura, J.D., Verrington, K., Wan, H., Pessaint, L., Ry, A.V., Blade, K., Strasbaugh, A., Cabus, M., Brown, R., Cook, A., Zouantchangadou, S., Teow, E., Anderson, H., Lewis, M.G., Cai, Y., Vhen, B., Schmidt, A.G., Reeves, R.K., Baric, R.S., Lauffenburger, D.A., Alter, G., Stoffels, P., Mammen, M., Hoof, J.V., Schuitemaker, H. and Barouch, D.H., 2020. Single-shot Ad26 vaccine protects against SARS-CoV-2 in rhesus macaques. *Nature* (2020), https://doi.org/10.1038/s41586-020-2607-z.

[30] Cohen, J., 2020. *COVID-19 Vaccine Protects Monkeys from New Coronavirus, Chinese Biotech Reports*. [online] Available at: https://www.sciencemag.org/news/2020/04/covid-19-vaccine-protects-monkeys-new-coronavirus-chinese-biotech-reports.

[31] Phelps, N., 2004. *The Great Compassion. Buddhism and Animal Rights*. New York: Lantern Books.

[32] Doke, S.K. and Dhawale, S.C., 2015. Alternatives to animal testing: A review. *Saudi Pharmaceutical Journal*, 23, 223-229.

[33] European Animal Research Association, 2020. *Covid-19 Research Using Monkeys*. [online] Available at: https://www.eara.eu/post/covid-19-research-using-monkeys.

[34] Rachels, J., 2003. *The Elements of Moral Philosophy*. Boston: McGraw-Hill.

[35] Camera, D., Dimitrova, Ir., Doynova, M., Jachacz, L., Kachakova, D., Kepka, M., Ould Isselmou, C.B., Vornier, J.P. and Yungarva., Tsv., 2008. *Transgenic and Cloned Animals: Ethical Problem?* Perugia: EU Socrates Erasmus European Community.

[36] Kunjara, P., 2015. Animals for scientific purposes act 2015 (2558 B.E.). *Proceedings of the 14th Chulalongkorn University Veterinary Conference CUVC: Responsible for Lives*. Bangkok, Thailand, April 20-22, 2015, 75.
[37] Singer, P., 2002. *Animal Liberation. The Definitive Classic of the Animal Movement*. New York: HarperCollins Publishers.
[38] Surasith, N., 2016. *Tipitaka Studies*. Translated by Veerakarn Kanokkamalade. Ayutthaya: Mahachulaongkornrajavidayalaya Press.
[39] Brunk, C.G., Hartley, S., 2013. *Designer Animals. Mapping the Issues in Animal Biotechnology*. Toronto: University of Toronto Press.
[40] Ubeysekara, A., 2019. *The Concept of Kamma in Theravada Buddhism*. [online] Available at: https://drarisworld.wordpress.com/2016/09/25/the-concept-of-kamma-in-theravada-buddhism/.
[41] Taniguchi, S., 2019. *Biomedical Ethics. From a Buddhist Perspective*. [online] Available at: https://enlight.lib.ntu.edu.tw/FULLTEXT/JR-MAG/mag133029.pdf.
[42] Ohnuma, R., 2017. *Unfortunate Destiny. Animals in the Indian Buddhist Imagination*. Oxford: Oxford University Press.
[43] Mahatthanadull, S., 2015. Buddhist response to environmental degradation under conceptual framework of the Five Niyāma. *Proceedings of the 1st MCU International Academic Conference (MIAC) on Buddhism and World Crisis*, Graduate School, MCU, Thailand, May 29, 2015, 65-78.
[44] Van Eenennaam, A.L., 2006. What is the future of animal biotechnology? *California Agriculture*, 60(3), 132-139.
[45] Payutto, P.A., 2017. *Buddhadhamma. The Laws of Nature and Their Benefits to Life*. 2nd ed. Translated by R. P. Moore. Bangkok: Buddhadhamma Foundation.
[46] Mahatthanadull, S. and Mahatthanadull, S., 2018. The five precepts: Criteria and the promotion of individual and social peace *JIABU*, 11(3), 180-193.
[47] Cambell, N.A., 1996. *Biology*. 4th ed. Menlo Park: The Benjamin/Cummings Publishing Company, Inc.
[48] Mahatthanadull, S. and Mahatthanadull, S., 2015. *Research Report on the Five Precepts: Criteria and the Promotion of Individual and Social Peace*. International Buddhist Studies College: Mahachulalongkornrajavidyalaya University.
[49] Rollin, B., 1996. *The Frankenstein Syndrome: Ethical and Social Issues in the Genetic Engineering of Animals*. Cambridge: Cambridge University Press.
[50] Doke, S.K. and Dhawale, S.C., 2015. Alternatives to animal testing: a review. *Saudi Pharmaceutical Journal*, 23(3), 223-229.
[51] Ranganatha, N. and Kuppast, I.J., 2012. A review on alternatives to animal testing methods in drug development. *International Journal of Pharmacy and Pharmaceutical Sciences*, 4, 28-32.
[52] Mushtaq, S., Das, Y.K. and Aksoy, A., 2018. Alternative methods to animal experiments. *Turkiye Klinikleri Journal of Medical Sciences*, 38(2), 161-170.
[53] Balls, M., 1994. Replacement of animal procedures: Alternatives in research, education and testing. *Laboratory Animals*, 28(3), 193-211.
[54] Xu, K.-P., Li, X.-F. and Yu, F.-S.X., 2000. Corneal organ culture model for assessing epithelial responses to surfactants. *Toxicological Science*, 58(2), 306-314.
[55] Arora, T., Mehta, A.K., Joshi, V., Mehta, K.D., Rathor, N., Mediratta, P.K. and Sharma, K.K., 2011. Substitute of animals in drug research: An approach towards fulfilment of 4R's". *Indian Journal of Pharmaceutical Sciences*, 73(1), 1-6.
[56] Taylor, K., 2019. Recent Developments in Alternatives to Animal Testing. [online] Available at: https://www.wellbeingintlstudiesrepository.org/cgi/viewcontent.cgi?article=1005&context=appamet.

Instructions for Authors

Current Applied Science and Technology journal contains research reports, articles concerning development work, reviews of the literature and research activities. The objectives are to publish and promote research contributions and innovative work in fields associated with applied science and technology. An electronic journal is provided on the website (https://www.tci-thaijo.org/index.php/cast/index). The editors reserve the right to require revision of the submitted manuscript as a condition for final acceptance.

The institute and the editorial board claim no responsibility for the contents or views expressed by the authors of individual articles. Copying is allowed provided that acknowledgement is made. All articles submitted for publication will be assessed by a group of distinguished.

Ethics:

The journal is committed to maintaining the high level of integrity in the content published and has a Conflict of Interest policy in place. The journal uses plagiarism detection software to screen the submissions. If plagiarism is found, the COPE guidelines on plagiarism will be followed. For more details, please see https://www.tci-thaijo.org/index.php/cast/navigationMenu/view/Publication_Ethics.

Page Charge: Free

Submission of Manuscripts:

Manuscripts must be written in English and submitted online. Manuscripts are to be reviewed (double blinded) by at least 3 referees specializing in relevant fields. Revised manuscripts have to be sent online.

All manuscripts should be submitted to: https://www.tci-thaijo.org/index.php/cast/index

Contact:

Editor of Current Applied Science and Technology
King Mongkut's Institute of Technology Ladkrabang
1 Soi Chalongkrung 1, Ladkrabang District,
Bangkok 10520, Thailand
Tel: 662-329-8136
Fax: 662-329-8221
Email: cast@kmitl.ac.th

Manuscript Preparation Guide:

General: Manuscripts must be typewritten using *Microsoft Word for Windows*, single-spaced with margin set-up (in page set up menu) as follows (see also the document template):

Top Margin	1.5"	Bottom Margin	1.5"
Left Margin	1.5"	Right Margin	1.5"

Good quality printouts using A4 paper size are required. Format should be a single column. Times New Roman font type is required. Font sizes for various text functions are as follows:

Text functions	Size *	Typeface
Title	14 (CT)	Bold
Author and co-authors	11 (CT)	Normal
Address for correspondence	11 (CT)	Normal
Abstract and main text	10 (LJ)	Normal
Section heading and number including "Abstract", "Acknowledgement", "References"	12 (CT)	Bold
Subsection heading and number	11 (LJ)	Bold

* CT = Center Text, LJ = Left Justified.

The corresponding author should be noted (included a Fax number and E-mail address) and indicated with an asterisk. Full postal addresses must be given for all co-authors, keyed to names (if required) by superscripted Arabic numbers.

Paper Length: Should not normally exceed 10 pages including figures and tables
Spelling: American English
Abstract: Should not exceed 250 words
Keywords: Should not exceed 8 keywords
Text: Authors are requested to use the following order when typing:-

All research reports (Full Length or Short Reports): Title, Authors, Affiliations, Abstract, Keywords, Introduction (in reserch papers this must be confined to relevant matters, and must not be a general review of cognate literature), Materials and Methods, Results and Discussion, Conclusions, Acknowledgements, References.

Reviews and Discussion Papers will be considered in any format appropriate to the purposes of the authors, although adherence to the general guidelines described above is encouraged.

Line Art Figures: Figures can be drawn using several packages such as Win Draw®, Auto CAD®, Corel Draw®, VISIO® etc.

Photographs: Actual size photographs are acceptable. However, they can also be put into a text stream using a good-resolution scanner. All photographs must be clear when printed in monochrome.

Graphs: Several packages available today can produce attractive and professional graph presentation. Some also provide curve-fitting function, which can be useful. However, two-dimensional bar charts are preferred. All graphs must be clear in monochrome printing.
Equations and complex expressions: Math CAD®, Math Writer® and Equation Editor® (included in Microsoft Word®) are acceptable for presentation of this type of material.

Citations: Citations in the text should be denoted by numbers between square brackets (i.e. [1, 2], [1-3], [1, 3-8]…) *in the order of first appearance in the text.*

References: References should be numbered to correspond with the text citations. References must be arranged as follows:

Books
Author's surname(s), Initials., Year. *Title of Book*. Edition. (only include this if not the first edition) Place of publication: Publisher.
Example:
[1] Einstein, A. 2019. *Relativity. The Special and the General Theory*. Ghaziabad: Samaira Book Publishers.

Chapters of edited books
Chapter author's surname(s), Initials., Year of book. Title of chapter. In**:** Book editor(s) initials. surnames, ed. or eds. *Title of Book*. Place of publication: Publisher, Chapter number or first and last page numbers.
Example:
[2] Smith, J.E., 2006. Public perception of biotechnology. In: C. Ratledge and B.Kristiansen, eds. *Basic Biotechnology*. Cambridge: Cambridge University Press, pp. 3-24.

E-books
Author's surname(s), Initials., Year, *Title of Book*. [e-book] Place of publication: Publisher. Available through: include e-book source/database, web address or URL.
Example:
[3] Willey, J., Sherwood, L. and Woolverton, C.J., eds. 2013. *Prescott's Microbiology*. 9th ed. [e-book] New York: McGraw-Hill. Available through: Libribook website < www.libribook.com>

Journal articles
Author's surname(s), Initials., Year. Title of article. *Full Title of Journal,* Volume number (Issue number), Page numbers.
Example:
[4] Ross, A.B., Junyapoon, S., Jones, J.M., Williams, A. and Bartle, K.D., 2005**.** A study of different soots using pyrolysis– GC– MS and comparison with solvent extractable material. *Journal of Analytical and Applied Pyrolysis*, 74(1-2), 494-501.

In case of online journal articles without page number:
Author's surname(s), Initials., Year. Title of article. *Full Title of Journal,* Volume number (Issue number), DOI**-**based link.
Example:
[5] Tanasupawat, S., Phongsopitanun, W., Suwanborirux, K., Ohkuma, M. and Kudo, T. 2016. *Streptomyces actinomycinicus* sp. nov., isolated from soil of a peat swamp forest. *International Journal of Systematic and Evolutionary Microbiology*, 66(1), https://doi.org/10.1099/ijsem. 0.000716.

Proceedings
Author's surname(s), Initials., Year. Title of article. *Full Title of Proceedings*, Place of Conference, Date, page numbers.
Example:
[6] Thanaboripat, D., Ruangrattanametee, V. and Srikitkademwat, K., 2010. Control of growth and aflatoxin production of aflatoxin producing fungi in corn by salts. *Proceedings of the 8th International Symposium on Biocontrol and Biotechnology*, Pattaya, Thailand, October 4-6, 2010, pp. 283-289.

Patent
Inventor surname(s), Initial(s)., Assignee, Year. *Title*. Place. Patent number (status, if an application).
Example:

[7] Leonard, Y., Super Sports Limited, 2008. *Tin Can Manufacture and Method of Sealing*. Canada. Pat. 12,789, 675.

Dissertation
Author's surname, Year of publication. *Title of Dissertation*. Level. Official name of University, Country.
Example:
[8] Sukcharoen, O., 2017. *Inhibitory Effect of Plant Essential Oils on Growth and Aflatoxin Production by Aspergillus flavus IMI 242684 and Aspergillus parasiticus IMI 283883.* Ph.D. King Mongkut's Institute of Technology Ladkrabang, Thailand.

Websites
Authorship or Source, Year. *Title of Document*. [online] Available at: include web site address/URL (Uniform Resource Locator).
Example:
[9] NHS Evidence, 2003. *National Library of Guidelines*. [online] Available at: http://www.library.nhs.uk/guidelines.

Acknowledgements: These should be as brief as possible.

Proofs:
Proofs will be sent to the corresponding author and *must* be returned as soon as possible. Corrections should be restricted to typesetting errors.

Copyright:

Page Numbering:
All pages must be sequentially numbered, preferably by using the automatic page numbering function on your computer.

Copyright Material:
It is the authors' responsibility to obtain written permission from the copyright holder (usually the book or journal publisher) to use copyright material, and to send a copy of this consent with the manuscript. This consent is not normally denied but it is an international legal requirement that it be obtained.

Note:

Please note that authors are urged to check their proofs carefully before returning, since the inclusion of late corrections cannot be guaranteed.

Author(s) are responsible for ensuring that the submitted manuscript fully meets the requirements specified in the above Instructions. Manuscripts which fail to do so will be returned unedited to the Author(s) for correction in accordance with the above requirements, before they can be submitted to the processes of Referee evaluation.

1.5"

TEMPLATE

Enter title here (14 PT type size, Title Case, Bold, Centered)

Author Information entered here:
Name (in full)

Affiliation
City
Country
(11 pt type size, upper and lower case, centered under the title)

How to Use This Document Template

Insert the information in your document in place of the text here. For the body of your document, use Times New Roman 10 pt. Font, upper and lower case, double-spaced. Allow an extra half space above a line containing superscripts and/or below a line containing subscripts. The whole text should be left-justified. The headings should be 12 pt size, uppercase, bold and centered.

1.5" 1.5"

Abstract (12pt)

Maximum 250 words here. (10 pt)
.....
.....
.....
.....
.....

Keywords: (10 pt)

Maximum of 8 words

1. Introduction (12 pt)

Clearly explain the nature of the problem, previous work, purpose, and contribution of the paper (10 pt).
.....
.....
.....
.....
.....

*Corresponding author: Tel.: ..... Fax: .....
E-mail: .....

1.5"

2. Materials and Methods (12 pt)

.....
.....
.....
.....

3. Results and Discussion (12 pt)

.....
.....…

4. Conclusions (12 pt)

Clearly indicate advantages, limitations and possible applications (10 pt).
.....
.....

5. Acknowledgements (12 pt)

A brief acknowledgement section may be included here (10 pt).
.....
.....

References (12 pt)

References must be numbered in the order cited in the manuscript and indicated in the text by a number in square brackets (e.g. [1, 2]) (10 pt).

Example of References must be arranged as follows:

[1] Barker, R. Kirk, J. and Munday, R.J., 1988. *Narrative Analysis*. 3rd ed. Bloomington: Indiana University Press.
[2] Samson, C., 1970. Problems of information studies in history. In: S. Stone, ed. *Humanities Information Research*. Sheffield: CRUS, pp. 44-68.
[3] Carlsen, J. and Charters, S., 2007. *Global Wine Tourism*. [e-book] Wallingford: CABI Pub. Available through: Anglia Ruskin University Library website <www.libweb.anglia.ac.uk>.
[4] Ross, A.B., Junyapoon, S., Jones, J.M., Williams, A. and Bartle, K.D., 2005. A study of different soots using pyrolysis–GC–MS and comparison with solvent extractable material. *Journal of Analytical and Applied Pyrolysis*, 74*(*1-2*)*, 494-501.
[5] Thanaboripat, D., Ruangrattanametee, V. and Srikitkademwat, K., 2010. Control of growth and aflatoxin production of aflatoxin producing fungi in corn by salts. *Proceeding of the 8th International Symposium on Biocontrol and Biotechnology*, Pattaya, Thailand, October 4-6, 2010, 283-289.

[6] Leonard, Y., Super Sports Limited., 2008. *Tin Can Manufacture and Method of Sealing*. Canada. Pat. 12,789, 675.
[7] Richmond, J., 2005. *Customer Expectations in the World of Electronic Banking: a Case Study of the Bank of Britain.* Ph.D. Anglia Ruskin University.
[8] NHS Evidence, 2003. *National Library of Guidelines*. [online] Available at: http://www.library.nhs.uk/guidelines

Note:

Tables and Graphs: Minimum of 10 pt type size, all captions should be upper and lower case, centered. Each table and figure must be on a separate page (or pages if required) , ***and must be embedded in the text.***

Illustrations and Photographs: Halftones, minimum of 10 pt type size, bold, captions should be in upper and lower case, centered. Images must be computer-designed with clearly visibility.

Contact

Editor of Current Applied Science and Technology
King Mongkut's Institute of Technology Ladkrabang
1 Soi Chalongkrung 1, Ladkrabang District
Bangkok 10520, Thailand
Tel: 662-329-8136 Fax: 662-329-8221
E-mail: cast@kmitl.ac.th
Website: https://www.tci-thaijo.org/index.php/cast/index

KING MONGKUT'S INSTITUTE OF TECHNOLOGY LADKRABANG
1 Soi Chalongkrung 1, Ladkrabang District Bangkok 10520, Thailand
Tel: 662-329-8136 Fax: 662-329-8221
E-mail: cast@kmitl.ac.th
Website: https://www.tci-thaijo.org/index.php/cast/index